26 February 2010 $10

Science

AAAS

INTERNATIONAL SCIENCE & ENGINEERING
VISUALIZATION CHALLENGE

CALL FOR ENTRIES

ENTRY DEADLINE: SEPTEMBER 15, 2010

SCIENCE AND ENGINEERING'S MOST POWERFUL STATEMENTS
ARE NOT MADE FROM WORDS ALONE

Visualization in all its forms has the power to illuminate and educate. It explains and makes clear all aspects of the world around us. It feeds insight and provokes curiosity.

The National Science Foundation (NSF) and the journal *Science*, published by the American Association for the Advancement of Science, invite you to participate in this year's Challenge. The competition recognizes scientists, engineers, visualization specialists, and artists who produce innovative work in visual communication.

Winning entries will be published in *Science* and *Science* Online, and will be displayed on the NSF web site.

Award Categories

- Photographs/Pictures
- Illustrations/Drawings
- Informational Posters and Graphics
- Interactive Games
- Non-Interactive Media

COMPLETE ENTRY INFORMATION:
WWW.NSF.GOV/NEWS/SCIVIS

NSF

Science
AAAS

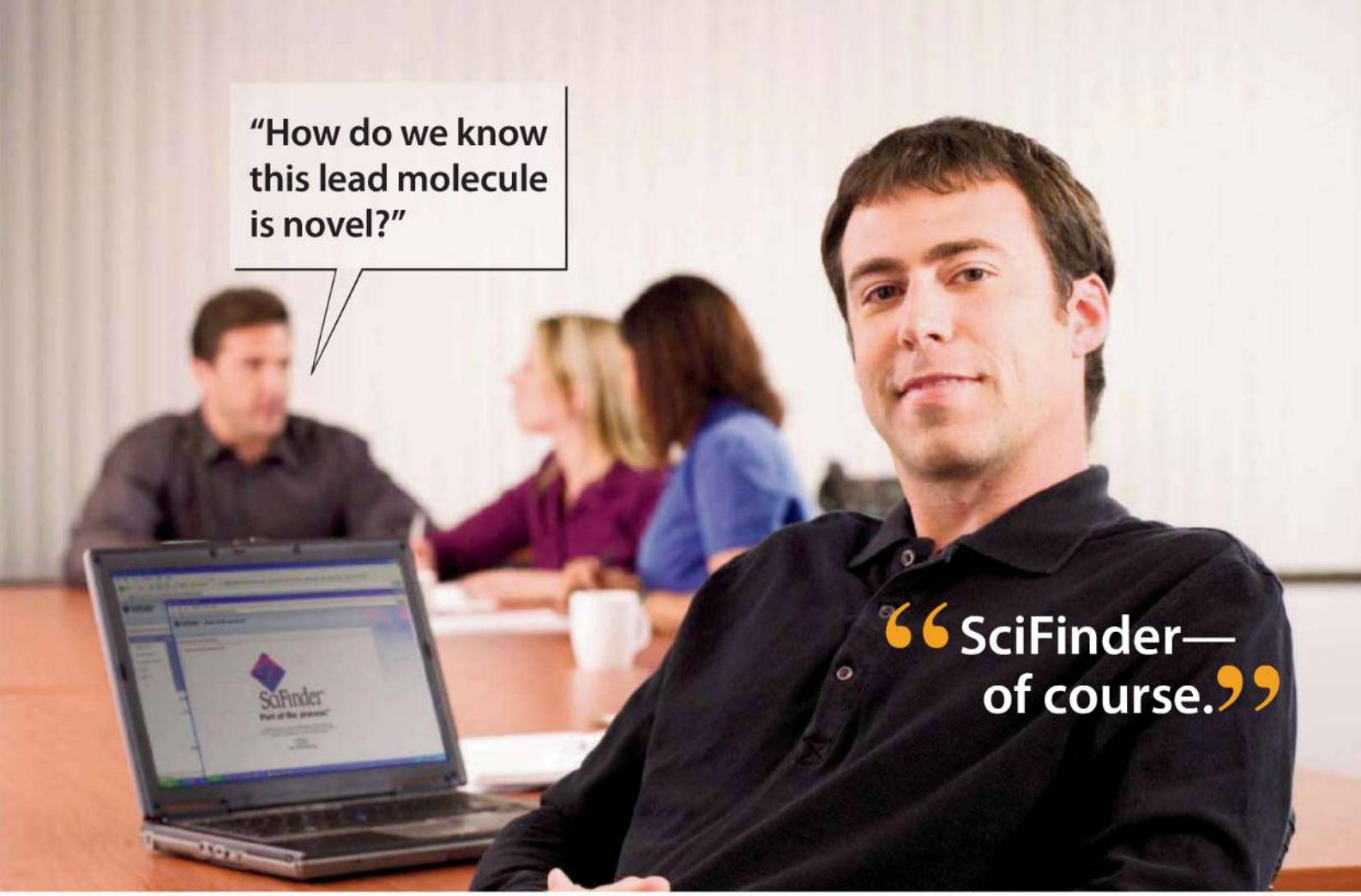

Need to assess the novelty of substances?
SciFinder is the answer.

It includes CAS REGISTRY,[SM] the most comprehensive substance information available, integrated with relevant journal articles and patents.

Give your research team the highest quality and most timely scientific information resource.

Make SciFinder an essential part of your research process.

For more information about SciFinder, visit www.cas.org or e-mail help@cas.org.

an essential

SciFinder®—Part of the process.™

CAS | SciFinder®

www.cas.org

CAS is a division of the American Chemical Society

Without high-quality biomarker data,
am I making the best decisions?

What is your risk tolerance?
WideScreen™ BeadPlex™ Multiplex Assays.
Assay solutions that are extensively
validated for clarity you can count on.
When it comes to biomarker patterns,
insight is everything.

That's what's in it for you. EMD Chemicals

Visit **www.emdbiosciences.com/widescreen** for technical information on the broad range of WideScreen™ products available. To order WideScreen™ products: USA and Canada 800.854.3417. Outside North America contact your local Merck office.
Refer to next page for details. ▶

EMD

WideScreen™ BeadPlex™ Multiplex Assays

for the xMAP® Technology Platform

Visit **www.emdbiosciences.com/widescreen** for technical information on the broad range of WideScreen™ products available. To order WideScreen™ products: USA and Canada 800.854.3417. Outside North America contact your local Merck office.

EMD NOVAGEN · CALBIOCHEM BIOSCIENCES

WideScreen™ BeadPlex™ Multiplex Assays for the Luminex® xMAP® Platform

WideScreen™ Biomarker Analysis for:

- Toxicity
- Cancer
- Cardiovascular Disease (CVD)
- Metabolism
- Inflammation
- Hormones
- Signaling Pathways

WideScreen™ BeadPlex™ Biomarker Assay Kits

Large portfolio of multiplex assays developed both internally at Merck KGaA, and with Rules Based Medicine (RBM)
Created using assays from RBM's HumanMAP® and Rat KidneyMAP® service portfolio
Focused on specific therapeutic areas and disease states
Our continually expanding portfolio includes:

Cancer:
- Human Cancer Panel 1 (Tumor Markers)
- Human Cancer Panel 2 (Growth Factors)
- Human Breast Cancer Panels (3)
- Human MMP Panel

Signaling Cancer Panels:
- Erk/MAPK Pathway Panels 1&2
- Receptor Tyrosine Kinase (RTK) Panel 1
- Phospho-Receptor Tyrosine Kinase (RTK) Panel 1
- Phospho-EGFR Profiling 9-plex

Coming soon:
- Receptor Tyrosine Kinase (RTK) Panel 2
- Phospho-Receptor Tyrosine Kinase (RTK) Panel 2

CardioVascular Disease:
- Human CVD Panel 1 (Apolipoprotein)
- Human CVD Panel 2 (Inflammation)
- Human CVD Panel 3
- Human CVD Panel 4
- Human CVD Panel 5 (Acute Phase)
- Human CVD Panel 6

Metabolism:
- Human Metabolism Panel 1
- Human Metabolism Panel 2
- Human Hormone Panel 1
- Rat Metabolism Panel 1

WideScreen™ BeadPlex™ Toxicity Assays

Panels of key toxicity biomarkers used to detect kidney impairment due to drug-induced toxicity. In 2008, the Predicitive Safety Testing Consortium (PSTC), a public-private consortium led by the Critical Path Institute, submitted a list of urinary biomarkers indicative of drug-induced kidney damage to the FDA and EMEA regulatory authorities. The FDA and EMEA have issued new guidelines on the submission of the biomarkers as indicators of kidney damage in pre-clinical studies. EMD, in partnership with RBM, has now released assay kits that include four of the seven newly accepted biomarkers (KIM-1, ß2M, Cystatin C, and Clusterin) along with six other key protein markers for kidney injury.

- Rat Kidney Toxicity Panel 1 (KIM-1, ß2-microglobulin, GSTα, TIMP-1, VEGF)
- Rat Kidney Toxicity Panel 2 (Cystatin C, NGAL, Calbindin, Clusterin, Osteopontin)

EMD

GE Healthcare
Life Sciences

GE02-10. First published January 2010.

Drop. Measure. Done.

NanoVue™ Plus: intelligent performance across all spectrophotometer applications

It's all the convenience you want in a spectrophotometer, packaged in a portable, ergonomic device. NanoVue Plus features a new hydrophobic, gold-colored sample plate coating that delivers outstanding results for sub-microliter amounts of proteins and nucleic acids. It operates without a PC and does not require time-consuming third-party path length recalibration.

NanoVue Plus enables easy protocol selection using advanced software that includes intuitive drop-down lists for the full range of CyDye™ fluorescent dyes, as well as lists for common fluors. Results can exported using a USB cable or Bluetooth™ connections for print via computer (PVC) or stored using the new SD card option. An integrated printer is also available.

- Swift, accurate analysis of 0.5 µl samples of nucleic acids and proteins
- Practical drop and measure mechanism
- Outstanding sample recovery
- Reliable and reproducible measurements
- Automatic self-calibration on start up
- Path length recalibration kit available as accessory

Experience the NanoVue Plus first hand.
Register for a trial at:

www.gelifesciences.com/tryNanoVuePlus

I ÄKTA I Amersham I Biacore I IN Cell Analysis I Whatman I GE Service I

imagination at work

EDITORIAL

NEWS OF THE WEEK

NEWS FOCUS

LETTERS

BOOKS *ET AL.*

POLICY FORUM

PERSPECTIVES

SCIENCE PRIZE ESSAY

CONTENTS continued >>

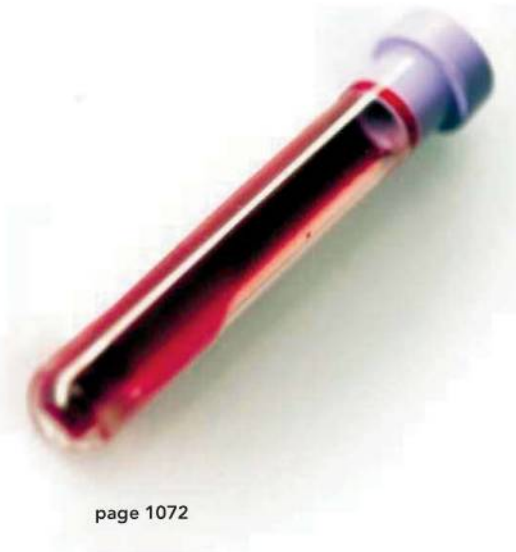

page 1072

pages 1091 & 1132

COVER

High-resolution (0.25 meters per pixel) hillshade map showing the topography of the San Andreas Fault in the Carrizo Plain of California. Two stream channels that bend at the fault have been displaced about 10 meters (lower right) by two earthquakes and 16 meters (upper left) by as many as five earthquakes, including the most recent earthquake in 1857. Blue indicates lower elevations. See pages 1117 and 1119.

Image: O. Zielke, J. R. Arrowsmith/Arizona State University; L. Grant Ludwig, S. O. Akçiz, G. R. Noriega/University of California, Irvine; topography data gathered by the B4 Project and processed by OpenTopography

DEPARTMENTS

Choose QIAGEN for detection

Detection platforms, assays, and analysis software by QIAGEN

Use QIAGEN® solutions from sample to result, and benefit from sensitive and reliable detection systems:

- **Quantitative, real-time PCR detection**
- **Automated analysis of DNA fragments and RNA**
- **Pyrosequencing® sequence-based DNA detection and quantification**
- **Optimized, ready-to-use assays and reagents**

Making improvements in life possible — www.qiagen.com

QIAGEN®

Sample & Assay Technologies

AUTODetect01105IWW

REVIEW

REPORTS

CONTENTS continued >>

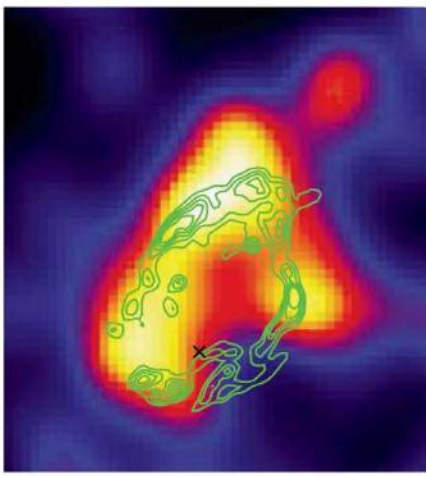

page 1103

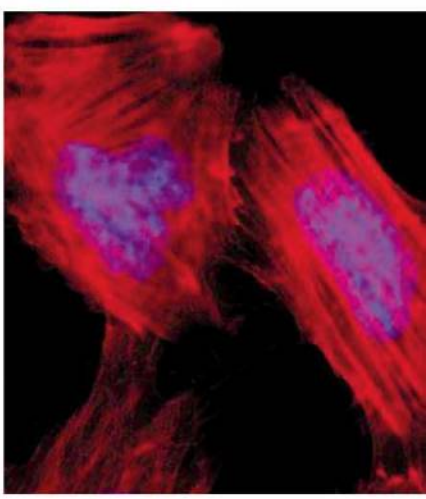

page 1139

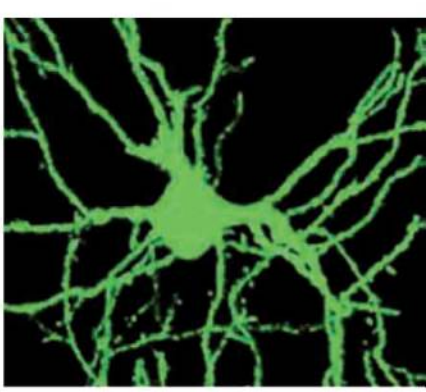

page 1145

abcam®

Bioactivity of human expressed proteins

Assays were conducted to compare the bioactivity of human expressed proteins and their non-human expressed counterparts such as *E.coli* expressed or other mammalian expressed proteins.

We do proteins too!

Over 8,000 proteins and peptides available, with 150 new products added every month. All supported by industry leading datasheets providing detailed application and technical data, just one click away!

Stay up-to-date on the latest developments with our human expressed proteins

- Optimal post-translational modifications
- Biological activity
- Fc chimera proteins offering advantages in dimerization

Visit **www.abcam.com/proteins** for more information

Abcam Inc.
1 Kendall Square, Ste 341
Cambridge, MA 02139-1517
USA

Tel: 1-617-225-2272
Toll free: 1-888-77-ABCAM
Toll free Fax: 1-866-739-9884

SCIENCEONLINE

SCIENCEXPRESS
www.sciencexpress.org

CKAMP44: A Brain-Specific Protein Attenuating Short-Term Synaptic Plasticity in the Dentate Gyrus
J. von Engelhardt et al.

A synaptic protein that regulates postsynaptic AMPA receptor responses has been cloned and functionally characterized.
10.1126/science.1184178

β_2-Adrenergic Receptor Redistribution in Heart Failure Changes cAMP Compartmentation
V. O. Nikolaev et al.

A change in the distribution of a signaling molecule on the surface of heart muscle cells may contribute to heart failure.
10.1126/science.1185988

Unicellular Cyanobacterial Distributions Broaden the Oceanic N_2 Fixation Domain
P. H. Moisander et al.

Nitrogen fixation in the South Pacific Ocean is partitioned among several microbe species with distinct ecophysiologies.
10.1126/science.1185468

Patterns of Diversity in Marine Phytoplankton
A. D. Barton et al.

Highest diversity occurs in physically dynamic mid-latitude zones; lowest diversity and highest biomass occur toward the poles.
10.1126/science.1184961

Constraints on the Formation Age of Cometary Material from the NASA Stardust Mission
J. E. P. Matzel et al.

Transport of inner solar system material to the Kuiper Belt and incorporation into comets took at least 2 million years.
10.1126/science.1184741

SCIENCENOW
www.sciencenow.org
Highlights From Our Daily News Coverage

Is a Dolphin a Person?

Dolphin intelligence poses tricky scientific and ethical questions.

Lack of Sleep Is Contagious

Sleep-deprived teens tend to have sleep-deprived friends and friends who use drugs.

The Mathematics of Clumpy Crime

Models may help police break up criminal hot spots.

SCIENCESIGNALING
www.sciencesignaling.org
The Signal Transduction Knowledge Environment

RESEARCH ARTICLE: Apoptotic Cells Activate the "Phoenix Rising" Pathway to Promote Wound Healing and Tissue Regeneration
F. Li et al.

PODCAST
C.-Y. Li and A. M. VanHook

Caspases in dying cells trigger the release of growth signals that promote tissue repair.

RESEARCH ARTICLE: DNA-PKcs Controls an Endosomal Signaling Pathway for a Proinflammatory Response by Natural Killer Cells
S. Rajagopalan et al.

Akt and DNA-dependent protein kinase are required for the activation of NF-κB by an endosomal receptor.

PERSPECTIVE: A New Role for RPTPσ in Spinal Cord Injury—Signaling Chondroitin Sulfate Proteoglycan Inhibition
Y. Duan and R. J. Giger

RPTPσ mediates the inhibitory effects of chondroitin sulfate proteoglycans on axonal growth.

PERSPECTIVE: ER Stress in Pancreatic β Cells—The Thin Red Line Between Adaptation and Failure
D. L. Eizirik and M. Cnop

The response of IRE1α to metabolic ER stress is modulated by its interaction with RACK1.

FUNDING SOURCES

Find grants and funding opportunities for research and training in cell signaling.

SCIENCECAREERS
www.sciencecareers.org/career_magazine
Free Career Resources for Scientists

Preparing for a Career in Venture Capital
E. Pain

Laia Crespo accumulated academic and business credentials to build a career in investment management.

For Physician-Scientist Couple, Success Is in Balance
K. Travis

Deepali Kumar and Atul Humar say their shared specialty helps them balance work and family life.

***Science* Careers Blog**
Science *Careers Staff*

Get frequent updates including advice, opinion, news, funding opportunities, and links to other online resources.

SCIENCETRANSLATIONAL MEDICINE
www.sciencetranslationalmedicine.org
Integrating Medicine and Science

RESEARCH ARTICLE: Development of Personalized Tumor Biomarkers Using Massively Parallel Sequencing
R. J. Leary et al.

PERSPECTIVE: Cancer Sequencing Gets a Little More Personal
L. Prokunina-Olsson and S. J. Chanock

Technology to detect personal genetic aberrations in cancer cells moves closer to the clinic.

RESEARCH ARTICLE: Adipocyte-Derived Factors Potentiate Nutrient-Induced Production of Plasminogen Activator Inhibitor-1 by Macrophages
P. Kishore et al.

PERSPECTIVE: Adipose Tissue Macrophages—A Piece of the PAI of Metabolic Syndrome
C. N. Lumeng

Macrophages within fat tissue release a hormone that contributes to atherosclerosis and insulin resistance.

SCIENCEPODCAST
www.sciencemag.org/multimedia/podcast
Free Weekly Show

Download the 26 February *Science* Podcast to hear about tracking circulating tumor cells, converting a biomass-derived compound into hydrocarbon fuel, your letters to *Science*, and more.

SCIENCEINSIDER
blogs.sciencemag.org/scienceinsider
Science Policy News and Analysis

SCIENCE (ISSN 0036-8075) is published weekly on Friday, except the last week in December, by the American Association for the Advancement of Science, 1200 New York Avenue, NW, Washington, DC 20005. Periodicals Mail postage (publication No. 484460) paid at Washington, DC, and additional mailing offices. Domestic individual membership and subscription (51 issues): $146 ($74 allocated to subscription). Domestic institutional subscription (51 issues): $910; Foreign postage extra: Mexico, Caribbean (surface mail) $55; other countries (air assist delivery) $85. First class, airmail, student, and emeritus rates on request. Canadian rates with GST available upon request, GST #1254 88122. Publications Mail Agreement Number 1069624. **Printed in the U.S.A.**

Change of address: Allow 4 weeks, giving old and new addresses and 8-digit account number. **Postmaster:** Send change of address to AAAS, P.O. Box 96178, Washington, DC 20090–6178. **Single-copy sales:** $10.00 current issue, $15.00 back issue prepaid includes surface postage; bulk rates on request. The identification code for *Science* is 0036-8075. *Science* is indexed in the *Reader's Guide to Periodical Literature* and in several specialized indexes.

AAAS
ADVANCING SCIENCE, SERVING SOCIETY

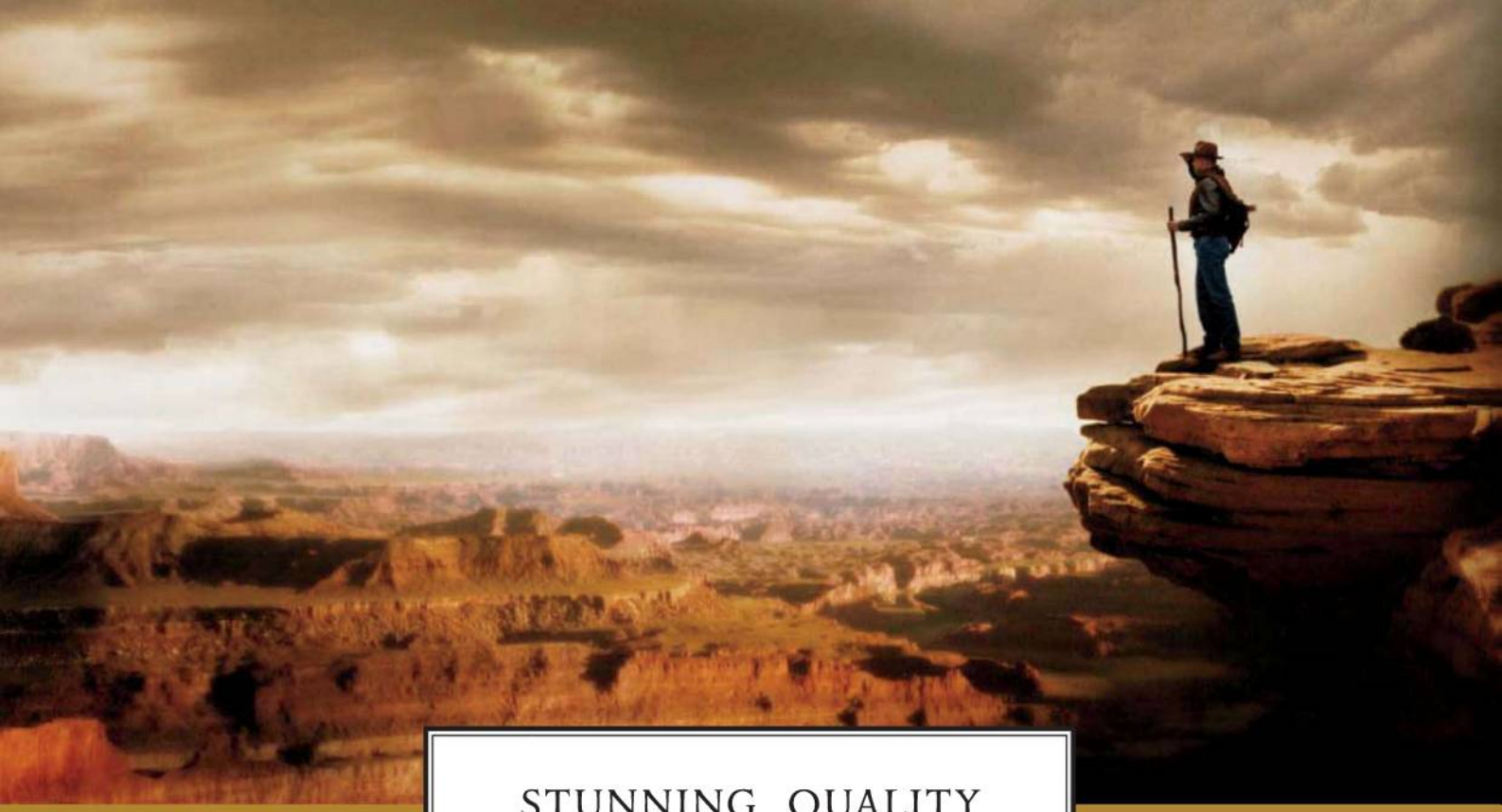

STUNNING QUALITY

Reagents for Sample Preparation from New England Biolabs

Introducing NEBNext™, a series of highly pure reagents that facilitate sample preparation for downstream applications such as next generation sequencing and expression library construction. Available in sets, master mixes and modules, these robust reagents undergo stringent quality controls and functional validation, ensuring maximum yield, convenience and value.

Sequencing coverage map of the *E. coli* genome after using NEBNext™ DNA Sample Prep Reagent Set 1 for Sample Preparation

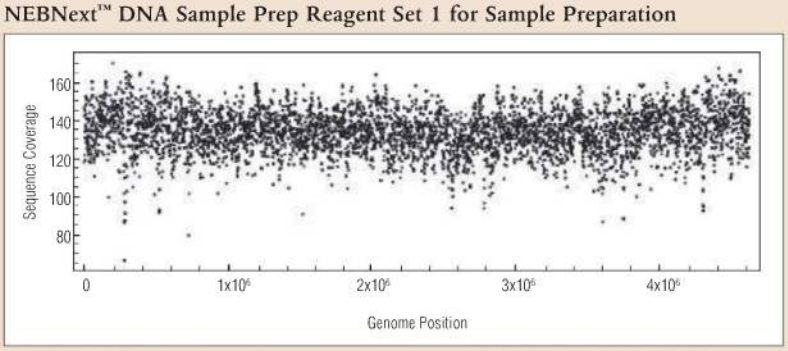

E. coli strain MG1655 gDNA was prepared with NEBNext DNA Sample Prep Reagent Set I and sequenced on an Illumina Genome Analyzer II.

For more information about NEBNext, including customized solutions, please contact NEBNext@neb.com.

Now available:
NEBNext™ dsDNA Fragmentase™
an enzyme-based solution for the fragmentation of DNA

CELEBRATING 35 YEARS

NEW ENGLAND BioLabs® Inc.
enabling technologies in the life sciences

CLONING & MAPPING	**DNA AMPLIFICATION & PCR**	RNA ANALYSIS	PROTEIN EXPRESSION & ANALYSIS	GENE EXPRESSION & CELLULAR ANALYSIS

www.neb.com

EDITED BY CAROLINE ASH

Difference, Not Diversity

In tropical forests, as in the ocean plankton, thousands of species may compete for the same resources. How they succeed in coexisting remains one of the central paradoxes in the study of biodiversity. Theory shows that coexisting species must partition the environment, but such partitioning is not obvious. Using data from coexisting forest trees in the southeastern United States, **Clark** (p. 1129) show that individual variation between members of the same species allows them to avoid direct competition: One plant may differ significantly from another in its requirements for light, nutrients, or moisture, yet remain within the general spectrum of features displayed by its conspecifics.

Critical Mediators

Helper T cells are the immune system's ringmasters, having a multiplicity of functions that mediate the body's immune responses to infections. Depending on the type of infection, $CD4^+$ helper T cells respond by secreting specific patterns of cytokines, which provide important cues to other subsets of immune cells. $CD4^+$ T cells with distinct cytokine profiles have been viewed classically as separate lineages; however, there is mounting evidence that these cells may not be terminally differentiated but are in fact quite plastic. **O'Shea and Paul** (p. 1098) review the current understanding of $CD4^+$ T cell subset differentiation and the underlying mechanisms that drive cell-lineage commitment.

Slip, Tripped, and Faulted

Earthquake risk assessment can be improved if we were able to quantify the recurrence and magnitude of slip events. Until recently though, a lack of sophisticated seismometers has forced us to rely on anecdotal evidence from those who survived major earthquakes or to look for clues in the landscape. **Zielke *et al.*** (p. 1119, published online 21 January; see the Perspective by **Scharer**) analyzed high-resolution images of the San Andreas Fault in southern California. The data showed that major surface ruptures, such as the 1857 Fort Tejon earthquake, resulted from slips of only about 5 meters; much less than previously thought. In a study that lends support to this discovery, **Grant Ludwig *et al.*** (p. 1117, published online 21 January; see the Perspective by **Scharer**) suggest from analysis of the geomorphic features of this region that several smaller earthquakes have occurred during recent centuries rather than infrequent but larger movements. The Perspective by **Scharer** (p. 1089) discusses how paleoseismological studies like these may be valuable for feeding data into earthquake prediction.

CREDITS (TOP TO BOTTOM): JAMES S. CLARK; GARCIA ET AL.

Lactic Fuels

In the quest to find sustainable alternatives to petrochemicals, a small cyclic ester, γ-valerolactone, derived from cellulose offers promising raw material. **Bond *et al.*** (p. 1110) show that carbon dioxide can be catalytically excised from the lactone efficiently at high pressure, leaving a mixture of butanes. In a second-stage reactor, the butanes can be strung together to form heavier hydrocarbons similar to those found in automotive and jet fuels. The method simultaneously yields fuel and a relatively pure stream of pressurized carbon dioxide amenable to sequestration or further chemical modification.

Cations in the Veins

Major events in Earth's history, from climate change to tectonic activity, can be revealed by reconstructing past conditions of the oceans. Clues from ancient ocean chemistry can be found in the cation content of fossilized microorganisms, marine carbonates, or salt deposits from old coastal zones. As these proxies are prone to inconsistencies between samples and methodologies, **Coggon *et al.*** (p. 1114, published online 4 February; see the Perspective by **Elderfield**) estimated past seawater composition from the geochemistry of resistant carbonate veins precipitated within fresh basalts on the sea floor. The sudden rise to modern-day levels of ocean magnesium:calcium and strontium:calcium ratios occurred about 24 million years ago, and can be explained by a decrease in seafloor hydrothermal activity combined with a decrease in river discharge.

Spin into Control

Spintronics—the use of the spin direction of subatomic particles to control on and off states, instead of electric charge—has the potential to create low-power electronics, because less energy is needed to flip spin states than to flip switches to create voltage barriers. Theoretical work hints that spin-polarized electrons from a ferromagnetic electrode can be controlled by a change in polarization created in a ferroelectric thin film. **Garcia *et al.*** (p. 1106, published online 14 January) fabricated an iron-barium titanate junction on a lanthanum strontium manganate substrate that acts as a spin detector. Local control of spin polarization was observed in the ferroelectric layer, which retained its polarization without any applied power.

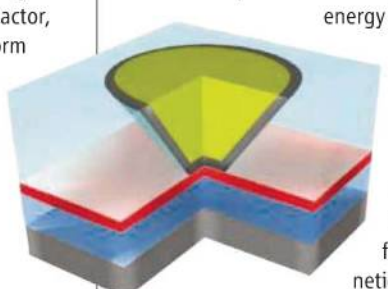

Continued on page 1057

Imagine not being able to recognize your best friend.

Today millions of people with Alzheimer's can no longer remember the ones they love. That number is expected to increase dramatically over the next 20 years. And it's one more reason MetLife Foundation continues to support research to find a cure. This year the Foundation honors the outstanding work of Todd E. Golde, MD, PhD, University of Florida, Gainesville, Edward H. Koo, MD, University of California, San Diego, Eckhard Mandelkow, PhD, and Eva-Maria Mandelkow, MD, PhD, Max-Planck-Institute for Structural Molecular Biology, Hamburg, Germany, with the MetLife Foundation Award for Medical Research.

MetLife Foundation
A leader in finding an Alzheimer's cure

Continued from page 1055

Recombinant Infectious Prions

Prion diseases are a group of fatal neurodegenerative disorders that include Creutzfeldt-Jakob disease in humans and bovine spongiform encephalopathy in cows. The prion hypothesis states that the infectious agent of these diseases is an aberrant conformational isoform of the normal prion protein (PrP^C), a glycosylphosphatidylinositol-anchored cell surface protein enriched in the central nervous system. The final proof for the prion hypothesis is to convert bacterially expressed recombinant PrP into an infectious prion, but this has been difficult to achieve. **F. Wang *et al.*** (p. 1132, published online 28 January; see the Perspective by **Supattapone**) put recombinant PrP purified from bacteria into mice and obtained all the characteristics of the infectious agent in prion disease. The recombinant form is not only resistant to proteinase-K, but also shows infectivity in cultured cells and causes rapid disease progression in wild-type mice, yielding both the behavioral and the neuropathological symptoms.

Tripartite Toxin

Luminescent bacterial symbionts of nematode worms that attack insects have long stirred interest in their possibilities for biological control. The bacteria produce a family of toxins composed of at least three subunits that resemble a widely occurring class of bacterial toxins also produced by human pathogens. **Lang *et al.*** (p. 1139) have elucidated the mode of action and structural interactions of some of these tripartite protein toxins and found that they poison the cell's actin cytoskeleton by catalyzing unusual reactions. One toxin mediated adenosine diphosphate (ADP)–ribosylation at threonine-148 to cause actin polymerization, another ADP-ribosylated Rho protein at glutamine-63, and both synergized to cause actin clustering and cell paralysis.

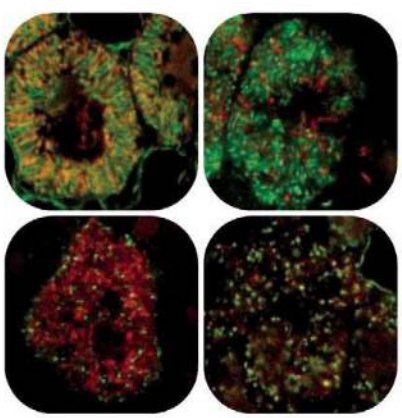

CREDIT: VAN DE VELDE ET AL.

Legume Symbiosome

Leguminous plants (peas and beans) are major players in global nitrogen cycling by virtue of their symbioses with nitrogen-fixing bacteria that are harbored in specialized structures, called nodules, on the plant's roots. **Van de Velde *et al.*** (p. 1122) show that the host plant, *Medicago truncatula* produces nodule-specific cysteine-rich peptides, resembling natural plant defense peptides. The peptides enter the bacterial cells and promote its development into the mature symbiont. In a complementary study, **D. Wang *et al.*** (p. 1126), have identified the signal peptidase, also encoded by the plant, that is required for processing these specialized peptides into their active form.

Bursty, Infrequent Noise

In gene regulatory networks, positive feedback loops can give rise to bistability and hysteresis in gene expression, thereby allowing switching mechanisms and memory effects. **To and Maheshri** (p. 1142; see the Perspective by **Levens and Gupta**) eschew the commonly held idea that sigmoidal promoter responses are required to achieve a steady-state bimodal response in a positive feedback loop. Instead, using a model and data from an experiment, they favor noisy gene expression and multiple, noncooperative transcription factor binding as an explanation for the bimodal response, and they expect that similar noisy systems are widespread in biology.

Inflexible Timing for Flexibility

During critical periods in early life, sensory experience molds circuits in the brain. In the visual cortex, blurring or occluding vision in one eye triggers a rapid reorganization of neuronal responses known as ocular dominance plasticity. The critical period for this plasticity depends on inhibitory neurotransmission. **Southwell *et al.*** (p. 1145) show that by transplanting embryonic precursors of inhibitory neurons into mice, a period of ocular dominance plasticity can be induced after the end of the normal critical period. These observations suggest that transplantation of inhibitory neurons has therapeutic potential for brain repair and for treating neurological disorders and inducing periods of brain plasticity.

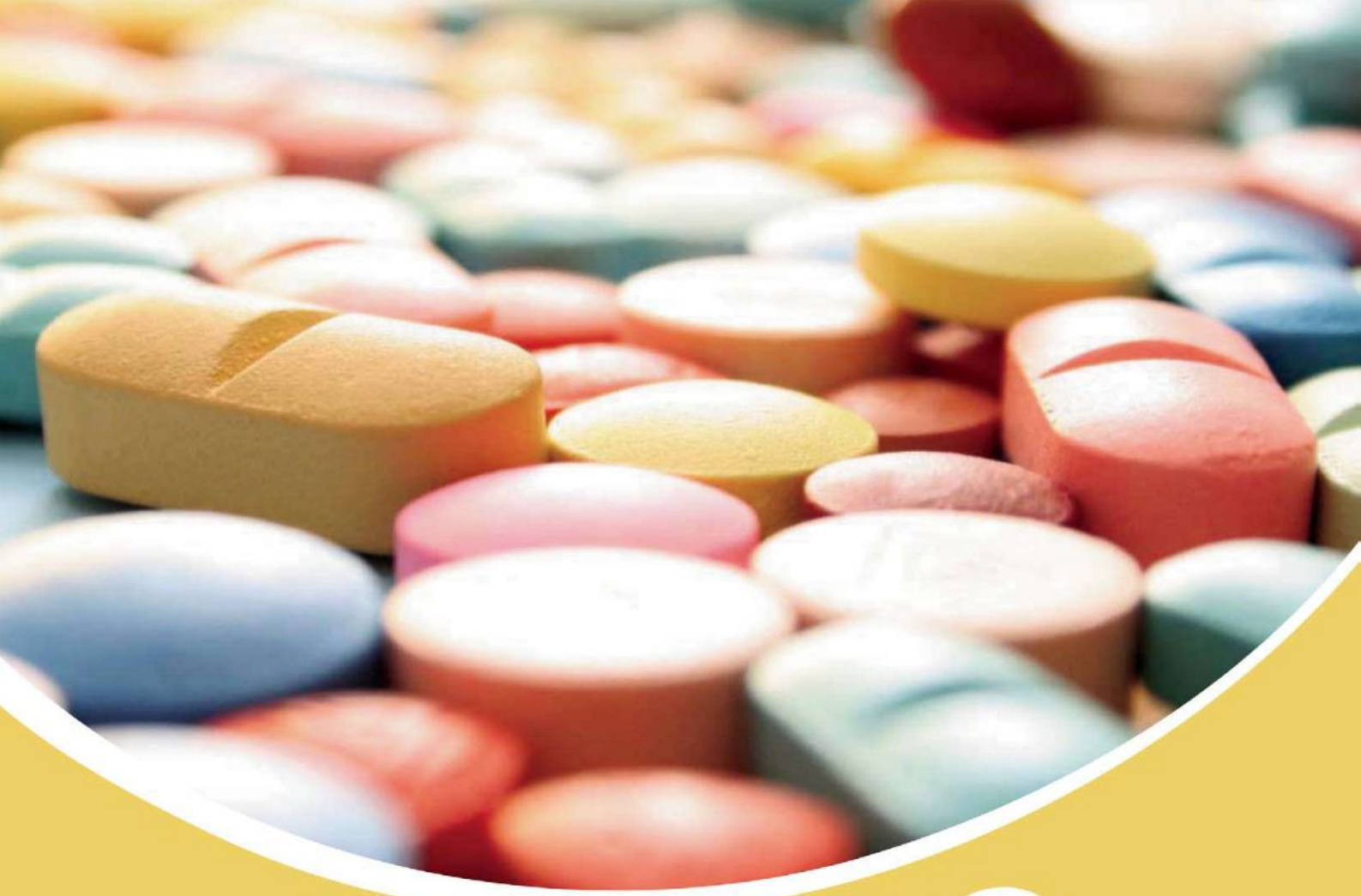

The smarter the mouse the quicker the drug gets to market.

From disease models that facilitate target identification, to humanized models that test the safety and efficacy of potential therapeutics, Taconic's "smart" mice play a pivotal role in speeding new drugs to market.

Taconic's rapidly expanding portfolio of fully licensed, off-the-shelf ADME-Tox transgenic models, as well as transgenic models for short term carcinogenicity testing provide valuable insights into how your drug will behave in humans.

Taconic introduces another breakthrough in *in vivo* compound testing with its new transADMET program. Developed in conjunction with CXR Biosciences, transADMET is transforming the discovery process by better predicting ADMET in humans. New humanized models are available now.

To learn how Taconic's "smart mice" can accelerate your research and help speed a drug to market, visit our website, **www.taconic.com/SOT**

Taconic
Smart Solutions To Improve Human Health

Timothy J. DeVoogd is a professor in the Department of Psychology and Field of Neurobiology and Behavior at Cornell University in Ithaca, NY. E-mail: tjd5@cornell.edu.

Science to Bridge the Americas

IT IS BROADLY RECOGNIZED ACROSS THE WESTERN HEMISPHERE THAT SCIENCE CAN PROVIDE ANSWERS to health and environmental problems and stimulate national development. But in a given region, scientists often face overwhelming barriers to conducting research, and there is far too little interaction among academia, industry, and government on an international level to effect change. Scientists in developing regions have repeatedly raised ways in which help from the United States could be transformational. It is now time to do more.

There are well-established U.S. academic and government programs that explore links between science and diplomacy and focus on forging robust scientific communities. For example, each year, the Jefferson Science Fellowship of the U.S. National Academies, in which I participated last year, selects up to 10 senior scientists across disciplines to work with the U.S. State Department or the U.S. Agency for International Development (USAID).* As a Jefferson Fellow, I traveled to universities, research institutes, and government agencies, seeking to enhance connections with foreign scientists. From my discussions with scientists and administrators across 12 countries in Latin America, several ideas repeatedly emerged for meeting the challenges ahead in health and environmental arenas, among others.

With minimal additional resources, the United States could bolster such interactions. For example, the U.S. Fulbright program, which supports about 7000 new grants each year for students, researchers, educators, and other professionals across disciplines, could make training in the sciences a larger proportion of its mandate. This program could provide financial support to aid each foreign scientist's return to his or her home country. Mexico provides this type of reentry support through CONACYT, but trainees in the United States who come from less-developed countries are likely to require U.S. funds for this purpose.

A dedicated program that supports visits of foreign scientists to a U.S. lab for as little as 1 to 2 months could also have a huge impact on science in Latin America. Participants could learn new approaches to a research question and become part of a larger research network. To encourage scientists who are trained abroad to return to positions at home, prolonged collaborations are also needed. Undertaking joint research projects in Latin America is difficult—funding is limited (U.S. agencies often restrict foreign expenditures), and grant deadlines for partners can be incompatible. To support such projects, a fund could be created with contributions from the science agencies of the participating countries; for less-developed countries, funds could also come from USAID.

Finally, many faculty members in Latin America would like to earn a Ph.D. in the United States but cannot leave family and job for long periods. U.S. universities could develop short intensive courses, Internet distance learning, and creative research programs to support the pursuit of an advanced degree. And with help from U.S. embassy staff in making arrangements, U.S. scientists visiting the Caribbean or Latin America for research or vacation could volunteer to spend time at a university, presenting their research and meeting with faculty and students.

Most countries in the Western Hemisphere have democratic governments and are eager for enhanced scientific interaction with the United States. Moreover, the U.S. State Department recognizes that "science diplomacy" in general is a powerful adjunct to other forms of international action. Supporting such efforts achieves the diplomatic goals of fostering mutual understanding while building human networks that link the United States with other countries. The cost is trivial compared to that of other forms of "hard diplomacy." The potential for scientific and societal payoffs is immense, as a better-linked scientific community will speed progress in responding to major problems that affect us all: health, energy, climate change, and preserving biodiversity. And even more importantly, programs that support international science broadly will position humanity to understand and meet the challenges yet to come.

– Timothy J. DeVoogd

10.1126/science.1183562

*http://sites.nationalacademies.org/pga/jefferson.

ECOLOGY

A Quick Sniff and She's Off

Insects often use their sense of smell to locate food; some carry disease-causing pathogens, and in general, being infected makes an organism smell more strongly. Several pathogens have evolved to exploit these odor-tracking behaviors to entrain their life cycles in advantageous ways. Mauck *et al.* show that infection by cucumber mosaic virus increases the amount of aphid-attracting volatiles emitted by their plant hosts. Despite the delectable odors, virus infection makes the host plant less palatable, and consequently the aphids don't feed for long. For cucumber mosaic virus, fickle visitors are not a problem because it happens to be a nonpersistent virus—one sip of infected sap is enough to imbibe an infectious dose. The repellent host hastens the vector's departure and the transmission of the virus to a new host. In contrast, persistent viruses, such as barley yellow dwarf virus, induce both sweet odors and juicy fruit, which encourage their aphid vectors to prolong their visits. This allows the virus to complete a lengthy replicative cycle within the insect, after which onward transmission occurs. — CA

Proc. Natl. Acad. Sci. U.S.A. **107**, 10.1073/pnas.0907191107 (2010).

GEOPHYSICS

Seismic Spinning

Some boundary layers in Earth's interior (including the crust/mantle and core/mantle boundaries) are often identified by sharp seismic discontinuities, whereas finer-scale interlayer structures require constraints from geochemistry and mineral physics to complement less obvious, or sometimes completely absent, seismological signals. For example, because some mantle minerals gradually change in structure or chemical composition with depth (and the associated pressure and temperature shifts), seismic velocities from these regions also vary along a gradient. Based on recent elasticity measurements of the abundant lower mantle mineral ferropericlase, Cammarano *et al.* computed seismic models that identify one such broad chemical or thermal gradient in the mid–lower mantle. The presence of this transition, which accounts for the preferential stability of high spin states of ferrous iron (Fe^{2+}) in ferropericlase, suggests that the viscosity and thermal conductivity of the mid-mantle may be different than previously thought. Specifically, recycled crustal material driven down into the mantle by subduction zones could flatten or broaden at this depth, which would affect the extent and dynamics of mantle mixing throughout Earth history. — NW

Geophys. Res. Lett. **37**, L03308 (2010).

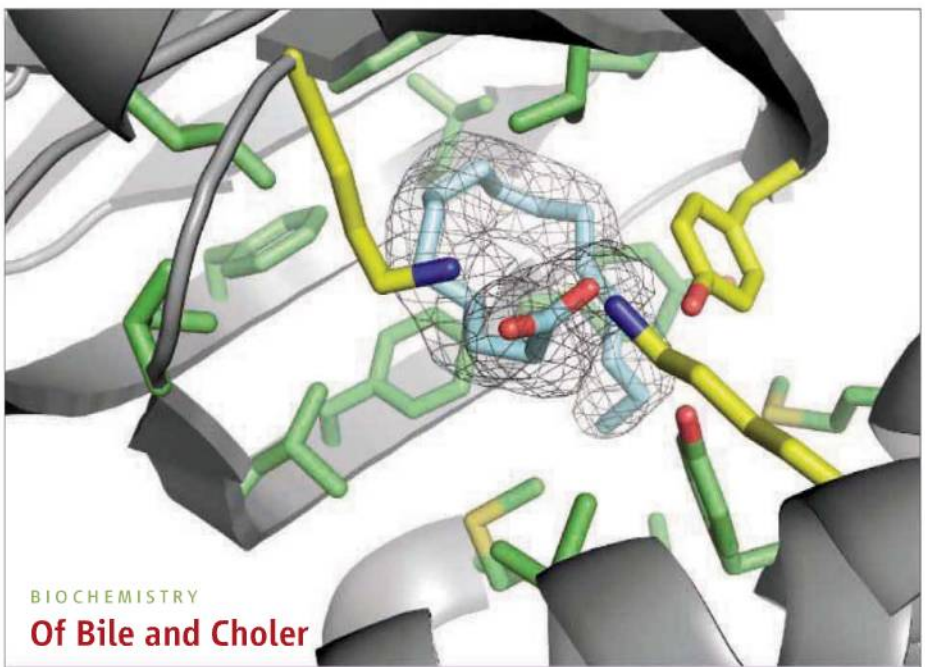

BIOCHEMISTRY

Of Bile and Choler

Vibrio cholerae is the Gram-negative bacterium that causes cholera, a disease that afflicts multitudes of people who lack access to a source of disinfected drinking water. When the bacterium enters the host's intestine, the master virulence regulator ToxT activates the expression of other virulence factors and cholera toxin. ToxT is a member of the AraC family of transcription factors; some of these regulate carbon metabolism (AraC) as dimers, whereas the stress response regulators (SoxS, Rob, and MarA) act as monomers. The promoters to which ToxT binds can be found singly and as inverted repeats. Lowden *et al.* have solved the ToxT crystal structure. It has an N-terminal regulatory domain and a C-terminal DNA binding domain that shares structural features with AraC, MarA, and Rob. ToxT is a monomer in the crystal, but helix α3 is analogous to the helix that mediates coiled-coil dimerization in AraC. The N-terminal domain contains a hydrophobic pocket that in the crystal is occupied by *cis*-palmitoleate (slate blue), and the activity of ToxT is known to be inhibited by components of bile. Palmitoleate binds to a lysine residue in the C-terminal domain and locks ToxT into a closed conformation that is not oriented to bind DNA and would also prevent dimerization. This conformation probably occurs in the lumen of the intestine where bile acids are present, yet in the mucus of the intestine, ToxT might be able to reorient into a conformation that can bind DNA and dimerize. — VV

Proc. Natl. Acad. Sci. U.S.A. **107**, 2860 (2010).

CHEMISTRY

Order at a Distance

The classic view of crystallization is the addition of atoms, colloids, or other small segments to a growing ordered crystal, where anisotropies in the growth are caused by differences in the thermodynamic or kinetic influences at different crystal faces. For some systems, such as metal oxides, nanocrystals are believed to form ordered aggregates through a fusion process. It has been proposed that these

CREDITS (TOP TO BOTTOM): LOWDEN *ET AL.*, *PROC. NATL. ACAD. SCI. U.S.A.* **107**, 10.1073/PNAS.0915021107 (2010); (PHOTO) PHOTOS.COM

primary crystals form a crystallographically aligned aggregate, even though each crystal unit is separated from the other by solvent. Yuwono *et al.* observe this process in the slow growth of crystals in solutions of ferrihydrite nanoparticles, using cryogenic transmission electron microscopy to preserve the structure of the sample at various ages. They observe the slow aggregation of primary crystals, with the formation of rodlike assemblies, which they speculate are composed of oriented goethite nanocrystals. They also note occasional twinned aggregates in which the angle at the junction matches that observed in a twinned goethite crystal. Under the beam intensity required for high-resolution imaging, the water between the crystals sublimes and the authors are able to see the crystallographic alignment of each of the primary units. — MSL

J. Am. Chem. Soc. **132**, 10.1021/ja909769a (2010).

IMMUNOLOGY

A Protective Shell

Originally carried primarily by forest mosquitoes living between the Tropics of Cancer and Capricorn, Chikungunya virus has become a growing public health threat in Africa, Asia, and parts of Europe. Infection is followed by fever, headache, and nausea and then by debilitating peripheral joint pain that can persist for months or even years. This alphavirus has adapted to urban vectors, such as the Asian tiger mosquito *Aedes albopictus*, which enhances its potential to spread worldwide. Akahata *et al.* describe the development of a protective vaccine by expressing the Chikungunya virus structural proteins in eukaryotic cells and purifying the resultant virus-like particles, which resemble the virus structurally but lack the encapsulated genomic RNA necessary for replication. Immunization of rhesus monkeys with the viruslike particles protected them against subsequent challenge with live virus, and the protective effect was shown to be mediated by the vaccine-induced humoral immune response (IgG). Previous attempts at making vaccines for Chikungunya virus have shown limited efficacy; hence these findings offer a step forward in the development of a protective vaccine for humans. — KLM

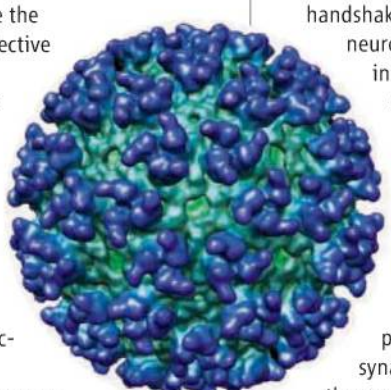

CREDIT: AKAHATA *ET AL.*, *NAT. MED.* **16**, 10.1038/NM.2105 (2010)

Nat. Med. **16**, 10.1038/nm.2105 (2010).

MATERIALS SCIENCE

Cations Minding the Gap

The band gap of a material—the energy threshold for excitation of electrons and thus the major determinant of properties ranging from color to conductivity—is usually set by the crystal structure of the constituent atoms or ions. It could prove useful for a variety of applications to be able to vary band gaps associated with a particular type of bulk framework in a systematic way, much as it is currently possible to do at the nanometer scale by tuning the size of dispersed individual particles. Qian *et al.* studied the assembly of the arsenic-based Zintl cluster As_7^{3-} with various cations and examined the effects of change transfer between cation and anion. The cations included Cs^+, cryptand-sequestered K^+ and Rb^+, and Au^+. The band gap, as determined from optical measurements, could be varied from 1.1 to 2.1 electron volts. Density functional calculations revealed that the changes mainly arose from variation in the positions of the lowest unoccupied orbitals, principally affected by the cations, although some changes were associated with charge transfer induced by the cations that led to covalent links between the clusters. — PDS

ACS Nano **4**, 235 (2010).

NEUROSCIENCE

Signal Effectors

Neurons convey information in part by transmission of small molecules such as γ-aminobutyric acid (GABA) across gaps termed synapses. The handshake between pre- and postsynaptic neurons that allows synapses to develop in the central nervous system is bolstered by surrounding astrocytes. Studying hippocampal neurons and astrocytes from embryonic rats, Hughes *et al.* show that the signals used by astrocytes to promote GABAergic (inhibitory) neuron development are different than those already shown to promote glutamatergic (excitatory) synapses. These signals encourage the growth of axons, but not dendrites, of the GABAergic neurons and seem not to affect the neurite length of glutamatergic neurons. Both the number and the density of synapses in GABAergic neurons are pumped up by signals from astrocytes. Although some potential mediating factors, such as the thrombospondins, have been excluded in this work, the relevant signaling proteins secreted by these astrocytes remain at the moment incognito. — PJH

Mol. Cell. Neurosci. **43**, 136 (2010).

www.sciencemag.org

Science

1200 New York Avenue, NW
Washington, DC 20005
Editorial: 202-326-6550, FAX 202-289-7562
News: 202-326-6581, FAX 202-371-9227
Bateman House, 82-88 Hills Road
Cambridge, UK CB2 1LQ
+44 (0) 1223 326500, FAX +44 (0) 1223 326501

Subscription Services For change of address, missing issues, new orders and renewals, and payment questions: 866-434-AAAS (2227) or 202-326-6417, FAX 202-842-1065. Mailing addresses: AAAS, P.O. Box 96178, Washington, DC 20090-6178 or AAAS Member Services, 1200 New York Avenue, NW, Washington, DC 20005

Institutional Site Licenses please call 202-326-6755 for any questions or information

Reprints: Author Inquiries 800-635-7181
Commercial Inquiries 803-359-4578

Permissions 202-326-7074, FAX 202-682-0816

Member Benefits AAAS/Barnes&Noble.com bookstore www.aaas.org/bn; AAAS Online Store www.apisource.com/aaas/ code MKB6; AAAS Travels: Betchart Expeditions 800-252-4910; Apple Store www.apple.com/eppstore/aaas; Bank of America MasterCard 1-800-833-6262 priority code FAA3YU; Cold Spring Harbor Laboratory Press Publications www.cshlpress.com/affiliates/aaas.htm; GEICO Auto Insurance www.geico.com/landingpage/go51.htm?logo=17624; Hertz 800-654-2200 CDP#343457; Office Depot https://bsd.officedepot.com/portalLogin.do; Seabury & Smith Life Insurance 800-424-9883; Subaru VIP Program 202-326-6417; VIP Moving Services www.vipmayflower.com/domestic/index.html; Other Benefits: AAAS Member Services 202-326-6417 or www.aaasmember.org.

science_editors@aaas.org	(for general editorial queries)
science_letters@aaas.org	(for queries about letters)
science_reviews@aaas.org	(for returning manuscript reviews)
science_bookrevs@aaas.org	(for book review queries)

Published by the American Association for the Advancement of Science (AAAS), *Science* serves its readers as a forum for the presentation and discussion of important issues related to the advancement of science, including the presentation of minority or conflicting points of view, rather than by publishing only material on which a consensus has been reached. Accordingly, all articles published in *Science*—including editorials, news and comment, and book reviews—are signed and reflect the individual views of the authors and not official points of view adopted by AAAS or the institutions with which the authors are affiliated.

AAAS was founded in 1848 and incorporated in 1874. Its mission is to advance science, engineering, and innovation throughout the world for the benefit of all people. The goals of the association are to: enhance communication among scientists, engineers, and the public; promote and defend the integrity of science and its use; strengthen support for the science and technology enterprise; provide a voice for science on societal issues; promote the responsible use of science in public policy; strengthen and diversify the science and technology workforce; foster education in science and technology for everyone; increase public engagement with science and technology; and advance international cooperation in science.

Information for Authors
See pages 352 and 353 of the 15 January 2010 issue or access www.sciencemag.org/about/authors

EDITOR-IN-CHIEF **Bruce Alberts**
EXECUTIVE EDITOR **Monica M. Bradford**
NEWS EDITOR **Colin Norman**
MANAGING EDITOR, RESEARCH JOURNALS **Katrina L. Kelner**
DEPUTY EDITORS **R. Brooks Hanson, Barbara R. Jasny, Andrew M. Sugden**

Editorial senior editors/commentary Lisa D. Chong, Brad Wible; **senior editors** Gilbert J. Chin, Pamela J. Hines, Paula A. Kiberstis (Boston), Marc S. Lavine (Toronto), Beverly A. Purnell, L. Bryan Ray, Guy Riddihough, H. Jesse Smith, Phillip D. Szuromi (Tennessee), Valda Vinson, Jake S. Yeston; **associate editors** Kristen L. Mueller, Jelena Stajic, Nicholas S. Wigginton, Laura M. Zahn; **research associate** Alexis Wynne Mogul; **online editor** Stewart Wills; **associate online editors** Robert Frederick, Tara S. Marathe; **web content developers** Martyn Green, Andrew Whitesell; **book review editor** Sherman J. Suter; **associate letters editor** Jennifer Sills; **editorial manager** Cara Tate; **senior copy editors** Jeffrey E. Cook, Cynthia Howe, Harry Jach, Barbara P. Ordway, Trista Wagoner; **copy editors** Chris Filiatreau, Lauren Kmec; **editorial coordinators** Carolyn Kyle, Beverly Shields; **publications assistants** Ramatoulaye Diop, Joi S. Granger, Jeffrey Hearn, Lisa Johnson, Scott Miller, Jerry Richardson, Jennifer A. Seibert, Brian White, Anita Wynn; **editorial assistants** Emily Guise, Michael Hicks, Patricia M. Moore, Miriam Weinberg; **executive assistant** Sylvia S. Kihara; **administrative support** Maryrose Madrid; **editorial fellow** Melissa R. McCartney

News deputy news editors Robert Coontz, Eliot Marshall, Jeffrey Mervis, Leslie Roberts; **contributing editors** Elizabeth Culotta, Polly Shulman; **news writers** Yudhijit Bhattacharjee, Adrian Cho, Jennifer Couzin, David Grimm, Constance Holden, Jocelyn Kaiser, Sam Kean, Richard A. Kerr, Eli Kintisch, Greg Miller, Elizabeth Pennisi, Robert F. Service (Pacific NW), Erik Stokstad, Jue Wang; **intern** Lauren Schenkman; **contributing correspondents** Jon Cohen (San Diego, CA), Daniel Ferber, Ann Gibbons, Robert Koenig, Andrew Lawler, Mitch Leslie, Charles C. Mann, Virginia Morell, Gary Taubes; **copy editors** Linda B. Felaco, Melvin Gatling, Melissa Raimondi; **administrative support** Scherraine Mack; **bureaus** San Diego, CA: 760-942-3252, FAX 760-942-4979; Pacific Northwest: 503-963-1940

Production director James Landry; **senior manager** Wendy K. Shank; **assistant manager** Rebecca Doshi; **senior specialists** Steve Forrester, Chris Redwood; **specialist** Anthony Rosen; **Preflight director** David M. Tompkins; **manager** Marcus Spiegler; **specialist** Jason Hillman

Art director Yael Kats; **associate art director** Laura Creveling; **senior illustrators** Chris Bickel, Katharine Sutliff; **illustrator** Yana Greenman; **senior art associates** Holly Bishop, Preston Huey, Nayomi Kevitiyagala; **art associate** Matthew Twombly; **photo editor** Leslie Blizard

***Science* International**

Europe (science@science-int.co.uk) **editorial: international managing editor** Andrew M. Sugden; **senior editor/commentary** Julia Fahrenkamp-Uppenbrink; **senior editors** Caroline Ash, Stella M. Hurtley, Ian S. Osborne, Peter Stern; **associate editor** Maria Cruz; **locum editor** Helen Pickersgill; **editorial support** Deborah Dennison, Rachel Roberts, Alice Whaley; **administrative support** John Cannell, Janet Clements, Louise Moore; **news: europe news editor** John Travis; **deputy news editor** Daniel Clery; **contributing correspondents** Michael Balter (Paris), John Bohannon (Vienna), Martin Enserink (Amsterdam and Paris), Gretchen Vogel (Berlin); **intern** Tim Wogan

Latin America contributing correspondent Antonio Regalado

Asia Japan Office: Asca Corporation, Tomoko Furusawa, Rustic Bldg. 7F, 77 Tenjin-cho, Shinjuku-ku, Tokyo 162-0808, Japan; +81 3 6802 4616, FAX +81 3 6802 4615, inquiry@sciencemag.jp; **asia news editor** Richard Stone (Beijing: rstone@aaas.org); **contributing correspondents** Dennis Normile [Japan: +81 (0) 3 3391 0630, FAX +81 (0) 3 5936 3531; dnormile@gol.com]; Hao Xin [China: +86 (0) 10 6307 4439 or 6307 3676, FAX +86 (0) 10 6307 4358; cindyhao@gmail.com]; Pallava Bagla [South Asia: +91 (0) 11 2271 2896; pbagla@vsnl.com]

EXECUTIVE PUBLISHER **Alan I. Leshner**
PUBLISHER **Beth Rosner**

Fulfillment Systems and Operations (membership@aaas.org); **director** Waylon Butler; **senior systems analyst** Nomuna Nyamaa; **customer service supervisor** Pat Butler; **specialists** Latoya Casteel, LaVonda Crawford, Vicki Linton, April Marshall; **data entry supervisor** Cynthia Johnson; **specialists** Shirlene Hall, Tarrika Hill, William Jones

Business Operations and Administration director Deborah Rivera-Wienhold; **assistant director, business operations** Randy Yi; **manager, business analysis** Eric Knott; **manager, business operations** Jessica Tierney; **financial analysts** Priti Pamnani, Celeste Troxler; **rights and permissions: administrator** Emilie David; **associate** Elizabeth Sandler; **marketing director** Ian King; **marketing managers** Allison Pritchard, Alison Chandler, Julianne Wielga; **marketing associates** Aimee Aponte, Mary Ellen Crowley, Wendy Wise; **marketing executive** Jennifer Reeves; **director, site licensing** Tom Ryan; **director, corporate relations** Eileen Bernadette Moran; **publisher relations, eresources specialist** Kiki Forsythe; **senior publisher relations specialist** Catherine Holland; **publisher relations, east coast** Phillip Smith; **publisher relations, west coast** Philip Tsolakidis; **fulfillment supervisor** Iquo Edim; **fulfillment coordinator** Carrie MacDonald; **marketing manager** Christina Schlecht; **marketing associate** Mary Lagnaoui; **electronic media: manager** Lizabeth Harman; **project manager** Trista Snyder; **assistant manager** Lisa Stanford; **senior production specialists** Ryan Atkins, Christopher Coleman, Walter Jones; **production specialists** Nichele Johnston, Kimberly Oster; **director, web and new media** Will Collins

advertising director, worldwide ad sales Bill Moran
commercial editor Sean Sanders: 202-326-6430
project director, outreach Brianna Blaser

Product (science_advertising@aaas.org); **midwest/w. canada** Rick Bongiovanni: 330-405-7080, FAX 330-405-7081; **east coast/e. canada** Laurie Faraday: 508-747-9395, FAX 617-507-8189; **west coast** Lynne Stickrod: 415-931-9782, FAX 415-520-6940; **uk/europe/asia** Roger Goncalves: TEL/FAX +41 43 243 1358; **japan** ASCA Corporation, Nanako Ide +81 (0) 3 6802 4616, FAX +81 (0) 3 6802 4615; ads@sciencemag.jp; **senior traffic associate** Deiandra Simms

worldwide associate director of *Science* Careers Tracy Holmes: +44 (0) 1223 326525, FAX +44 (0) 1223 326532

Classified (advertise@sciencecareers.org); **u.s.: sales manager** Daryl Anderson: 202-326-6543; **midwest** Tina Burks: 202-326-6577; **east coast** Alexis Fleming: 202-326-6578; **west/south central** Nicholas Hintibidze: 202-326-6533; **sales coordinators** Rohan Edmonson, Shirley Young; **sales** Susanne Kharraz, Dan Pennington, Alex Palmer; **sales assistant** Lisa Patterson; **japan** ASCA Corporation, Jie Chin +81 (0) 3 6802 4616, FAX +81 (0) 3 6802 4615; careerads@sciencemag.jp; **advertising support manager** Karen Foote: 202-326-6740; **advertising production operations manager** Deborah Tompkins; **senior production specialist/graphic designer** Amy Hardcastle; **senior production specialist** Robert Buck; **senior traffic associate** Christine Hall

It becomes you.

Introducing the 3500 Series Genetic Analyzer.

Get ready to make an amazing discovery: the new 8-capillary and 24-capillary 3500 Series Genetic Analyzers take DNA analysis to an entirely new level of performance. A level where your daily workflow seems like a natural extension of your own intuition. Where precise, quality-assured data inspires greater confidence. And where a new consumables design and intuitive software interface keep you current and in control.

Take a closer look, and you'll find the new 3500 and 3500xL Genetic Analyzers are like second nature. Which is our first priority when it's your data.

Discover the 3500 System at **www.appliedbiosystems.com/3500Series**

Easy-to-Use Consumables

Control at Your Fingertips

Quality-Assured Data

applied biosystems
part of life technologies

Africa's Iron-Age Healers?

Last month, archaeologists working at a site in northern Ghana uncovered the most detailed evidence yet of a highly sophisticated and previously unknown Iron Age society. A team led by Benjamin Kankpeyeng of the University of Ghana in Legon excavated part of an earthen mound containing 92 whole and broken terra-cotta figurines of humans and mythical creatures. Radiocarbon dates from similar mounds in the region place the time between 600 C.E. and 1200 C.E.

The mound, which miraculously escaped decades of heavy looting in the region, may have served as an ancient shrine. Team co-director Timothy Insoll of the University of Manchester in the United Kingdom says the figurines have what appear to be libation holes to hold ritual drinks for a deity. There's also a ritually arranged human skull: "The jaw was removed, the skull was turned face-down, and the teeth were snapped out and placed nearby," Insoll says.

The finds open a major window on ritual life in West Africa before the Islamic era, says Christopher DeCorse, an archaeologist at Syracuse University in New York state: "It's analogous to the discovery of Upper Paleolithic rock art in Europe."

The deposits, which included grindstones for pulverizing plants, could be related to "traditional healing practices," Kankpeyeng notes. The team hopes to find further clues from the nearby remains of ancient riverbank settlements. The group has been excavating the site of Yikpabongo, first discovered in 1985, since 2007.

Heated Politics

The fallout from "Climategate" is raining down into state politics. On 9 February, the Utah House of Representatives passed a resolution stating that there is no evidence that the world is warming and urging the U.S. Environmental Protection Agency (EPA) to revoke its "endangerment" ruling that carbon dioxide is a threat to public health.

Apparently referring to the controversial leaked e-mails from a climate center in the United Kingdom (*Science*, 4 December 2009, p. 1329), the Utah resolution contends that "communications between climate researchers around the globe … indicate a well organized and ongoing effort to manipulate global temperature data."

Citing the same concerns, the state of Texas on 16 February sued EPA to overturn the endangerment finding. The same day, Virginia's attorney general filed court petitions questioning EPA's ruling.

The Utah resolution, backed by all of the Republican representatives, passed 56 to 17. The bill now goes to the state Senate, which is 72% Republican.

Dimly Lit Teens

Video games and texting are not the only reasons teenagers don't go to bed when they should. Lack of exposure to outdoor light is messing with their bodily rhythms and keeping them from getting sleepy when they should, according to research from the Rensselaer Polytechnic Institute (RPI) in Troy, New York.

A team led by Mariana Figueiro of RPI's Lighting Research Center conducted an experiment at a well-lit school in Chapel Hill, North Carolina, which has skylights that allow students maximal exposure to daylight. For 5 days, 11 eighth-graders wore orange glasses that blocked short-wavelength blue light, the kind that lab experiments have shown is important for setting the circadian clock. Researchers found that at the end of the week, the onset of sleep-inducing melatonin in the children was delayed by a half-hour.

"The amount of light we get indoors is below threshold for activation of the circadian system," says Figueiro, whose report appeared last week in *Neuroendocrinology Letters*. This contributes to the fact that "some kids can't fall asleep before 2 or 3 a.m."

Brown University sleep expert Mary Carskadon says the experiment lacked controls. But she agrees with Figueiro that the shortage of outdoor light in most schools—compounded by the indoor-oriented existence of the modern teen—may be contributing substantially to below-par school performance.

SAINT LOSES HER HEAD

For more than 600 years, citizens of the parish of Vadstena in Sweden have venerated two skulls said to have been those of St. Birgitta (1303–1373) and her daughter Katarina.

In the 1950s, anthropologists scrutinized the skulls and concluded that they were from women aged 60 to 70 years and 50 to 55 years, which could have fit the mother-daughter scenario. But modern science has shattered the myth.

Marie Allen, a forensic geneticist from Uppsala University in Sweden, used the relics to test her new method for analyzing mitochondrial DNA (mtDNA) from degraded samples. MtDNA from the two skulls, which is inherited only from the mother, showed both were female but "they were certainly not mother and daughter," Allen says. What's more, carbon-14 dating revealed that St. Birgitta's putative skull is at least a century too old to be the real thing. The other skull is a couple of centuries too late.

Allen, who published her results in *PLoS ONE* on 16 February, says the parish is not too disappointed with the findings: "They are very open-minded, and they wanted to know the truth about their relics."

CREDITS (TOP TO BOTTOM): TIM INSOLL; PHOTOS.COM; HERMANN RODE

Mapping mood disorders
1068

AAAS meeting: Science in a changed climate
1070

DRUG SAFETY

New Network to Track Drugs and Vaccines in Pregnancy

Pregnant women worry about—and avoid—exposure to virtually everything that might be risky, from tap water to soft cheeses. Many also jettison drugs they need, for fear of harming their baby.

Unfortunately, existing data are fuzzy about the dangers of using—or going without—key medications. "We can tell you what happens in a rat or a rabbit," says Christina Chambers, an epidemiologist at the University of California, San Diego. But a pregnant woman? For most medications, "we are flying by the seat of our pants," says Chambers, a situation she calls "appalling and frustrating." As a result, both doctors and patients are jittery about whether to continue or drop potentially risky treatments during pregnancy.

A new effort to bring risks into focus is being launched this week with $12.5 million from two U.S. agencies. It will start by examining asthma medications called short-acting beta agonists, as well as flu vaccines and antivirals for influenza. Called VAMPSS (the Vaccines and Medications in Pregnancy Surveillance System), the program will be funded for 5 years by the Agency for Healthcare Research and Quality and for 2 years by the Biomedical Advanced Research and Development Authority and coordinated by the American Academy of Allergy, Asthma, and Immunology. An advisory committee that includes members from pediatric and obstetric groups and the Centers for Disease Control and Prevention will guide VAMPSS's research.

This push for data began 8 years ago. Chambers and two of her colleagues—asthma specialist Michael Schatz of the Kaiser Permanente Medical Center in San Diego, California, and Allen Mitchell, who directs the Slone Epidemiology Center at Boston University—had spent years researching the issue. But their studies were hampered by too few volunteers and potentially imprecise data from mothers asked to remember every pill they'd taken.

The new program aims to get more robust results by bringing together two long-standing efforts. The first, led by Mitchell, has collected information over the years on 37,000 babies, most of them with congenital malformations, and their mothers. Mitchell plans to recruit at least 2000 more babies in each of the next 2 years for VAMPSS.

Playing it safe. Flu vaccines top the list of therapies to be studied in pregnancy.

Chambers, meanwhile, is one of the leaders of the Organization of Teratology Information Specialists (OTIS). It counsels between 70,000 and 100,000 pregnant women and health-care providers each year in the United States and Canada about drug and other exposures in pregnancy and lactation. It also invites some callers to enroll in research studies in which they and their babies are followed over time. OTIS will recruit thousands of these women for the VAMPSS studies on asthma and flu treatments and flu vaccines.

OTIS takes an approach that improves the quality of the data: It works with women before their babies are born. But its cohorts are often too small to link a specific medication with a specific birth defect. On the flip side, the project headed by Mitchell has the statistical power to focus on one birth defect at a time, but it relies on mothers to recall exposures during pregnancy. By conducting studies in sync on the same treatment or vaccine, there's "no question" that VAMPSS will be superior to existing efforts and far more systematic, says Gideon Koren, who directs the Motherisk Program at the Hospital for Sick Children in Toronto, Canada, which is part of OTIS's North American network.

The government support helps fill a serious gap. "It's not a secret that most drug companies … don't want anything to do with pregnancy," says Koren. Drug companies so far have declined to help fund VAMPSS. To survive long-term and branch out to other drugs and vaccines, as its leaders hope it will, it needs industry money.

VAMPSS is coming together now partly because of the H1N1 flu. H1N1 was "a situation that seemed to be uniquely affecting pregnant women" who were at high risk for complications if they contracted it, says Schatz, a past president of the allergy academy. Meanwhile, the U.S. Food and Drug Administration (FDA) is asking companies to focus more on drug safety in pregnancy after a drug is approved. In December, FDA announced it was setting up the Medication Exposure in Pregnancy Risk Evaluation Program, which relies on insurance company databases to look for signals.

VAMPSS is focused as much on demonstrating safety as on finding hazards. "In some ways there's more benefit" to showing safety than risk, says Chambers, because women and their babies can be harmed by a poorly controlled disease. Studies of pregnant women with asthma have found that those who have asthma attacks are more likely to give birth to babies with low birth weight and, in one study, with birth defects.

But just how reassuring can any study be?

CREDIT: BLOOMBERG/GETTY IMAGES

Cancer in circulation
1072

The end of random-source lab animals?
1076

"It's been really difficult" to prove that drugs or vaccines are safe in pregnancy, says Allison McGeer, an infectious disease specialist at Mount Sinai Hospital in Toronto, who is studying flu vaccines in pregnancy. Although McGeer believes flu vaccines are safe, she hesitates to prescribe antiviral drugs to pregnant women who are mildly ill or as a preventive treatment. "Those of us who don't deal routinely with pregnant women are very afraid to do anything," she says.

One area not addressed by VAMPSS and most other studies is whether medications taken during pregnancy can cause effects in children years later, such as learning difficulties in school. "We need to focus more on the long-term effects," says Lars Pedersen, an epidemiologist and obstetrician at Aarhus University in Denmark, who has studied antidepressants and other drugs in pregnancy. But that is not easy to do.

It's not so much that "drugs are out there causing problems," says Schatz, although some probably are. The bigger challenge, he believes, is the uncertainty: Which drugs are dangerous to a fetus, and which are not?

–JENNIFER COUZIN-FRANKEL

PHYSICS

Century-Long Debate Over Momentum of Light Resolved?

What is the formula for the momentum of light zipping through a transparent material? That may sound like a question on a high-school physics quiz, but physicists have been debating the matter ever since two different formulas were proposed more than 100 years ago. Now Stephen Barnett, a theorist at the University of Strathclyde in Glasgow, U.K., says he has resolved the famed "Abraham-Minkowski dilemma." Both formulas are correct, he says, but they denote different things and apply in different contexts.

Others had suggested that each formula might be correct in its own way, but Barnett spells out precisely when each is relevant, says Robert Boyd of the University of Rochester in New York state. "Steve tells you how to apply them correctly," Boyd says. "I think [the work] has a good chance of being definitive."

Everyone agrees that the momentum of a photon zinging through empty space is given by a fundamental constant divided by the light's wavelength. When the light enters a medium such as glass or a gas, however, it slows down, which is why a lens bends light. What then happens to the light's momentum? Key to this question is the material's "index of refraction," the ratio of light's speed in a vacuum to its speed in the material, a number typically larger than one. In 1908, German mathematician Hermann Minkowski argued that the momentum of light in a material equals its momentum in the vacuum multiplied by the index of refraction, making it greater than the vacuum momentum. A year later, his compatriot, physicist Max Abraham, argued that the momentum of light in a material equals the vacuum momentum *divided* by the index, making it smaller than the vacuum momentum.

Thought experiments and real-world data can be found to support each formula. For example, imagine a photon speeding toward a block of glass (see diagram). Together, the glass and the photon possess a total mass and energy that flows in the same direction as the photon. According to Newton's laws of motion, that flow should continue unabated as the photon passes through the glass. But within the glass, the photon slows down. So to maintain constant energy flow, the glass has to recoil in the same direction. From this premise, a little algebra leads to Abraham's formula for the photon's momentum in the glass.

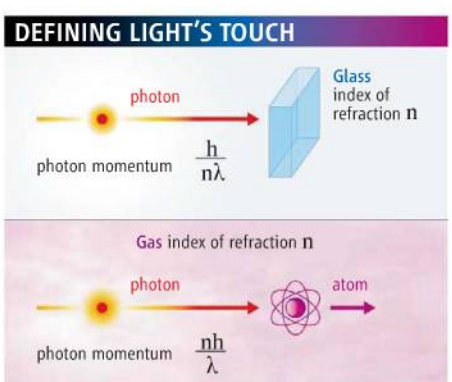

Riddle me this. Incompatible equations for a photon's momentum have long puzzled physicists.

On the other hand, imagine firing a photon at an atom in a gas. Suppose the atom can absorb light of a wavelength slightly longer than that of the approaching photon. Then to soak up the photon, the atom must speed away from the light source so that from its perspective the light wavelength stretches—just as a siren's pitch dips if you're in a car rushing away from the siren. The size of that "Doppler shift" is proportional to the gas's index of refraction. Starting from that premise, a little math yields Minkowski's formula.

Actually, Barnett argues in the 19 February issue of *Physical Review Letters*, the two cases describe different kinds of momentum. Abraham's formula gives the "kinetic momentum"—essentially the mechanical punch the photon packs as it hits the glass. Any experiment to measure such a punch will agree with Abraham's formula. Minkowski's formula gives the subtler "canonical momentum"—which, loosely speaking, is tied to the wave nature of light and is higher in a material than in vacuum because the light's wavelength is shorter in the material. Any experiment to probe wave effects will jibe with Minkowski's formula.

More technically, the canonical momentum is a mathematical quantity connected to movements in space. A theorist can write down a quantum "wave function" describing an atom sitting in an electromagnetic field. To move the atom to another spot, the theorist must change the wave function by performing a specific mathematical operation that involves the canonical momentum. That's why in the thought experiment with the moving atom, it's the canonical momentum that counts.

Given the debate's long history, few expect the work to win immediate acceptance. "Various people have taken rather strong views, you might say verging on religious beliefs," says Paul Lett, a physicist at the U.S. National Institute of Standards and Technology in Gaithersburg, Maryland. Barnett says he's game to take on the naysayers, however: "If somebody exposes some flaw, then I suppose I shall have to—Oh, they won't!"

–ADRIAN CHO

CREDIT: A. CHO AND M. TWOMBY/SCIENCE

PSYCHIATRY

Experts Map the Terrain of Mood Disorders

There's been a lot of debate over efforts to revise psychiatry's *Diagnostic and Statistical Manual of Mental Disorders* (*DSM*), and one of the issues generating extensive discussion is the connection between depression and anxiety. Anxiety isn't on the list of symptoms for major depression, but "most cases of depression are anxious depression," notes David Goldberg of London's Institute of Psychiatry.

This is part of a broader conversation about how the American Psychiatric Association's (APA's) teams assembling a new *DSM-V* edition can "deconstruct" psychiatric illnesses, recognizing that few exist in their pure form; rather, comorbidity and cross-cutting features are the norm (*Science*, 12 February, p. 770).

Depression is a prime example. It can coexist with practically any other psychiatric condition. And when it's the primary complaint, many other factors can shape its course. "There are a lot of [comorbid] symptoms that categorical diagnoses don't reflect … that really affect outcome," says psychiatrist Jan Fawcett of the University of New Mexico School of Medicine in Albuquerque, chair of the *DSM-V* work group on mood disorders. Substance abuse and anxiety are two of the most important. Indeed, *DSM-V* authors are debating whether the relationship between anxiety and depression is so close that they should be subsumed into a supercategory of human hopelessness, fear, and existential angst.

DSM-IV, currently in use, gives a menu of nine symptoms for "major depression," a diagnosis that afflicts about 17% of the population at some point in life, according to the U.S. National Comorbidity Survey. (Bipolar illness—depression alternating with mania—affects another 1%.) Missing from the list is anxiety; yet, says Fawcett, anxious depressives are at greater risk for suicide, and there's a "staggering" fivefold difference in response to antidepressants, with nonanxious depressives doing much better. Fawcett's group is therefore recommending that "mixed anxiety depression," a condition that has been residing in the Appendix of *DSM-IV*, be promoted to a free-standing diagnosis.

Deep blue. Tracing a line between depression and anxiety can be difficult.

But giving anxiety a higher status within depression raises other categorical questions. The "anxiety disorders" are currently a separate category that includes generalized anxiety disorder, phobias, and panic, as well as obsessive-compulsive disorders and post-traumatic stress disorder. The symptoms defining the latter two are far more varied than those associated with depression and anxiety.

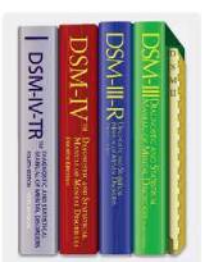

DSM-V
Third in a series

The mood work group spent a lot of time agonizing over the relationship between anxiety and depression at a conference on the subject at the Institute of Psychiatry in 2007. Much new data have revealed a close relationship between the two, but some of it is conflicting. Both family studies and whole-genome surveys show that the two disorders share some of the same genes. On the other hand, imaging and neurochemistry data—including drug responses—suggest important differences. The anxious brain "doesn't look the same" as the depressed one, says APA President Alan Schatzberg, a psychiatrist at Stanford University in Palo Alto, California. Twin studies have shown "a common, underlying genetic vulnerability," he says, but environmental factors seem to determine whether a twin becomes anxious or depressed.

At another border area of depression's bleak realm, major depression is sometimes hard to distinguish from bipolar illness, in which depression alternates with mania—characterized by grandiosity, hyperactivity, racing thoughts, and wild schemes. "There's a raft of reports of major depressives with [only] one or two manic symptoms," says Fawcett. Because such individuals are at risk of full-blown bipolar illness—which is often not diagnosed for years—and also because some antidepressants can trigger a manic episode in the vulnerable, his group decided to slightly lower the bar for a bipolar diagnosis.

Depression also has a murky border with psychosis, which involves delusions (often paranoid) and hallucinations. Bipolar illness and schizophrenia have traditionally been thought of as separate disorders. But genetic and brain-imaging studies over the past decade have undermined this separation, says APA psychiatrist Darrell Regier, co-chair of the *DSM-V* effort. Both bipolar and schizophrenic patients exhibit common biological abnormalities, including anomalous brain waves and eye movements, notes Goldberg. And in bipolar I, the more severe form, psychosis is not unusual. Genetic studies have shown that vulnerability to psychosis appears as a "common denominator" in some families with both schizophrenia and bipolar illness, Schatzberg says. Some psychiatrists see the two as ends of a continuum, with "schizoaffective disorder"—a utilitarian diagnosis for people showing symptoms of depression and schizophrenia but not qualifying for either diagnosis—somewhere in the middle.

All involved with the *DSM-V* process emphasize that no one yet knows what the final product will look like. On the Web site where proposed revisions are posted (www.dsm5.org), diagnoses are currently grouped for convenience under *DSM-IV* categories, Regier says. But, he adds, "we are very seriously considering a reorganization" in which anxiety and depression are combined under a supercategory of "internalizing disorders." Still, says Regier, it's all very much a work in progress. The final organization will not be determined until changes have been tested in field trials. **–CONSTANCE HOLDEN**

CREDIT: VINCENT VAN GOGH

Suicide Scale

Because severity of depression is not a good indicator of whether a patient is suicidal, the mood group is proposing two "suicide assessment scales" for youths and adults, based on a review of the literature on completed suicides, to help in the process of diagnosing any mental disorders. Proposed risk factors include history of suicide attempt, living alone, "angry impulsivity," drug or alcohol abuse, chronic pain, and a suicide plan. **–C.H.**

STEM EDUCATION

DOE Reworks Student Initiative to Prepare Energy Researchers

Having learned that bigger isn't always better, the U.S. Department of Energy (DOE) has downsized a proposal to train more scientists and engineers to work in a low-carbon economy.

Last year, Energy Secretary Steven Chu won President Barack Obama's backing for a $115 million education initiative dubbed RE-ENERGYSE (REgaining our ENERGY Science and Engineering Edge). It was designed to support activities along the entire training spectrum, from postdoctoral fellowships to hands-on learning for elementary students, with a special focus on preparing technicians for jobs in the burgeoning clean-energy sector.

Federal lawmakers weren't very impressed (*Science*, 10 July 2009, p. 130). They worried that RE-ENERGYSE overlapped with other federal activities to improve science, technology, engineering, and mathematics (STEM) education, notably those at the National Science Foundation (NSF) and the Department of Education, as well as at the Workforce Development for Teachers and Scientists program within DOE's Office of Science. In the end, Congress did not give DOE any money for RE-ENERGYSE in its 2010 budget.

CREDIT: DOE

"We've scaled back. We're going to start small."

—KRISTINA JOHNSON, DOE

But this month, the president's 2011 budget request contains a slimmed-down RE-ENERGYSE, with a price tag of $50 million—$35 million for higher education and $15 million for technical training and precollege outreach. The need for more skilled workers hasn't gone away, says Kristina Johnson, under secretary for energy, who helped to craft the program and would oversee it. But DOE has learned its lesson, she says: "We've scaled back. We're going to start small, and we'll try to build it up once we see what's working."

For example, Johnson says that DOE's workforce development program, overseen by Science Under Secretary Steven Koonin, is "taking the lead" on graduate research fellowships, with a request for 170 new fellows in 2011 to join a class of 160 funded this year. In comparison, the new RE-ENERGYSE would support only 60 fellows in 2010, instead of the 150 to 200 requested last year. However, RE-ENERGYSE's fellows would be encouraged to work on clean-energy topics, while the Office of Science fellows would be spread across most basic-science disciplines.

Johnson has also trimmed plans for another key element in the initiative: the creation of master's degree programs in interdisciplinary energy studies. DOE is requesting money for two rather than four such collaborations across departmental lines. The idea is modeled on an engineering management program that Johnson expanded while dean at Duke University in Durham, North Carolina.

RE-ENERGYSE's activities at the precollege level "haven't been defined yet," Johnson admits. But there, too, the goal is to produce more clean-energy scientists and engineers. "This year, about 6% of entering college students say they are interested in engineering, and about 4.4% of them graduate with an engineering degree," she explains. "It's pretty hard to compete globally when you're relying on such a small segment of the population to provide the innovations we need. We know from studies NSF has done that we lose kids in grades three to five. And if they don't maintain an interest in science and math, they won't take enough courses to be able to become an engineer."

A congressional aide on the spending panel that controls DOE's budget says that members were taken aback last year by the size of the initiative as well as its scope. "We're still concerned about whether RE-ENERGYSE complements or overlaps with existing STEM education programs," says the aide. But "it sounds like they heard us."

–JEFFREY MERVIS

ScienceInsider

From the *Science* Policy Blog

The U.S. National Institutes of Health (NIH) has widened its definition of what constitutes a **human embryonic stem cell** to keep up with what's happening in the lab. The new definition would include lines derived from embryos before the blastocyst stage. http://bit.ly/b8jJy]

The U.S. government has formally closed its investigation of **Bruce Ivins**. A 92-page report summarizes why it believes the Army researcher who killed himself in July 2008 was the 2001 anthrax mail bomber. http://bit.ly/daAtvZ

A veteran science policymaker is the new head of the European Research Council's scientific council. **Helga Nowotny** is replacing founding president Fotis Kafatos. http://bit.ly/ddPr4L

This week's launch of **an instrument to measure the extent and thickness of polar ice** has been delayed after the European Space Agency became concerned about the Russian rocket that will place the CryoSat-2 spacecraft into its highly inclined orbit. http://bit.ly/caR6qg

New York state officials have accused a former researcher from the University at Buffalo of hiring three actors to give false testimony that helped clear him of research misconduct charges in a 2004 case. **William Fals-Stewart**, an expert on addiction, was arrested and charged with attempted grand larceny, perjury, identity theft, and other crimes. http://bit.ly/cHiAVZ

The man in charge of the recent Copenhagen climate conference, **Yvo de Boer**, has resigned his United Nations post and will join the consulting giant KPMG to work on climate and sustainability issues. http://bit.ly/9XdmNO

Raynard Kington, who ran NIH during the transition from Elias Zerhouni to Francis Collins, is leaving as deputy NIH director to become president of Grinnell College in Iowa. http://bit.ly/cDkuX8

For the full postings and more, go to **blogs.sciencemag.org/science/insider**.

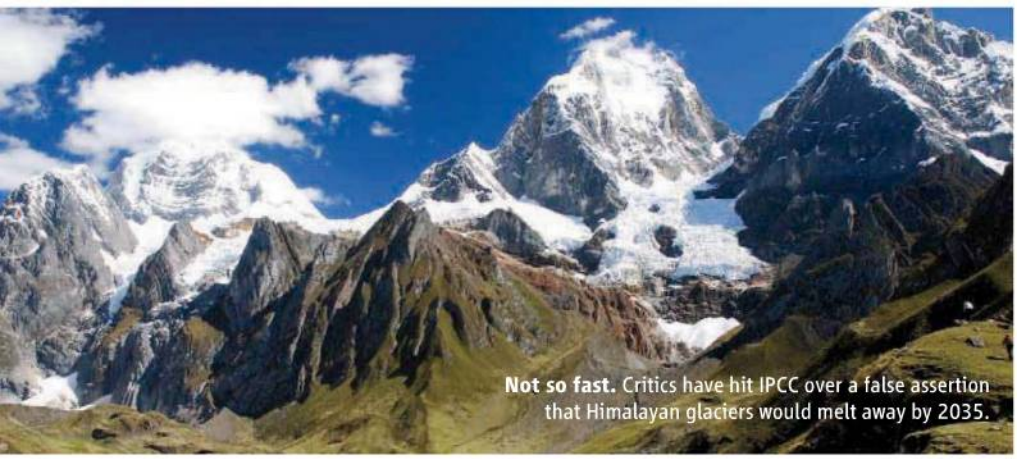

Not so fast. Critics have hit IPCC over a false assertion that Himalayan glaciers would melt away by 2035.

Scientists Grapple With 'Completely Out of Hand' Attacks on Climate Science

A symposium organized at the last minute at the annual meeting of the American Association for the Advancement of Science (the publisher of *Science*) by two of the world's most prominent scientific organizations addressed recent attacks on an increasingly beleaguered climate science community. The panel met in the uncertain aftermath of the stolen e-mails affair and critiques of the Intergovernmental Panel on Climate Change (IPCC) (*Science*, 12 February, p. 768).

The symposium was convened by U.S. National Academy of Sciences President Ralph Cicerone, in conjunction with AAAS, at a time when flaws in the latest IPCC report, and even the legitimacy of climate science, have made headlines. E-mails uncovered late last year revealed instances of scientists on the panel discussing withholding data and documents from those with opposing views, conspiring to keep contradictory papers out of influential reports, and encouraging colleagues to delete e-mails.

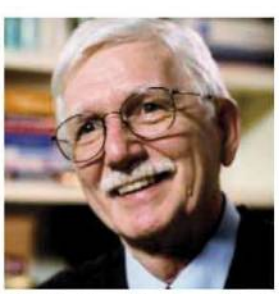

E-mail etiquette. Gerald North says scientists should not sound like bloggers.

Despite a drumbeat of studies that corroborate the conclusion that the planet is warming and human activities are largely responsible, these recent skirmishes "have really shaken the confidence of the public in the conduct of science [overall]," said Cicerone, citing a number of recent polls on the public perception of science. "The situation is completely out of hand," said climate scientist Gerald North of Texas A&M University in College Station, who has served as an IPCC reviewer. "One guy e-mailed me to say I'm a 'whore for the global warming crowd.' " His PowerPoint presentation at the meeting included a slide quoting conservative talk show host Glenn Beck, who suggested that scientists commit "hara-kari" to atone. "Scientists cannot use the same tone and rhetorical style as commentators and bloggers," North said.

Although much of the session at the meeting, titled "Ensuring the Transparency and Integrity of Scientific Research," focused on what Harvard University oceanographer and former AAAS head James McCarthy called the "abominable" press coverage, scientists owned up to their share of the blame. Small errors in the 2007 report were "careless," said McCarthy, but IPCC should have done a full and public examination to describe how they had come about: "The names of the authors, who was on the review, what happened—it all should have been up there, and it wasn't done. And I think that the institution was hurt as a result," he said.

The community allowed "the situation to get out of control," said Sheila Jasanoff of Harvard University. She said in general scientists had to connect better to the public. "There is a kind of arrogance—we are scientists and we know best," Jasanoff said. "That needs to change." —**ELI KINTISCH**

The Latest on Geoengineering

Preliminary findings presented here suggest that some proposed techniques to cool the planet manually may have fewer barriers than previously thought. But many technical and societal barriers remain.

Even before they got to the sessions, the scientists had to contend with a smattering of activists with drums, cameras, and a megaphone alleging that the government is already performing geoengineering through the spraying of particles, in so-called chemtrails.

Physicist David Keith of the University of Calgary in Canada addressed the concept of spreading aerosol droplets in the stratosphere, where they could block a small fraction of the sun's rays. A paper published last year in *Environmental Research Letters* suggested that the leading proposal, spraying

Is a Dolphin a Person?

Are dolphins as smart as people? And if so, shouldn't we be treating them a bit better? Those were the questions scientists and philosophers debated at a session here on Sunday.

Dolphins, it turns out, are pretty darn smart. Panelist Lori Marino, an expert on cetacean neuroanatomy at Emory University in Atlanta, said they may be Earth's second smartest creature, after humans, of course.

Bottlenose dolphins have bigger brains than humans (1600 grams versus 1300 grams), and they have a brain-to-body-weight ratio greater than that of great apes (but smaller than that of humans), said Marino. "They are the second most encephalized beings on the planet."

But it's not just size that matters. Dolphins also have a very complex neocortex, the part of the brain responsible for problem solving, self-awareness, and various other traits we associate with human intelligence. And researchers have found spindle neurons in dolphin brains called von Economo neurons that in humans and apes have been linked to emotions, social cognition, and even theory of mind: the ability to sense what others are thinking. Overall, said Marino, "dolphin brains stack up quite well to human brains."

What dolphins do with their brains is also impressive. Cognitive psychologist Diana

sulfur dioxide gas, wouldn't work. Sulfur dioxide is converted in the atmosphere into droplets of sulfuric acid, which would clump and fall out of the sky before they could have much cooling effect. To get around this problem, Keith and colleagues have proposed using airplanes to spray droplets of the acid itself, rather than sulfur dioxide. In unpublished data, the team found that injecting only "a few megatons per year" of sulfuric acid could be more than twice as effective at blocking radiation as starting with sulfur dioxide.

While scientists are finding ways to overcome the engineering challenges, the environmental effects of planet-hacking techniques remain uncertain. One challenge in geoengineering a warmed planet is simultaneously restoring temperatures while minimizing disruption of rain and precipitation. (Stratospheric particles lower the total amount of energy striking Earth, the driver of precipitation.)

In previous modeling efforts, adding sun-blocking particles uniformly across the globe has tended to undercool the poles while overcooling the equator. So Kenneth Caldeira, a climate scientist at the Carnegie Institution for Science in Stanford, California, modeled various approaches to try to counteract a severe warming—the result of a doubling of preindustrial CO_2 concentration. In work yet to be published, he distributed the particles unevenly to try to minimize those effects; for example, by putting more at the poles versus the equator. (Global warming is greatest in the Arctic.) In models, that strategy helped fix the undercooling/overcooling problem, but it worsened the effects on precipitation. "There's a complex problem of how do you balance the damage that you do against the benefit," said Caldeira.

That said, simulating either geoengineering approach to counteract global warming—distributing particles globally or focusing on the poles—suggests a cooler world with less disruption of rain patterns than one in which warming continues unabated. "In a high-global-warming world, more people would be better off with geoengineering, but some people would be worse off," he said.

–ELI KINTISCH

Reiss of Hunter College of the City University of New York has been working with dolphins in aquariums for most of her career, and she said their social intelligence rivals that of the great apes. Dolphins can recognize themselves in a mirror, a sign of self-awareness. They can understand complex gesture "sentences" from humans. And they can learn to poke an underwater keyboard to request toys. "Much of their learning is similar to what we see with young children," said Reiss.

So if dolphins are so similar to people, shouldn't we be treating them more like people? "The very traits that make dolphins interesting to study," said Marino, "make confining them in captivity unethical." She noted, for example, that, in the wild, dolphins have a home range of about 100 square kilometers. In captivity, they roam one 10-thousandth of one percent of this area.

Far worse, Reiss said, is the massive dolphin culling ongoing in some parts of the world, which she documented with a graphic video of dolphins being drowned and stabbed in places like the Japanese town of Taiji.

Thomas White, a philosopher at Loyola Marymount University in Redondo Beach, California, suggested that dolphins aren't merely like people—they may actually be people, or at least, "nonhuman persons." Defining exactly what it means to be a person is difficult, White said, but dolphins seem to fit the checklist many philosophers agree on. There are the obvious ones: They're alive, aware of their environment, and have emotions; but they also seem to have personalities, exhibit self-control, and treat others appropriately, even ethically. When it comes to what defines a person, said White, "dolphins fit the bill."

Social smarts. Dolphins display many of the same behaviors humans do.

CREDIT: PHOTOS.COM

Still, experts caution that the scientific case for dolphin intelligence is based on relatively little data. "It's a pretty story, but it's very speculative," says Jacopo Annese, a neuroanatomist at the University of California, San Diego. Despite a long history of research, scientists still don't agree on the roots of intelligence in the human brain, he says. "We don't know, even in humans, the relationship between brain structure and function, let alone intelligence." And, Annese says, far less is known about dolphins.

–DAVID GRIMM

With reporting by Greg Miller.

More Highlights From AAAS 2010

Science reporters posted more than two dozen blog entries and podcasts from the meeting. Here is a sample. For full coverage, see www.sciencenow.org. And to see what our guest bloggers had to say, see news.sciencemag.org/sciencebloggers.

A Sexy Treatment for Traumatic Brain Injury
The hormone progesterone is best known for its work in the female reproductive system, where it plays various roles in supporting pregnancy. But starting next month, it will be the focus of a phase III clinical trial for traumatic brain injury. Researchers hope an infusion of progesterone given within a few hours of a car accident or other trauma will help prevent brain damage.

The Mathematics of Clumpy Crime
Even in a sprawling city like Los Angeles, California, crimes still clump together. Mathematical models presented at the meeting show that such crime hot spots form when previous crimes attract more criminals to a neighborhood. By understanding how these blobs form, researchers hope to help police break them up.

Are 'Test Tube Babies' Healthy?
When Louise Brown was born on 25 July 1978, she kicked off an era. The first "test tube baby" is a mother herself now, and she's been joined by millions of others born with the help of in vitro fertilization (IVF). But are babies born via IVF the same as those born naturally? Researchers have discovered some subtle genetic differences.

Drive Green, Make Money
Widespread adoption of plug-in electric vehicles could dramatically cut greenhouse gas pollution and reduce U.S. dependence on foreign oil. And results of a new electric-car pilot project provide added incentive to go electric: Car owners could return unused electricity to the grid and make real money doing so.

Science Is Kryptonite for Superheroes
Hollywood has a message for scientists: If you want something that's 100% accurate, go watch a documentary. A panel of screenwriters for superhero-driven movies and TV shows like *Watchmen* and *Heroes* said that their job is to get the characters right, not the science.

Cancer's Circulation Problem

Researchers are counting and examining the rare cells shed by a primary tumor that circulate in the blood, but will these studies help patients?

IT GIVES SURGEON

Stefanie Jeffrey great satisfaction that most of the women whose breast tumors she removes will go on to lead healthy lives, their cancer gone for good. But in about 25% of her patients, the cancer will reappear, having spread to their bones or other organs. Yet physicians have no easy way to know whether a woman's breast tumor has metastasized or whether treatments are keeping a cancer in check. Often they and their patient find out only when a new tumor is large enough to cause symptoms or show up with imaging technologies. By then, "it's often too late" for a cure, says Jeffrey. "It's very frustrating not knowing which patients will develop metastases or how best to treat those who do."

A solution to Jeffrey's frustration may come at her lab bench at Stanford University in Palo Alto, California, rather than in her operating room. She and other researchers are exploring a new window for tracking the spread of cancer: the vanishingly few tumor cells that circulate in a patient's blood.

It's been recognized for decades that cancers metastasize because primary tumors shed cells into the blood, which carries them to other organs where they seed new tumors. It's these metastases, not the primary tumors, that cause 90% of cancer deaths. Only in the past 10 years, however, have researchers figured out how to efficiently capture circulating tumor cells (CTCs) from a blood sample. Clinical researchers are now counting CTCs every few weeks in patients with several types of metastatic cancer, a crude but potentially useful measure for gauging whether a treatment is working. Researchers have also begun to analyze CTCs for certain gene variants or proteins that indicate a patient's tumor is susceptible to a particular drug. This kind of "liquid biopsy," which may allow physicians to follow cancer changes over time and tailor treatment, has spurred at least two dozen academic groups and companies to come up with new CTC detection devices.

The growing ability to detect and analyze CTCs could also galvanize the development of drugs designed to block metastasis, says Joan Massagué, a metastasis researcher at Memorial Sloan-Kettering Cancer Center in New York City. Compared to waiting for secondary tumors to appear, monitoring CTC counts may give companies a shortcut for measuring whether an antimetastasis drug works.

At the same time, CTC research faces hurdles. Any new CTC detection technology is considered a disease monitoring device by U.S. regulators and must be validated in clinical trials—a slow, costly process. And because CTCs are so rare and hard to capture—there may be as few as one cancer cell in a billion blood cells—most separation strategies are thought to miss some of the cancer cells. Moreover, researchers don't yet have a good handle on whether the cells they're collecting from people's blood are the ones that can seed new tumors.

Online
sciencemag.org
Podcast interview with author Jocelyn Kaiser.

Further analysis of CTCs could answer that question and confirm that the picture of metastasis developed over the past decade in animal studies is the same in people. "In some way, the big missing piece has been access to these cells," says Daniel Haber, director of the Massachusetts General Hospital (MGH) Cancer Center in Boston.

Rare, but important

The first report of blood-borne cells shed by a solid tumor came in 1869 from an Australian physician named Thomas Ashworth. Using a microscope, he examined blood from a patient who died of metastatic cancer, spotting cells that looked identical to the cells in the patient's tumors. Such cells "may tend to throw some light upon the mode of origin of multiple tumours existing in the same person," Ashworth presciently wrote.

But only in the 1990s did clinicians fully realize the potential value of CTCs. The inspiration came in part from work on rare primary tumor cells found lodged in a cancer patient's bone marrow long before metastasis was evident. Studies in Europe suggested that patients with these so-called disseminated tumor cells in their bone marrow had a poorer prognosis. Frequent bone marrow biopsies aren't practical, however, so researchers began to look to CTCs in blood samples, says Klaus Pantel, a medical oncologist at the University Medical Center Hamburg-Eppendorf in Germany.

Also motivating the interest in CTCs has been the recent development of molecularly targeted cancer therapies that work best on patients whose tumors have a particular mutation. This spurred a push to develop devices to efficiently capture and analyze CTCs, which could potentially serve as a surrogate for the tumor itself, Pantel says.

One of the first widespread CTC detectors, called CellSearch, works for cancers that arise in the epithelial tissue lining organs such as the breast and colon. The device traps CTCs using magnetic beads coated with an antibody that sticks to a protein called epithelial cell adhesion molecule (EpCAM) that's found on the tumor cells but not on blood cells. But before technicians can use a microscope to count the CTCs, they must stain the trapped cells with other antibodies to distinguish the tumor-derived ones from white blood cells that linger as contamination.

CellSearch demonstrated its potential in 2004, when a study of 177 breast cancer

CREDIT: ISTOCKPHOTO.COM

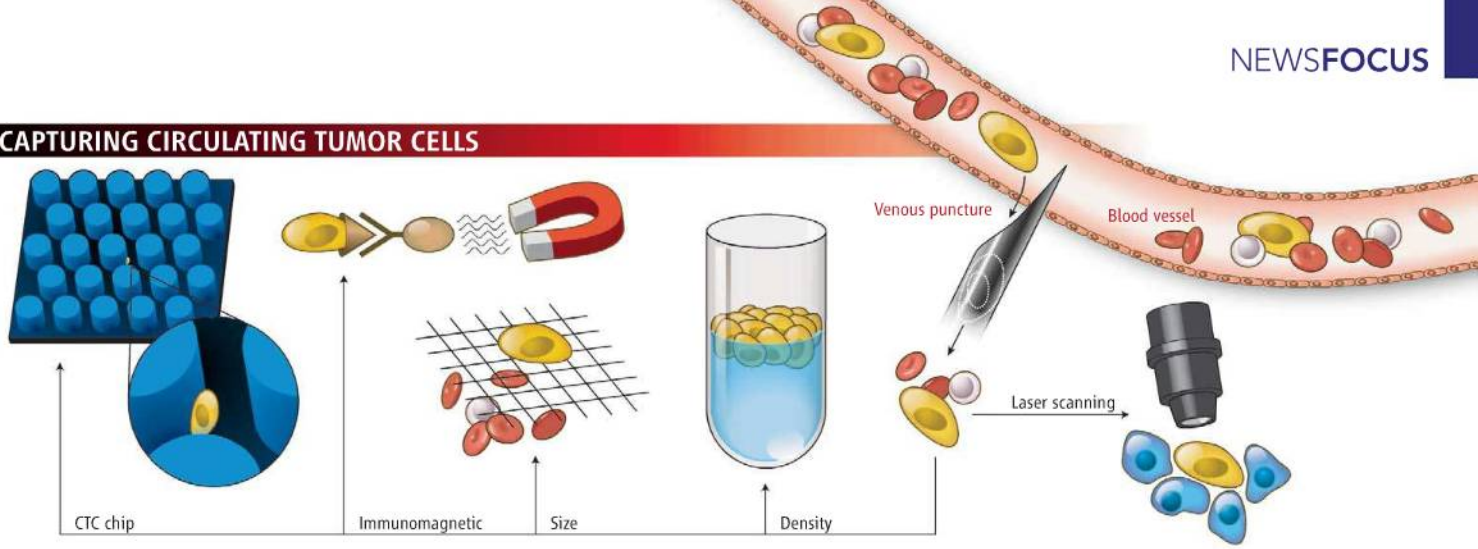

Needle in a haystack. Devices for separating the rare tumor cells (yellow) in a blood sample include a silicon chip studded with microscopic posts, magnetic beads coated with antibodies, filters, density-based centrifuges, and laser detection. Antibodies or genetic analyses are then used to identify and characterize the cells.

patients showed that women with at least five CTCs per 7.5 milliliters of blood had a poorer prognosis than those with fewer or no CTCs. Based on these results, that year the U.S. Food and Drug Administration approved CellSearch as a device for managing the progression of metastatic breast cancer. Manufacturer Veridex later won approval for using CellSearch to monitor metastatic colon and prostate cancers.

One CellSearch test on a blood sample costs about $600, far less than $1500 or more for a PET or CT scan that may only spot significantly sized tumors, notes Massimo Cristofanilli of the Fox Chase Cancer Center in Philadelphia, Pennsylvania, who led the breast cancer trial. CellSearch "will be extremely useful for oncologists," he says.

Just how useful remains uncertain. When the American Society of Clinical Oncology issued its most recent guidelines for treating breast cancer in 2007, it cautioned against making treatment decisions based on CTCs just yet. To confirm the utility of CTC monitoring, experts want a prospective study to show that switching treatments when a patient's CTC levels rise, rather than waiting until an imaging scan shows progression, extends lives. A randomized breast cancer trial now enrolling 500 women in the United States with metastatic breast cancer aims to provide this evidence within the next few years.

More than a number

Counting cells barely scratches the surface of how oncologists want to use CTCs. "My problem with counting is, say the cell count is up and the drug isn't working. What drug do you switch to?" says Jeffrey. She and others want to analyze CTCs for molecular changes in a person's cancer that would point toward particular treatments. For example, only women with breast cancer whose tumor cells express the receptor HER2 respond to the drug Herceptin. Researchers reported 6 years ago that some women whose primary tumors were HER2-negative later had CTCs that were positive for HER2, suggesting that their cancer had mutated. Monitoring CTCs might therefore identify women who were initially ineligible for Herceptin but who would later qualify for the drug.

To detect such molecular changes routinely, researchers say they need to improve on CellSearch, which often finds only a few, if any, CTCs in a cancer patient and yields impure cells that can't be analyzed in much depth. One newer device is a silicon chip developed by Haber and MGH biomedical engineer Mehmet Toner. Called the CTC Chip, it has 78,000 microscopic posts coated with EpCAM antibodies that let blood cells pass by but trap live tumor cells; as with CellSearch, these cells are then dyed with markers and detected with a microscope. In a 2007 *Nature* paper on the CTC Chip, the MGH team reported that 67 of 68 mostly metastatic cancer patients had CTCs, while controls had none.

The MGH group later used the chip to capture CTCs from lung cancer patients for genetic analysis. In a 2008 *New England Journal of Medicine* article, the MGH group reported extracting DNA from these CTCs and detecting key mutations in the gene for a cell surface protein called EGFR—including a genetic change indicating that some patients' cancer had become resistant to the potent drug they were receiving.

Haber's team has a $15 million, 3-year grant from Stand Up To Cancer, a U.S. telethon to raise money for cancer research, to further improve the test—it's slow, requiring about 6 hours per sample—and incorporate it into clinical trials at several other cancer centers.

Devices like the CTC chip and CellSearch that use EpCAM to fish out cancer cells in blood have a potentially significant drawback: They miss CTCs that lack EpCAM, possibly because the cells have gone through the so-called epithelial-mesenchymal transition (EMT), a process in which some tumor cells become less sticky as they're breaking free and entering the blood. Nor can EpCAM methods detect non-epithelial cancers, such as sarcomas.

To combat these problems, some labs are using cocktails of antibodies to try to pick up more CTCs. Others are experimenting with so-called negative filtration, which uses antibodies to remove blood cells from a sample and leave behind tumor cells. Still others are working on CTC trapping methods that don't rely on antibodies. A size-based membrane filter—CTCs tend to be larger and less dense than blood cells—developed by a team led by pathologist Richard Cote of the University of Miami in Florida wins the record for speed: It's essentially a big syringe, and in just 90 seconds it squeezes a blood sample through a filter, leaving behind tumor cells. Yet another approach is to smear whole blood on a slide, stain the cells with various fluorescent markers, then use a laser to rapidly count the cells.

A particular device "may be better depending on what you're trying to do. It's up to you to prove it," says oncologist Howard Scher of Sloan-Kettering. CTC detectors may also soon face a challenge from growing efforts to analyze blood samples for free-floating DNA shed by tumor cells (see sidebar, p. 1074).

One reason researchers are hotly pursuing better CTC detectors is the prospect of a test that is sensitive enough to detect a person's initial tumor early in its development.

SOURCE: ADAPTED FROM K. PANTEL *ET AL.*, *NATURE REVIEWS CANCER* 8 (MAY 2008)

Keeping Tabs on Tumor DNA

While many researchers are working on using tumor cells in blood to track cancer (see main text), Bert Vogelstein's group at Johns Hopkins University has been doggedly pursuing a related idea: monitoring free-floating tumor DNA in blood. A new study suggests that advances in DNA sequencing may make this approach a strong alternative.

Detecting naked DNA shed by a tumor isn't quite as daunting as capturing circulating cancer cells, which requires physically separating multiple kinds of cells. But it isn't easy, either. For several years, Vogelstein's team has tried to detect tumor DNA in a cancer patient's blood by searching for DNA with subtle mutations in known cancer genes. But not all patients' tumors carry such mutations. And the polymerase chain reaction (PCR) technique used to amplify and detect these single-DNA-base changes can generate false positives.

While cataloging mutations in cancers, the Johns Hopkins group hit upon a potentially better way to fish out tumor DNA. They noticed that all solid tumors had large chromosomal rearrangements that were unique to that patient's tumor. Rapid advances in DNA-sequencing technology have now made it practical to systematically look for such large-scale changes. In *Science Translational Medicine* this week, the Johns Hopkins team reports taking biopsies of breast or colon tumors from six people and sequencing the entire genome in each tumor's cells. In each case, the researchers identified rejiggered chromosomes specific to the tumor but not seen in a person's normal DNA.

The researchers then showed they could use PCR to pick out scant amounts of this distinctive tumor DNA from normal DNA, even if it constituted as little as 0.001% of the overall DNA sample. They next analyzed the blood of two people who had colon tumors that had been biopsied and genome-sequenced but not yet been removed. The blood of both tested positive for their specific cancer biomarker, whereas blood from healthy people tested negative. Finally, the researchers used the genetic fingerprint of one colon tumor to track that patient's response to various treatments (see graph). The amount of tumor DNA in the person's plasma declined in the hours after surgery, rose during the next few weeks, and then dropped again after chemotherapy and surgery for a secondary tumor in the liver.

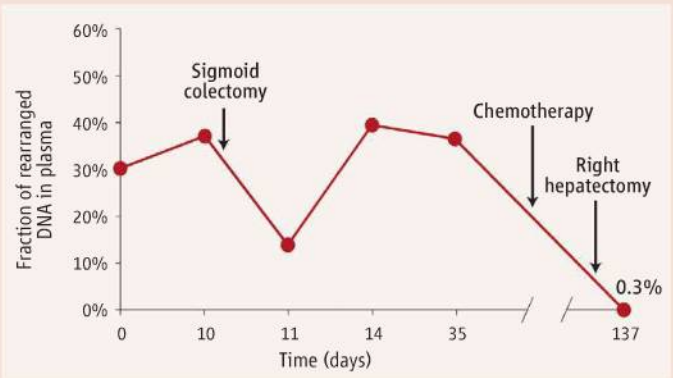

Cancer clue. Levels of free-floating tumor DNA in a colon cancer patient's blood plasma fluctuated during treatment.

Compared with single-base mutations, the chromosomal biomarkers are "extraordinarily specific. The chance of getting a false positive is essentially zero," says Johns Hopkins's Victor Velculescu, who led the pilot study. They could also be used to detect tumor DNA in other fluids and tissues.

Klaus Pantel of the University Medical Center Hamburg-Eppendorf in Germany, who studies both circulating whole tumor cells and free tumor DNA, enviously admits that his group has thought about the same genome-sequencing strategy. "It is a great approach," he says. But as Pantel and the study authors themselves note, the costs—$5000 per patient just to find the unique chromosome changes—must still come down significantly before the strategy could be available for routine use. And Howard Scher of the Memorial Sloan-Kettering Cancer Center in New York City cautions that tests for whole tumor cells and free-floating tumor DNA needed to be compared head to head in clinical trials to know which is more useful for a specific purpose.

–J.K.

"We're not ready for early detection, but the principle is there," says Haber. Bioengineers are also working on ways to physically filter CTCs out of the blood to prevent metastasis. Some oncologists seem skeptical that you could get rid of every last cancer cell without causing harmful side effects, but the National Cancer Institute is funding research on the topic.

Dangerous seeds?

Whatever the technique, CTC researchers are still struggling with the question of whether the cells they're capturing are the seeds for new tumors. Teams are chipping away at the problem by probing CTCs for the expression of genes thought to be involved in the EMT process or for stem cell markers. The latter is a more recent development as more cancer researchers have begun to believe that the cells initiating tumors have stem cell properties (*Science*, 24 August 2007, p. 1029). Several teams, including Cristofanilli's and Jeffrey's, have been finding CTCs that express EMT or stem cell genes.

Growth spurt. A mouse tumor generated from cultured CTCs (*right*) was twice as large as a regular tumor after 3 weeks.

A few labs are going a step further, trying to directly show that human CTCs can cause new tumors. "If anybody can prove that the few CTCs in human samples grow in mice, it would be almost a proof of their stem cell nature," says Pantel.

This, however, requires isolating sufficient numbers of living CTCs, which only a few labs have managed to do. Jeffrey's group has implanted cells cultured from a human cancer cell line in mouse mammary tissue, waited for tumors to grow, then isolated live CTCs from these mice using a new device that her team invented. When these CTCs were cultured and implanted in another set of mice, the resulting tumors grew larger and spread faster than tumors from the original cell line, her team reported online in January in the *British Journal of Cancer*. "These cells definitely were involved in metastasis," Jeffrey says. She eventually wants to culture CTCs from patients and implant them in mice to see if tumors form.

Cancer biologists are paying more and more attention to such experiments. "I'm thinking of CTCs all the time," says Massagué. If the details of these cells can reveal how human cancers spread, they may offer new ways of stopping it in its tracks.

–JOCELYN KAISER

CREDITS (TOP TO BOTTOM): LEARY *ET AL.*, *SCIENCE TRANSLATIONAL MEDICINE*/AAAS; K. AMERI *ET AL.*, *BRITISH JOURNAL OF CANCER* **102** (2010)

PLANETARY SCIENCE

Iceball Mars Proving a Tough Place to Find Liquid Water

Although Mars was once awash in flowing water, all the water found by orbiting radars has long been tied up in recurring ice ages

"The running joke is that somebody's about to announce the discovery of water on Mars, again," says planetary scientist Robert Grimm of the Southwest Research Institute (SwRI) in Boulder, Colorado. Actually, it was more than 30 years ago that researchers first discovered water on Mars, more than a million cubic kilometers of it frozen in the north polar ice cap.

More recently, water has been turning up far and wide on Mars, but—like the two polar caps—all of it is quite solidly frozen. "On a global scale, Mars has been cold, frozen, and dominated by ice for a long, long time," says planetary scientist Michael Mellon of the University of Colorado, Boulder. This frozen (or sometimes vaporous) water is looking increasingly dynamic, dancing across the planet between recurring ice ages. But radar's deep probing is pushing the search for liquid water—and possible oases of life—deeper and deeper into the planet.

Planetary scientists reported the latest water-ice findings at December's American Geophysical Union (AGU) meeting in San Francisco, California. Jeffrey Plaut of the Jet Propulsion Laboratory (JPL) in Pasadena, California, and Mars Advanced Radar for Subsurface and Ionosphere Sounding (MARSIS) team members reported detecting ice-rich deposits as deep as 1 kilometer beneath the 3-million-square-kilometer Dorsa Argentea Formation near the south polar cap. From its perch on the European Space Agency's Mars Express orbiter, MARSIS beams microwave pulses at the surface. A part of each pulse may reflect back from buried geologic strata. Compared with most rock, ice is relatively transparent to microwaves, so when microwaves easily penetrate deep into the subsurface, that implies the area is rich in ice.

Planetary geologists such as James Head of Brown University aren't surprised that roughly equal amounts of ice and rock underlie Dorsa Argentea. They had already recognized the sinuous ridges and channels of the region as lingering markers of a now-vanished ice cap. When its base was melting a couple of billion years ago, that cap was far larger than today's.

Where that ice cap's water went remains a mystery. So does the current whereabouts of the far more copious water that soaked Mars during its "warm and wet" era more than 4 billion years ago. But radar is on water's trail. At next week's Lunar and Planetary Science Conference (LPSC) in Houston, Texas, Plaut and team members on SHARAD (SHAllow RADar)—the radar flying on NASA's Mars Reconnaissance Orbiter—will report that ice is indeed abundant across the 1000-kilometer span of the Deuteronilus Mensae area on the edge of the great northern lowlands.

Geologists had inferred the presence of buried ice, but with repeated SHARAD passes, it can now be seen that there are hundreds of meters of nearly pure ice—covered by a few meters of protective rocky debris—in almost every valley and piled against almost every mesa across nearly all of Deuteronilus Mensae. Head and colleagues have shown from geological studies that this ice is just the residue of glaciers that hundreds of millions of years ago flowed off high plateaus from ice sheets up to 800 meters thick. Climate modeling has shown that when Mars nods far over on its axis—as it does on time scales of tens of thousands to millions of years—the solar energy added to the polar regions can drive water from the ice caps to snow out in mid-latitudes and form ice sheets (*Science*, 11 April 2003, p. 234).

Another residue from cyclic martian ice ages may still pervade high latitudes just centimeters beneath the surface. Analysis of cosmic-ray–induced gamma-ray and neutron emissions had pointed to water ice in the top meter of martian soil down to a latitude of 40°; the Phoenix lander touched some of that ice. But at the AGU meeting, both the SHARAD and the MARSIS teams reported signs of abundant high-latitude ice down as deep as a few tens of meters in both hemispheres. That's "exactly what we'd predict," says Head; Phoenix ice is a residue of past snow-fed glaciation. On the other hand, the Phoenix team and especially Mellon have argued that Phoenix ice is all just atmospheric water vapor that formed a dense frost between soil grains. That debate continues, although in an abstract for LPSC, Phoenix team member Michael Hecht of JPL jumps ship and argues for a glacial origin.

Ironically enough, the Mars radars were designed to hunt not for ice but for the missing liquid water from the planet's early days. Planetary scientists thought they would find liquid water in aquifers as radar probed as much as 5 kilometers beneath the surface. "We had expectations of a shallow aquifer, but we don't have any detections," Plaut said at the AGU meeting. "There are few if any large, shallow aquifers on Mars," he now says. Aquifers "are probably there," he adds, "just too deep to see."

Unfortunately, the radars are not probing as deeply as even the most pessimistic predictions, says planetary geophysicist Roger Phillips of SwRI, Boulder, a member of both radar teams. The problem may be radar-blocking clays. And radar has detected a rocky crust unbowed by the weight of the overlying north polar cap. That means less crust-weakening—and ice-melting—heat is flowing up from the interior than geophysicists had assumed, so any subterranean water would be frozen well beyond the reach of radar. So while geologists continue sorting out the climate history of Mars as frozen into the planet's ice, geophysicists will likely have to come up with another, more penetrating probe of the Red Planet. **–RICHARD A. KERR**

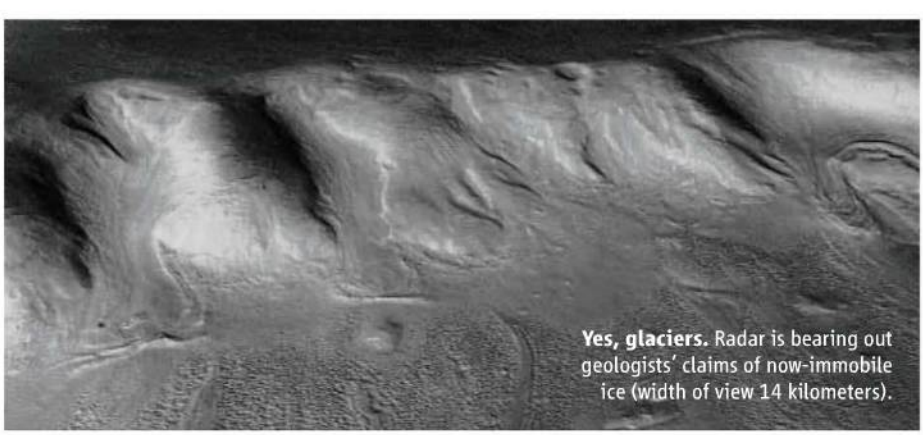

Yes, glaciers. Radar is bearing out geologists' claims of now-immobile ice (width of view 14 kilometers).

CREDIT: NASA/MRO/CTX/RENDERING BY JAMES DICKSON

Motley crew. Dogs gathered from a variety of sources await transport at a Class B dealer facility.

ANIMAL RESEARCH

Dog Dealers' Days May Be Numbered

Legislators want to shut down the pipeline of "random source" dogs and cats to laboratories, but some researchers worry about the impact on science

In the summer of 2005, a 1-year-old Labrador mix with brindle markings arrived on a truck at the University of Minnesota, Minneapolis. The dog, one of a handful of ostensibly unwanted canines rounded up by an animal dealer from local pounds, was to be implanted with an experimental heart device and eventually euthanized. But this dog was hardly unwanted. When research technicians passed a handheld scanner over his shoulder blades, they detected a microchip that they traced back to a man, three states away, desperately searching for his pet, Echo.

Cases like Echo's demonstrate what can happen when the so-called Class B dealer system breaks down. For more than 4 decades, individuals licensed by the U.S. Department of Agriculture (USDA) have collected dogs and cats from shelters, breeders, and other sources and sold them to research facilities. Proponents say these dealers provide genetically diverse breeds of various sizes and ages that can't be obtained from traditional laboratory animal suppliers and that are essential in some types of research. But detractors point to a history of misconduct, from stolen pets to animal cruelty, and have been trying for years to shut down the system. "By using these animals, we risk losing our credibility with the public," says Robert Whitney, who oversaw animal resources programs at the National Institutes of Health (NIH) for more than 20 years. "It's an Achilles' heel for research."

Last year, the National Academy of Sciences (NAS) released a report that backed up what Whitney and fellow thinkers have been saying. "Class B dealers are not necessary for supplying dogs and cats for NIH-funded research," it said, and recommended ways to phase out the system. The report is also giving fuel to a congressional bill that would ban these dealers outright.

But many in the research community are fighting back, even those who don't use Class B dealers. "These actions are premature," says Alice Ra'anan, director of Government Relations and Science Policy at the American Physiological Society (APS), which represents more than 10,000 scientists, doctors, and veterinarians. Any such ban, she says, would delay important research projects and could shut down others entirely. "It would be enormously disruptive."

The rise of animal welfare

Ironically, it was a case much like Echo's that helped create the Class B dealer system. In 1965, a Dalmatian named Pepper was stolen from a farm in Pennsylvania and sold to a research hospital in New York, where she died in a cardiac pacemaker experiment before her owners could locate her. The following year, *Life* magazine published "Concentration Camps for Dogs," a photo exposé of emaciated dogs, cats crammed into chicken crates, and other abuses at the property of a Maryland dealer who sold animals to research facilities.

Lab cat. Random-source cats may harbor important diseases not found in purpose-bred animals.

The stories galvanized the public, and in 1966 President Lyndon Johnson signed the Laboratory Animal Welfare Act into law. The legislation mandated the humane treatment of dogs, cats, and other laboratory animals. It also created two types of licenses—Class A and Class B—for selling animals to research. Class A dealers could sell only animals that they had raised themselves, while Class B dealers could sell animals they had acquired from "random sources," such as pounds, breeders, and even other dealers. Class A facilities tended to be large corporate entities that bred animals on site, while Class B dealers often ran smaller, "mom-and-pop" operations.

By the 1970s, the Class B dealer system was thriving. NAS estimates that there were about 200 dealers supplying thousands of dogs and cats to U.S. laboratories.

These animals proved critical to advances in science and medicine. Large-chested Dalmatians like Pepper helped doctors develop some of the first artificial-heart devices and lung-transplant procedures. And cats and dogs gathered from the general population harbored a variety of genetic diseases and infections that led to insights into everything from sleep apnea to AIDS.

Yet, despite USDA regulation, stolen and abused animals continued to show up at research institutions. So, in 1990, Congress toughened the Animal Welfare Act. Shelters now had to hold animals for 5 days before selling them to Class B dealers, and—as part of a new USDA "traceback" program—the dealers had to provide extensive documentation about where they got their animals, often detailing multiple sources over several states. Some shelters began refusing to sell cats and dogs to Class B dealers entirely.

The biggest blow to the Class B system came in 2003, when a member of a humane organization—Last Chance for Animals—infiltrated the Arkansas facility of a Class B dealer named C. C.

CREDITS (TOP TO BOTTOM): ANIMAL WELFARE INSTITUTE; RICHARD B. LEVINE/NEWSCOM

Baird and went public with accounts of sick, abused, and dying animals, many of which appeared to be former pets. The case became fodder for an HBO documentary and resulted in the largest investigation of animal abuse in U.S. history. USDA, blamed for not properly enforcing the Animal Welfare Act, intensified its traceback program and began unannounced quarterly inspections of Class B facilities.

The intense regulation took its toll. Today, only 11 Class B dealers sell dogs and cats to research facilities (hundreds of others sell nonhuman primates, pigs, and other animals), and more than half of these are under intense USDA scrutiny. Together, they supply about 3000 dogs and cats—about 3% of the 90,000 or so used in U.S. research.

Yet critics have been unable to shut down the system entirely. In 1996, federal legislators first introduced the Pet Safety and Protection Act, which would have outlawed the sale of cats and dogs to researchers from Class B dealers. But APS and other research groups opposed it, and it has failed to pass every year it has been proposed. That may change with the release of last year's NAS report.

"Concentration camps." A photo from the 1966 *Life* magazine exposé that helped create the Class B dealer system.

CREDIT: STAN WAYMAN/TIME LIFE PICTURES/GETTY IMAGES

The leash tightens

The report seems damning in its conclusions. Commissioned by Congress in response to Echo, C. C. Baird, and other incidents, it found that although Class B dog and cat dealers had provided a vital service to biomedicine, the system was now obsolete and even potentially damaging to research. "There is a minority of dealers that are totally legitimate and doing the job well," says Stephen Barthold, the chair of the report committee and director of the Center for Comparative Medicine at the University of California, Davis. "But others have sullied the reputation and are taking down the whole thing."

Class B dealers, the report found, were no longer providing the valued diversity they had in the past. Shut out of shelters and forced to rely on breeders and private owners, the dealers were selling researchers primarily young hounds and beagles—essentially the same type of dogs Class A dealers were providing. "We could not find any compelling evidence that these animals were unique," says Barthold.

The committee also concluded that, because of limited resources, USDA could not properly regulate the Class B system. "USDA is supposed to ensure compliance," says Barthold, "but they've done a bad job." And that meant stolen and abused animals could still end up in U.S. research labs. "It's a very negative public stigma that, personally, I don't think NIH needs," Barthold says. USDA refutes those claims: "The record over the years shows that we've enforced the system very well," counters Robert Gibbens, who oversees USDA regulation of Class A and B dealers in the western United States.

The NAS committee recommended several ways to phase out the Class B dog and cat system. It suggested that researchers get their animals directly from pounds and shelters. It advised paying Class A dealers to provide older and more genetically diverse animals. And it proposed that universities or NIH set up consortia to share dogs and cats, as has been done for primates and rodents. "There are so many possible sources for these animals," says Cathy Liss, president of the Washington, D.C.–based Animal Welfare Institute (AWI), which has tried to find a middle ground between groups like APS and those who want to eliminate cat and dog research entirely. "It's about trying to ensure integrity in the supply."

But these ideas have not sat well with scientists who still rely on the Class B system. "All of the possibilities … wouldn't work as far as I'm concerned," says a cardiovascular researcher who asked to remain anonymous so as not to draw attention to his university. For more than 30 years, he has used large and old random-source dogs from Class B dealers to study cardiovascular diseases and develop medical devices. Class A dealers don't stock these dogs, he says, because it's more economical for them to sell puppies. Nor can he get them from shelters, because most no longer sell to researchers. And he says he doesn't understand why NIH or Class A dealers should breed extra dogs and cats for terminal research, when millions of shelter animals are euthanized every year.

"There may not be a lot of groups in America still using Class B dogs for research," he says, "but the numbers do not reflect the importance of the research being done."

End of the pipeline?

Still, the end seems near for Class B dog and cat dealers. Last fall, Representative Mike Doyle (D–PA) and Senator Daniel Akaka (D–HI) reintroduced identical versions of the Pet Safety and Protection Act (H.R. 3907 and S. 1834, respectively). With the National Academies' report, "we're in a better position to pass this bill than we've ever been," says Doyle. NIH's response to the report, which is expected this spring, could include halting future funding for research that uses Class B dogs and cats.

Even APS seems to acknowledge that the system is on its way out. The society has endorsed the NAS report, and Ra'anan says it wants to work with NIH to develop viable alternatives. She's arguing for a 5-year transition period, especially for labs that have ongoing projects with random-source animals. "This is not something that can be done overnight," she says, "but we need to get the ball rolling."

Some universities have already started. Duke, Yale, and MIT, for example, discourage their researchers from obtaining cats and dogs from Class B dealers. Says AWI's Liss: "Institutions need to step up to the plate."

At least one dealer says it is planning on shutting down on its own. "I don't see how the system can continue to survive like this," says Janice Hodgins, who has run a Class B facility in Howell, Michigan, with her husband since 1960. At one time, the operation housed more than 300 dogs and cats, used in everything from hip-replacement studies to mental health research. Today, they have just nine. "There's been a lot of things learned through random-source animals," she says, "but I feel like we're on the losing end of this now."

–DAVID GRIMM

LETTERS

edited by Jennifer Sills

Sowing the Seeds of Soil Conservation

IN THEIR PERSPECTIVE ("MONITORING EARTH'S CRITICAL ZONE," 20 November 2009, p. 1067), D. deB. Richter Jr. and M. L. Mobley argue for the importance of monitoring Earth's belowground critical zone for sustaining life and humanity. Their message echoes a similar call from a different era. "The Nation that destroys its soil destroys itself." These words of President Franklin Delano Roosevelt in his 1937 letter to all state governors referred to the Soil Conservation Act of 1935, which recognized the need to sustain soil resources. The Standard Soil Conservation District law was subsequently adopted by all 50 states, plus Puerto Rico and the Virgin Islands. Historical aerial photos across the country from 1947 to 2004 (*1*) provide evidence that the law has been effective in protecting many farmlands and show that visible erosion in the form of gullies is now almost nonexistent in comparison with the erosion that occurred in the 1930s. In the decades since the Natural Resources Conservation Service started the National Resources Inventory in 1982, soil erosion on U.S. croplands has decreased 43% (*2*).

Fighting erosion. Contour stripcropping is one method used to protect soils.

Laws like the one President Roosevelt championed in the 1930s are more important today than ever. Urban sprawl, land degradation, environmental pollution, and anthropogenically accelerated erosion (to name just a few) are detrimental to sustainable food production and quality water supply for the growing world population. Modern soil vulnerability to global change and anthropogenic threats (beyond just croplands) is unprecedented. This issue was not addressed in the 1930s law but could have devastating effects. Monitoring and protecting the belowground critical zone is a crucial step to ensure that we do not lose ground for sustainability.

HENRY LIN

Department of Crop and Soil Sciences, The Pennsylvania State University, University Park, PA 16802, USA. E-mail: henrylin@psu.edu

References

1. L. E. Mathews, *Aerial Photography Field Office Historical Imagery Holdings for the United States Department of Agriculture* (2005); www.apfo.usda.gov/Internet/FSA_File/vault_holdings2.pdf.
2. Natural Resources Conservation Service, *National Resources Inventory 2003 Annual NRI: Soil Erosion* (2007); www.nrcs.usda.gov/technical/NRI/2003/SoilErosion-mrb.pdf.

Spain's Budget Neglects Research

RESEARCH AND INNOVATION ARE CRUCIAL for the development and well-being of society. Now, in times of economic downturn, the urgency of changing the economic model to provide sustainable growth has become apparent. However, investment in R&D is the first collateral damage in the Spanish national budget, and many regional governments have also cut spending; all this in spite of the fact that Spain only dedicates 1.35% of its gross national product to R&D (*1*). These cuts will deeply affect aspiring researchers; researchers with temporary contracts will find that, after years of work and training, their contracts may not be renewed.

R&D has been completely neglected in the recent special anti-crisis measures, referred to as "Plan-E" (*2*), even though funds dedicated to science and its infrastructure would have met the same goals and been profitable in subsequent years. A training program for future researchers and technicians would have provided opportunities for laid-off workers from other sectors. It would also have been an excellent time to promote R&D in the private sector.

Unfortunately, the Spanish science system also has endemic deficits, such as continuous changes in management personnel and structure; lack of a fixed calendar of calls; bureaucratic delays; arbitrariness in the selection, promotion, and stabilization of personnel; and paralysis of necessary legislative initiatives.

We believe that it is time to demand a binding, long-term commitment from all parties to equip the Spanish science system with stability and prestige; a real increase in funding for R&D, so that spending first equals and then exceeds the European average; and rational planning to support the different stages of scientific careers.

The authors of this Letter have written a manifesto (*3*), summarized here, that has the support of many scientific groups. We believe that the moment has arrived for the scientific community to join forces. Learn more about our mission at www.investigaresfuturo.org.

XOSÉ AFONSO ÁLVAREZ,[1,2] NOEMÍ CABRERA-POCH,[3,4,5] ANA CANDA-SÁNCHEZ,[1,6] CARLOS FENOLLOSA,[4,7]* ELENA PIÑERO,[1,8] MARK J. VAN RAAIJ,[9,10] EVA SÁNCHEZ COBOS,[11,12] IGNACIO SEGURA PÉREZ,[1,13] FRANCISCO J. TAPIADOR,[3,14] ANA M. TORRADO AGRASAR[15,16]

CREDIT: RON NICHOLS/USDA-NRCS

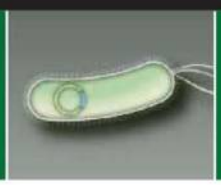

Prion protocol
1091

SPORE prize essay
1095

[1]Federación de Jóvenes Investigadores. [2]Universidade de Lisboa, 1649-003 Lisboa, Portugal. [3]Asociación Nacional de Investigadores Ramón y Cajal. [4]Plataforma por la Investigación. [5]Instituto de Investigaciones Biomédicas de Madrid, CSIC-UAM, 28029 Madrid, Spain. [6]MRC Toxicology Unit, Lancaster Road, LE1 9HN Leicester, UK. [7]Molecular Modelling and Bioinformatics Lab, Instituto Nacional de Bioinformática, Parc Científic de Barcelona, 08028 Barcelona, Spain. [8]Marine Biogeochemie–Marine Geosysteme, IFM-GEOMAR, Leibniz-Institut für Meereswissenschaften (an der Universität Kiel), 24148 Kiel, Germany. [9]Asociación para el Avance de la Ciencia y la Tecnología en España. [10]Departamento de Biología Estructural, Instituto de Biología Molecular de Barcelona–CSIC, Parc Científic de Barcelona, 08028 Barcelona, Spain. [11]Asociación de Investigadores Juan de la Cierva. [12]Departamento de Química, Física, Facultad de Ciencias, Universidad de Granada, 18071 Granada, Spain. [13]Mechanical Engineering Division, CARTIF Technology Centre, Parque Tecnológico de Boecillo, 205, 47151 Boecillo, Valladolid, Spain. [14]Institute of Environmental Sciences (ICAM), Universidad de Castilla-La Mancha, 45071 Toledo, Spain. [15]Asociación de Investigadores Parga Pondal. [16]Facultade de Ciencias, Universidade de Vigo, 32004 Ourense, Spain.

*To whom correspondence should be addressed. E-mail: carlesfe@mmb.pcb.ub.es

References

1. Instituto Nacional de Estadística, Notas de Prensa (2009); www.ine.es/prensa/np575.pdf.
2. Gobierno de España, "¿Qué es el Plan E?" Plan Español para el Estímulo de la Economía y el Empleo; www.plane.gob.es/que-es-el-plan-e/.
3. Plataforma por la Investigación, "Research is an investment in the future"; http://porlainvestigacion.blogspot.com/2010/02/research-is-investment-in-future.html.

LIFE IN SCIENCE

The Cow Ate My Fieldwork

Life is easier today than when I studied stream temperature more than half a century ago. Unlike today, when scientists can collect data with automatic loggers, we had to be in the stream for every data point, night and day.

Back then, during winter nights, a fire and an improvised shelter made life more comfortable. An alarm clock rang when it was time to read the thermometer. During summertime, we set up shelters in haystacks. I have good memories of those nights: shooting stars, nocturnal birds, and moonlight. However, I eventually realized that I had to choose between good data and pleasant memories. So I went high-tech: a mercury thermograph. The device was clumsy and heavy, but it could paint a week's temperatures on paper on a rotating drum. I had decided to investigate a weak trend in my haystack data with the new equipment. Four weeks of extraordinary high summer had confirmed an increasing trend. Now, at the last and most critical station, the thermograph had painted the temperatures of another high-summer week. How exciting it was to remove the paper from the drum and discover the trend that I had suspected—data destined for future textbooks! Eager to duplicate the findings, I changed the paper on the drum, leaving the saved graph safe under the weight of a stone. Busy and excited, I was not aware that I had company. No, it was not a farmer's young daughter, but a farmer's young and very inquisitive calf. In a split second, he snatched my paper graph from under the stone with his long tongue and ran.

I pursued the fleeing beast, got a firm hold on its tail, lost my balance, and was drawn through water and dirt, only to watch the mischievous creature slowly and deliberately consume my data.

Needless to say, this was the end of the high summer. And of my venture into fluvial temperature regimes.

BENT LAUGE MADSEN

Danish National Agency of Forest and Nature (retired). E-mail: bent@laugemadsen.dk

EDITOR'S NOTE

This is an occasional feature highlighting some of the day-to-day humorous realities that face our readers. Can you top this? Submit your best stories at www.submit2science.org.

CREDIT: PETER HOEY/WWW.PETERHOEY.COM

The Permanence Debate

E. KINTISCH ("DEFORESTATION MOVES TO THE fore in Copenhagen," News of the Week, 11 December 2009, p. 1465) identifies a number of issues hindering an agreement on Reducing Emissions from Deforestation and Forest Degradation (REDD). However, he does not mention permanence, which has dogged the REDD discussions for some time (*1*). Many negotiators fear that reductions in loss of forest carbon stocks may be credited and rewarded now, but that the forest may later disappear (whether cut or affected by die-off due to climate changes). They contrast this scenario with that of fossil fuels, for which they argue that savings are permanent.

This argument is flawed. There is a finite quantity of fossil fuel underground. Clean technology slows the rate at which it is extracted and burned, but eventually it will all be converted to CO_2. REDD will slow the rate at which carbon is emitted from forests in an analogous way. The conceptual muddle about permanence occurs when people confuse "stocks" with the "rate of change of stocks." Reduced emissions from deforestation and forest degradation are, like fossil fuel reductions, calculated on the basis of lowered annual losses compared to business as usual, not on the basis of stock remaining.

There is only one difference between stocks of fossil carbon and stocks of living carbon, in terms of permanence. Carbon lost due to deforestation or forest degradation in one place can be replaced by reforestation or enhancing carbon stocks in degraded forests elsewhere, whereas fossil fuels cannot be replaced at all.

MARGARET SKUTSCH[1]* AND BEN H. J. DE JONG[2]

[1]Centro de Investigaciones en Geografía Ambiental, Universidad Nacional Autónoma de México (UNAM), Morelia, Mexico. [2]Unidad Villahermosa, El Colegio de la Frontera Sur (ECOSUR), Villahermosa, Mexico.

*To whom correspondence should be addressed. E-mail: mskutsch@ciga.unam.mx

Reference

1. M. Dutschke, A. Angelsen, in *Moving Ahead with REDD: Issues, Options and Implications*, A. Angelsen, Ed. (CIFOR, Bogor, Indonesia, 2008), pp. 77–86.

Letters to the Editor

Letters (~300 words) discuss material published in *Science* in the previous 3 months or issues of general interest. They can be submitted through the Web (www.submit2science.org) or by regular mail (1200 New York Ave., NW, Washington, DC 20005, USA). Letters are not acknowledged upon receipt, nor are authors generally consulted before publication. Whether published in full or in part, letters are subject to editing for clarity and space.

BIOMEDICINE

Of HeLa and Human Lives

Leigh Krietsch Boerner

It is hard to imagine a scientist who hasn't heard of HeLa cells. Rapidly reproducing and amazingly robust, these cervical cancer cells have become indispensable in modern biomedical research. Their nearly ubiquitous cell line has been used in innumerable experiments that required a human cell culture. It has served in work ranging from the creation of a polio vaccine, to the development of leukemia treatments, to discoveries in cloning and gene mapping.

Despite the vast amounts of scientific data on HeLa, most people know very little about the cells' origin. Obviously they came from a woman, but who was she? HeLa, from the initial letters of the donor's first and last names, provides a small clue. Commonly reported as Helen Larson or Helen Lane, her actual name was Henrietta Lacks. But just knowing her name does not tell us that she was poor, that she was black, or that she was largely uneducated. It does not tell us how she died, moaning in agony, in the free ward of Johns Hopkins Hospital in 1951, when she was barely 31 years old, leaving behind five children. Nor does it tell us how her cells were taken without her knowledge and without her consent.

Rebecca Skloot's *The Immortal Life of Henrietta Lacks* does tell us all these things—and more. It gives us Henrietta's life, laid out like a cell under a microscope. And like any good scientific research, this beautifully crafted and painstakingly researched book raises nearly as many questions as it answers: questions about ethics, racism, and, most importantly, humanity.

Skloot (who teaches creative nonfiction at the University of Memphis) twines together the strands of HeLa cells and Henrietta Lacks and of "Henrietta's family … and their lifelong struggle to make peace with the existence of those cells, and the science that made them possible." She does that so eloquently one can't imagine the story being told any other way. Most notably, Skloot presents people in a completely straightforward manner. She does not insert her own opinions of them, just gives us the details and lets us decide for ourselves.

Her approach is particularly important in regards to the scientists, especially Richard TeLinde (chair of the hospital's gynecology department) and George Gey (head of tissue culture research at Hopkins). TeLinde, who was collecting biopsies from patients for a cervical cancer study, offered Gey samples from which to attempt to grow some cells. Having been trying for over 30 years to establish an "immortal" cell line, Gey jumped at the chance. He and Margaret Gey succeeded at culturing Lacks's cells and discovered their amazing capacity for reproduction.

The Immortal Life of Henrietta Lacks

by Rebecca Skloot

Crown, New York, 2010. 392 pp. $26, C$32. ISBN 9781400052172.

In a time when it's fashionable to demonize scientists, Skloot generously does not pin any sins to the lapels of the researchers. She just lets them be human. The humanity of Gey comes out in particular relief. Instead of spending his time publishing his HeLa results, Gey flew around the country helping other labs set up the culturing techniques he had developed, and he gave away HeLa cells. Eventually, he was scooped by a lab to which he had distributed cells.

CREDIT: COURTESY THE LACKS FAMILY AND CROWN

Henrietta and David Lacks. She died in 1951, while the cancer that killed her lives on in HeLa.

Did Gey or TeLinde really see Lacks as a person, possessing rights about what happened to her cells? Likely not: they saw her as a patient. At the time, it was generally held that physicians could use patients treated in a free ward as research subjects (with such use seen as a form of payment). But Mary Kubicek, Gey's young lab assistant, did eventually recognize Lacks as more than a cell source. After Lacks died, Kubicek was sent to collect additional samples directly from the body. Noticing the toenails Lacks had meticulously kept painted red, she "'started imagining her sitting in her bathroom painting those toenails, and it hit me for the first time that those cells we'd been working with all this time and sending all over the world, they came from a live woman. I'd never thought of it that way.'"

Anyone who has ever worked with HeLa cells will find it easy to relate to this revelation. Some years back, I injected a drug our lab group had synthesized into a group of HeLa cells. I watched the treated cells through a fluorescence microscope, the blue dots of drug shining out like stars from the white of Henrietta's cells, and thought, "Who was this person?"

At 16, Skloot asked the same question after hearing about Henrietta Lacks in a biology class. She could find little information then, but curiosity kept the story in the back of her mind. Eventually, she returned to it and spent 10 years researching and writing her book, during which she got Lacks's reticent family to talk to her.

The book's first half intertwines the stories of Lacks and the science of HeLa. The second half binds together the author's own desire to learn Lacks's story with that of Lacks's daughter, Deborah. Veering from the road usually trod by journalists, Skloot forms a close emotional bond with Deborah Lacks and becomes a character in her own book. Such a presence can be risky, but she makes it work. Skloot presents Deborah's emotionally charged story of confusion and loss in the same unassuming style with which she told the scientists' stories: she does not judge, just tells what happened. And by writing her story this way, Skloot draws in anyone who, like her and me, has ever wondered who was the person from which researchers obtained HeLa.

In the prologue, Skloot remarks, "The Lackses challenged everything I thought I knew about faith, science, journalism, and race." Similarly, Skloot challenges much of what we believe of ethics, tissue owner-

The reviewer is at the Department of Chemistry, Indiana University, Bloomington, IN 47405, USA. Web page: http://ljkboerner.wordpress.com

ship, and humanity. Looking back, it may seem easy to say that those cells never should have been taken from Lacks in the first place. But can you imagine a world without HeLa cells? Without the advancements that they've helped us make?

The HeLa cells I used in my experiment, now two years past, still sit at the back of my waste cabinet. I just can't seem to throw them away. Likewise, the story that Skloot tells is something that will not be easily forgotten. Thanks to the author's narrative skills, it is a tale that one experiences rather than reads. Through her cells, Henrietta Lacks was already immortal. But with this book, Skloot may make her story immortal as well.

10.1126/science.1186755

GEOPHYSICS

The Prediction Puzzle

Christopher H. Scholz

Predicting the Unpredictable
The Tumultuous Science of Earthquake Prediction

by Susan Hough

Princeton University Press, Princeton, NJ, 2010.
269 pp. $24.95, £16.95.
ISBN 9780691138169.

The devastating San Francisco earthquake of 1906 produced various reactions among scientists and the general population. It provided the first demonstration that earthquakes were the result of slip on a previously recognized fault, which had been steadily strained over time by tectonic movements. Grove Karl Gilbert proposed in 1909 that by measuring such deformation, one could estimate the expected time for the next such earthquake, the basis for what is now called long-term earthquake prediction. He wrote "and now … the people of the civilized earth—the lay clients of the seismologist—would be glad to know whether the time has yet come for a scientific forecast of the impending tremor." (*1*)

Local business leaders took a different view. They proclaimed that the city was destroyed by fire (a far less fearsome menace) and not by the earthquake, ignoring the fact that the earthquake caused both the fires and the city's inability to extinguish them. In 1915, they celebrated the rebirth of the city by hosting the Panama-Pacific International Exposition. It took place in an area, later called the Marina District, built on landfill that included earthquake rubble. This latter bit of hubris was rewarded by the extensive damage from liquefaction of that landfill by the 1989 Loma Prieta earthquake.

As suggested in the subtitle of Susan Hough's *Predicting the Unpredictable*, the topic of earthquake prediction—both within the scientific community and in its relation with the public—has always been tumultuous. Thus, as she relates, Bailey Willis, a leading geologist and Stanford professor, led a campaign in the 1920s to call attention to earthquake hazards in California, only to have his reputation besmirched by a counter-campaign led by business interests.

Hough, a seismologist with the U.S. Geological Survey (USGS), offers a history of earthquake prediction science. Her account focuses on the American experience and particularly on the USGS, which is the primary U.S. agency for earthquake science. It is written for a general audience, and she manages to convey concepts while keeping the science clear. Earthquake prediction became an announced goal of U.S. earthquake research during the 1970s, and most of the book covers the period since then. Hough describes all the memorable pitfalls and pratfalls of this era with an equanimity that is remarkable, considering the contentiousness of the subject matter.

The long-term prediction scheme outlined by Gilbert has become standard practice for estimating seismic hazards in regions with known active faults. It was the basis of the belated warning by Eric Calais and colleagues of the recent earthquake in Haiti, and it underlay some of the debated predictions of the Loma Prieta earthquake that Hough briefly recounts. Her book's main topic, however, is what the public usually thinks of as earthquake prediction: the forecasting, in a time frame of weeks or months, of the time, location, and magnitude of an impending earthquake.

We do not yet know whether or not such short-term prediction is possible. It requires the existence of some precursory phenomena that are both sufficiently universal and diagnostic. One approach is to look for indications of an advanced state of stress that might signal an impending earthquake. Hough reviews attempts, now mostly forsaken, of this type, which have been sometimes based on theory, sometimes on empiricism. Another approach is to find a precursor that foreshadows earthquake initiation. Current theory of earthquake stability, for example, predicts a nucleation stage during which stable sliding occurs on a patch of the fault where the earthquake will initiate. The theory, however, is presently too sketchy to be very useful.

Short-term prediction research is a poorly posed problem, because carrying out a field experiment to identify precursors requires that one has already made a prediction. Two experiments of this type have been attempted. The Japanese identified the "Tokai gap," a section of plate boundary near Shizuoka that seemed long overdue for a major quake. Similar reasoning led the USGS to predict an earthquake would occur in 1988 on a short section of the San Andreas Fault near Parkfield, in central California. Both areas were heavily instrumented to detect precursors. In the meantime, despite (and perhaps to spite) these attentions, other, less-studied faults in California and Japan ruptured in damaging earthquakes. The 1995 earthquake that heavily damaged Kobe occurred on a known, but slowly moving and unmonitored fault: an embarrassment to the Japanese earthquake prediction program. The Tokai gap earthquake has yet to occur. In California, the Parkfield earthquake long outlasted its prediction window. When it finally occurred in 2004, it initiated at the south end of the fault segment—rather than, as expected, in the north, where the bulk of the instrument cluster had been installed. Another kind of hubris was repaid.

As *Predicting the Unpredictable* reminds us, after 100 years, it seems that the answer to Gilbert's rhetorical question is: Not yet.

The reviewer is at the Department of Earth and Environmental Sciences, Lamont-Doherty Earth Observatory, Columbia University, 61 Route 9W, Palisades, NY 10964, USA. E-mail: scholz@ldeo.columbia.edu

While instruments waited at Parkfield. Damage in San Francisco's Marina District from the 1989 Loma Prieta earthquake.

CREDIT: C. E. MEYER/USGS

References
1. G. K. Gilbert, *Science* **29**, 121 (1909).

10.1126/science.1187372

INTELLECTUAL PROPERTY

Fixing the Legal Framework for Pharmaceutical Research

The outdated Hatch-Waxman Act and judicial retroactivity challenge costly development of new pharmaceuticals.

Sherry M. Knowles

The cost of drug research and development (R&D) has increased from ~$230 million per drug in the early 1980s to $1.2 billion today, with R&D currently requiring about 10 to 15 years per drug (*1*–*4*). This investment of time and money cannot be sustained without a legal system that provides sufficient time to recoup the investment and to secure a reasonable return, as well as the ability to make important business decisions that remain correct over a long period of time. Pharmaceutical companies have historically relied on two kinds of market protection: (i) the exclusive ownership of their own clinical research and (ii) patents. However, the U.S. Hatch-Waxman Act (*5*), which is designed to strike a balance between innovative pharmaceutical research and access to generic drugs, is flawed. Further, U.S. courts sometimes retroactively change standards for patent protection long after large R&D efforts have been initiated, which increases the risk to defend and rely on patent protection.

The Hatch-Waxman Act

The 1984 Hatch-Waxman Act applies to pharmaceuticals, not biologic products. It allows producers of generic drugs to use, without cost, all preclinical and clinical data to support approval of the drug that were filed by innovator pharmaceutical companies with the U.S. Food and Drug Administration (FDA) (*6*). Five years after approval of a "new chemical entity" innovator drug, a generic company can simply reference the innovator's data to support the generic drug application (*7*–*9*). If the innovator company does not have a patent protecting the product or if a court rules the patent invalid or nonenforceable, the generic company can then obtain approval to sell the drug, simply by referencing the innovator data and submitting only enough data to demonstrate that the innovator and generic drugs are bioequivalent (*10*). Furthermore, the usefulness of a patent on a drug typically only begins after drug approval, and the FDA requires 10 to 15 years of preapproval R&D after a patent application is filed. So, in exchange for the forced sharing of data with generics, under Hatch-Waxman, innovators are granted up to five additional years of post–drug approval patent protection, but in no event can the patent extend more than 14 years after the drug approval (the "14-year cap").

How does this quid pro quo work in practice? The 5-year data exclusivity period was a political compromise 26 years ago during Hatch-Waxman negotiations without substantial supporting economic analysis. This period is vastly inadequate today and rarely covers the breakeven point for reimbursement of R&D costs. Because of this, new drugs are almost never developed without patent protection, which limits the number of new drugs created (as not all useful drugs are patentable).

For those few drugs that are developed without patent protection or that lose patent protection through court decisions, does the forced sharing of expensive clinical research data with generics amount to a federal taking of property from the innovator pharmaceutical company? The "Takings Clause" of the Fifth Amendment provides that "private property" shall not "be taken for public use, without just compensation" (*11*). In the past 26 years, the cost of drug development has increased sixfold, and the period of data exclusivity given to innovator pharmaceutical companies for new drugs is still half the period given for pesticides (*12*). Without a change to update the law to increase the period of data exclusivity, compensation from the government for the involuntary use of innovator R&D data files by generic companies to obtain drug approvals seems fair.

Once a U.S. patent is granted, which the Patent Office intends to take ~3 years, the patent has a term of 20 years after the filing date (*13*). However, as discussed above, under Hatch-Waxman, the new drug gets capped at 14 years of useful post–drug approval patent term. This creates the situation where a relatively unregulated, simple, inexpensive invention may receive 17 years or more of useful patent term, whereas more expensive and important pharmaceutical innovations get useful patent terms capped at 14 years (*14*).

Changing Requirements for Patentability

A patent application filed today on a pharmaceutical innovation will not be used to defend a market for about 15 years. What will the law look like in 2025? How can companies make long-term investment decisions that remain accurate over 15 years or more?

"The Supreme Court is reconsidering … what constitutes patentable subject matter. At what point does an idea pass from an abstract theory to a patentable invention?"

Under the U.S. Constitution, Congress makes laws, and the courts interpret and apply them. However, there may be little practical difference to a corporation between changing a law and changing the interpretation of a law. Both change the rules of the game. However, when Congress passes laws, they apply prospectively, whereas when courts reinterpret the law, the new interpretation is applied retrospectively to business decisions that occurred sometimes long before (*15*). When a significant change in interpretation of a statute alters the burden to prove patentability, it can convert valid patents into invalid patents, or invalid patents into valid patents. The former can eviscerate the value of research programs, and the latter can create increased infringement exposure. Both disrupt well-settled expectations, which can affect the outcome of long-term business decisions and can have an effect indistinguishable from a congressional change in law.

In 2007, the U.S. Supreme Court issued the landmark decision *KSR* v. *Teleflex* (*16*), in which the court changed the longstanding interpretation of the statutory requirements to prove nonobviousness of an invention. This case has been perceived by some as weakening patent protection by holding an invention unpatentable if there are a finite number of identified predictable alternatives that would

Chief Patent Counsel, GlaxoSmithKline, King of Prussia, PA 19406, USA. E-mail: sherry.m.knowles@gsk.com

be obvious to try. The prior law had emphasized that obviousness required a reasonable expectation of success (*17*). The case also, for the first time, sanctioned the combination of references from unrelated fields to prove obviousness (*18*) and held that "ordinary creativity" may not qualify for patent protection. In this way some have argued that the bar for patentability was raised without the type of public debate and stakeholder voice that occurs during the consideration of a new law in Congress. Also, it applied retroactively. Some research programs funded by biologic or pharmaceutical companies in reasonable reliance on the old law were suddenly at risk of no patent protection, with a potential wasting of employee time and resources (*19*).

In the case of *In re Bilski* (*20*, *21*), the Supreme Court is reconsidering how to interpret the statute covering what constitutes patentable subject matter (*22*). At what point does an idea pass from an abstract theory to a patentable invention? Relevant to the pharmaceutical industry could be the patentability of medical diagnostic methods, assays, and the use of biomarkers (*23*).

In *Ariad* v. *Lilly*, the U.S. Court of Appeals for the Federal Circuit (CAFC), is reconsidering how to interpret a statute that defines how much and what kind of patent disclosure is necessary to provide an adequate description of an invention (*24*–*26*). This statute, with wording that has not changed in 57 years, could thereafter be reconsidered by the U.S. Supreme Court. Is it sufficient that a patent applicant teach how to obtain an innovation, or must the applicant go further and actually provide sufficient detail on what the invention is, such as physical characteristics of the innovation itself, to establish that the applicant had possession of the invention at the time of filing? For example, is it sufficient to teach how to obtain a new pharmaceutical drug, gene, or protein, or must one describe exactly what the new drug, gene, or protein is?

Retroactive judicial decisions can have several effects. They can facilitate the increase of challenges by generic producers under Hatch-Waxman, which compresses the pay-back period for drugs. They can stop R&D investment decisions that have already been made and could prevent a product from reaching the market because of patentability issues. They can also potentially prevent some R&D from taking place to begin with.

An issued patent is property just like a piece of land or a house (*27*, *28*). When a federal judicial decision dramatically changes the law, such that a valid patent becomes invalid, has the federal government taken private property in violation of the federal Constitution? Application of the Fifth Amendment is not clearly limited to legislative and executive action; nothing in its text bars extension of the takings clause to judicial action. This question continues to be debated (*29*, *30*).

Conclusion

The time has come to rethink the right legal framework to promote and protect investment in pharmaceutical research and development. The Hatch-Waxman Act should be amended to increase the period of R&D data exclusivity from 5 to 14 years (consistent with the current patent term cap) (*31*). This should substantially increase the number of drugs in the R&D pipeline, which could greatly benefit patients and ultimately benefit generic companies. The act should also be amended to allow at least one patent term on the drug to begin on FDA approval. In this way, the innovator is not penalized for the lengthy federal regulatory review process. In addition, to provide an environment that supports long-term good faith business decisions and protect justified prior reliance by innovators, Congress should pass a law that gives an appellate court discretion to mark a decision for prospective application only, if it overrules a prior interpretation of patent statutory law.

References and Notes

1. J. A. DiMasi, H. G. Grabowski, *Manag. Decis. Econ.* **28**, 469 (2007).
2. J. A. DiMasi, *Pharmacoeconomics* **20** (Suppl 3), 1 (2002).
3. J. A. DiMasi, R. W. Hansen, H. G. Grabowski, *J. Health Econ.* **22**, 151 (2003).
4. J. A. DiMasi, R. W. Hansen, H. G. Grabowski, L. Lasagna, *J. Health Econ.* **10**, 107 (1991).
5. The Drug Price Competition and Patent Term Restoration Act of 1984, 21 U.S. Code (U.S.C.) § 355.
6. 21 U.S.C. § 355(c)(3)(E)(ii).
7. This 5-year term is often referred to as a "data exclusivity period" but may be considered a forced data-sharing requirement.
8. M. J. Higgins, S. J. Graham, *Science* **326**, 370 (2009).
9. If a generic company files an abbreviated new drug application during the 5-year period and certifies that a listed innovator patent is invalid or not infringed, the FDA will stay approval of the generic drug for 30 months during patent litigation, up to a cap of 7.5 years. See (*32*).
10. The cost to generic companies of demonstrating bioequivalence typically pales in comparison to the cost to innovator companies of collecting preclinical and clinical safety and efficacy data.
11. U.S. Const. amend. V.
12. In *Ruckelshaus* v. *Monsanto Company* (*33*), the U.S. Supreme Court held that a federal law that allows companies to rely on innovator pesticide data to get approval for a generic version 10 years after first approval is not a taking of property, as Monsanto was aware of the law when it submitted its innovator data for pesticide approval. However, in the post-Monsanto case of *Palazollo* v. *Rhode Island* (*34*), the Supreme Court held that takings claims cannot be defeated merely because the legislature has amended a statute to give prospective notice of some new limitation on property. Hence, Hatch-Waxman is not insulated from takings claims involving patents issued after that statute was passed, and the economic impact of the outdated law supports compensation.
13. Contents and term of patent; provisional rights, 35 U.S.C. § 154.
14. As one example, U.S. Patent No. 6,637,447 covering the "Beerella" an umbrella that snaps onto a beer bottle has 18 years of useful patent life, whereas U.S. Patent No. 6,713,485 on a metastatic breast cancer therapy has 13.5 years of useful life.
15. If a court makes a ruling prospective only, it appears to cross the line into the policy-making function reserved for the political branches. See (*35*).
16. *KSR Int'l Co.* v. *Teleflex, Inc.*, 550 U.S. 398 (2007).
17. *Amgen* v. *Chugai Pharmaceuticals Co.*, 927 F. 2d 1200, 1208–1209 (Fed. Cir.), cert. denied 502 U.S. 856 (1999).
18. In so holding, the Supreme Court overruled the prior "teaching, suggesting, motivation" test for obviousness that required that a reference itself contain the motivation to combine it with a second reference (*36*).
19. In the mid-1990s, the CAFC issued the landmark decisions of *In re Deuel* (*37*), and *Regents of the Univ. of Cal.* v. *Eli Lilly & Co.* (*38*). *Deuel* ruled that "knowledge of a protein does not give one a conception of a particular DNA encoding it." In the Lilly case, the court held that one cannot obtain a patent on cDNA simply by providing a probe and explaining how to use the probe to isolate cDNA, even if the protein encoded by the cDNA is known. Rather, the applicant must disclose the sequence of the DNA to get a claim to the DNA. Years later, the CAFC was compelled to overrule *Deuel* because the Supreme Court referred to that case with disfavor in its 2007 KSR opinion (*16*). The court held that a gene was not patentable to Amgen because its protein was known, even though the patent application was filed only 3 years after the *Deuel* decision. See (*39*).
20. 545 F.3d 943 (Fed. Cir 2008); cert granted 556 U.S. 1 (1 June 2009).
21. The oral argument was heard 9 November 2009, with a written decision expected soon.
22. 35 U.S.C. § 101.
23. *Bilski* pertains to a method for hedging risk in commodity trading. The decision being appealed holds that an innovation is patentable only if it involves a "machine or transformation."
24. 35 U.S.C. §112.
25. Ariad Pharms., *Inc.* v. *Eli Lilly & Co.*, 560 F.3d 1366 (Fed. Cir. 2009); U.S. Patent No. 6,410,516 (filed 5 June 1995); *Ariad Pharms., Inc.* v. *Eli Lilly & Co.*, No. 2008-1248, 2009 WL 2573004 (Fed. Cir. 21 August 2009).
26. CAFC heard full-court oral argument in *Ariad* v. *Lilly* on 7 December 2009, with a decision due shortly. See also (*40*).
27. *Consolidated Fruit-Jar Co.* v. *Wright*, 84 U.S. 92, 96 (1876).
28. *Patlex Corp.* v. *Mossinghoff*, 758 F.2d 594, 599 (Fed. Cir. 1985).
29. J. N. Bunch, *Tex. Law Rev.* **83**, 1747 (2005).
30. D. R. Cahoy, . *Am. Bus. Law. J.* **41**, 1 (2003).
31. The current congressional debate about whether to impose a data exclusivity requirement for follow on biologics focuses on 12 to 14.5 years. S. 1695 and H. 1548.
32. 21 U.S.C. § 355 (j)(5)(B)(iii).
33. *Ruckelshaus* v. *Monsanto Company*, 467 U.S. 986; 1005 (1984) [citing (*41*)].
34. *Palazollo* v. *Rhode Island*, 533 U.S. 606, 626–630 (2001).
35. *Harper* v. *Va. Dep't of Taxation*, 509 U.S. 86, 97 (1993).
36. *In re Grabiak*, 769 F. 2d 729 (Fed. Cir. 1985).
37. *In re Deuel*, 51 F.3d 1552 (Fed. Cir. 1995).
38. *Regents of the Univ. of Cal.* v. *Eli Lilly & Co.*, 119 F.3d 1559 (Fed. Cir. 1997).
39. *In re Kubin*, 561 F.3d 1351 (Fed. Cir. 2009).
40. Brief for GlaxoSmithKline as Amicus Curiae Supporting Defendant-Appellant Eli Lilly & Company, No. 2008-1248 (Fed. Cir. 19 November 2009) (en banc).
41. *PruneYard Shopping Ctr.* v. *Robins*, 447 U.S. 74, 83 (1980).

10.1126/science.1184188

ATMOSPHERIC SCIENCE

Observing Weather from Space

Since the first weather satellite was launched 50 years ago, satellite observations have revolutionized weather forecasting.

Stanley Q. Kidder[1] and Thomas H. Vonder Haar[2]

On 1 April 1960, the world's first weather satellite, the Television Infrared Observation Satellite 1 (TIROS 1), was launched from Cape Canaveral, Florida, into a 99-min orbit at an altitude of about 725 km. The cylindrical (1.1-m diameter, 0.48-m tall), 120-kg spacecraft was spin-stabilized, rotating between 8 and 12 times per min. It carried two television cameras that pointed parallel to the spin axis and could take 32 pictures per orbit (*1*). Although the results were modest by today's standards (see the figure), TIROS 1 revolutionized the field of meteorology.

Weather forecasting is an initial-value problem: One observes the weather (preferably globally) at a particular time, and then uses equations or simple extrapolation to propagate the weather into the future. The complexities of integrating the equations and of modeling the physics of the three phases of water that exist on Earth (and which most people consider to be the weather) are not to be underestimated, but nor is observing the initial state of the weather. Due to the sheer size of Earth's atmosphere, 40,000 km in circumference, satellite platforms are the only ones from which the entire atmosphere can be observed. From land, only about one quarter of the atmosphere can be observed.

After 1945, the first cloud photographs were taken from cameras mounted on balloons and rockets. However, balloon- and rocket-mounted cameras could take pictures only very infrequently when a rocket or balloon was launched, not daily, as meteorologists needed. Meteorologists thus eagerly awaited the launch of a satellite carrying a cloud camera (*2*). Progress was rapid after the success of TIROS 1, which returned 19,389 meteorologically useful images in its 79-day life (*1*). In the next decade, the United States launched 24 civilian meteorological satellites, including the first Sun-synchronous satellite (Nimbus 1) and the first geosynchronous meteorological satellite (ATS 1); the former Soviet Union launched a similar number of meteorological satellites (*3*). All meteorologically important portions of the electromagnetic spectrum, from the microwave to the ultraviolet, were sampled for the first time. Succeeding decades have each seen dozens of meteorological satellites launched by countries around the world.

The first meteorological satellites were designed to take snapshots of clouds, which are the main feature in visible or infrared images (see the figure). From these images—especially from geosynchronous satellites, which allow "movies" of the weather to be made—meteorologists learned to identify and forecast meteorological systems such as low- and high-pressure systems, fronts, jet streams, severe thunderstorms, tropical storms, and snow storms (*4*, *5*).

Forecasters make short-term forecasts (up to 6 hours) largely by extrapolating the motion of weather systems observed with satellites. Almost all forecasts longer than 6 hours are made using numerical weather prediction (NWP) models. Satellite observations enable retrieval of the atmospheric properties necessary to initialize NWP models: temperature, humidity, wind direction, and wind speed as functions of pressure. Temperature and humidity are retrieved from measurements on the wings of gaseous absorption bands, either in the infrared or microwave parts of the spectrum. Winds can be measured by tracking clouds in geostationary infrared images, by measuring the backscattered radiation from the wind-roughened sea surface using satellite-borne radars, or by measuring the polarization of microwave radiation emitted and reflected by the ocean surface (*6*). Today, more than 95% of data available to NWP models come from satellites (*7*). By one measure of forecast accuracy, 5-day forecasts are now as good as 3-day forecasts were 25 years ago, and forecasts in the conventionally data-sparse Southern Hemisphere have become as accurate as those in the Northern Hemisphere (*8*).

In addition, meteorologically important quantities are now retrieved that are not yet well assimilated into NWP models. These include precipitation (from passive micro-

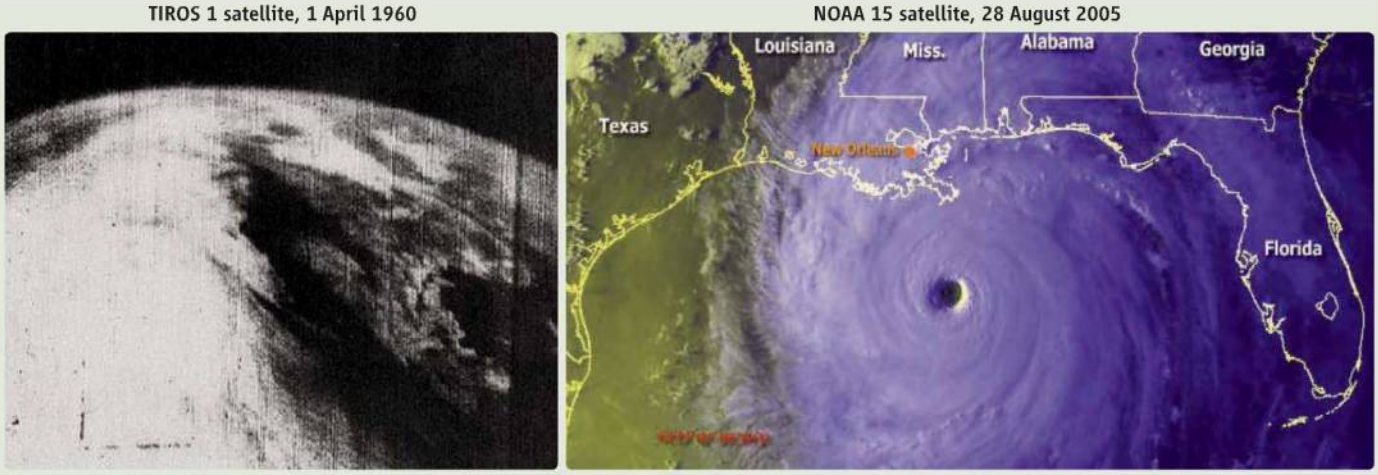

What a difference 50 years make. (Left) The first image from TIROS 1. Nova Scotia is in the lower right quarter. The television camera was pointing to the west. A cloud formation is visible in the lower left quarter. **(Right)** Hurricane Katrina on 28 August 2005 at 2332 UTC, as seen from the NOAA 15 satellite. The image is composed of visible (yellow) and infrared (blue) observations.

CREDITS: (LEFT) NASA; (RIGHT) NOAA

[1]Cooperative Institute for Research in the Atmosphere (CIRA), Colorado State University, Fort Collins, CO 80523, USA. [2]Department of Atmospheric Science and CIRA, Colorado State University, Fort Collins, CO 80523, USA. E-mail: kidder@cira.colostate.edu; vonderhaar@cira.colostate.edu

wave sensors and radars); cloud cover and cloud phase (from traditional passive visible and infrared measurements and from newer active instruments); snow cover, sea ice cover, and soil moisture (mostly from passive microwave instruments, which can sense through clouds); smoke, dust, volcanic ash, and other aerosols (from a variety of passive sensors); and gases, including carbon dioxide, sulfur dioxide, and ozone (from infrared and ultraviolet spectrometers). All of these quantities will gradually become part of improved NWP models and forecasts.

In the 50 years since TIROS 1, many fields other than meteorology have benefited from space-based observations, including atmospheric science, climate studies, oceanography, hydrology, ecology, and geology (*9*). It is becoming increasingly clear that these fields are interrelated. When a volcano erupts, the dust becomes a meteorological problem and a threat to aviation. Changes in sea surface temperatures alter the tracks of storm systems. Changes in atmospheric composition affect climate and air quality. Future satellite sensors will thus serve a variety of fields. A list of missions has been recommended as a result of the U.S. National Research Council's decadal survey for Earth science (*10*, *11*), and many other missions are planned by other countries (*12*, *13*).

The first 50 years of space-based Earth observation progressed from crude observations to scientific understanding to stewardship of the atmosphere and of Earth. Today's space-based observations will likely appear crude in 50 years (*14*). The new observations will result in many scientific insights and should help humanity to weather what could be the worst of global warming and other environmental problems.

References and Notes

1. J. G. Vaeth, *Weather Eyes in the Sky: America's Meteorological Satellites* (Ronald Press, New York, 1965).
2. H. Wexler, *J. Br. Interplanet. Soc.* **13**, 269 (1954).
3. P. K. Rao, S. J. Holmes, R. K. Anderson, J. S. Winston, P. E. Lehr, *Weather Satellites: Systems, Data, and Environmental Applications* (American Meteorological Society, Boston, 1990).
4. M. J. Bader *et al.*, Eds., *Images in Weather Forecasting: A Practical Guide for Interpreting Satellite and Radar Imagery* (Cambridge Univ. Press, Cambridge, UK, 1995).
5. R. C. Sheets, *Weather Forecast.* **5**, 185 (1990).
6. S. Q. Kidder, T. H. Vonder Haar, *Satellite Meteorology: An Introduction* (Academic Press, San Diego, CA, 1995).
7. Monthly statistics on the data used in U.S. NWP models are at www.nco.ncep.noaa.gov/sib/counts.
8. A. J. Simmons, A. Hollingsworth, *Q. J. R. Meteorol. Soc.* **128**, 647 (2002).
9. National Research Council, *Earth Observations from Space: The First 50 Years of Scientific Achievements* (National Academies Press, Washington, DC, 2008).
10. National Research Council, *Earth Science and Applications from Space: National Imperatives for the Next Decade and Beyond* (National Academies Press, Washington, DC, 2007).
11. National Research Council, *Satellite Observations to Benefit Science and Society: Recommended Missions for the Next Decade* (National Academies Press, Washington, DC, 2008).
12. World Meteorological Organization (WMO), www.wmo.int/pages/index_en.html.
13. Committee on Space Research (COSPAR), http://cosparhq.cnes.fr.
14. National Research Council, *America's Future in Space: Aligning the Civil Space Program with National Needs* (National Academies Press, Washington, DC, 2009).

10.1126/science.1185867

ENGINEERING

Intelligent Infrastructure for Energy Efficiency

A substantial fraction of wasted energy can be recovered by extending insights from the architecture of the Internet to the infrastructure of buildings.

Neil Gershenfeld,[1] Stephen Samouhos,[1,2] Bruce Nordman[3]

Buildings use 40% of the primary energy supplied in the United States, and more than 70% of all generated electricity (*1*), primarily for heating, cooling, and lighting. About 20% of the energy used by buildings can potentially be saved by correcting faults, including malfunctions and unnecessary operation (*2*). Initial deployments of advanced control systems currently in development suggest that they can save an additional 10 to 20% (*3*). The energy efficiency resource recoverable through such improved building controls and fault detection corresponds to the output from hundreds of power plants, equivalent to more than one-third of the coal-fired power production in the United States (*1*). Realizing these substantial savings will require introducing intelligence into the infrastructure of buildings, to distribute the optimization of their operation and detection of their faults.

Intelligent infrastructure extends "smart grid" initiatives that seek to save energy by allowing utilities to manage loads, such as turning off air conditioners during peak demand (*4*). However, a grid cannot be smart if it is connected to dumb devices. Currently, modifying a building is costly and labor-intensive; it can cost $1000 to add a control point containing a $1 sensor to a building, requiring a skilled installer to connect it to a central controller that then must be reconfigured. This situation is analogous to computing and communications before the Internet, when terminals and telephones were connected to mainframes and central office switches.

The Internet allowed applications to reside where information is created and consumed, from reading e-mail to viewing virtual worlds. In this way, its applications are independent of how the network connecting them is constructed (*5*). This observation is equally applicable to building infrastructure: Sensors and actuators can compute and communicate to solve problems locally rather than having functions fixed by a central controller (*6*).

Many of the candidate standards for smart building systems are recreating rather than extending the development of the Internet. There are, however, important differences between high-performance buildings and networks. Installation lifetimes for buildings are measured in decades, and the cost of installation and maintenance can dwarf the cost of devices. Events can happen over seasons (such as cooling versus heating) rather than seconds, requiring efficient handling of slow rather than fast events. Operation must often be unsupervised, air and water as well as information must be moved, and people are an integral part of the building system. Each of these practical considerations presents new research challenges; they cannot be addressed simply by making better use of available technologies.

A testbed for intelligent infrastructure for energy efficiency (I2E), shown in panel A of the figure, consists of 100 nodes (*7*) that cost about $1 each but contain interfaces for sensors and loads, implement Internet Protocol (IPv6) communications over the dc control wiring already in the building, and provide an

[1]Center for Bits and Atoms, Massachusetts Institute of Technology, Cambridge, MA 02138, USA. [2]Building Technologies, Massachusetts Institute of Technology, Cambridge, MA 02138, USA. [3]Lawrence Berkeley National Laboratory, Berkeley, CA 94720, USA. E-mail: gersh@cba.mit.edu, bnordman@lbl.gov, stratos@mit.edu

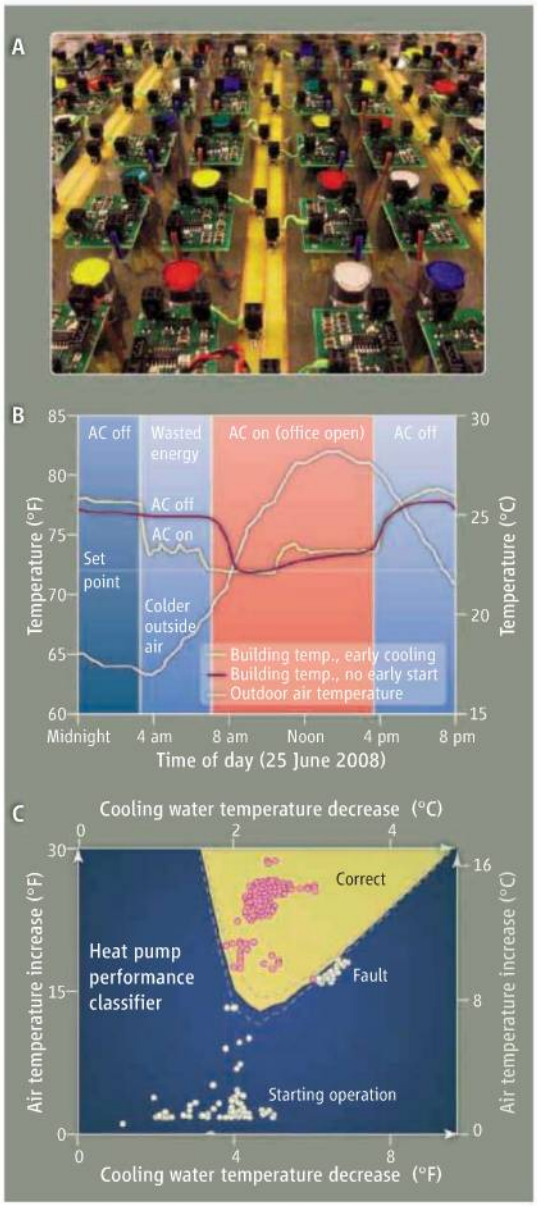

Bringing energy loss under control. (**A**) A key element for intelligent infrastructure for energy efficiency (I2E) is sensing and controlling the state of a building. The testbed shown has 100 embedded IPv6 Web servers, each with sensor inputs and control outputs, at a component cost of roughly $1. (**B**) Measured responses, based on I2E testbed data, for an office building with an oversized air conditioner that turns on 4 hours early (blue), versus an appropriate start time closer to the start of the workday (red). (**C**) Classification of a heat pump's operation based on analysis of drops in water temperature and increase in air temperature. Pattern recognition with a convex kernel method separates clusters of normal operation (yellow region) from starting operation conditions, as well as a separate set of responses that appear to reflect faulty operation (blue region).

embedded Web server. At wiring junctions, changes in impedance will cause part of a signal to be reflected, which is prevented in high-speed networks by adding active terminations. However, signal impulses in building wiring will decay on the order of the time it takes them to transit the building, typically microseconds. By communicating to embedded devices with transient impulses slower than this rate (megabits per second), a network can be connected in an arbitrary way (*8*). This approach minimizes complexity rather than maximizes capacity and supports any available signaling medium and data rate. A key feature of the scalability of the Internet—its ability to operate in the same way as more connections and devices are added—has been its use of protocol definitions (*9*) that do not limit performance numbers, unlike candidate standards for building systems that fix these parameters (*10*).

Another aspect of scalability has been hierarchical routing, which can provide global connectivity even for low-power devices with unreliable connections (*11*). By embedding Web servers in individual sensors and actuators to present and control their state, a new device can document its own capabilities, rather than have its functions defined in advance as done today (*12*).

An example of how this works is shown in panel B of the figure, which presents data collected from sensors in an I2E testbed installation, an office building at MIT. Air conditioners with excess capacity for the actual building load were automatically turning on at 4:30 a.m. to cool the building for a workday starting 4 hours later, even though the building could be cooled in 30 min. Even worse, in the early morning the outside air was colder than the desired temperature; the most efficient strategy would have been to bring in outside air. Efficient building air handlers do have dampers to regulate the mixing of outside air; however, another I2E testbed study found a mixing unit failing to mix because of unexpected internal recirculation.

To be able to respond to such changing conditions, an I2E system must integrate control of all of the degrees of freedom in a building and adapt to their actual configuration. If networked intelligence is embedded into all of an I2E system's devices, the system can use them to implement controllers that have the same structure as the system being controlled (*13*).

Historically, building infrastructure faults have been detected (if at all) with simple setpoint alarms; more recently, machine learning techniques have been applied that require supervised training (*14*). Modern methods for pattern recognition, such as convex kernel methods (*15*), allow anomalies to be found in unlabeled data without iterative learning procedures; panel C of the figure shows such a decision surface found for a heat pump that identifies its faulty operation.

There are also opportunities for saving energy with dense networks of intelligent actuators as well as sensors. Heating and cooling pumps and fans have been found to contribute more than 50% of the HVAC-related energy usage in commercial buildings (*16*). This includes kinetic energy in moving air and water, drag in pipes and ducts, and internal losses. Efficiency is maximized by minimizing velocity and drag, which can be accomplished by distributing a greater number of smaller impellers over internal surfaces, rather than just a few large ones at inlets or exhausts (*17*).

The energy benefits in these I2E systems will be negated if their control systems consume more energy than they save. Because the relevant operational time scales are measured in hertz rather than gigahertz, most of the clock cycles in a conventional processor will be wasted. This static power consumption can be minimized by using asynchronous logic that is driven by events rather than by a clock. Because building architecture changes much more slowly than computer architecture, the embedded computing should ideally be reconfigurable as well as asynchronous, so that choices such as word sizes or instruction sets are not fixed in the construction of a building. These constraints suggest the use of reconfigurable asynchronous logic in building infrastructure, an area of active research originally developed for use in high-performance computing (*18*).

I2E faces operational as well as technological hurdles to widespread adoption. Building codes evolve slowly to reflect worst-case experiences and are applied on a case-by-case basis, whereas computer codes are developed much more rapidly and are debugged by finding and fixing errors. Construction costs typically do not reflect life-cycle operational costs, which are accounted for independently. Individual building controls do not currently have access to economic data that could convey to occupants the costs of their actions (in dollars, CO_2 emissions, or utility load).

Bridging between these worlds will not be accomplished with an investment at a single point in the system. Intelligent building infra-

structure can be thought of as a long "green" tail distribution of many small savings that add up to a major opportunity for reducing energy consumption, while also improving a building's responsiveness to its occupants. This presents corresponding challenges that are at the frontiers of distributed computing and communications; rather than replicating the history of their development, today's best practices can be extended to this largest of all programming environments—the built environment.

References and Notes

1. U.S. Department of Energy, *Buildings Energy Data Book* (http://buildingsdatabook.eere.energy.gov, 2009).
2. K. W. Roth *et al.*, *Energy Impact of Commercial Building Controls and Performance Diagnostics*, TIAX (http://apps1.eere.energy.gov/buildings/publications/pdfs/corporate/pnnl-15149_market_assessment.pdf, 2005).
3. M. R. Brambley *et al.*, *Advanced Sensors and Controls for Building Applications: Market Assessment and Potential R&D Pathways* (http://apps1.eere.energy.gov/buildings/publications/pdfs/corporate/pnnl-15149_market_assessment.pdf, 2005).
4. National Institute of Standards and Technology, Smart Grid Interoperability Standards Project (http://nist.gov/smartgrid/).
5. J. H. Saltzer *et al.*, *ACM Trans. Comput. Syst.* **2**, 277 (1984).
6. N. Gershenfeld *et al.*, *Sci. Am.* **291**, 76 (2004).
7. D. Kopp, Sarvanet, personal communication (2009).
8. N. Gershenfeld, D. Cohen, *IEEE Circ. Dev.* **22**, 48 (2006).
9. DARPA Internet Program Protocol Specification RFC 791 (www.ietf.org/rfc/rfc0791.txt, 1981).
10. ZigBee Alliance (www.zigbee.org/).
11. Internet Engineering Task Force (http://tools.ietf.org/html/draft-ietf-roll-of0-00).
12. BACnet (www.bacnet.org/).
13. C. Langbort *et al.*, *IEEE Trans. Automat. Contr.* **49**, 1502 (2004).
14. M. Krarti, *J. Sol. Energy Eng.* **125**, 331 (2003).
15. A. Rahimi, B. Recht, in Proceedings of the 8th European Conference on Computer Vision Workshop on Statistical Learning in Computer Vision, Prague, 2004 (http://groups.csail.mit.edu/vision/vip/papers/rahimi-ncut.pdf).
16. California Measurement Advisory Council (www.calmac.org, 2003).
17. A. Sun, unpublished results.
18. N. Gershenfeld *et al.*, in POPL '10 (ACM SIGACT-SIGPLAN Symposium on Principles of Programming Languages), 17 to 23 January 2010, Madrid (http://phm.cba.mit.edu/papers/09.11.POPL.pdf).

10.1126/science.1174082

MOLECULAR BIOLOGY

Reliable Noise

David Levens[1] and Ashutosh Gupta[1,2]

Assessing how the noise created in transcription factor regulatory circuits affects gene expression is essential to understanding network operation and output.

Most measurements of gene expression assess large numbers of cells to improve precision and reduce the "standard error" (the standard deviation of the mean). Yet, the standard deviation of the fluctuations of a measured property, such as cell proliferation, over time in a single cell (in a system at equilibrium or steady state) or across a cell population, scaled to the mean of the measured property, is defined as "noise." Despite this pejorative, a full accounting of noise provides insights into the pathways and mechanisms controlling a measured property. On page 1142 of this issue, To and Maheshri demonstrate that noise itself can generate a system that switches spontaneously between high and low gene expression (*1*). This finding implies that fluctuation in the numbers of regulatory molecules may drive physiological transitions without having to precisely specify the numbers of other molecules needed to prepare chromatin and make RNA. However, these same fluctuations might initiate and sustain pathological states, so mechanisms to suppress such fluctuations must also exist.

The basic experimental scheme used by To and Maheshri involves expressing TetVP16, a recombinant transcription factor, from a weak minimal promoter bearing either one or seven binding sites for TetVP16 itself. This positive feedback arrangement mimics a commonly occurring biological regulatory motif (*2*). Reporter genes encoding fluorescent proteins that are driven by either promoter are then used to monitor transcriptional output in cells. Upon the graded removal of doxycycline, a compound that inhibits the binding of TetVP16 to DNA, a cell population can transition from low to high reporter gene expression in this system.

To and Maheshri observed that with a single TetVP16 binding site in the promoter, the entire cell population increased reporter gene expression gradually and coherently. However, with seven TetVP16 binding sites, even at low doxycycline concentrations, a single burst of transcription could drive enough TetVP16 expression to enable visualization by sustained high reporter expression, the result of a high transcription output state in individual cells that sporadically relaxed to low output. The high-output state was associated with bursts of transcription that were less frequent, and either of longer duration or of higher intensity compared to bursts observed in the low-output state. Because only a single polymerase can initiate transcription at a promoter at one time, prolonging a burst to include more successive rounds of transcription initiation will increase output relative to more frequent, but short bursts.

The same bimodal pattern of low and high gene expression was also observed with a stronger promoter bearing just one TetVP16 binding site. Thus, cooperative binding of TetVP16 was excluded as the cause of the switch from low to high transcription output. This two-state system is distinct from the monotonic curve defined by calculations based solely upon the binding constants and concentrations of interacting molecular species in the absence of cooperativity. The study of To and Maheshri also reveals the difficulty of rigorously accounting for the biologically relevant species of macromolecules. To construct a working mathematical model, the authors had to correct for a cytoplasmic reservoir of inactive TetVP16 molecules and for

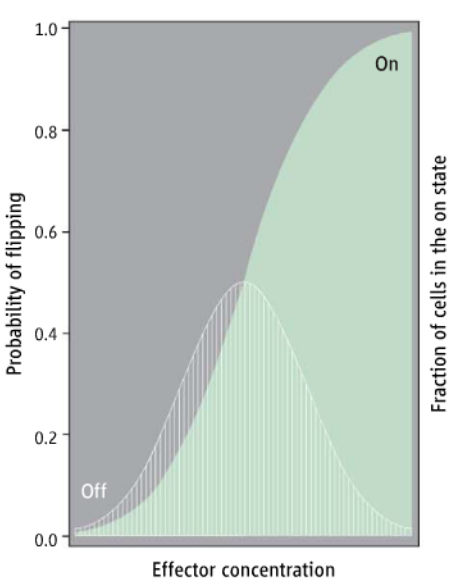

Dynamic system stability. The fracton of cells expressing a gene is a function of the concentration of an effector molecule (as in the system used by To and Maheshri). At very low or high effector concentrations, the expression system is often off (gray) or on (green). At intermediate concentrations, the system is bimodal, flipping between both states (region with lines). Nevertheless, the overall system is stable.

CREDIT: N. KEVITTYAGALA/SCIENCE

[1]Laboratory of Pathology, Center for Cancer Research, National Cancer Institute, Bethesda, MD 20892, USA. [2]Department of Physics, University of Maryland, College Park, MD 20742, USA. E-mail: levensd@mail.nih.gov

the ubiquitination of TetVP16, a modification that generates the most transcriptionally relevant species, but a species that is unstable (marked for proteolysis).

Cross-regulating and self-regulating transcription factor regulatory circuits are common, and describing how noise is suppressed or amplified as it is transmitted through these networks may be essential to understanding their operation. The inherent statistical fluctuations around the mean output of a weak promoter [about one transcript per cell (*3*)] generate intrinsic noise. For long-lived gene products, this noise can be averaged away over time. But if the gene product is a short-lived transcription factor, then this intrinsic noise is amplified and propagated onto each of the transcription factor's target genes as extrinsic noise (*4*–*6*). Depending on the quality and number of transcription factor binding sites, as well as on the architecture, context, and strength of their associated promoters, different target genes may be tuned to switch to high output at different concentrations of transcription factor (*7*). Positive feedback onto the gene encoding the transcription factor itself, fixes the stochastic switch in the "on" position.

Such stochastic switching in a uniform population of unicellular organisms generates a range of responses to a defined stress and increases the likelihood of survival. This sort of switching may also be critical during metazoan development. Whereas the nematode *Caenorhabditis elegans* hardwires the fate of each of its 959 cells (*8*), the 10^{13} cells of the human body are unlikely to be explicitly programmed, and so some form of probabilisitic specification is required. When the number of cells in a developmental field is sufficiently large, precise stochastic switching may be guaranteed by chance. This would seem to be especially appropriate for genes encoding effectors whose synthesis and release from a small number of cells elicit a cell nonautonomous response, ultimately recruiting a cohort of cells to the same switched fate. Thus, a defined physiological or developmental state may be viewed as an "attractor" (*9*), generating a stable system, despite the fluctuations of individual cells (see the figure).

However, for some genes, even a pulse of inappropriate expression may provoke untoward consequences, and so unscheduled stochastic switching may need to be suppressed in some cases. For example, even a brief increase in the concentration of the transcription factor Myc in some cells provokes programmed cell death (*10*). The problem becomes how to suppress stochastic pulses that might put the system into an unfavorable state, while ensuring that proper switching, driven by bona fide signaling, is allowed (*11*). End-product feedback regulation would be inherently too slow to control noise in this situation. Indeed, in the case of human Myc, transcription generates dynamic DNA supercoiling that when sufficiently intense, provokes a change in DNA conformation. This threshold-dependent change in DNA conformation serves as a real-time sensor of the intensity of ongoing transcription, enabling the effector components of this system to intercept incipient fluctuations and suppress noise, while transmitting true signals (*12*–*14*). Similar adaptations might be anticipated for genes that are required at uniform, low levels of expression, whereas other mechanisms are likely to expand the dynamic ranges of genes, probing the limits of expression space.

References and Notes

1. T.-L. To, N. Maheshri, *Science* **327**, 1142 (2010).
2. U. Alon, *An Introduction to Systems Biology: Design Principles of Biological Circuits* (Chapman & Hall, London, 2006).
3. D. J. Lockhart, E. A. Winzeler, *Nature* **405**, 827 (2000).
4. M. B. Elowitz *et al.*, *Science* **297**, 1183 (2002).
5. N. Maheshri, E. K. O'Shea, *Annu. Rev. Biophys. Biomol. Struct.* **36**, 413 (2007).
6. J. M. Raser, E. K. O'Shea, *Science* **304**, 1811 (2004).
7. F. H. Lam, D. J. Steger, E. K. O'Shea, *Nature* **453**, 246 (2008).
8. J. E. Sulston, E. Schierenberg, J. G. White, J. N. Thomson, *Dev. Biol.* **100**, 64 (1983).
9. K. T. Alligood, T. Sauer, J. A. Yorke, *Chaos: An Introduction to Dynamical Systems* (Springer, New York, 1997).
10. N. Senoo-Matsuda, L. A. Johnston, *Proc. Natl. Acad. Sci. U.S.A.* **104**, 18543 (2007).
11. H. J. Chung, D. Levens, *Mol. Cells* **20**, 157 (2005).
12. L. R. Benjamin *et al.*, *Proc. Natl. Acad. Sci. U.S.A.* **105**, 18296 (2008).
13. F. Kouzine, S. Sanford, Z. Elisha-Feil, D. Levens, *Nat. Struct. Mol. Biol.* **15**, 146 (2008).
14. J. Liu *et al.*, *EMBO J.* **25**, 2119 (2006).

10.1126/science.1187268

GEOPHYSICS

Changing Views of the San Andreas Fault

Katherine Scharer

A combination of high-resolution laser imaging with improved radiocarbon dating techniques is providing new ways to view earthquake behavior.

The magnitude 7.0 earthquake that struck Haiti on 12 January 2010 is a reminder of the devastation caused by large earthquakes. Because recurrence of large (*M*7–8) earthquakes is rare, on the order of centuries, studying the past behavior of a fault guides future expectations. Paleoseismologists examine the stratigraphic and geomorphic history of deposits and landforms along a fault for evidence of past ruptures. Such observations provide information on when earthquakes happened, what parts of the fault failed, and the size of the earthquakes. The collected geologic data form the backbone of probabilistic seismic hazard analyses (*1*) used by the insurance and engineering industries and are increasingly used to explore models of lithosphere rheology and fault interaction (*2*, *3*). Because of sparse data, however, inferences about patterns of strain accumulation and release are a common occurrence. On pages 1119 and 1117 of this issue, Zielke *et al.* (*4*) and Grant Ludwig *et al.* (*5*) present data and interpretations providing an exciting new view that questions fault behavior models that have been applied to the south central San Andreas Fault for decades, highlighting the value of revisiting old problems with new techniques.

Fault behavior models describe the amount of slip (the relative displacement of points on opposite sides of a fault), length, and location of ground-rupturing earthquakes along a fault (see the figure, panels A and B). In the 1980s, observations of 8 to 10 m of slip measured for the most recent large earthquake (in 1857) and inferred for the two preceding earthquakes along the Carrizo Plain section of the southern San Andreas Fault contributed to the development of the characteristic and uniform slip models (*6*, *7*). A fundamental premise of both models was that every rupture that crossed a specific region of the fault produced similarly large slip, and thus controlled the frequency of earthquakes along that segment. If correct, then the timing of large ruptures like the *M*7.9 in 1857 seemed to be controlled by properties of the fault in the Carrizo Plain (*8*). In comparison, the variable-slip model allows the slip, rupture location, and length to change with each earthquake (*6*).

Department of Geology, Appalachian State University, Boone, NC 28608, USA. E-mail: scharerkm@appstate.edu

Both the slip and age of each earthquake are needed to constrain a fault behavior model, and the challenge is to find a location where single-earthquake slip can be determined. The ideal geomorphic feature for identifying slip is a straight channel oriented perpendicular to a strike-slip fault (in strike-slip faults, the ground moves essentially horizontally). During large earthquakes, the sections of the channel upstream and downstream of the fault will be offset and thus record slip (see the figure, panel C). Each subsequent earthquake will increase the slip, so older channels are more offset.

The Carrizo Plain has dozens of offset channels and thus provides a great opportunity to investigate slip (*8*, *9*). Zielke *et al.* examined newly available LiDAR (light detection and ranging)–based topographic data along the 1857 rupture. LiDAR data provide high-density, submeter resolution and wide, relatively uniform spatial extent, giving Earth scientists a new mechanism to explore surface morphology. By carefully reconstructing offsets revealed in the topography, Zielke *et al.* found that ~5 m of slip occurred along the Carrizo Plain section in 1857. This observation contradicts the ~9.5 m of slip previously reported (*9*) and questions the uniqueness of the Carrizo Plain section in the 1857 event. Further, they provide an enticing view into the fault history by showing that older channels are also offset in multiples of ~5 m.

Like previous studies (*9*, *10*), however, the topographic data studied by Zielke *et al.* provide offset only, with no means to determine the number of earthquakes that contributed to each stream offset. The dates of individual ancient earthquakes are typically determined by excavating sections of the fault where sediment accumulates rapidly. Each rupture disturbs the existing layers and is capped by subsequent deposits (see the figure, panel C). Ages of individual earthquakes are determined by unraveling the successive disruptions and radiocarbon dating of organic material in the sediments. Slip associated with individual earthquakes is determined by tying the timing of channel incision into the radiocarbon-dated stratigraphy.

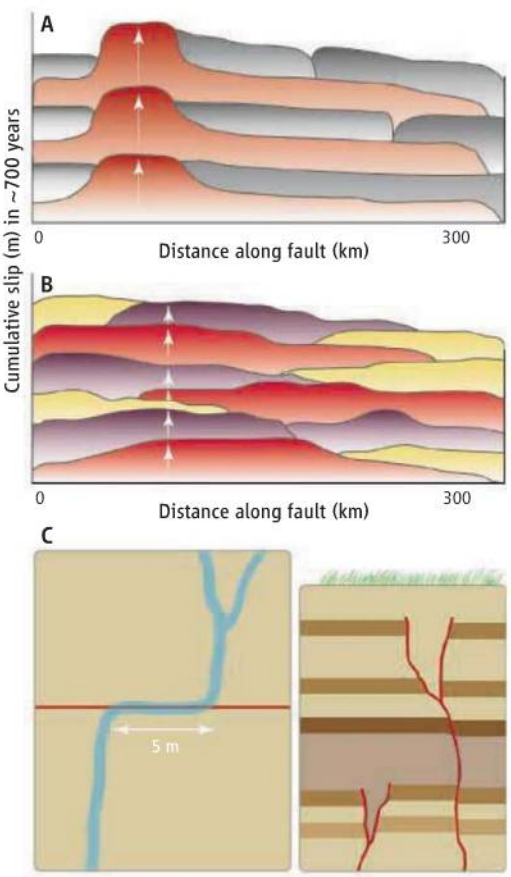

On the move. Fault behavior models are distinguished by the shape of accumulated ruptures over time. Each shape shows the distribution of slip along the fault in an individual earthquake, and each successive earthquake adds slip over time. Arrows highlight differences in slip-per-earthquake at the same location along the fault. The slip may be characteristically large, as shown in the uniform slip model (**A**), and produce a regular pattern of ruptures, or it may change with each earthquake, as shown in the variable slip model (**B**), and produce a more complicated pattern. (**C**) Cartoons showing examples of a stream offset by fault (left) and two earthquakes preserved in sediments (right).

Applying these principles, Grant Ludwig *et al.* have made a careful study of an incised alluvial fan in the Carrizo Plain and found that the amount of slip during the last five earthquakes varies from >0.5 to 5.3 m. These results provide critical insight into the meaning of the observations made by Zielke *et al.*, because they show that the accumulation of ~5 m of slip may require multiple earthquakes, and if completed in one earthquake, ~5 m of slip appears to be an upper limit along this section. Grant Ludwig *et al.* also report that earthquakes occur more frequently than previously found. Key to this conclusion was the use of new radiocarbon dating techniques that permit dating of rice-sized pieces of organic material. This is an appreciable improvement over traditional methods that required >50 g of sample, thus limiting the number of samples that could be dated (*11*).

Given the evidence that some variability in slip occurs, what is the appropriate fault behavior model for the south central San Andreas Fault? Do most of the ~5-m offsets result from one earthquake or several? The variable-slip model implies a power-law relationship between earthquake frequency and magnitude (*6*), but this distribution underestimates the number of large earthquakes on individual faults (*12*), suggesting that it does not describe faults with high slip rate. Defining a fault behavior model requires determination of the endpoints of past ruptures. Recognizing abrupt and significant variation (40%) in slip measured along modern ruptures (*13*), we cannot know whether small slip is due to a small earthquake or the tail end of a large earthquake. Locating the site relative to the past rupture is critical for determining the persistence of segments on the fault and is important for earthquake forecasts and studies of earthquake interaction along the fault (*1*, *3*). To do so requires more sites with slip-per-earthquake and short-term slip rates, paired with long earthquake histories that examine the recurrence behavior on the fault (*14*, *15*) and longer-term slip rates. Such data, augmented with additional records that are temporally variable (such as climate data), can be folded into numerical (*3*) and probabilistic approaches (*16*). This should enable investigators to leverage empirical data to arrive at a rupture history for the south central San Andreas Fault, rather than relying on a model.

References

1. 2007 Working Group on California Earthquake Probabilities, *The Uniform California Earthquake Rupture Forecast, Version 2*, Open-File Report 2007-1437 and California Geological Survey Special Report 203 (2008).
2. K. M. Johnson, G. E. Hilley, R. Burgmann, *J. Geophys. Res.* **112**, B07408 (2007).
3. J. Van Aalsburg *et al.*, *Phys. Earth Planet. Inter.* **163**, 149 (2007).
4. O. Zielke *et al.*, *Science* **327**, 1119 (2010); published online 21 January 2010 (10.1126/science.1182781).
5. L. Grant Ludwig, S. O. Akçiz, G. R. Noriega, O. Zielke, J R. Arrowsmith, *Science* **327**, 1117 (2010); published online 21 January 2010 (10.1126/science.1182837).
6. D. P. Schwartz, K. J. Coppersmith, *J. Geophys. Res.* **89**, 5681 (1984).
7. K. Sieh, in *Earthquake Prediction—An International Review* D. W. Simpson, P. G. Richards, Eds. (American Geophysical Union, Washington, DC, 1981), pp. 181–207.
8. K. E. Sieh, R. H. Jahns, *Geol. Soc. Am. Bull.* **95**, 883 (1984).
9. K. E. Sieh, *Bull. Seismol. Soc. Am.* **68**, 1421 (1978).
10. J. Liu-Zeng *et al.*, *J. Geophys. Res.* **111**, B02306 (2006).
11. S. O. Akciz, L. Grant Ludwig, J. R. Arrowsmith, *J. Geophys. Res.* **114**, B01313 (2009).
12. C. Scholz, *The Mechanics of Earthquakes and Faulting* (Cambridge Univ. Press, Cambridge, ed. 2, 2002).
13. S. G. Wesnousky, *Bull. Seismol. Soc. Am.* **98**, 1609 (2008).
14. T. Parsons, *Geophys. Res. Lett.* **35**, L21301 (2008).
15. K. M. Scharer, R. J. Weldon II, T. E. Fumal, G. P. Biasi, *Bull. Seismol. Soc. Am.* **97**, 1054 (2007).
16. G. P. Biasi, R. J. Weldon II, *Bull. Seismol. Soc. Am.* **99**, 471 (2009).

10.1126/science.1186770

BIOCHEMISTRY

What Makes a Prion Infectious?

Nonproteinaceous cofactors may be essential to generate infectious prions.

Surachai Supattapone

Prions are unconventional infectious agents that cause fatal neurological illnesses such as Creutzfeldt-Jakob disease, bovine spongiform encephalopathy, and scrapie. Many hypotheses have been advanced to explain the chemical composition of infectious prions and the mechanism of their formation in the neurons of infected hosts, but none has yet been proven. Perhaps the most provocative proposal has been the "protein-only" hypothesis, which posits that the infectious agent is composed exclusively of a misfolded, host-encoded protein called the prion protein (PrP). However, three decades of investigation have yielded no direct experimental proof for this stringent hypothesis. Moreover, various biochemical studies have suggested that nonproteinaceous cofactors may be required to produce infectious prions, possibly by forming physical complexes with PrP (*1*–*4*). On page 1132 of this issue, Wang *et al*. demonstrate the importance of cofactors for producing recombinant infectious prions in vitro (*5*). Another study by Li *et al*. suggests that endogenous cofactors may also influence the strain properties of prions in cells (*6*).

Misfolded PrP that is associated with disease can convert normal PrP into an aberrant form. In a subset of cases, aggregates of misfolded PrP form amyloid fibers, which can accumulate and form plaques in the brain. A central prediction of the protein-only hypothesis is that it should be possible to generate prions with high specific infectivity by chemically refolding PrP in vitro in the absence of other cellular components. The specific infectivity of an infectious agent is measured by an end-point titration bioassay of a known quantity of the agent in susceptible, wild-type hosts. Previous studies have shown that using chemical denaturants to fold purified recombinant PrP (produced by genetically engineered bacteria) into amyloid fibrils yields products with minimal infectivity (*7*, *8*). Although end-point titration was not performed in these studies, extremely low specific infectivity may be inferred because wild-type rodents failed to develop clinical disease when inoculated with samples of highly concentrated protein.

Department of Biochemistry, Dartmouth Medical School, Hanover, NH 03755, USA. E-mail: supattapone@dartmouth.edu

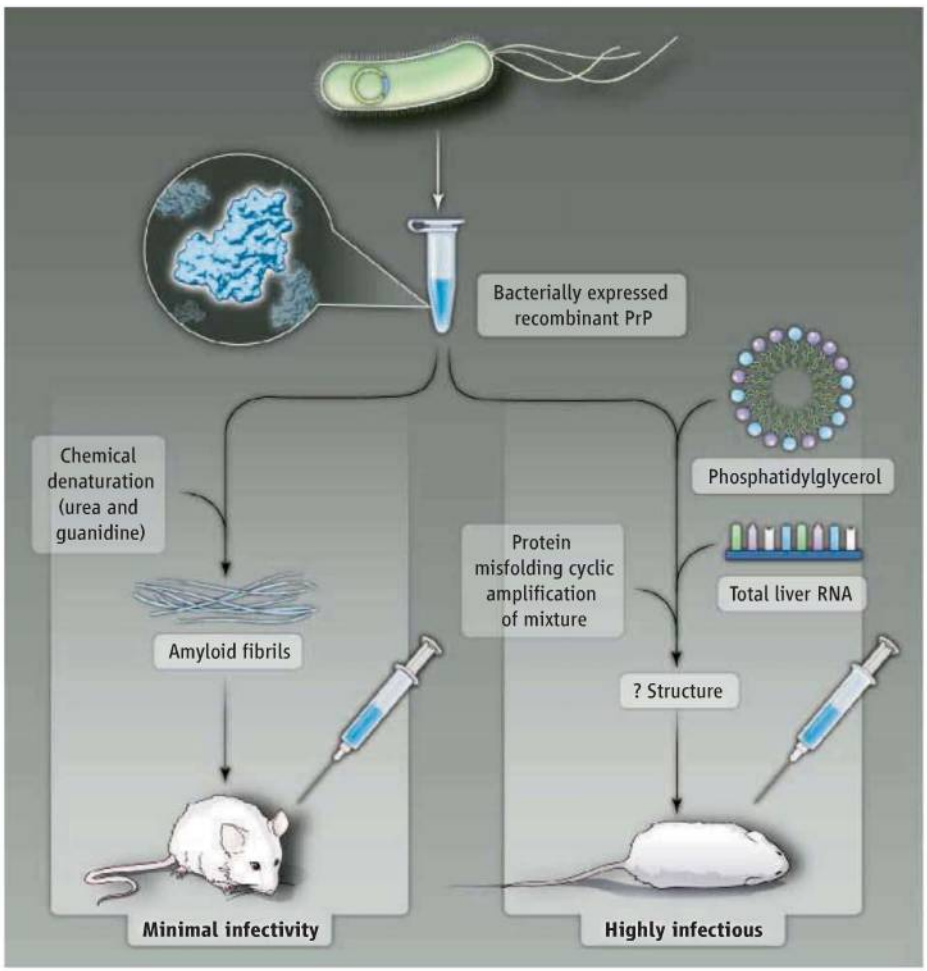

CREDIT: Y. GREENMAN/SCIENCE

Extra ingredients. Two different biochemical protocols yield recombinant PrP with different infectivity. (**Left**) Minimally infectious amyloid fibrils are formed by incubating recombinant PrP with chemical denaturants. (**Right**) Mixing recombinant PrP with phospholipid and RNA produces highly infectious prions.

By contrast, a mixture of native PrP and lipid molecules purified from noninfected hamster brain, plus synthetic polyadenylic acid RNA molecules, resulted in the de novo formation of prions whose specific infectivity was comparable to that of naturally occurring prions (*3*). Although these results indicated that nonproteinaceous cofactors were necessary for generating native prions, it remained unknown whether the addition of such cofactors could facilitate the production of infectious prions from recombinant PrP (*9*).

In a major advance, Wang *et al*. report that mixing recombinant PrP with total liver RNA and synthetic 1-palmitoyl-2-oleoyl-phosphatidylglycerol (POPG) lipid molecules produces bona fide infectious prions (*5*). Building upon their earlier work showing that POPG promotes the conversion of PrP into an aberrant, protease-resistant conformation (*2*), Wang *et al*. used the protein misfolding cyclic amplification technique (*10*) to generate recombinant prions de novo. Remarkably, the resulting recombinant prions were infectious to wild-type mice and displayed unique strain characteristics (prion strains are self-propagating variants with distinct PrP conformations and infectious phenotypes). Although an end-point titration bioassay was not performed, a 100% fatality rate among inoculated animals and a short incubation period between inoculation and disease onset suggest high specific infectivity. The contrast between the bioassay results obtained with recombinant prions formed with lipid and polyanionic cofactors and those obtained using recombinant PrP

amyloid fibrils (*7*, *8*) argues that cofactors likely facilitated the formation of prions with high specific infectivity from recombinant PrP (see the figure).

If endogenous cofactors participate in prion conversion, it is reasonable to anticipate that they might also constrain PrP structure and influence the properties of different prion strains in cells. Consistent with this possibility, Li *et al*. observed that infecting different cell types with prions can cause phenotypic "mutation" and selection of prion strains, as detected by a new rapid strain-typing assay. It may be that cell type–dependent differences in non-PrP factors could be responsible for the observed evolution of prion strains because all of the cell types examined expressed identical endogenous PrP molecules.

Wang *et al*. and Li *et al*. each have developed powerful methods that can be used to answer critical questions in future studies. It will be important to determine whether cofactors are essential components of an infectious complex, or simply catalyze the formation of prions exclusively composed of PrP. Identifying the endogenous cofactors that facilitate the formation of prion strains in different cell types is also of interest. And a biophysical comparison of the protein structures of the infectious recombinant prions produced by Wang *et al*. and the minimally infectious PrP amyloid (produced by chemically induced refolding of recombinant PrP) could reveal the structural features that encode prion infectivity. After decades of speculation, it may finally be possible to determine the molecular basis of prion infectivity experimentally.

References

1. C. Wong *et al*., *EMBO J.* **20**, 377 (2001).
2. F. Wang *et al*., *Biochemistry* **46**, 7045 (2007).
3. N. R. Deleault, B. T. Harris, J. R. Rees, S. Supattapone, *Proc. Natl. Acad. Sci. U.S.A.* **104**, 9741 (2007).
4. J. C. Geoghegan *et al*., *J. Biol. Chem.* **282**, 36341 (2007).
5. F. Wang, X. Wang, C.-G. Yuan, J. Ma, *Science* **327**, 1132 (2010); published online 28 January 2010. (10.1126/science.1183748).
6. J. Li, S. Browning, S. P. Mahal, A. M. Oelschlegel, C. Weissmann, *Science* **327**, 869 (2010); published online 31 December 2009 (10.1126/science.1183218).
7. G. Legname *et al*., *Science* **305**, 673 (2004).
8. N. Makarava *et al*., *Acta Neuropathol.* **119**, 177 (2010).
9. J. I. Kim, K. Surewicz, P. Gambetti, W. K. Surewicz, *FEBS Lett.* **583**, 3671 (2009).
10. J. Castilla, P. Saa, C. Hetz, C. Soto, *Cell* **121**, 195 (2005).

10.1126/science.1187790

CLIMATE

Seawater Chemistry and Climate

Reconstructions of past seawater chemistry provide insights into the driving forces behind long-term climate change.

Harry Elderfield

The chemical composition of the ocean is determined by rivers, submarine hot springs, and ocean sediments that add or remove elements to seawater. Throughout the oceans, the more abundant elements have near constant ratios to salinity (a measure of total dissolved salts). Thus, records of their past concentrations in seawater should tell us how active these sources and sinks were over long time scales. However, reliable archives of past seawater chemistry have been difficult to find (*1*). On page 1114 of this issue, Coggon *et al*. address this problem by measuring magnesium/calcium and strontium/calcium ratios in calcium carbonate (calcite) veins recovered from ocean crust buried under sediments (*2*). Their Mg/Ca record for the past 180 million years agrees with previous work (*1*), but the Sr/Ca record does not (*3*). The results have implications not only for seawater chemistry but also for climate change.

Earth's climate changes on several time scales. Over tens to hundreds of thousands of years, variations in Earth's orbit around the Sun alter the amount and distribution of external heating. The resulting changes in climate occur within the framework of tectonic processes that take place over millions of years. Driven by Earth's internal heat, tectonics shapes climate by recycling carbon between Earth's interior and surface. Tectonic forcing of climate is crucial for a habitable planet. Our closest planetary neighbors, Mars and Venus, have carbon dioxide in their atmospheres but were unable to escape runaway "icebox" (Mars) and "greenhouse" (Venus) conditions. For Earth to avoid such a fate, a negative feedback must keep runaway warming or cooling in check. Over million-year time scales, it is commonly thought that atmospheric CO_2 reflects a balance between input from volcanic activity and removal by silicate rock weathering feedback (see the figure). This balance, and how it may have changed, is reflected in the chemical composition of the oceans.

The calcite veins studied by Coggon *et al*. were formed by seawater flowing through the upper oceanic crust on the flanks of mid-ocean ridges. The authors dated the veins based on their $^{87}Sr/^{86}Sr$

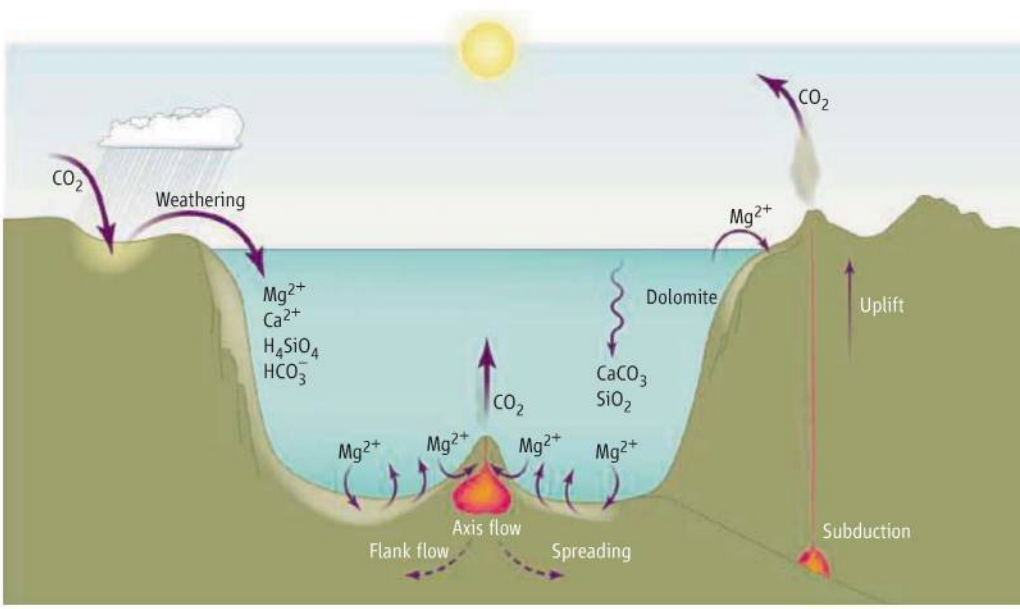

Long-term climate change and ocean chemistry. On million-year time scales, climate is driven by the input of CO_2 to the atmosphere by plate tectonics. The atmospheric CO_2 reservoir is small and would raise global temperatures unchecked without a chemical weathering carbon feedback. Coggon *et al*. (*2*) have improved understanding of the global Mg cycle, which shares some similarities with the carbon cycle.

Earth Sciences Department, Cambridge University, Cambridge CB2 3EQ, UK. E-mail: he101@cam.ac.uk

ratios and then converted the calcite Mg/Ca and Sr/Ca ratios to seawater values (*2*). The resulting Mg/Ca ratios were ~1 mmol/mol from 180 to 60 million years ago and then rose to today's value of 5.4 mmol/mol. This pattern agrees with other studies using different approaches (*1*).

Coggon *et al*. explain this pattern based on two classic models (*4*, *5*), in which seawater gains Mg from river input and loses Mg during hydrothermal circulation through ocean ridges (see the figure). Hydrothermal processes dominate Mg removal today, but Wilkinson and Algeo (*4*) have argued that removal as dolomite (a sedimentary carbonate rich in Mg) dominated the Mg budget over long periods in the past. Only ~10% of today's sedimentary sink is as dolomite (*6*).

How do the Sr/Ca data fit into this picture? Coggon *et al*.'s seawater Sr/Ca values are ~3 μmol/mol from 180 to 20 million years ago and then tripled to modern values. In contrast, earlier studies found higher values in the past than today (*3*). Coggon *et al*. attribute this discrepancy to uncertainty over Sr partitioning into biogenic carbonates. Literature data show that hydrothermal vent fluids have lower Sr/Ca than does seawater (*7*), and Coggon *et al*. attribute the increasing seawater Sr/Ca (as for Mg/Ca) to a decreasing influence of hydrothermal activity over time. However, Sr and Ca concentrations in hydrothermal fluids vary and may be both higher and lower than seawater values (*7*). When normalized to chloride to account for phase separation, Sr concentrations are, in fact, about two times higher than modern seawater; the Sr/Ca ratios are only lower than in modern seawater because Ca is on average five times higher. Therefore, the situation is more complex. For example, if Ca added from vents is removed as carbonate sediments, then the impact of hydrothermal activity will be to increase Sr/Ca, not lower it.

A key feature of the models (*4*, *5*) is the rate at which Mg is stripped from seawater during hydrothermal alteration in the ocean crust (see the figure). However, estimates of this rate differ widely, with implications for understanding seawater chemistry and long-term climate change.

Many studies have used estimates based on seafloor spreading rates and seafloor generation histories (*8*) that show a decrease of 50% or more in ridge production (and hence Mg removal at ridge crests) in the past 100 million years. This makes sense: Mg removal at ridge crests decreases, and seawater Mg/Ca increases. Lower ridge production also implies a decrease in CO_2 production. This lowers atmospheric CO_2, which leads to a decrease in chemical weathering, less CO_2 removal, and thus a negative feedback on climate. One geochemical model that has taken this approach is the influential BLAG model (*9*), in which the atmospheric CO_2 cycle is driven by the rate of seafloor generation.

However, in 2002, Rowley (*10*) showed that the present distribution of seafloor ages is consistent with an almost constant rate of oceanic crustal area of 3.4 km^2 per year for the past 180 million years. He concluded that "a constant rate of ridge production has important implications for models of sea level and pCO_2"—to which we can add, the history of seawater chemistry. How can the Mg/Ca ratio of seawater decrease through time if its major sink has remained constant?

Coggon *et al*. do not use Rowley's result but instead refer to Müller *et al*. (*11*), who argued that Rowley's approach is invalid. Rowley (*12*) has criticized the assumptions made by Müller *et al*. in extrapolating the spreading history or age distribution of oceanic lithosphere. Errors in estimates of the crustal production of seafloor that has been subducted are likely to be very large.

If Rowley is correct, then how could constant global ridge production lead to changing hydrothermal seawater Mg/Ca? One idea is that fast- and slow-spreading ridges may behave differently. Another, pointed out by Coggon *et al*., is that oceanic crust is altered on ridge flanks. Flanks buried by sediments may remain warm enough long enough to promote Mg removal (*13*).

At present, geophysical constraints on crustal production rate seem to be weaker than geochemical ones, yet they are crucial for the long-term climate balance of CO_2. Taken together with our knowledge of seawater chemistry, they offer the promise to understand the interactions between solid earth processes and the biogeochemical cycles of the major ions in the oceans.

References and Notes

1. H. D. Holland, in *The Oceans and Marine Geochemistry, Vol. 6*, H. Elderfield, Ed. (Elsevier, Oxford, 2003), pp. 583–625.
2. R. M. Coggon *et al*., *Science* **327**, 1114 (2010); published online 4 February 2010 (10.1126/science.1182252).
3. C. H. Lear *et al*., *Science* **287**, 269 (2000).
4. B. H. Wilkinson, T. J. Algeo, *Am. J. Sci.* **289**, 1158 (1989).
5. R. J. Spencer, L. A. Hardie, in *Fluid-Mineral Interactions*, Spec. Pub. 2, R. J. Spencer, I.-M. Chou, Eds. (Geochemical Society, St. Louis, MO, 1990), pp. 409–419.
6. E. T. Tipper *et al*., *Earth Planet. Sci. Lett.* **250**, 241 (2006).
7. M. R. Palmer, *Earth Planet. Sci. Lett.* **109**, 37 (1992).
8. S. E. McCauley, D. J. DePaolo, in *Tectonic Uplift and Climate Change*, W. F. Ruddiman, Ed. (Plenum, New York, 1997), pp. 427–467.
9. R. A. Berner, *Am. J. Sci.* **291**, 39 (1991).
10. D. B. Rowley, *Geol. Soc. Am. Bull.* **114**, 927 (2002).
11. R. D. Müller *et al*., *Science* **319**, 1357 (2008).
12. D. B. Rowley, *J. Geol.* **116**, 587 (2008).
13. H. Elderfield *et al*., *Earth Planet. Sci. Lett.* **172**, 151 (1999).

14. I thank J. Maclennan, S. Turchyn, and M. Bickle for helpful discussions.

10.1126/science.1186769

CELL BIOLOGY

Turning Off Inflammation Signaling

Srividya Sriskantharajah and Steven C. Ley

A cytosolic protein controls interactions between key ubiquitin-conjugating enzymes, thereby regulating the expression of proinflammatory genes.

The name A20 may sound unassuming for a protein, but polymorphisms in the *A20* gene locus have been identified as risk alleles for Crohn's disease, systemic lupus erythematosus, rheumatoid arthritis, type I diabetes, psoriasis, and atherosclerosis, suggesting important functions for A20 protein in autoimmunity. A20 is also a tumor suppressor for several types of B cell cancer, including Hodgkin's lymphoma and diffuse large B cell lymphoma (*1*). On page 1135 of this issue, Shembade *et al*. describe the means by which A20 acts through the transcription factor nuclear factor κB (NF-κB) to control inflammation (*2*).

Division of Immune Cell Biology, Medical Research Council, National Institute for Medical Research, London NW7 1AA, UK. E-mail: sley@nimr.mrc.ac.uk

NF-κB regulates the expression of genes involved in inflammation and immunity (*3*), and its chronic activation is associated with several human autoimmune diseases and cancers. Consequently, under normal conditions, NF-κB activation is transient and tightly controlled (see the figure). Inhibitor of NF-κB (IκB) proteins retain inactive NF-κB in the cytoplasm of unstimulated cells. Proinflammatory ligands, such as tumor necrosis factor (TNF), lipopolysaccharide (LPS), and interleukin-1 (IL-1), activate the IκB kinase (IKK) complex to phosphorylate IκBs, inducing their degradation. This releases associated NF-κB to translocate into the nucleus and activate the transcription of genes that promote inflamma-

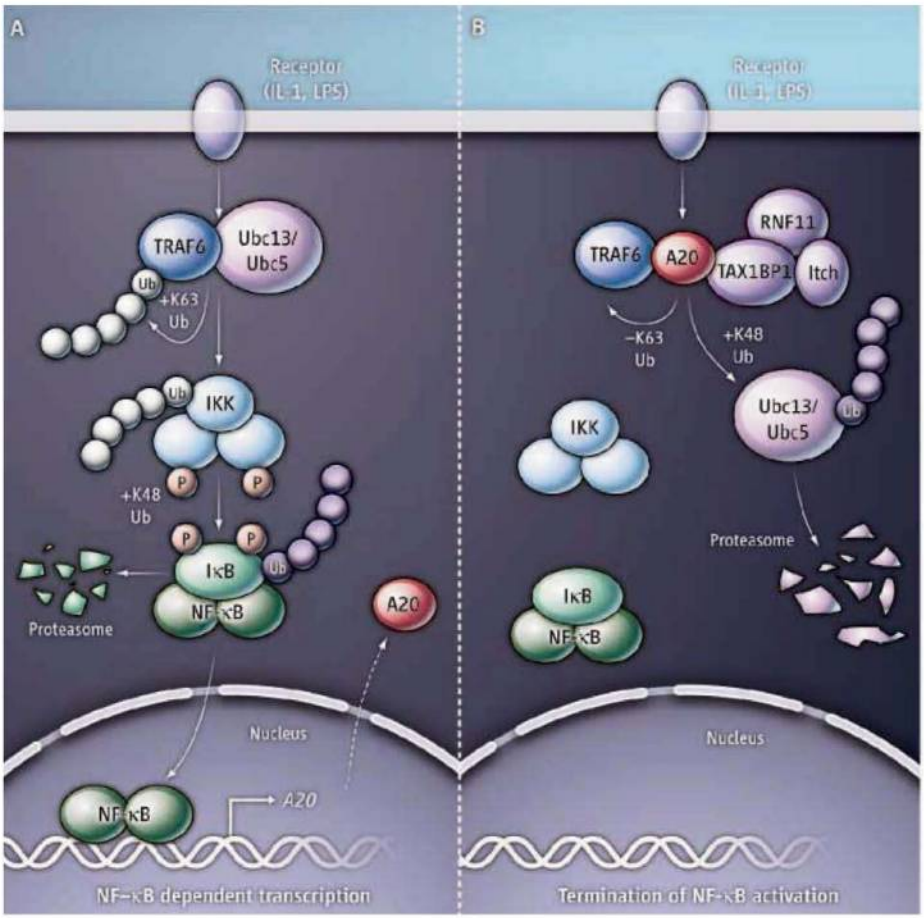

A20 in control. IL-1 and LPS stimulate the association of the E3 ligase TRAF6 with the E2 enzyme Ubc13 (or Ubc5). This promotes the autoubiquitination of TRAF6, which then activates the IKK complex and the transcription factor NF-κB. NF-κB targets include proinflammatory genes, but also the gene that encodes A20. A20, in a complex with TAX1BP1 and the E3 ligases Itch and RNF11, promotes the removal of ubiquitin chains from TRAF6, and disrupts TRAF6 association with Ubc13 (or Ubc5), terminating IKK and NF-κB activation. A20-TAX1BP1 also induce the delayed proteasomal degradation of Ubc13.

tion. However, one target is the gene encoding A20 (also called TNFAIP3), a negative feedback regulator that terminates IKK and NF-κB activation (*1*).

A20 can block activation of NF-κB by the cytokine TNF through a "ubiquitin-editing" process (*4*), but it has not been clear whether this function is also elicited in response to LPS and IL-1. Following cell stimulation by TNF, A20 modifies a cytosolic protein called receptor-interacting protein 1 (RIP1). A20 removes activating chains of ubiquitin molecules linked together by a specific lysine residue (K63), and facilitates the addition of similar chains linked together by another lysine (K48), thus targeting RIP1 for proteasomal degradation. This prevents activation of the IKK complex, and consequently NF-κB. In addition, an adaptor protein called Tax1-binding protein 1 (TAX1BP1) must recruit A20 and two E3 ubiquitin ligases (Itch and RNF11) to RIP1, to facilitate the switch in ubiquitination (*1*). A20 has an ovarian tumor (OTU) deubiquitinase domain at its amino terminus and a zinc-finger ubiquitin-binding domain (ZnF4) at its carboxyl terminus, and both are required for NF-κB inhibition (*4*). However, it is not known whether Itch, RNF11, or A20 itself functions as the E3 ligase that directly links ubiquitin chains to RIP1.

TNF receptor-associated factor (TRAF) proteins transduce signals from activated Toll-like receptor 4 in response to LPS, or IL-1 and TNF cytokine receptors, to different intracellular signaling pathways, including those that regulate IKK and NF-κB. In response to the LPS and IL-1, A20 removes an activating ubiquitin chain on the protein TRAF6, thereby abolishing its E3 ligase activity, an event that is required for NF-κB activation (*1*). However, it has remained unclear whether the ubiquitin-editing function of A20 is involved, as TRAF6 is not degraded (as is the outcome when A20 acts on RIP1). Shembade *et al.* show that LPS- and IL-1–induced activation of NF-κB is blocked by A20, because A20 disrupts interactions between key E2 and E3 enzymes that control activation of the IKK complex. Specifically, A20 binds to TRAF6, which prevents TRAF6 from associating with the E2-conjugating enzyme Ubc13 (Ubc13 normally triggers TRAF6 autoubiquitination and activation) (*5*). A20-TRAF6 interaction also requires the adaptor protein TAX1BP1.

The requirement for the E2 enzyme Ubc13 in NF-κB activation is cell type- or stimulus-specific (*5*), and recent experiments indicate that TNF activates the IKK complex through the E2 enzyme Ubc5, rather than Ubc13 (*6*). Shembade *et al.* show that A20, in a complex with TAX1BP1, disrupts the association of the E2 enzyme Ubc5 with the E3 ligases cIAP1 and TRAF2 upon TNF stimulation, and also disrupts the association of Ubc5 with the E3 ligase TRAF6 in response to IL-1. A20 can therefore control E3 ligase function in both Ubc13- and Ubc5-dependent NF-κB signaling pathways.

Although the cytokines TNF and IL-1 stimulate K48-linked ubiquitination of the E2 enzyme Ubc13, its subsequent proteolysis occurs several hours after cytokine stimulation. It is therefore unclear whether Ubc13 degradation is important for the acute inhibitory effects that A20 has on IKK activation, but it may play a role when stimulation is chronic. For example, Tax, the transforming oncoprotein of human T cell leukemia virus-type I, persistently activates NF-κB by protecting Ubc13 from degradation by A20 (*2*).

The findings of Shembade *et al.* raise questions about how A20 turns off NF-κB signaling in TNF-stimulated cells. For example, it is not known whether the ubiquitin-editing function of A20 occurs simultaneously with its inhibition of E2-E3 enzyme interactions, or if it is an alternate mechanism to down-regulate IKK activation. Both mechanisms indicate essential roles for the OTU and ZnF4 domains of A20, consistent with their requirement for the inhibitory effect of A20 on NF-κB activity. However, the roles of the ubiquitinating and deubquitinating functions of A20 for controlling E2-E3 enzyme interactions are not known. But the detailed insights provided by Shembade *et al.* suggest that pharmacological inhibition of the E2 ligases that A20 controls, such as Ubc13 or Ubc5, may be beneficial in treating certain autoimmune diseases and cancer.

References

1. L. Vereecke, R. Beyaert, G. van Loo, *Trends Immunol.* **30**, 383 (2009).
2. N. Shembade *et al.*, *Science* **327**, 1135 (2010).
3. S. Vallabhapurapu, M. Karin, *Annu. Rev. Immunol.* **27**, 693 (2009).
4. I. E. Wertz *et al.*, *Nature* **430**, 694 (2004).
5. Z. J. Chen, L. J. Sun, *Mol. Cell* **33**, 275 (2009).
6. M. Xu *et al.*, *Mol. Cell* **36**, 302 (2009).

10.1126/science.1187271

SPORE: *SCIENCE* PRIZE FOR ONLINE RESOURCES IN EDUCATION

On the Cutting Edge: Teaching Help for Geoscience Faculty

A place is described for faculty to share their teaching expertise and to remain current with advances in geoscience.

Cathryn A. Manduca,[1]* David W. Mogk,[2] Barbara Tewksbury,[3] R. Heather Macdonald,[4] Sean P. Fox,[1] Ellen R. Iverson,[1] Karin Kirk,[1] John McDaris,[1] Carol Ormand,[1] Monica Bruckner[1]

In contrast to science, which makes progress at the level of the community and where individual work builds on all that has come before, teaching science has often been an individual enterprise. Typically, faculty create courses in isolation, without the benefit of knowledge of others' classroom experiences or research on how students learn (*1*, *2*). Building a culture of sharing and communal improvement in support of undergraduate geoscience teaching is the goal of the On the Cutting Edge professional development program.

To this end, On the Cutting Edge has offered a series of professional development workshops for geoscience faculty and graduate students since 2002. Participants share their teaching experiences, learn from leaders in geoscience and other disciplines, and develop new online resources in support of teaching geoscience (*3*) (see the figure, right). Many of the workshops focus on specific topics in geoscience education. Emerging themes, such as teaching with visualizations and data; core courses in the undergraduate major, such as structural geology; and rapidly changing content areas, such as climate change, are all included. Other workshops, repeated each year, help faculty design or revise a course, pretenure faculty manage their careers, and postdoctoral students and graduate students prepare for an academic career. This range of workshop topics has been successful in engaging a wide spectrum of geoscience faculty in learning more about geoscience teaching.

Workshop participants generate much of the Web site content. Here, participants in the 2008 Teaching Introductory Geoscience workshop work together to improve their contributions to the teaching activity collection.

To date, ~1400 geoscience faculty from more than 450 geoscience departments have participated in On the Cutting Edge workshops. Participants from research universities, comprehensive universities, liberal arts colleges, and 2-year colleges are selected on the basis of scientific and educational expertise, as well as to provide a diverse array of viewpoints.

The On the Cutting Edge Web site (http://serc.carleton.edu/NAGTWorkshops/) is one of the program's most important innovations for allowing faculty to learn from one another about teaching. The Web site is a key resource for workshop participants as they prepare for their workshop experience; it provides tools for interaction, sharing, and collaboration during the workshop and records insights gained at the workshop. After the workshop, the Web site provides information and resources and supports changes in instruction for both participants and the larger community. The Web site also illuminates the linkages between science content, pedagogical strategies, teaching activities, assessments, and research on learning.

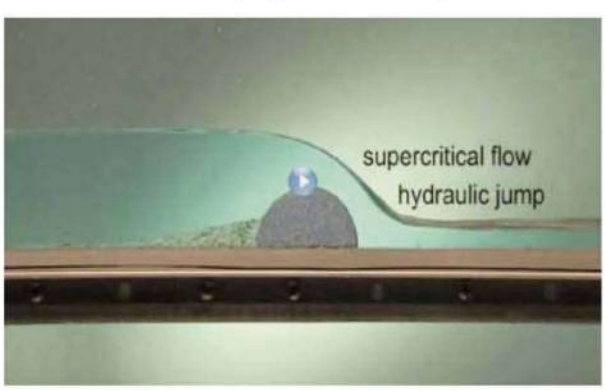

Many Web site users are searching for video or other visualizations. This video of a flume study of water flowing over a dam is part of a collection of videos for teaching river geomorphology developed by Little River Research and Design, with funding from the Missouri Department of Natural Resources. From this page, users can easily explore other related materials and ideas for teaching geomorphology, including a collection of teaching activities and syllabi.

The Web site is a joint creation of the workshop participants and the project team of On the Cutting Edge. The conveners work with staff to create pages that introduce the topics of the workshop and build a foundation for workshop discussions. For example, before a workshop on the role of the affective domain in geoscience teaching, pages reviewing the definition of the affective domain, a framework for its application to teaching, and an introduction to the literature were developed. Workshop participants prepare for the workshop by reviewing materials on the Web site and contributing examples from their own teaching. In another example, participants from a 2009 workshop on teach-

[1]Science Education Resource Center, Carleton College, Northfield, MN 55057, USA. [2]Department of Earth Sciences, Montana State University, Bozeman, MT 59717, USA. [3]Geology Department, Hamilton College, Clinton, NY 13323, USA. [4]Geology Department, College of William and Mary, Williamsburg, VA 23187, USA.

*Author for correspondence. E-mail: cmanduca@carleton.edu

CREDIT: (TOP) DAVE TEWKSBURY

ing paleontology submitted descriptions of their courses and two activities that they have used in the classroom. These examples are collected through a structured Web-based format in advance of the workshop, which allows participants to learn about their colleagues' work before they meet at the workshop and automatically produces a valuable, easily searched collection for use by all interested faculty (*4*).

During the workshop, participants document the results of their discussions and work together via the Web site. For example, participants in the affective domain workshop described dilemmas that they had faced in teaching and discussed a variety of possible responses, based on the presentations and information gained at the workshop. They developed these discussions into a set of Web pages that they can use for their own reference and that are available to others. Increasingly, workshops also provide opportunities for participants to review and improve teaching activities submitted before the workshop, enhancing the quality of the materials shared through the Web site.

Following the workshop, the On the Cutting Edge project team reviews materials generated by the workshop and creates a topical site designed to present this information to geoscience faculty who did not attended the workshop.

The On the Cutting Edge site now has 33 topical sections based on the workshops offered to date. These include more than 1200 community-contributed teaching activities ranging from in-class activities that make lecture interactive to designs for laboratory activities. Web statistics show that 16,000 users returned to the site six or more times last year to find ideas or materials for teaching, to learn about a new method or topic, to find out what their colleagues are doing in their teaching, to find geoscience visualizations, or to obtain information to assist with career planning or advancement (see the figure, page 1095, bottom). We estimate that ~25% of these users are geoscience faculty, including roughly equal numbers of workshop participants and other geoscience faculty. Other users include faculty in other disciplines, teachers of elementary through high-school pupils, students, and others.

Workshop participants use the Web site to refresh their memory, to make use of resources discussed at the workshop in their teaching, and to expand their knowledge in areas addressed by workshops other than the one they attended. For example, one participant in the Introductory Geoscience workshop developed a dinosaur course by combining ideas learned at the workshop with materials from the online course design tutorial available from a workshop he did not attend. The result was a course that used a student project as a central element to tie together concepts addressed throughout the course. Similarly, geoscience faculty who have not attended workshops are using the Web site to learn about different aspects of geoscience teaching and to find out more about what their colleagues are doing in their courses. This combination gives them confidence to try new methods in their teaching.

We know less about use by those outside geoscience, but use patterns suggest that they are also learning about pedagogy, finding visualizations, and exploring teaching examples. Of intensive sessions (those viewing 10 or more pages), 38% include views of activity pages. Learning does not stop with the activities, however; 20% of intensive sessions include visits to a module describing a pedagogic method.

The combination of workshops and Web sites has influenced the practice of individual geoscience faculty in the classroom (*5*). Multiple surveys indicate that 80% of respondents have made specific changes to their teaching practices with a measurable shift toward active-learning techniques. Interviewees can identify specific changes and trace them to lessons learned at the workshop or from the Web site. Critical to supporting these changes is a student-centered view of learning (*6*), which is developed at the workshops. Past participants use phrases such as "eye-opener" or "seismic shift" to describe this change in viewpoint.

Beyond the impacts on individual faculty, the On the Cutting Edge program has created a new culture; faculty learn from one another and share resources to improve teaching. The workshops encourage discussions about teaching, whereas the Web site allows faculty to quickly discover what others are doing. We are beginning to see spontaneous contribution of teaching materials through our online submission forms, actions that reflect the beginnings of a self-sustaining community of sharing.

In the future, On the Cutting Edge will offer several workshops in 2010 on topics central to improved teaching in the geosciences: teaching complex systems, using the Geographic Information System and remote sensing in geoscience, and teaching through fieldwork. We continue to work to engage a larger fraction of geoscience faculty in this community and, this year, will expand our virtual workshop series by offering workshops on service learning, teaching about the deep earth, designing effective courses, and teaching online courses. All will yield new additions to the Web site, which we invite you to explore and enjoy.

About the Authors

Authors Macdonald, Mogk, and Tewksbury are full-time geoscience faculty, in addition to leading the On the Cutting Edge program. Cathryn Manduca (left) is the executive director of the National Association of Geoscience Teachers and the director the Science Education Resource Center (SERC) at Carleton College, which uses workshops and Web sites to help faculty to be better teachers in all disciplines and engages in projects that support geoscience education at all levels. All the authors have received national awards for contributions to geoscience education and have served as leaders in geoscience professional societies. As SERC's technical director, Fox has developed the content management system that supports community development by the On the Cutting Edge Web site. Iverson, SERC's evaluation director, leads the data collection effort for the Web site and workshops. Kirk, McDaris, Ormand, and Bruckner manage the Web site, steward the content, and create a coherent resource from the contributions of community members.

References and Notes

1. R. H. Macdonald, C. A. Manduca, D. W. Mogk, B. J. Tewksbury, *J. Geosci. Educ.* **53**, 237 (2005).
2. C. A. Manduca, E. R. Iverson, S. P. Fox, F. McMartin, *D-Lib* **11** (2005); www.dlib.org/dlib/may05/fox/05fox.html.
3. R. H. Macdonald, C. A. Manduca, D. W. Mogk, B. J. Tewksbury, in *Invention and Impact: Building Excellence in Undergraduate Science, Technology, Engineering, and Mathematics (STEM) Education* (AAAS, Washington, DC, 2004), pp. 233–240.
4. C. A. Manduca, S. Fox, E. R. Iverson, *D-Lib* **12** (2006); www.dlib.org/dlib/december06/manduca/12manduca.html.
5. On the Cutting Edge Evaluation Summary, http://serc.carleton.edu/NAGTWorkshops/evaluation.html.
6. S. Loucks-Horsley *et al.*, *Designing Professional Development for Teachers of Science and Mathematics* (Corwin, Thousand Oaks, CA, ed. 2, 2003).
7. On the Cutting Edge is sponsored by the National Association of Geoscience Teachers, contributes to the National Science Digital Library, and is supported by NSF's Division of Undergraduate Education under grants 0127310, 0127141, 0127257, 0127018, 0618482, 0618725, and 0618533. Any opinions, findings, conclusions, or recommendations expressed in this Web site are those of the authors and do not necessarily reflect the views of NSF.

10.1126/science.1183028

SCIENCE AND SOCIETY

Science-Rights Coalition Has Global Impact in First Year

One group studied the human impacts of gold mining in Guinea. Another analyzed the economic aid to rebuild New Orleans' hurricane-ravaged infrastructure. And others are working to improve on a vital tradition, assessing the most effective ways to protect scientists from political persecution.

Productive partners. Villagers in Madhya Pradesh join Geoscientists Without Borders in a water study for the Indian state.

PHOTO CREDIT: DANIEL MATZ

It was a busy first year for the AAAS-led Science and Human Rights Coalition and the "On-call" Scientists. At 2 days of meetings at the association's Washington, D.C. headquarters, Coalition members encouraged volunteer efforts and charted ambitious new initiatives.

The Coalition has created a "starter kit" to help scientific organizations develop their own human rights programs, built a comprehensive bibliography of science and human rights materials, and taught researchers to respond to alleged rights violations.

Building on this foundation, the Coalition plans a substantial campaign in 2010 to support a United Nations covenant on the universal access to scientific knowledge.

Science and human rights "benefit from each other's strengths," said Jessica Wyndham, project director in the AAAS Science and Human Rights Program. "Scientists bring technical knowledge to human rights problems, and human rights organizations help scientists realize the potential impacts of their research."

Since its founding in 1977, the program has promoted science-based solutions to investigate mass atrocities, develop encryption technologies to protect human rights communication, and analyze satellite imagery to document human rights violations. The program also offers a service to publicize threats against scientists around the globe.

When Susan Hinkins became chair of the American Statistical Society's committee on scientific freedom and human rights, "it felt as if every new chair of the committee had to reinvent the process and rebuild the connections," she said. "So I was very eager to participate in the development of the Coalition."

A year after its debut, the Coalition has grown to include more than 45 member or affiliate societies—including the American Psychological Association and Sigma Xi, the research society—and 50 individual members.

Participants at the 22 January meeting discussed the ethical dilemmas surrounding scientific research for the military, as well as stories from survivors of human rights violations.

In one session, groups such as Geoscientists Without Borders demonstrated how researchers can use their tools and training to benefit communities in unexpected ways.

The group, part of the Society of Exploration Geophysicists, is part of an ongoing project to develop evacuation plans and shelters for communities along Sumatra's remote southwestern coast after a devastating 9.1 magnitude earthquake hit the island in 2004.

Volunteers used tsunami and earthquake rupture modeling to design tall evacuation towers, said Program Manager Rhonda Jacobs. The new designs "would allow residents to climb above the tsunami, as opposed to outrunning it by moving inland," she explained.

Programs such as AAAS's "On-call" Scientists, which connected researchers with the projects in Guinea and New Orleans, can have an immediate impact on communities in need, they agreed.

"As scientists, we have a love for finding answers and strive during our careers to use our research for beneficial activities," said Alexander Mihai Popovici, current committee chair of Geoscientists Without Borders. "It is great to see both these passions come together, bringing basic human rights and the benefits of science to people who need it."

A day before the meeting, the Coalition's Working Group on the Welfare of Scientists held a training session on the best practices for defending scientists against human rights violations. With its partner Scholars at Risk, an international network of higher education institutions, the working group offered a primer in international and regional human rights laws pertaining to scientists.

—Benjamin Somers and Becky Ham

BIOSECURITY

Synthetic DNA Plan Limits Risk, Experts Say

Significant advances in synthetic gene production have raised a critical question for industry leaders and national security experts: How can the research and trade in tailor-made DNA continue while assuring that the materials aren't available to criminals and terrorists?

Proposed federal guidelines can secure genetic material that could be used to create harmful pathogens without stifling promising research in medicine, agriculture, and energy production, experts said at an 11 January meeting at AAAS. The guidelines propose voluntary screening of both potential buyers and the sequences they are seeking.

While some participants suggested fine-tuning, "the overall sentiment was that the guidance is well thought out, facilitates advances in scientific knowledge, and allows for international engagement," says a summary from the AAAS Center for Science, Technology and Security Policy (the summary is available at www.aaas.org/go/synth_dna).

Following the release of the guidelines last November, the U.S. Department of Health and Human Services and the Department of State asked AAAS to convene a group to informally evaluate the draft guidance. Nearly 100 researchers, industry representatives, and policy experts gathered at the meeting organized by Gerald Epstein, director of the AAAS Center, and Kavita Berger, the Center's associate program director for biosecurity.

Mechanisms Underlying Lineage Commitment and Plasticity of Helper CD4$^+$ T Cells

John J. O'Shea* and William E. Paul

CD4$^+$ T cells are critical for host defense but are also major drivers of immune-mediated disease. These T cells specialize to become distinct subsets and produce restricted patterns of cytokines, which are tailored to combat various microbial pathogens. Although classically viewed as distinct lineages, recent work calls into question whether helper CD4$^+$ T cell subsets are more appropriately viewed as terminally differentiated cells or works in progress. Herein, we review recent advances that pertain to this topic and the mechanisms that contribute to helper CD4$^+$ T cell commitment and plasticity. The therapeutic implications of these new findings are also considered.

Faced with innumerable microbial pathogens, antigen-inexperienced naïve CD4$^+$ T cells orchestrate immune responses by differentiating into T helper (T_H) cell populations that secrete distinct sets of cytokines. In this manner, they tailor their responses to the character of the threat encountered, providing help to B lymphocytes and CD8$^+$ cytotoxic T cells and activating the cells of the innate immune system. The importance of CD4$^+$ T cells is vividly illustrated in the range of infections that afflict HIV-infected individuals when their blood CD4$^+$ T cell numbers decline. CD4$^+$ T cells also play critical roles in the pathogenesis of autoimmunity, asthma, allergy, and likely cancer. The concept of distinct T_H cell lineages has been a useful paradigm for the conceptualization of CD4$^+$ T cell differentiation, but immunologists are now rethinking how T_H cell subsets should be viewed. Are distinct T_H subsets really different lineages, and, if so, how plastic are they in altering or modifying their committed state? Or, do T_H cells lack features of end stage commitment and readily alter their profile of secreted products? Certainly, there is increasing evidence in vitro that differentiated CD4$^+$ T cell populations can alter the range of cytokines they produce, although whether this occurs as readily in vivo remains unclear. Understanding the molecular basis of CD4$^+$ T_H cell differentiation and of the process through which cells alter their cytokine-producing potential will likely provide interesting insights into subset specification and gene regulation. Equally, these insights may allow the development of strategies to alter T_H cell function in circumstances of autoimmunity or allergy or alternatively, when a response is mounted against a pathogenic microbe or a tumor cell that is appropriate in specificity but inappropriate in type.

Molecular Immunology and Inflammation Branch, National Institute of Arthritis and Musculoskeletal and Skin Diseases, Laboratory of Immunology, National Institute of Allergy and Infectious Disease, National Institutes of Health, Bethesda, MD 20892–1616, USA.

*To whom correspondence should be addressed. E-mail: osheajo@mail.nih.gov

Why Should We Think of Subsets of Cytokine-Producing CD4$^+$ T Cells as Differentiated Lineages?

Nearly a quarter of a century ago, it was recognized that cytokine production by T_H cells was not stochastic (*1*). Rather, T cell clones could be divided into two subsets, T_H1 and T_H2, which respectively produced the signature cytokines interferon (IFN)-γ and interleukin (IL)-4 and IL-13 (Fig. 1). Importantly, selective cytokine production was a stable feature of multiply passaged T_H1 and T_H2 cell lines. T_H1 and T_H2 cells also preferentially expressed particular cytokine and chemokine receptors. Both subsets were thought to provide help to B cells, although they "instructed" the class-switching mechanism toward different immunoglobulin (Ig) classes [see discussion of T follicular helper (Tfh) cells in the next section]. Their selective cytokine production was important for the proper elimination of microbial pathogens, intracellular microbes for T_H1 cells, and helminths for T_H2 cells (*2*). These subsets also expressed lineage-specifying transcription factors (T-bet and GATA3), and overexpression of these "master regulators" induced the production of the stereotypic cytokine (*3*). The concept of stable, terminally differentiated T_H cells made sense: After exposure to a particular pathogen, memory T cells would "remember" to make responses not only of the correct specificity but also of the appropriate type.

How Does Increasing Subset Complexity Fit with Existing Models?

Although this paradigm was a useful construct for understanding immunoregulation and to define the molecular mechanisms that shaped CD4$^+$ T cell differentiation, the dualistic view of T_H cell lineages was complicated by the recognition of new subsets of T_H cells. CD4$^+$ CD25$^+$ regulatory T cells (T_{reg}s) were identified and found to be critical for the preservation of immune tolerance (*4*–*6*). Besides thymic-derived T_{reg}s (natural or nT_{reg}s), it was shown that naïve T cells in the periphery could acquire immunosuppressive properties and become induced Tregs (iT_{reg}s). Both T_{reg} subsets express the forkhead transcriptional repressor, Foxp3 (*5*, *6*). Absence of Foxp3 results in widespread autoimmunity and absence of T_{reg}s, whereas its overexpression confers immunosuppressive functions (*5*, *6*). Consequently, Foxp3 was designated as the T_{reg} master regulator. Although the biologic significance of T_{reg}s is well established, the relative importance of nT_{reg}s and iT_{reg}s is still unresolved. No decisive tests to differentiate their function in physiologic settings and particularly in humans have yet been devised.

The next "lineage" recognized was cells that selectively produced IL-17 (T_H17 cells), which also seemed to have their own master transcription factor, the orphan retinoid receptor, Rorγt (*7*, *8*). The recognition of T_{reg}s and T_H17 cells improved our understanding of immunoregulation and provided insights into the pathogenesis of autoimmunity, but whether T_{reg}s and T_H17 cells behaved like polarized T_H1 and T_H2 cells was unclear. For one, T_{reg}s and T_H17 cells both require transforming growth factor–β (TGFβ) for their induction (*9*). Tfh cells are yet another CD4$^+$ T cell population with a particular function, helping B cells make antibody responses to T cell–dependent antigens (*10*–*12*). They aid in the development of germinal centers (specialized regions within secondary lymphoid tissues that promote B cell immunity) and promote immunoglobulin class switch recombination and affinity maturation. Tfh cells express Bcl6, their master regulator transcription factor (*13*–*15*), but unlike T-bet and GATA3, Bcl6 is a transcriptional repressor. Whether Tfh cells are truly a population (lineage) parallel to T_H1, T_H2, T_H17, and iT_{reg} cells or a particular state of some or all of these cells is unresolved (*10*–*12*). Tfh cells have distinct properties and phenotypes (e.g., expression of CXCR5, ICOS, and Bcl6); however, individual Tfh cells may produce T_H1 or T_H2 signature cytokines, depending on the conditions of their initial activation (*10*–*12*). Thus, are IL-4– or IFN-γ–producing Tfh cells members of a Tfh lineage that then acquires a distinct cytokine-producing potential, or is "Tfh-ness" a property of T_H1, T_H2, and possibly T_H17 cells acquired much in the same way that these cells become central memory cells, effector memory cells, or tissue-seeking effector cells? Of course, if the latter is the case, then a discussion of plasticity for Tfh cells is the same as discussing plasticity among the conventional effector lineages. Although these new discoveries increase the complexity of the T_H response and raise questions of how decision-making in the differentiation process occurs, they could still be accommodated

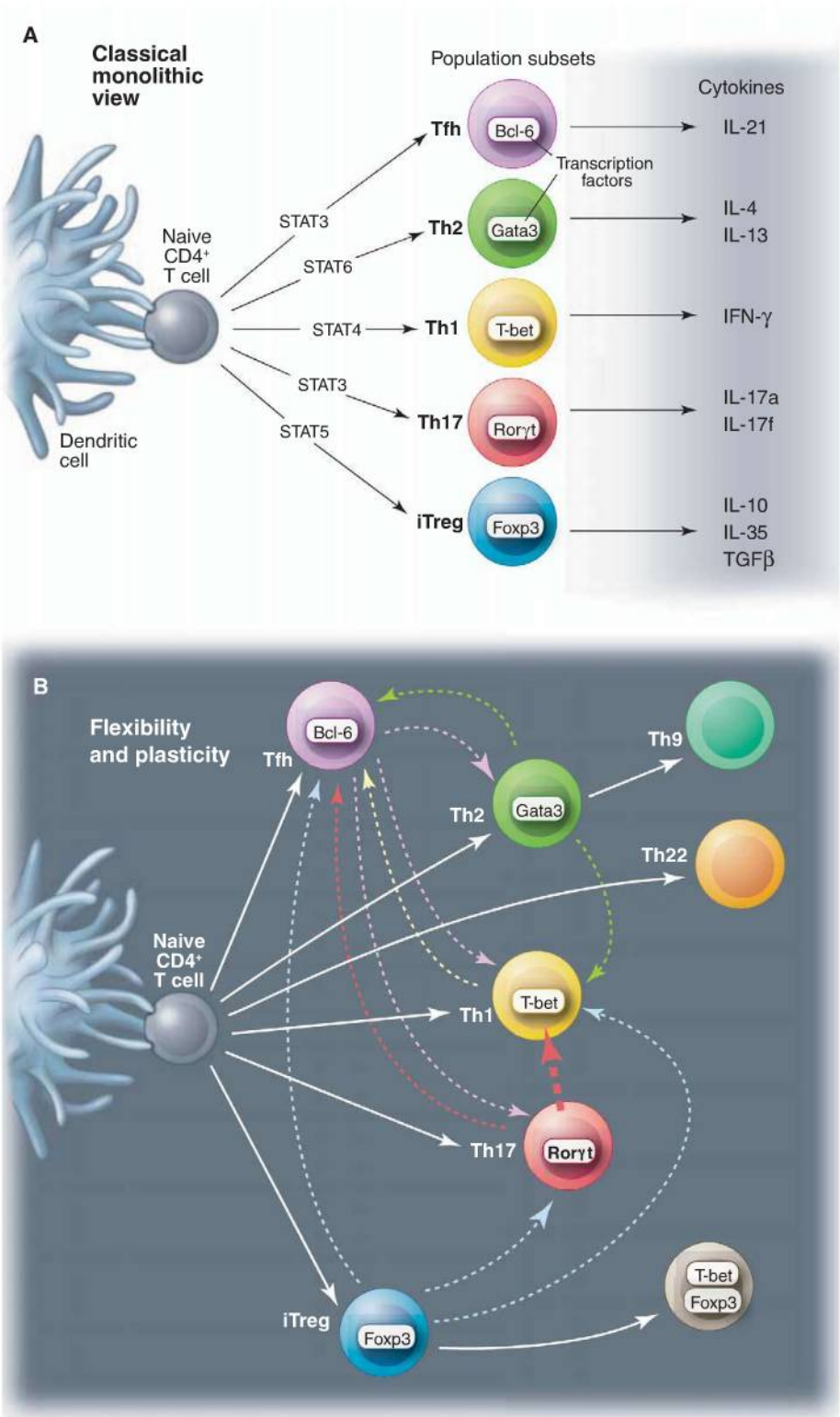

Fig. 1. Helper T cell differentiation. **(A)** The classical monolithic view: lineages and master regulators. Initial studies arising from in vitro cultured T_H1 and T_H2 cells led to the idea that these subsets behaved like lineages, meaning that their phenotype (i.e., selective cytokine production) was inflexible. Accordingly, these subsets expressed lineage-defining transcription factors that were sufficient to impart this selective cytokine production. As newer subsets of cytokine producing cells were identified, they too were viewed as stable lineages. **(B)** Flexibility and plasticity of helper T cells. Recent studies of T_H cells have revealed more flexibility in cytokine production than predicted by earlier work, and there are now many examples of plasticity of T_H cell phenotype. $CD4^+$ T cells can change their profile of cytokine production, and there are now circumstances in which the expression of master regulators is transient or instances where cells express more than one master regulator.

within the end-stage differentiation paradigm. T cell fates need not be restricted to two or even four T_H cell lineages; on the contrary, given the many microbial pathogens, one could imagine the need for multiple specialized subsets. But how the system determines the character of the threat and makes appropriate decisions as to what the dominant response will be grows increasingly complicated with each additional "lineage."

To What Extent Is Cytokine Production Plastic?

More challenging than the identification of new T_H cell subsets was the emergence of evidence that cytokine expression is not as stable as initially thought; indeed, there are now many examples of flexible cytokine production (*9*, *10*, *16*). Once thought to be a T_H2 cytokine, IL-10 is now recognized as produced by multiple cell subsets: T_H1, T_H2, Tregs, and T_H17 cells (Fig. 2). Similarly, T_H2 cells can acquire IL-9–producing capacity in the presence of TGFβ (*17*), but IL-9 can also be produced by T_H17 cells (*18*). Acquisition of IFN-γ–producing potential by T_H17 cells, particularly the simultaneous production of IL-17 and IFN-γ, is a common occurrence, especially in vivo (*19*, *20*). T_H17 cells can even extinguish production of their cytokine signature, becoming selective IFN-γ producers (*21*–*23*). Although T_H1 cells do not become IL-17 producers, under the right circumstances they can make IL-13 (*24*). T_H17 cells produce IL-22, but cells that make IL-22 and not IL-17 have recently been identified (*25*, *26*). Simultaneous production of IL-22 and IFN-γ also occurs and, indeed, IL-22 was originally viewed as a T_H1 cytokine. More concerning for the firmly fixed notion of cytokine production, however, is the finding that in vitro differentiated, IL-4–producing T_H2 cells specific for lymphocytic choriomeningitis virus (LCMV) produce IFN-γ when transferred into mice subsequently infected with LCMV (*27*). Whether cells primed in vivo under robust T_H2-inducing conditions show an equal propensity to acquire IFN-γ–producing capacity has not been established.

Collectively, these findings argue for much flexibility in cytokine production, but the true frequency with which T_H cells alter their cytokine-producing potential in vivo is still uncertain. More precisely, to what extent do cells really change? Not just by expressing a cytokine that they formerly did not, but rather by altering the major properties that define T_H cells. To the extent that such plasticity is a major feature of immune responses, the stakes are raised in the effort to understand how the system reads pathogen threats and orders up the right response.

Is Expression of Master Regulators Stable?

What is clearly problematic for a strict lineage commitment model of T_H cell differentiation is that the expression of master regulators that drive differentiation is not fixed. For instance,

it now appears that Foxp3$^+$ T_{reg} cells are heterogeneous and that transient expression of Foxp3 is a common event (*28*). Many studies show that Foxp3 expression can be extinguished and that former T_{reg}s can acquire the ability to produce pro-inflammatory cytokines (*28*–*31*). This phenomenon is enhanced in the setting of autoimmunity. More disturbing is that T_H cells can also express more than one master regulator. Cells expressing Foxp3 and T-bet are present at sites of inflammation and limit that inflammation (*32*). T_{reg}s can simultaneously express Foxp3, RORγt, and the transcriptional repressor Runx3 (*33*, *34*). Alternatively, Foxp3$^+$ cells can differentiate into Tfh cells in Peyer's patches in the gut, implying that they acquire Bcl6 expression (*35*).

So what does all this mean? Recent studies indicate that flexibility in expression of master regulators and cytokines is relatively common. Whether this will be true for T_H cell populations primed in vivo will require much additional analysis, and whether this potentiality translates into change in phenotype under physiologic conditions also remains to be established. Such plasticity may have evolutionarily selective value: To the extent that aging humans and mice rely more and more on memory CD4$^+$ T cells to respond to newly encountered pathogens, freezing the phenotype of memory cells could lead to inappropriate responses to new threats. So, perhaps our earlier "evolutionary" argument for stability is not so compelling after all.

What Mechanisms Underlie Commitment and Plasticity?

Flexibility in cytokine production by CD4$^+$ T cells does not easily square with conventional models of helper cell lineage commitment and raises the question of whether these notions are still useful. If flexibility and/ or plasticity is the rule, what governs such changes in production of individual cytokines or wholesale changes in the properties of cells? In this context, it is useful to revisit the concept of lineage commitment and consider recent advances that shed new light on terminal differentiation.

Defining factors that regulate lineage commitment and plasticity is not new, nor is it unique to T cells. Arguments regarding determinism and flexibility in developmental biology arise from the earliest experiments in model organisms. These lessons show that morphogens drive expression of lineage-specifying transcription factors, a classic example being the TGF-β–related cytokine, activin, that promotes mesoderm differentiation by inducing the T-box protein Brachyury. Other transcription factors of the homeobox, signal transducer and activator of transcription (STAT), NF-κB, Notch, and Forkhead families have similar, critical roles in development. A key aspect of commitment is that not only are genes turned on by transcription factors but also that genes conferring alternative fates are repressed.

Preferential gene expression is heritable, and diverse epigenetic modifications ensure that this is the case. As a result, cell identity remains stable without continued external signals. Cell stability is also controlled by microRNA (miRNA) expression (*36*). These short single-stranded noncoding RNAs repress target mRNAs by inhibiting translation and enhancing mRNA decay. From this perspective, T_H cell differentiation resembles classical lineage commitment. Cytokines provide morphogen-like signals, inducing expression of lineage-specifying transcription factors that belong to the same families that are critical for development in general. The stability of cytokine production is also preserved by epigenetic modifiation. Studied predominantly in in vitro differentiated cells, lineage-defining cytokine genes (*Ifng*, *Il4*, and *Il17*) have the predicted permissive and repressive epigenetic modifications (*29*, *37*). Both the *Il4* and *Ifng* genes also show striking CpG demethylation, an epigenetic modification that is associated with gene expression, in their promoters and in enhancer regions during the process of differentiation to T_H2 and T_H1 cells, respectively. The region upstream of exon-1 of the *Foxp3* gene is also strongly methylated in non-T_{reg}s but is largely demethylated in nT_{reg}s (*38*). Thus, the ability of different T_H cells to selectively produce cytokines looks like commitment; however, even classical lineage commitment does not exclude flexibility.

Although commitment indicates that the developmental fate of a cell and its progeny is restricted, it is divided into two phases: specification and determination. The former implies reversibility, whereas the latter connotes irreversible commitment. It might be reasonable to posit, then, that many CD4$^+$ T cell subsets are specified but rarely become fully determined. This makes sense because, unlike sessile cells in organs like the brain or heart, T cells migrate; irreversible commitment might be disadvantageous under changing conditions. To completely discard the notion of determination, however, would be premature. Cells grown in tissue culture over long periods of time can act like determined cells, but to what extent does this mimic physiology? Nonetheless, the demonstration that terminally differentiated cells can become inducible pluripotent stem cells and generate a new organism just by expressing four transcription factors puts all determination at risk (*39*). Thus, plasticity is relative, not absolute. Importantly, there are also other examples of reprogramming in which de-differentiation back to stem cells is not required (*40*). Such examples represent extraordinary examples of plasticity, but they are artificial. Regardless, these insights establish the principle that transcription factor expression dramatically alters cell fate, even in highly differentiated cells. One implication is that, rather than assuming that expression of a master regulator implies a discrete function, we should be thinking more about gradients of transcription factors such as Rorγt, Foxp3, and T-bet and repressors like Bcl6 and Blimp1. As we better understand the extrinsic and intrinsic signals that influence expression of transcription factors and transcriptional repressors, we might be surprised by the plasticity that emerges.

As indicated above, epigenetic modifications help ensure that phenotype does not change, even in the absence of extrinsic signals; however, epigenetic marks are not immutable. Intriguingly, the epigenetic modifications of the genes encoding T-bet and GATA3 are more complex than one might expect a priori. Unlike the signature cytokine genes, the genes encoding the master regulators for T_H1 and T_H2 cells have both repressive and permissive marks in opposing lineages (*29*). This pattern has been denoted as bivalency and is typical of genes in stem cells that are poised for induction (*41*). Furthermore, epigenetic modifications are dynamic, and H3K27 demethylases (Jumonji d3 and UTX) can remove repressive marks (*42*). Of note, when isolated Foxp3$^+$ cells were transferred into autoimmune recipients and Foxp3 expression was down-regulated, the Foxp3 locus became remethylated (*28*).

miRNAs are another factor that influences the stability of Foxp3 gene expression. Deleting the genes encoding the miRNA processing enzymes Dicer and Drosha in T_{reg}s results in loss of Foxp3 expression, and the resultant T cells have the capacity to become effectors (*43*).

Similarly, deletion of the transcriptional repressor Bcl-6 results in the expression of a large number of miRNAs (*13*). Thus, regulation of miRNAs has the potential of being an important mechanism in preserving and altering helper cell phenotype, but we need to understand when and how expression of key miRNAs is altered physiologically and how they influence epigenetic regulation.

Lineages Versus Subsets: Who Cares?

For those not directly involved, the question of stability versus plasticity of subpopulations might be viewed as a tempest in a teapot: Who cares whether a T_H cell represents a determined or potentially plastic lineage or a subset? From a cell biologist's perspective, the distinction might seem arbitrary or even pretentious; however, this is not just a pedantic distinction and there are very pragmatic reasons for carefully considering this question. In fact, the prospect of lineage commitment versus flexible programs for T cells has direct implications for disease pathogenesis and the success of therapeutic interventions. A variety of autoimmune and allergic inflammatory disorders are associated with the presence of T_H cells of particular types, and these cells have a major influence on, even controlling the pathophysiology of, these disorders. If T cell responses are plastic, one should be able to reset the clock therapeutically. The allergen-specific T_H2 cells of asthmatics and others might be altered in vivo and thus interrupt the disorder. In multiple sclerosis and early type I diabetes, the destructive

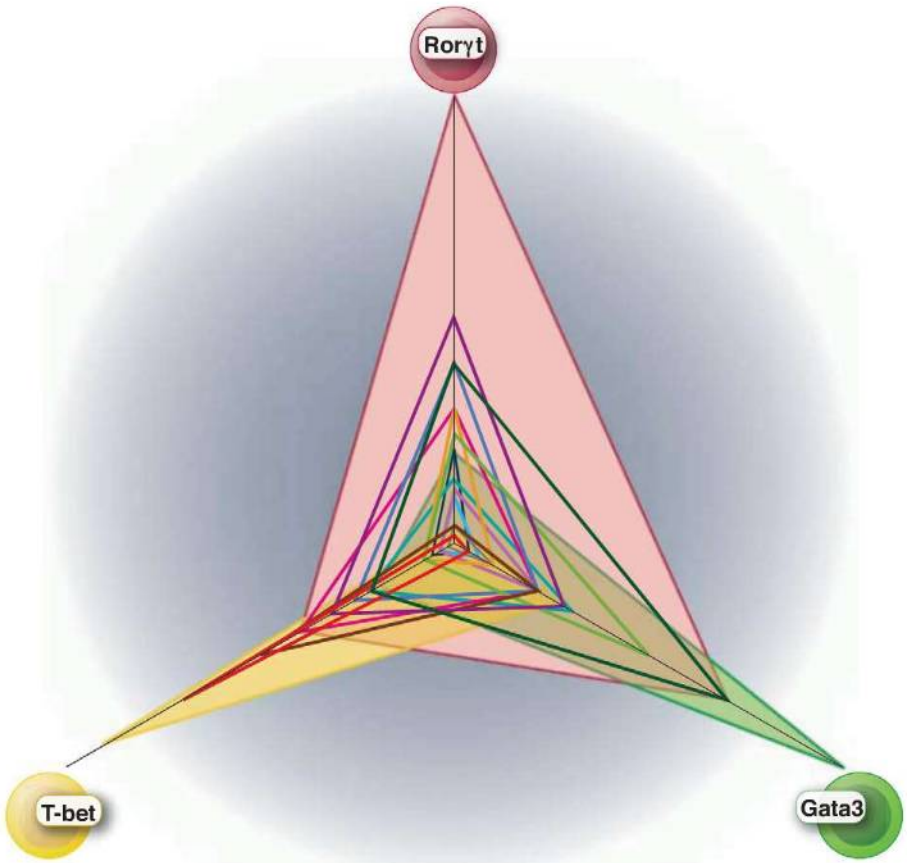

Fig. 2. A more nuanced view of T_H cell differentiation: dynamic expression of transcription factors. Although T cells preferentially express particular transcription factors (for simplicity, only three important factors are depicted in this figure), recent insights suggest that it is probably more accurate to view the process of T_H cell differentiation in the context of varying ratios of transcription factors, whose expression is regulated by an array of extrinsic and intrinsic factors. T cell subsets can express more than one "master regulator," and they may have different functions during the life of a T cell. GATA3 and Rorγt, for instance, both regulate T cell in addition to helper cell differentiation. Rather than viewing transcription factor expression as an "all or none" proposition, it may be more reasonable to consider that an array of helper T cells exist with varying ratios of different transcription factors and consequently graded properties. Viewed in this context, plasticity may be an intrinsic feature of helper T cells. Furthermore, the few transcription factors shown in the figure are undoubtedly a vast oversimplification; it is more likely that a panoply of transcription factors contribute to the specialized function of T_H cells.

T_H1 and/or T_H17 cells might be altered to more-benign T_H2 cells. A better understanding of the molecular mechanisms that stabilize committed cytokine production may provide new therapeutic opportunities or revise our approaches for treating such diseases. Of course, there is also a down side. Administering T_{reg}s in some mice with autoimmunity ameliorates disease. Administration of human T_{reg}s is being considered as a treatment for various severe human autoimmune diseases. It could be disastrous if these cells were to become inflammatory T_H17 cells.

The issue is important for another reason: The question of commitment versus flexibility is a fundamentally important and interesting cell biological problem. T_H cells represent outstanding models for understanding how extrinsic factors in the microenvironment influence intrinsic factors to ultimately control gene expression. T cell biologists have generated a wealth of tools (e.g., numerous knockout mice), and, with any luck, studies from T cell differentiation might provide valuable lessons for other biologists.

What Are the Challenges for Future Research?

It has been unquestionably useful in advancing our understanding of immune cell function to recognize that B cells, T cells, and different T cell subsets ($CD4^+$, $CD8^+$, α/β, γ/δ, and natural killer T cells) constitute distinct lineages that do not interconvert. Although new subsets of T_H cells continue to be elevated to the status of "lineages," there are really no accepted criteria for what qualifies a cell for this august designation. The selective production of cytokines is the sine qua non for a subset, but this definition is tautologic and consequently leads to considerable confusion. T_H1 cells make IFN-γ, but are all IFN-γ–producing $CD4^+$ T cells T_H1 cells? IL-22–producing cells make IFN-γ, but are they then T_H1s or T_H22s? Can a cell be a T_H1/T_H22, or should this be a new "lineage"? In the simplest view, T_H cell lineages express lineage-defining transcription factors, but, as discussed, we know that transcription factor expression is dynamic; a particular subset can express more than one master regulator, and expression of these factors can be lost or induced. It is impractical to suggest that it is time to call a moratorium on T_H lineages, and it is equally unlikely that all immunologists will agree on the criteria for lineage versus subset; there will always be lumpers and splitters. Minimally though, concepts such as fate determination and lineage commitment should not be used lightly; they do have biological implications albeit imprecise. Immunologists need to recognize that, in most cases, this is just shorthand and that we should not become entangled by our own semantic distinctions. We should certainly not infer stable function on the basis of the presence of a transcription factor or the production of cytokine; in fact, it might be safer to view cytokine-producing subsets in probabilistic terms. Certain factors increase the likelihood of stably producing a cytokine, but many factors, ranging from transcription factor expression to epigenetic modifications and miRNA expression, need to be quantified to predict with more accuracy that a helper cell will behave more like a differentiated cell.

It is also timely to gain a more sophisticated understanding of T cell–expressed transcription factors and repressors. Reductionist approaches are of course essential in trying to make sense of complex biological processes; however, the risk is that the concepts that emerge may be overly simplistic. Although it has been convenient to refer to master regulators, the limitations of such an approach are becoming increasingly evident, and a more nuanced view of transcription factor function is appropriate (Fig. 2). For instance, GATA3 is important in the acquisition of IL-4–producing capacity, but once T_H2 status has been achieved GATA3 can be deleted without abolishing the capacity of a T_H2 cell to produce IL-4. Even more interesting, although GATA3 appears essential to achieve T_H2 status, this does not necessarily mean that GATA3 expression has to rise for a cell to become a T_H2 cell. In vitro, introducing constitutively active STAT5a by retroviral transduction into cells being differentiated under T_H1 conditions results in repression of T-bet and acquisition of IL-4–producing capacity (*44*). GATA3 levels in these STAT5a overexpressors are as low or lower than in T_H1 cells, but that modest amount of GATA3 is essential. Constitutively active STAT5a fails to cause T_H2 differentiation in conditional GATA3-deleted mice. Thus, it may well be that the concentration of the required transcription factor may vary depending on the concentration of other transcription factors and, once a differentiated state is induced, that factor may be dispensable. Similarly, we have long known that, although T-bet and STAT4 are important for T_H1

differentiation, absence of either does not abrogate IFN-γ production. We also know that IFN-γ acting through STAT1 promotes T-bet expression (*45*, *46*). Given our present level of sophistication and technological capabilities, we should be more able to appreciate that transcription factors and repressors work in complex regulatory circuits; embracing their complexity will be the key to really understanding how they work. Rather than thinking about presence or absence of a transcription, it will be more fruitful to consider levels and ratios as they change during the course of immune stimulation (Fig. 2). In fact, like other aspects of hematopoietic cell differentiation, one needs to think of an array of transcription factors participating in concert with one another (*47*, *48*). Here's the good news: Improved computational approaches and more sophisticated assessment of dynamic interactions between transcription factors are in sight (*49*). High-throughput, comprehensive approaches, such as chromatin immunoprecipitation with massive parallel sequencing, will facilitate more profound and global views of transcription factor function. This technique also allows genome-wide analysis of epigenetic modifications; thus, the interplay between transcription factors and epigenetic changes can be assessed. High-throughput sequencing can also be used to measure RNA expression, including mRNA, miRNAs, and long noncoding mRNAs. Thus, we can comprehensively measure transcription factor binding, epigenetic modifications, and expression of miRNA and mRNA; however, we will have to deal with all these data. Modern technology allows a comprehensive set of data to be acquired, but to put the massive number of pixels into a true picture of the status of the cell is a daunting task. The sheer immensity of the challenge makes this a logical area for an integrated systems approach involving a concerted and organized effort among several laboratories.

Adding yet another dimension of difficulty is cell heterogeneity, even among cells that have been subjected to identical differentiation regimes. Ideally, it would be desirable to obtain information about gene expression and epigenetic modifications on individual cells, although this is not technically possible at present. The classical studies on helper T cell differentiation have relied heavily on in vitro manipulation; indeed, this has been a criterion for a lineage—stability of cytokine production after extended in vitro passage with resistance to cytokines that might alter fate decision—but this is both a strength and weakness. Although the new T_H lineages have not been subjected to this standard, stability based on in vitro passage is surely not the gold standard that we would like to apply; in vivo clearly trumps in plastico. Moreover, there is little standardization regarding in vitro differentiation; each laboratory does things a little differently. The critical issue will be to define whether T_H cells generated in vivo during the course of infection or autoimmune disease behave as lineages or not. This will need to be done over substantial time, not just a few days or weeks. Fate-mapping studies, using genetically engineered mice in which deletion of a stop signal is determined by cytokine expression and thus cells acquire a permanent marker based on an initial differentiation decision, can be of particular value for the assessment of in vivo differentiation. Coupling this technology with intravital imaging will certainly improve our chances of understanding physiologic helper cell fates, because anatomical considerations undoubtedly contribute to T cell differentiation. Advances in basic immunology have led to many new therapies, including biologics and small molecules that influence the actions of cytokines. These new therapies provide an exciting opportunity to probe whether such precise therapies can influence T_H differentiation and plasticity. Similarly, as new vaccines are developed, it will be useful to assess their impact with more sophisticated measures of helper cell function and differentiation. Hopefully, these advances can be useful in the prevention or treatment of human disease.

References and Notes

1. T. R. Mosmann, H. Cherwinski, M. W. Bond, M. A. Giedlin, R. L. Coffman, *J. Immunol.* **136**, 2348 (1986).
2. A. K. Abbas, K. M. Murphy, A. Sher, *Nature* **383**, 787 (1996).
3. C. Dong, R. A. Flavell, *Sci. STKE* **2000**, pe1 (2000).
4. E. M. Shevach, *Nat. Rev. Immunol.* **2**, 389 (2002).
5. S. Sakaguchi, T. Yamaguchi, T. Nomura, M. Ono, *Cell* **133**, 775 (2008).
6. S. Z. Josefowicz, A. Rudensky, *Immunity* **30**, 616 (2009).
7. B. Stockinger, M. Veldhoen, B. Martin, *Semin. Immunol.* **19**, 353 (2007).
8. P. Miossec, T. Korn, V. K. Kuchroo, *N. Engl. J. Med.* **361**, 888 (2009).
9. Y. K. Lee, R. Mukasa, R. D. Hatton, C. T. Weaver, *Curr. Opin. Immunol.* **21**, 274 (2009).
10. L. Zhou, M. M. Chong, D. R. Littman, *Immunity* **30**, 646 (2009).
11. N. Fazilleau, L. Mark, L. J. McHeyzer-Williams, M. G. McHeyzer-Williams, *Immunity* **30**, 324 (2009).
12. C. King, S. G. Tangye, C. R. Mackay, *Annu. Rev. Immunol.* **26**, 741 (2008).
13. A. Awasthi, V. K. Kuchroo, *Science* **325**, 953 (2009).
14. R. J. Johnston *et al.*, *Science* **325**, 1006 (2009).
15. R. I. Nurieva *et al.*, *Science* **325**, 1001 (2009).
16. X. Zhou, S. Bailey-Bucktrout, L. T. Jeker, J. A. Bluestone, *Curr. Opin. Immunol.* **21**, 281 (2009).
17. M. Veldhoen *et al.*, *Nat. Immunol.* **9**, 1341 (2008).
18. W. Elyaman *et al.*, *Proc. Natl. Acad. Sci. U.S.A.* **106**, 12885 (2009).
19. N. J. Wilson *et al.*, *Nat. Immunol.* **8**, 950 (2007).
20. Z. Chen, C. M. Tato, L. Muul, A. Laurence, J. J. O'Shea, *Arthritis Rheum.* **56**, 2936 (2007).
21. Y. K. Lee *et al.*, *Immunity* **30**, 92 (2009).
22. D. Bending *et al.*, *J. Clin. Investig.* **119**, 565 (2009).
23. G. Shi *et al.*, *J. Immunol.* **181**, 7205 (2008).
24. N. Hayashi *et al.*, *Proc. Natl. Acad. Sci. U.S.A.* **104**, 14765 (2007).
25. T. Duhen, R. Geiger, D. Jarrossay, A. Lanzavecchia, F. Sallusto, *Nat. Immunol.* **10**, 857 (2009).
26. S. Trifari, C. D. Kaplan, E. H. Tran, N. K. Crellin, H. Spits, *Nat. Immunol.* **10**, 864 (2009).
27. M. Löhning *et al.*, *J. Exp. Med.* **205**, 53 (2008).
28. X. Zhou *et al.*, *Nat. Immunol.* **10**, 1000 (2009).
29. L. Xu, A. Kitani, I. Fuss, W. Strober, *J. Immunol.* **178**, 6725 (2007).
30. G. Wei *et al.*, *Immunity* **30**, 155 (2009).
31. N. Komatsu *et al.*, *Proc. Natl. Acad. Sci. U.S.A.* **106**, 1903 (2009).
32. M. A. Koch *et al.*, *Nat. Immunol.* **10**, 595 (2009).
33. L. Zhou *et al.*, *Nature* **453**, 236 (2008).
34. F. Zhang, G. Meng, W. Strober, *Nat. Immunol.* **9**, 1297 (2008).
35. M. Tsuji *et al.*, *Science* **323**, 1488 (2009).
36. K. R. Cordes *et al.*, *Nature* **460**, 705 (2009).
37. C. B. Wilson, E. Rowell, M. Sekimata, *Nat. Rev. Immunol.* **9**, 91 (2009).
38. S. Floess *et al.*, *PLoS Biol.* **5**, e38 (2007).
39. S. Yamanaka, *Philos. Trans. R. Soc. London Ser. B* **363**, 2079 (2008).
40. Q. Zhou, D. A. Melton, *Cell Stem Cell* **3**, 382 (2008).
41. B. E. Bernstein *et al.*, *Cell* **125**, 315 (2006).
42. X. Zhou *et al.*, *J. Exp. Med.* **205**, 1983 (2008).
43. R. J. Johnston *et al.*, *Science* **325**, 1006 (2009).
44. J. Zhu *et al.*, *Nat. Immunol.* **5**, 1157 (2004).
45. A. A. Lighvani *et al.*, *Proc. Natl. Acad. Sci. U.S.A.* **98**, 15137 (2001).
46. V. T. Thieu *et al.*, *Immunity* **29**, 679 (2008).
47. C. Georgescu *et al.*, *Proc. Natl. Acad. Sci. U.S.A.* **105**, 20100 (2008).
48. E. V. Rothenberg, J. E. Moore, M. A. Yui, *Nat. Rev. Immunol.* **8**, 9 (2008).
49. A. Barski *et al.*, *Cell* **129**, 823 (2007).

50. J.O'S. and W.E.P. are supported by the National Institute of Arthritis and Musculoskeletal and Skin Diseases and National Institute of Allergy and Infectious Disease intramural research programs, respectively.

10.1126/science.1178334

Gamma-Ray Emission from the Shell of Supernova Remnant W44 Revealed by the Fermi LAT

A. A. Abdo,[1]* M. Ackermann,[2] M. Ajello,[2] L. Baldini,[3] J. Ballet,[4] G. Barbiellini,[5,6] M. G. Baring,[7] D. Bastieri,[8,9] B. M. Baughman,[10] K. Bechtol,[2] R. Bellazzini,[3] B. Berenji,[2] R. D. Blandford,[2] E. D. Bloom,[2] E. Bonamente,[11,12] A. W. Borgland,[2] J. Bregeon,[3] A. Brez,[3] M. Brigida,[13,14] P. Bruel,[15] T. H. Burnett,[16] S. Buson,[9] G. A. Caliandro,[13,14] R. A. Cameron,[2] P. A. Caraveo,[17] J. M. Casandjian,[4] C. Cecchi,[11,12] Ö. Çelik,[18,19,20] A. Chekhtman,[1,21] C. C. Cheung,[18] J. Chiang,[2] S. Ciprini,[11,12] R. Claus,[2] I. Cognard,[22] J. Cohen-Tanugi,[23] L. R. Cominsky,[24] J. Conrad,[25,26]† S. Cutini,[27] C. D. Dermer,[1] A. de Angelis,[28] F. de Palma,[13,14] S. W. Digel,[2] E. do Couto e Silva,[2] P. S. Drell,[2] R. Dubois,[2] D. Dumora,[29,30] C. Espinoza,[31] C. Farnier,[23] C. Favuzzi,[13,14] S. J. Fegan,[15] W. B. Focke,[2] P. Fortin,[15] M. Frailis,[28] Y. Fukazawa,[32] S. Funk,[2] P. Fusco,[13,14] F. Gargano,[14] D. Gasparrini,[27] N. Gehrels,[18,33] S. Germani,[11,12] G. Giavitto,[34] B. Giebels,[15] N. Giglietto,[13,14] F. Giordano,[13,14] T. Glanzman,[2] G. Godfrey,[2] I. A. Grenier,[4] M.-H. Grondin,[29,30] J. E. Grove,[1] L. Guillemot,[29,30] S. Guiriec,[35] Y. Hanabata,[32] A. K. Harding,[18] M. Hayashida,[2] E. Hays,[18] R. E. Hughes,[10] M. S. Jackson,[25,26,36] G. Jóhannesson,[2] A. S. Johnson,[2] T. J. Johnson,[18,33] W. N. Johnson,[1] T. Kamae,[2] H. Katagiri,[32] J. Kataoka,[37,38] J. Katsuta,[39,40] N. Kawai,[37,41] M. Kerr,[16] J. Knödlseder,[42] M. L. Kocian,[2] M. Kramer,[31,43] M. Kuss,[3] J. Lande,[2] L. Latronico,[3] M. Lemoine-Goumard,[29,30] F. Longo,[5,6] F. Loparco,[13,14] B. Lott,[29,30] M. N. Lovellette,[1] P. Lubrano,[11,12] A. G. Lyne,[31] G. M. Madejski,[2] A. Makeev,[1,21] M. N. Mazziotta,[14] J. E. McEnery,[18] C. Meurer,[24,25] P. F. Michelson,[2] W. Mitthumsiri,[2] T. Mizuno,[32] C. Monte,[13,14] M. E. Monzani,[2] A. Morselli,[44] I. V. Moskalenko,[2] S. Murgia,[2] T. Nakamori,[37] P. L. Nolan,[2] J. P. Norris,[45] A. Noutsos,[31] E. Nuss,[23] T. Ohsugi,[32] N. Omodei,[3] E. Orlando,[46] J. F. Ormes,[45] D. Paneque,[2] D. Parent,[29,30] V. Pelassa,[23] M. Pepe,[11,12] M. Pesce-Rollins,[3] F. Piron,[23] T. A. Porter,[47] S. Rainò,[13,14] R. Rando,[8,9] M. Razzano,[3] A. Reimer,[48,2] O. Reimer,[48,2] T. Reposeur,[29,30] L. S. Rochester,[2] A. Y. Rodriguez,[49] R. W. Romani,[2] M. Roth,[16] F. Ryde,[36,26] H. F.-W. Sadrozinski,[47] D. Sanchez,[15] A. Sander,[10] P. M. Saz Parkinson,[47] J. D. Scargle,[50] C. Sgrò,[3] E. J. Siskind,[51] D. A. Smith,[29,30] P. D. Smith,[10] G. Spandre,[3] P. Spinelli,[13,14] B. W. Stappers,[31] F. W. Stecker,[18] M. S. Strickman,[1] D. J. Suson,[52] H. Tajima,[2]‡ H. Takahashi,[32] T. Takahashi,[39] T. Tanaka,[2]‡ J. B. Thayer,[2] J. G. Thayer,[2] G. Theureau,[22] D. J. Thompson,[18] L. Tibaldo,[8,4,9] O. Tibolla,[53] D. F. Torres,[54,49] G. Tosti,[11,12] A. Tramacere,[2,55] Y. Uchiyama,[2]‡ T. L. Usher,[2] V. Vasileiou,[18,19,20] C. Venter,[18,56] N. Vilchez,[42] V. Vitale,[44,57] A. P. Waite,[2] P. Wang,[2] B. L. Winer,[10] K. S. Wood,[1] R. Yamazaki,[32] T. Ylinen,[36,58,26] M. Ziegler[47]

Recent observations of supernova remnants (SNRs) hint that they accelerate cosmic rays to energies close to ~10^{15} electron volts. However, the nature of the particles that produce the emission remains ambiguous. We report observations of SNR W44 with the Fermi Large Area Telescope at energies between 2×10^8 electron volts and 3×10^{11} electron volts. The detection of a source with a morphology corresponding to the SNR shell implies that the emission is produced by particles accelerated there. The gamma-ray spectrum is well modeled with emission from protons and nuclei. Its steepening above ~10^9 electron volts provides a probe with which to study how particle acceleration responds to environmental effects such as shock propagation in dense clouds and how accelerated particles are released into interstellar space.

Galactic cosmic rays (GCRs) are thought to be accelerated in the expanding shock waves of supernova remnants (SNRs) (*1*, *2*), a conjecture that has been strengthened by recent observations of young SNRs in x-rays (*3*) and TeV gamma rays (*4*–*6*). Magnetic field amplification is essential to make the maximum particle energy attainable large enough to explain the GCRs (*7*). It also implies that a large fraction of the kinetic energy released by a supernova explosion is transferred to cosmic rays (*8*). If strong magnetic fields are present in the gamma-ray–emitting region, the TeV images of young SNRs (*4*–*6*) are more likely to show the accelerated protons and nuclei via their hadronic interactions with the ambient gas and subsequent π^0 decays into gamma rays. However, the identification has been inconclusive because high-energy electrons can also shine in gamma rays via bremsstrahlung and/or inverse Compton processes. Observations in the GeV domain are necessary to disentangle the emission mechanisms by means of spectral differences in this energy band.

Environmental effects can complicate the interpretation of the gamma-ray emission. For instance, enhanced π^0-decay emission can be expected in those SNRs interacting with a molecular cloud (*9*, *10*) because of the higher gas density, which makes the interactions between cosmic-ray nuclei and the gas more frequent. Yet the dense gas slows down the shock and the overall acceleration efficiency, and the acceleration rate can be much reduced because of interactions between the shock and dense gas. Even without strong shell-cloud interactions, the shock is decelerated in the late stage of SNR evolution. Such evolution of particle acceleration (*11*, *12*) can be probed with observations of GeV to TeV gamma rays from SNRs.

Here, we report GeV observations of the middle-aged (~2.0×10^4 years) SNR W44 with the Large Area Telescope (LAT) on board the Fermi Gamma-ray Space Telescope. W44 is known to be interacting with a molecular cloud on the basis of observations of lines of CO (*13*), OH masers (*14*), and near- and mid-infrared (IR) from shocked H_2 (*15*, *16*). In the GeV domain, the EGRET instrument aboard the Compton Gamma Ray Observatory detected a source in the vicinity of the SNR (*17*), although its association with W44 was not clear. The Fermi LAT is a pair-conversion detector capable of measuring gamma rays in the GeV domain (*18*). We analyzed the Fermi LAT data accumulated between 4 August 2008 and 13 July 2009 in the region around W44. Details of event selections for this analysis are summarized in the supporting online material (SOM).

The gamma-ray emission spatially associated with SNR W44 is visible in Fig. 1, well above the GeV emission from the Galactic disc. The source corresponds to 0FGL J1855.9+0126 in the Fermi bright source list (*19*). A detailed analysis reveals that the GeV emission is significantly extended (see SOM) compared with that of a point source case. Therefore, it is difficult to attribute most of the gamma rays to the radio pulsar in W44, PSR B1853+01 (*20*), or its pulsar wind nebula (PWN), which extends only ~1′ to 2′ in x-rays (*21*) and radio (*22*). To extract the gamma-ray morphology of the source, we applied an image deconvolution technique (Fig. 2 and SOM). The resemblance between the gamma-ray and infrared-ring morphologies supports the inference that the bulk of the emission comes from the SNR shell rather than from the unresolved pulsar.

To test the source morphology and determine its spectrum, we performed a maximum likelihood analysis (*23*). The gamma-ray emission model used in the analysis includes individual sources detected in the 11 months, the Galactic diffuse emission (resulting from cosmic-ray interactions with interstellar medium and radiation), and an isotropic component (extragalactic and instrumental backgrounds). For the diffuse backgrounds, we used models released by the LAT collaboration (*23*). In order to quantitatively confirm that the gamma-ray emission is associated with the SNR shell, we compared the likelihood values obtained with the following source shapes:

(i) a point source, (ii) a uniform flux within an ellipse, (iii) a uniform flux within an elliptical ring, and (iv) a uniform elliptical ring plus a point source at the pulsar position (Fig. 2). The single elliptical ring yields the best likelihood and rejects the filled ellipse and point source hypotheses at the >8 σ and >16 σ confidence levels, respectively. The extended ring emission is detected at the 62 σ confidence level above the intense and structured Galactic background in this direction. These results, together with the lack of detection of an additional point source at the pulsar position in case iv, imply that the bulk of the gamma rays comes from the shell, as suggested by the deconvolved image. The 95% upper limit to pulsar and/or PWN flux is 1.6×10^{-7} photons cm^{-2} s^{-1} above 100 MeV. We also searched for gamma-ray pulsation from PSR B1853+01 by using ephemerides provided by the Jodrell Bank and Nançay radio telescopes as in (*24*) but valid through July 2009. However, none was seen (H test < 5).

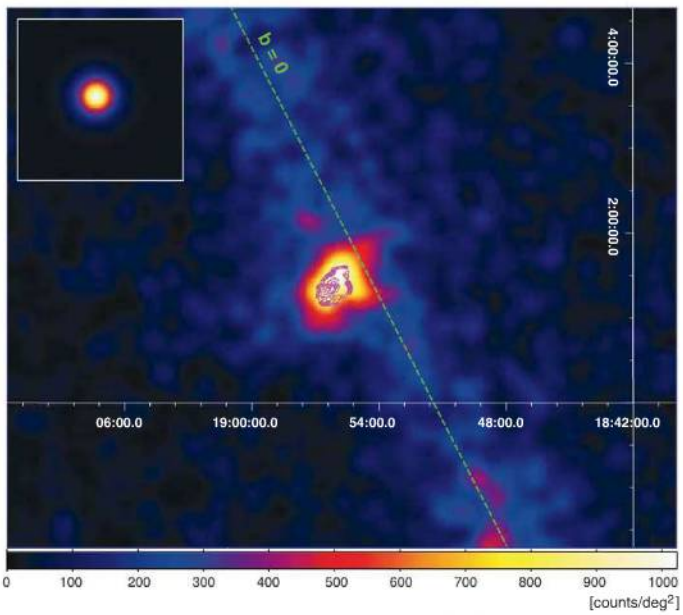

Fig. 1. Fermi LAT image (2 to 10 GeV) of the region where SNR W44 is located. North is up and east is to the left. The color scale indicates count per solid angle on a linear scale. The dotted green line corresponds to the Galactic plane (b = 0°). The radio image of W44 as seen in 20-cm wavelength by the Very Large Array (*31*) is overlaid as the magenta contours. **(Inset)** An image of a simulated point source. In the simulation, spectral parameters of the W44 emission are assumed.

The spectral energy distribution (SED) of the source is seen to steepen toward high energies (Fig. 3). To obtain general characteristics of the spectrum, we fitted it with simple functions. For a broken power law where the photon index is abruptly changed at a break energy, the photon indices are $\Gamma_1 = 2.06 \pm 0.03$ [1σ statistical error (stat)] ± 0.07 [1σ systematic error (sys)] at low energy and $\Gamma_2 = 3.02 \pm 0.10$ (stat) ± 0.12 (sys) at high energy with a break energy of $E_{break} = 1.9 \pm 0.2$ (stat) ± 0.3 (sys) GeV. The likelihood-ratio test between a broken and a single power law disfavors the latter at the significance of 14 σ. The resulting gamma-ray flux integrated above 100 MeV (*25*) amounts to $F_{>100\ MeV} = [1.22 \pm 0.05\ (stat) \pm 0.23\ (sys)] \times 10^{-6}$ photons cm^{-2} s^{-1}.

The shell-like morphology and spectral shape of the GeV emission provide information about its origin in the SNR. Most of the emission comes from the SNR shell, which is known to interact with molecular clouds. When high-energy particles interact with dense gas, two emission processes become important: π^0 decays and electron bremsstrahlung. Simple model curves with dominant π^0-decay emission fit the data reasonably well (see SOM for description of the model). In the model, protons and electrons are injected with the constant rate and fixed spectral shape over the age of the SNR (2.0×10^4 years). Although the age should include some uncertainties, the results, particularly in the Fermi LAT energy range, are insensitive to the assumed age. The ratio of injected electrons to protons was fixed at $K_{ep} = 0.01$ to be roughly consistent with

[1]Space Science Division, Naval Research Laboratory, Washington, DC 20375, USA. [2]W. W. Hansen Experimental Physics Laboratory, Kavli Institute for Particle Astrophysics and Cosmology, Department of Physics and SLAC National Accelerator Laboratory, Stanford University, Stanford, CA 94305, USA. [3]Istituto Nazionale di Fisica Nucleare (INFN), Sezione di Pisa, I–56127 Pisa, Italy. [4]Laboratoire Astrophysique Instrumentation Modélisation, Commissariat à l'Énergie Atomique (CEA)–Institut de Recherche sur les Lois Fondamentales de l'Univers (IRFU)/CNRS/Université Paris Diderot, Service d'Astrophysique, CEA Saclay, 91191 Gif sur Yvette, France. [5]Istituto Nazionale di Fisica Nucleare, Sezione di Trieste, I–34127 Trieste, Italy. [6]Dipartimento di Fisica, Università di Trieste, I–34127 Trieste, Italy. [7]Rice University, Department of Physics and Astronomy, MS–108, Post Office Box 1892, Houston, TX 77251, USA. [8]Istituto Nazionale di Fisica Nucleare, Sezione di Padova, I–35131 Padova, Italy. [9]Dipartimento di Fisica "G. Galilei," Università di Padova, I–35131 Padova, Italy. [10]Department of Physics, Center for Cosmology and Astro-Particle Physics, The Ohio State University, Columbus, OH 43210, USA. [11]Istituto Nazionale di Fisica Nucleare, Sezione di Perugia, I–06123 Perugia, Italy. [12]Dipartimento di Fisica, Università degli Studi di Perugia, I–06123 Perugia, Italy. [13]Dipartimento di Fisica "M. Merlin" dell'Università e del Politecnico di Bari, I–70126 Bari, Italy. [14]Istituto Nazionale di Fisica Nucleare, Sezione di Bari, 70126 Bari, Italy. [15]Laboratoire Leprince-Ringuet, École Polytechnique, CNRS/Institut National de Physique Nucléaire et de Physique des Particules (IN2P3), Palaiseau, France. [16]Department of Physics, University of Washington, Seattle, WA 98195–1560, USA. [17]Istituto di Astrofisica Spaziale e Fisica Cosmica, Istituto Nazionale di Astrofisica (INAF), I–20133 Milano, Italy. [18]NASA Goddard Space Flight Center, Greenbelt, MD 20771, USA. [19]Center for Research and Exploration in Space Science and Technology (CRESST), NASA Goddard Space Flight Center, Greenbelt, MD 20771, USA. [20]University of Maryland, Baltimore County, Baltimore, MD 21250, USA. [21]George Mason University, Fairfax, VA 22030, USA. [22]Laboratoire de Physique et Chemie de l'Environnement (LPCE), LPCE UMR 6115 CNRS, F–45071 Orléans Cedex 02, France, and Station de Radioastronomie de Nançay, Observatoire de Paris, CNRS/Institut National des Sciences de l'Univers (INSU), F–18330 Nançay, France. [23]Laboratoire de Physique Théorique et Astroparticules, Université Montpellier 2, CNRS/IN2P3, Montpellier, France. [24]Department of Physics and Astronomy, Sonoma State University, Rohnert Park, CA 94928–3609, USA. [25]Department of Physics, Stockholm University, AlbaNova, SE–106 91 Stockholm, Sweden. [26]The Oskar Klein Centre for Cosmoparticle Physics, AlbaNova, SE–106 91 Stockholm, Sweden. [27]Agenzia Spaziale Italiana (ASI) Science Data Center, I–00044 Frascati (Roma), Italy. [28]Dipartimento di Fisica, Università di Udine and Istituto Nazionale di Fisica Nucleare, Sezione di Trieste, Gruppo Collegato di Udine, I–33100 Udine, Italy. [29]Centre d'Études Nucléaires Bordeaux Gradignan, Université de Bordeaux, UMR 5797, 33175 Gradignan, France. [30]Centre d'Études Nucléaires Bordeaux Gradignan, CNRS/IN2P3, UMR 5797, Gradignan 33175, France. [31]Jodrell Bank Centre for Astrophysics, School of Physics and Astronomy, The University of Manchester, Manchester M13 9PL, UK. [32]Department of Physical Sciences, Hiroshima University, Higashi-Hiroshima, Hiroshima 739–8526, Japan. [33]University of Maryland, College Park, MD 20742, USA. [34]Istituto Nazionale di Fisica Nucleare, Sezione di Trieste, and Università di Trieste, I–34127 Trieste, Italy. [35]University of Alabama in Huntsville, Huntsville, AL 35899, USA. [36]Department of Physics, Royal Institute of Technology (KTH), AlbaNova, SE–106 91 Stockholm, Sweden. [37]Department of Physics, Tokyo Institute of Technology, Meguro City, Tokyo 152–8551, Japan. [38]Waseda University, 1-104 Totsukamachi, Shinjuku-ku, Tokyo 169–8050, Japan. [39]Institute of Space and Astronautical Science, Japan Aerospace Exploration Agency (JAXA), 3-1-1 Yoshinodai, Sagamihara, Kanagawa 229–8510, Japan. [40]Department of Physics, Graduate School of Science, University of Tokyo, 7-3-1 Hongo, Bunkyo-ku, Tokyo 113–0033, Japan. [41]Cosmic Radiation Laboratory, Institute of Physical and Chemical Research (RIKEN), Wako, Saitama 351–0198, Japan. [42]Centre d'Étude Spatiale des Rayonnements, CNRS/Université Paul Sabatier (UPS), BP 44346, F–30128 Toulouse Cedex 4, France. [43]Max-Planck-Institut für Radioastronomie, Auf dem Hügel 69, 53121 Bonn, Germany. [44]Istituto Nazionale di Fisica Nucleare, Sezione di Roma "Tor Vergata," I–00133 Roma, Italy. [45]Department of Physics and Astronomy, University of Denver, Denver, CO 80208, USA. [46]Max-Planck Institut für Extraterrestrische Physik, 85748 Garching, Germany. [47]Santa Cruz Institute for Particle Physics, Department of Physics and Department of Astronomy and Astrophysics, University of California at Santa Cruz, Santa Cruz, CA 95064, USA. [48]Institut für Astro- und Teilchenphysik and Institut für Theoretische Physik, Leopold-Franzens-Universität Innsbruck, A–6020 Innsbruck, Austria. [49]Institut de Ciencies de l'Espai (IEEC-CSIC), Campus UAB, 08193 Barcelona, Spain. [50]Space Sciences Division, NASA Ames Research Center, Moffett Field, CA 94035–1000, USA. [51]NYCB Real-Time Computing Incorporated, Lattingtown, NY 11560–1025, USA. [52]Department of Chemistry and Physics, Purdue University Calumet, Hammond, IN 46323–2094, USA. [53]Max-Planck-Institut für Kernphysik, D–69029 Heidelberg, Germany. [54]Institució Catalana de Recerca i Estudis Avançats (ICREA), 08010 Barcelona, Spain. [55]Consorzio Interuniversitario per la Fisica Spaziale (CIFS), I–10133 Torino, Italy. [56]North-West University, Potchefstroom Campus, Potchefstroom 2520, South Africa. [57]Dipartimento di Fisica, Università di Roma "Tor Vergata," I–00133 Roma, Italy. [58]School of Pure and Applied Natural Sciences, University of Kalmar, SE–391 82 Kalmar, Sweden.

*National Research Council Research Associate, National Academy of Sciences, Washington, DC 20001, USA.
†Royal Swedish Academy of Sciences Research Fellow.
‡To whom correspondence should be addressed. E-mail: ttanaka@slac.stanford.edu (T.T.); uchiyama@slac.stanford.edu (Y.U.); htajima@slac.stanford.edu (H.T.)

the cosmic-ray composition observed at Earth, where K_{cp} is defined as a ratio of particle numbers at $p = 1$ GeV/c. The ambient gas density was assumed to be $n = 100$ cm^{-3}, which is the estimated averaged density in the molecular cloud interacting with W44 (*15*). Both proton and electron spectra have a spectral break at $p_{br} = 9$ GeV/c. The power-law indices are $s_1 = 1.74$ below the break, whereas the indices are $s_2 = 3.7$ above the break. The spectral indices below the break were chosen to explain the observed radio synchrotron spectrum with $\alpha = \Gamma - 1 = 0.37$ (*26*). In this model, the total kinetic energy of protons and electrons integrated above 100 MeV amount to $W_p = 6 \times 10^{49}$ erg and $W_e = 1 \times 10^{48}$ erg. The spectral index of $s_1 = 1.73$ deduced from the radio index is harder compared with $s_1 = 2.0$ expected from the standard acceleration theory. The flat radio spectrum might be due to processes such as reacceleration of preexisting cosmic-ray electrons (*27*). In such cases, spectral index of protons could be different from that of electrons. Assuming the standard value of $s_1 = 2.0$ yields $s_2 = 3.3$ and $p_{br} = 7$ GeV/c for protons.

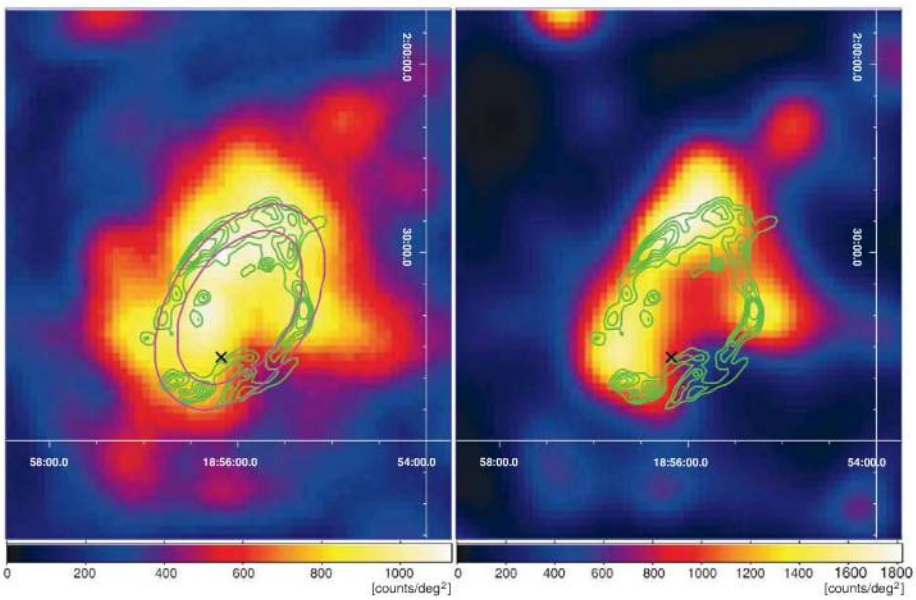

Fig. 2. Close-up images (2 to 10 GeV) of the SNR W44 region obtained with Fermi LAT. (**Left**) Count map. (**Right**) Deconvolved image that should be used to see the large-scale structure of the source, not to discern small structures with angular scales of <10′, which can be affected by statistical fluctuations. Such features should therefore not be taken as indicative of the true source morphology. The black cross on each image indicates the location of a radio pulsar, PSR B1853+01, which is believed to be associated with SNR W44 because its estimated distance of 3 kpc and characteristic age of 2 ×10^4 years are consistent with those independently obtained for the SNR (*20*). The green contours represent the 4.5-μm IR image by the Spitzer Space Telescope Infrared Array Camera (*16*), which traces shocked H_2. The magenta ellipses in the left image describe the spatial models used for the maximum likelihood analysis. Uniform emission inside the outer ellipse and uniform emission in the region between the inner and outer ellipses were among the models considered for the spatial distribution.

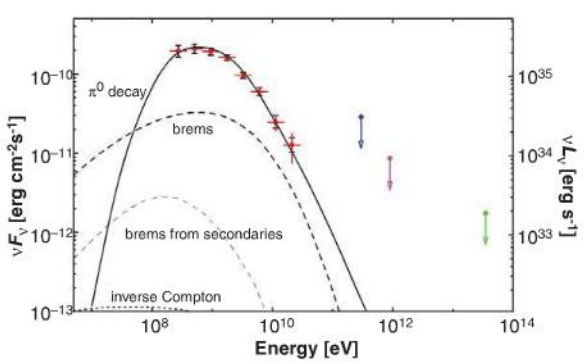

Fig. 3. Fermi LAT spectral energy distributions (SEDs) of SNR W44. The gamma-ray flux of each point was obtained by binning the gamma-ray data in a range of 0.2 to 30 GeV into eight energy intervals and performing a binned likelihood analysis on each energy bin. The source shape is assumed to be the elliptical ring shown in Fig. 2. The vertical red lines and the black caps represent 1 σ statistical errors and systematic errors, respectively. The SED is insensitive to the choice of reasonable diffuse background models within the ~10% level. It is also insensitive to the choice of the gamma-ray source shape between the elliptical ring and filled ellipse. Each curve corresponds to contributions from each emission process: π^0 decay (solid), electron bremsstrahlung (dashed), inverse Compton scattering (dots), and bremsstrahlung from secondary electrons and positrons, which are decay products of $\pi^\pm$ produced by the same hadronic interactions as π^0 production (thin dashed) for a simple model in which most of the emission detected by the Fermi LAT is attributed to π^0 decays. The spectra of protons and electrons have a form of $\propto p^{-s_1}(1 + p/p_{br})^{s_1 - s_2}$. A magnetic field of $B = 70$ μG is given from the radio flux, which is not shown here. In addition to the Fermi LAT data, currently available upper limits in the TeV energies by Whipple (*32*) (blue), High Energy Gamma Ray Astronomy (HEGRA) (*33*) (magenta), and Milagro (*34*) (green) are plotted. Because the Whipple and HEGRA upper limits are given in flux integrated above their threshold energies, we converted them to energy flux assuming power-law spectra with photon indices of 3.0.

Although not necessarily relevant to the shell-cloud interaction, another emission process, inverse Compton scattering of electrons, can in principle produce gamma rays at GeV energies. In the model shown in Fig. 3, the calculated gamma-ray flux from inverse Compton scattering is ~1 × 10^{-13} erg cm^{-2} s^{-1} at ~100 MeV to 1 GeV when the interstellar radiation field (*28*) at the location of W44 is assumed as target photons for electrons. The interstellar radiation field includes optical radiation from stars with the energy density of 0.96 eV cm^{-3} and infrared radiation with 0.93 eV cm^{-3} in addition to the cosmic microwave background at 0.26 eV cm^{-3}. In order for the inverse Compton emission to be enhanced to the flux level of the Fermi LAT spectrum, total energy in electrons is required to be as large as ~10^{51} erg, or the local soft photon field should be denser at least by one order of magnitude than the interstellar radiation field to reduce the total electron energy to <10^{50} erg. SNR W44 itself is an infrared radiation source and can provide additional target photons for the inverse Compton process. However, estimated energy density of infrared photons from W44 is 0.69 eV cm^{-3} (*29*), which is even lower than that of the interstellar radiation field. Therefore, it is unlikely that the inverse Compton scattering is the dominant emission mechanism in the GeV band. For the same reason, it is difficult to attribute the gamma-ray emission to the PWN, from which inverse Compton radiation is generally expected in the GeV band.

Instead, if one attempts to attribute the bulk of the gamma-ray flux to electron bremsstrahlung, the break in the Fermi LAT spectrum requires a break in the parent electron spectrum. In order to explain the power-law radio spectrum up to 10 GHz (*26*) at the same time, a strong magnetic field more intense than ~100 μG is necessary to have the corresponding break in the synchrotron spectrum at a frequency higher than 10 GHz. In this case, a high ambient density greater than ~1000 cm^{-3} is needed to explain the Fermi LAT flux (see SOM for modeling details). A strong magnetic field and high gas density are plausible if the observed emission is radiated mostly from the region where the shell is interacting with dense gas (*15*). However, electron bremsstrahlung can dominate over π^0-decay emission in the GeV band only with $K_{cp} > 0.1$, far greater than the observed cosmic-ray composition ratio near Earth.

Most plausible is that π^0 decays are responsible for the gamma-ray emission, although the bremsstrahlung scenario cannot be ruled out completely. In order to fit the Fermi LAT spectrum with π^0-decay emission, a spectral break in the proton spectrum is needed at fairly low energy, around 10 GeV/c. One possible mechanism to explain the spectral break is that particles escape from their acceleration sites, that is, the SNR shells. Theories predict that very high energy particles above ~TeV can be confined only during the early stage of SNR evolution (*11*, *12*). Because W44 is a middle-aged SNR with estimated age of ~2.0×10^4 years, most particles accelerated up to higher energies in the past could have escaped from its shell and cannot contribute to the gamma-ray emission we are observing now.

In the case of W44, the effect of particle escape can be enhanced because of the interaction between the shell and the dense, largely neutral molecular gas. Magnetic turbulence, which is required to confine and efficiently accelerate particles, is considered to be substantially damped. Thus, particles can easily escape from the shell at an earlier stage of SNR evolution (*30*) compared with the case where an SNR is expanding in a more rarefied medium. For W44, parts of the shock are expanding into clumps and interclump gas with densities of ~10 to ~100 cm^{-3} (*15*). The Fermi LAT spectrum indicates that the slow shock velocity (<500 km s^{-1}) and efficient damping can limit the maximum particle energy to a few GeV. Our results for W44 demonstrate the capability of the Fermi LAT for morphological and spectral studies of GeV emission from Galactic SNRs, which allow us to study the escape of energetic particles from SNR shells into interstellar space, the evolution of SNR shocks during the age of the SNR, and the impact of a dense environment.

References and Notes

1. R. Blandford, D. Eichler, *Phys. Rep.* **154**, 1 (1987).
2. M. A. Malkov, L. O'C. Drury, *Rep. Prog. Phys.* **64**, 429 (2001).
3. S. P. Reynolds, *Annu. Rev. Astron. Astrophys.* **46**, 89 (2008).
4. F. A. Aharonian *et al.*, *Nature* **432**, 75 (2004).
5. F. A. Aharonian *et al.*, *Astron. Astrophys.* **464**, 235 (2007).
6. F. A. Aharonian *et al.*, *Astrophys. J.* **661**, 236 (2007).
7. A. R. Bell, S. G. Lucek, *Mon. Not. R. Astron. Soc.* **321**, 433 (2001).
8. E. G. Berezhko, H. J. Völk, *Astron. Astrophys.* **492**, 695 (2008).
9. F. A. Aharonian, L. O'C. Drury, H. J. Völk, *Astron. Astrophys.* **285**, 645 (1994).
10. L. O'C. Drury, F. A. Aharonian, H. J. Völk, *Astron. Astrophys.* **287**, 959 (1994).
11. V. S. Ptuskin, V. N. Zirakashvili, *Astron. Astrophys.* **429**, 755 (2005).
12. S. Gabici, F. A. Aharonian, *Astrophys. J.* **665**, L131 (2007).
13. M. Seta *et al.*, *Astron. J.* **127**, 1098 (2004).
14. I. M. Hoffman, W. M. Goss, C. L. Brogan, M. J. Claussen, *Astrophys. J.* **627**, 803 (2005).
15. W. T. Reach, J. Rho, T. H. Jarrett, *Astrophys. J.* **618**, 297 (2005).
16. W. T. Reach *et al.*, *Astron. J.* **131**, 1479 (2006).
17. J. A. Esposito, S. D. Hunter, G. Kanbach, P. Sreekumar, *Astrophys. J.* **461**, 820 (1996).
18. W. B. Atwood *et al.*, *Astrophys. J.* **697**, 1071 (2009).
19. A. A. Abdo *et al.*, *Astrophys. J.* **183** (suppl.), 46 (2009).
20. A. Wolszczan, J. M. Cordes, R. J. Dewey, *Astrophys. J.* **372**, L99 (1991).
21. R. Petre, K. D. Kuntz, R. L. Shelton, *Astrophys. J.* **579**, 404 (2002).
22. D. A. Frail, E. B. Giacani, W. M. Goss, G. Dubner, *Astrophys. J.* **464**, L165 (1996).
23. Fermi Science Support Center, http://fermi.gsfc.nasa.gov/ssc/.
24. A. A. Abdo *et al.*, The first Fermi Large Area Telescope catalog of gamma-ray pulsars, http://arxiv.org/abs/0910.1608.
25. Although the analysis was performed by using events above 200 MeV, the quoted flux was obtained by extrapolating the best-fit function down to 100 MeV to make it easier to compare the value with past publications on GeV gamma-ray observations.
26. G. Castelletti, G. Dubner, C. Brogan, N. E. Kassim, *Astron. Astrophys.* **471**, 537 (2007).
27. A. M. Bykov, R. A. Chevalier, D. C. Ellison, Y. A. Uvarov, *Astrophys. J.* **538**, 203 (2000).
28. T. A. Porter, I. V. Moskalenko, A. W. Strong, *Astrophys. J.* **648**, L29 (2006).
29. O. C. de Jager, A. Mastichiadis, *Astrophys. J.* **482**, 874 (1997).
30. V. S. Ptuskin, V. N. Zirakashvili, *Astron. Astrophys.* **403**, 1 (2003).
31. D. J. Helfand, R. H. Becker, R. L. White, A. Fallon, S. Tuttle, *Astron. J.* **131**, 2525 (2006).
32. J. H. Buckley *et al.*, *Astron. Astrophys.* **329**, 639 (1998).
33. F. A. Aharonian *et al.*, *Astron. Astrophys.* **395**, 803 (2002).
34. A. A. Abdo *et al.*, *Astrophys. J.* **700**, L127 (2009).

35. The Fermi LAT Collaboration acknowledges support from a number of agencies and institutes for both development and the operation of the LAT as well as scientific data analysis. These include NASA and Department of Energy in the United States; CEA/Irfu, IN2P3/CNRS, and Centre National d'Études Spatiales in France; ASI, INFN, and INAF in Italy; Ministry of Education, Culture, Sports, Science, and Technology, High Energy Accelerator Research Organization (KEK) and JAXA in Japan; and the K. A. Wallenberg Foundation, the Swedish Research Council, and the National Space Board in Sweden.

Supporting Online Material

www.sciencemag.org/cgi/content/full/science.1182787/DC1
Materials and Methods
SOM Text
Figs. S1 and S2
References and Notes

2 October 2009; accepted 29 December 2009
Published online 7 January 2010;
10.1126/science.1182787
Include this information when citing this paper.

Ferroelectric Control of Spin Polarization

V. Garcia,[1] M. Bibes,[1]* L. Bocher,[2] S. Valencia,[3] F. Kronast,[3] A. Crassous,[1] X. Moya,[4] S. Enouz-Vedrenne,[5] A. Gloter,[2] D. Imhoff,[2] C. Deranlot,[1] N. D. Mathur,[4] S. Fusil,[1,6] K. Bouzehouane,[1] A. Barthélémy[1]

A current drawback of spintronics is the large power that is usually required for magnetic writing, in contrast with nanoelectronics, which relies on "zero-current," gate-controlled operations. Efforts have been made to control the spin-relaxation rate, the Curie temperature, or the magnetic anisotropy with a gate voltage, but these effects are usually small and volatile. We used ferroelectric tunnel junctions with ferromagnetic electrodes to demonstrate local, large, and nonvolatile control of carrier spin polarization by electrically switching ferroelectric polarization. Our results represent a giant type of interfacial magnetoelectric coupling and suggest a low-power approach for spin-based information control.

Controlling the spin degree of freedom by purely electrical means is currently an important challenge in spintronics (*1*, *2*). Approaches based on spin-transfer torque (*3*) have proven very successful in controlling the direction of magnetization in a ferromagnetic layer, but they require the injection of high current densities. An ideal solution would rely on the application of an electric field across an insulator, as in existing nanoelectronics. Early experiments have demonstrated the volatile modulation of spin-based properties with a gate voltage applied through a dielectric. Notable examples include the gate control of the spin-orbit interaction in III-V quantum wells (*4*), the Curie temperature T_C (*5*), or the magnetic anisotropy (*6*) in magnetic semiconductors with carrier-mediated exchange interactions; for example, (Ga,Mn)As or (In,Mn)As. Electric field–induced modifications of magnetic anisotropy at room temperature have also been reported recently in ultrathin Fe-based layers (*7*, *8*).

[1]Unité Mixte de Physique CNRS/Thales, 1 Avenue Augustin Fresnel, Campus de l'Ecole Polytechnique, 91767 Palaiseau, France, and Université Paris-Sud, 91405 Orsay, France. [2]Laboratoire de Physique des Solides, Université Paris-Sud, CNRS UMR-8502, 91405 Orsay, France. [3]Helmholtz-Zentrum-Berlin, Berliner Elektronen-Speicherring Gesellschaft für Synchrotronstrahlung (BESSY), Albert-Einstein-Strasse 15,12489 Berlin, Germany. [4]Department of Materials Science, University of Cambridge, Cambridge, CB2 3QZ, UK. [5]Thales Research and Technology, 1 Avenue Augustin Fresnel, Campus de l'Ecole Polytechnique, 91767 Palaiseau, France. [6]Université d'Evry-Val d'Essonne, Boulevard François Mitterrand, 91025 Evry cedex, France.

*To whom correspondence should be addressed. E-mail: manuel.bibes@thalesgroup.com

A nonvolatile extension of this approach involves replacing the gate dielectric by a ferroelectric and taking advantage of the hysteretic response of its order parameter (polarization) with an electric field. When combined with (Ga, Mn)As channels, for instance, a remanent control of T_C over a few kelvin was achieved through polarization-driven charge depletion/accumulation (*9*, *10*), and the magnetic anisotropy was modified by the coupling of piezoelectricity and magnetostriction (*11*, *12*). Indications of an electrical control of magnetization have also been provided in magnetoelectric heterostructures at room temperature (*13*–*17*).

Recently, several theoretical studies have predicted that large variations of magnetic properties may occur at interfaces between ferroelectrics and high-T_C ferromagnets such as Fe (*18*–*20*), Co_2MnSi (*21*), or Fe_3O_4 (*22*). Changing the direction of the ferroelectric polarization has been predicted to influence not only the interfacial anisotropy and magnetization, but also the spin polarization. Spin polarization [i.e., the normalized difference in the density of states (DOS) of majority and minority spin carriers at the Fermi level (E_F)] is typically the key parameter controlling the response of spintronics systems, epitomized by magnetic tunnel junctions in which the tunnel magnetoresistance (*TMR*) is related to the electrode spin polarization by the Jullière formula (*23*). These predictions suggest that the nonvolatile character of ferroelectrics at the heart of ferroelectric random access memory technology (*24*) may be exploited in spintronics devices such as magnetic random access memories or spin field-effect transistors (*2*). However, the nonvolatile electrical control of spin polarization has not yet been demonstrated.

We address this issue experimentally by probing the spin polarization of electrons tunneling from an Fe electrode through ultrathin ferroelectric $BaTiO_3$ (BTO) tunnel barriers (Fig. 1A). The BTO polarization can be electrically switched to point toward or away from the Fe electrode. We used a half-metallic $La_{0.67}Sr_{0.33}MnO_3$ (LSMO) (*25*) bottom electrode as a spin detector in these artificial multiferroic tunnel junctions (*26*, *27*). Magnetotransport experiments provide evidence for a large and reversible dependence of the *TMR* on ferroelectric polarization direction.

The tunnel junctions that we used in this study are based on BTO(1 nm)/LSMO(30 nm) bilayers grown epitaxially onto (001)-oriented $NdGaO_3$ (NGO) single-crystal substrates (*28*). The large (~180°) and stable piezoresponse force microscopy (PFM) phase contrast (*28*) between negatively and positively poled areas (Fig. 1B, top) indicates that the ultrathin BTO films are ferroelectric at room temperature (*29*). The persistence of ferroelectricity for such ultrathin films of BTO arises from the large lattice mismatch with the NGO substrate (–3.2%), which is expected to dramatically enhance ferroelectric properties in this highly strained BTO (*30*). The local topographical and transport properties of the BTO(1 nm)/LSMO(30 nm) bilayers were characterized by conductive-tip atomic force microscopy (CTAFM) (*28*). The surface is very smooth with terraces separated by one-unit-cell–high steps, visible in both the topography (*29*) and resistance mappings (Fig. 1B, bottom). No anomalies in the CTAFM data were observed over lateral distances on the micrometer scale.

We defined tunnel junctions from these bilayers by a lithographic technique based on CTAFM (*28*, *31*). Top electrical contacts of diameter ~10 to 30 nm can be patterned by this nanofabrication process. The subsequent sputter deposition of a 5-nm-thick Fe layer, capped by a

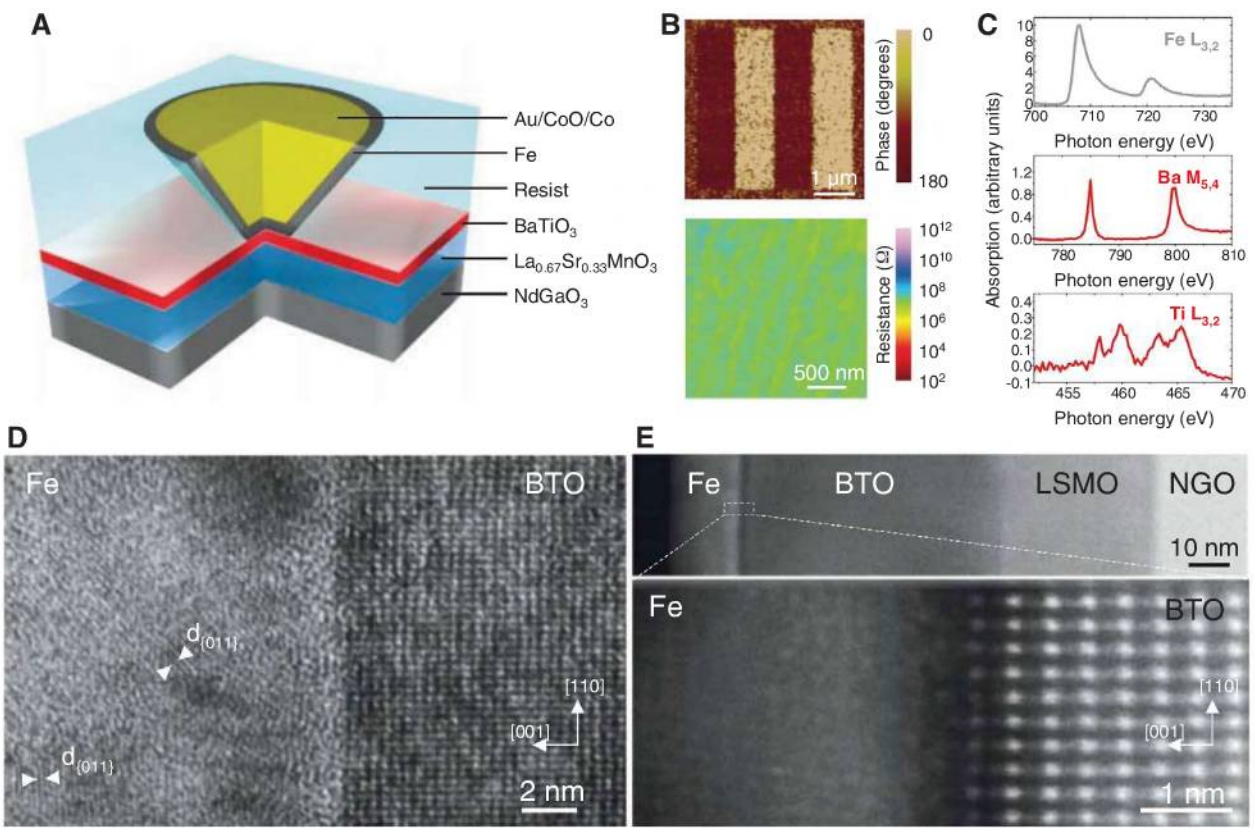

Fig. 1. (**A**) Sketch of the nanojunction defined by electrically controlled nanoindentation. A thin resist is spin-coated on the BTO(1 nm)/LSMO(30 nm) bilayer. The nanoindentation is performed with a conductive-tip atomic force microscope, and the resulting nano-hole is filled by sputter-depositing Au/CoO/Co/Fe. (**B**) (Top) PFM phase image of a BTO(1 nm)/LSMO(30 nm) bilayer after poling the BTO along 1-by-4–μm stripes with either a negative or positive (tip-LSMO) voltage. (Bottom) CTAFM image of an unpoled area of a BTO(1 nm)/LSMO(30 nm) bilayer. Ω, ohms. (**C**) X-ray absorption spectra collected at room temperature close to the Fe $L_{3,2}$ (top), Ba $M_{5,4}$ (middle), and Ti $L_{3,2}$ (bottom) edges on an AlO_x(1.5 nm)/Al(1.5 nm)/Fe(2 nm)/BTO(1 nm)/LSMO(30 nm)//NGO(001) heterostructure. (**D**) HRTEM and (**E**) HAADF images of the Fe/BTO interface in a Ta(5 nm)/Fe(18 nm)/BTO(50 nm)/LSMO(30 nm)//NGO(001) heterostructure. The white arrowheads in (D) indicate the lattice fringes of {011} planes in the iron layer. [110] and [001] indicate pseudotetragonal crystallographic axes of the BTO perovskite.

Au(100 nm)/CoO(3.5 nm)/Co(11.5 nm) stack to increase coercivity, defined a set of nanojunctions (Fig. 1A). The same Au/CoO/Co/Fe stack was deposited on another BTO(1 nm)/LSMO(30 nm) sample for magnetic measurements. Additionally, a Ta(5 nm)/Fe(18 nm)/BTO(50 nm)/LSMO(30 nm) sample and a AlO_x(1.5 nm)/Al(1.5 nm)/Fe(2 nm)/BTO(1 nm)/LSMO(30 nm) sample were realized for structural and spectroscopic characterizations.

We used both a conventional high-resolution transmission electron microscope (HRTEM) and the NION UltraSTEM 100 scanning transmission electron microscope (STEM) to investigate the Fe/BTO interface properties of the Ta/Fe/BTO/LSMO sample. The epitaxial growth of the BTO/LSMO bilayer on the NGO substrate was confirmed by HRTEM and high-resolution STEM images. The low-resolution, high-angle annular dark field (HAADF) image of the entire heterostructure shows the sharpness of the LSMO/BTO interface over the studied area (Fig. 1E, top). Figure 1D reveals a smooth interface between the BTO and the Fe layers. Whereas the BTO film is epitaxially grown on top of LSMO, the Fe layer consists of textured nanocrystallites. From the in-plane (a) and out-of-plane (c) lattice parameters in the tetragonal BTO layer, we infer that $c/a = 1.016 \pm 0.008$, in good agreement with the value of 1.013 found with the use of x-ray diffraction (*29*). The interplanar distances for selected crystallites in the Fe layer [i.e., ~2.03 Å (Fig. 1D, white arrowheads)] are consistent with the {011} planes of body-centered cubic (bcc) Fe.

We investigated the BTO/Fe interface region more closely in the HAADF mode of the STEM (Fig. 1E, bottom). On the BTO side, the atomically resolved HAADF image allows the distinction of atomic columns where the perovskite A-site atoms (Ba) appear as brighter spots. Lattice fringes with the characteristic {100} interplanar distances of bcc Fe (~2.86 Å) can be distinguished on the opposite side. Subtle structural, chemical, and/or electronic modifications may be expected to occur at the interfacial boundary between the BTO perovskite-type structure and the Fe layer. These effects may lead to interdiffusion of Fe, Ba, and O atoms over less than 1 nm, or the local modification of the Fe DOS close to E_F, consistent with ab initio calculations of the BTO/Fe interface (*18*–*20*).

To characterize the oxidation state of Fe, we performed x-ray absorption spectroscopy (XAS) measurements on a AlO_x(1.5 nm)/Al(1.5 nm)/Fe(2 nm)/BTO(1 nm)/LSMO(30 nm) sample (*28*). The probe depth was at least 7 nm, as indicated by the finite XAS intensity at the La $M_{4,5}$ edge (*28*), so that the entire Fe thickness contributed substantially to the signal. As shown in Fig. 1C (top), the spectrum at the Fe $L_{2,3}$ edge corresponds to that of metallic Fe (*32*). The XAS spectrum obtained at the Ba $M_{4,5}$ edge (Fig. 1C, middle) is similar to that reported for Ba^{2+} in (*33*). Despite the poor signal-to-noise ratio, the Ti $L_{2,3}$ edge spectrum (Fig. C, bottom) shows the typical signature expected for a valence close to 4+ (*34*). From the XAS, HRTEM, and STEM analyses, we conclude that the Fe/BTO interface is smooth with no detectable oxidation of the Fe layer within a limit of less than 1 nm.

After cooling in a magnetic field of 5 kOe aligned along the [110] easy axis of pseudocubic LSMO (which is parallel to the orthorhombic [100] axis of NGO), we characterized the transport properties of the junctions at low temperature (4.2 K). Figure 2A (middle) shows a typical resistance–versus–magnetic field $R(H)$ cycle recorded at a bias voltage of –2 mV (positive bias corresponds to electrons tunneling from Fe to LSMO). The bottom panel of Fig. 2A shows the magnetic hysteresis loop $m(H)$ of a similar unpatterned sample measured with superconducting quantum interference device (SQUID) magnetometry. When we decreased the magnetic field from a large positive value, the resistance dropped in the –50 to –250 Oe range and then followed a plateau down to –800 Oe, after which it sharply returned to the high-resistance state. We observed a similar response when cycling the field back to large positive values. A comparison with the $m(H)$ loop indicates that the switching fields in $R(H)$ correspond to changes in the relative magnetic configuration of the LSMO and Fe electrodes from parallel (at high field) to antiparallel (at low field). The magnetically softer LSMO layer switched at lower fields (50 to 250 Oe) compared with the Fe layer, for which coupling to the exchange-biased Co/CoO induces larger and asymmetric coercive fields (–800 Oe, 300 Oe). The observed $R(H)$ corresponds to a negative $TMR = (R_{ap} - R_p)/R_{ap}$ of –17% [R_p and R_{ap} are the resistance in the parallel (p) and antiparallel (ap) magnetic configurations, respectively; see the sketches in Fig. 2A]. Within the simple Jullière model of *TMR* (*23*) and considering the large positive spin polarization of half-metallic LSMO (*25*), this negative *TMR* corresponds to a negative spin polarization for bcc Fe at the interface with BTO, in agreement with ab initio calculations (*18*–*20*).

As predicted (*35*–*38*) and demonstrated (*29*) previously, the tunnel current across a ferroelectric barrier depends on the direction of the ferroelectric polarization. We also observed this effect in our Fe/BTO/LSMO junctions. As can be seen in Fig. 2B, after poling the BTO at 4.2 K to orient its polarization toward LSMO or Fe (with a poling voltage of $VP- \approx -1$ V or $VP+ \approx 1$ V, respectively; see Fig. 2B sketches), current-versus-voltage $I(V_{DC})$ curves collected at low bias voltages showed a finite difference corresponding to a tunnel electroresistance as large as $TER = (I_{VP+} - I_{VP-})/I_{VP-} \approx 37\%$ (Fig. 2B, inset). This *TER* can be interpreted within an electrostatic model (*36*–*39*), taking into account the asymmetric deformation

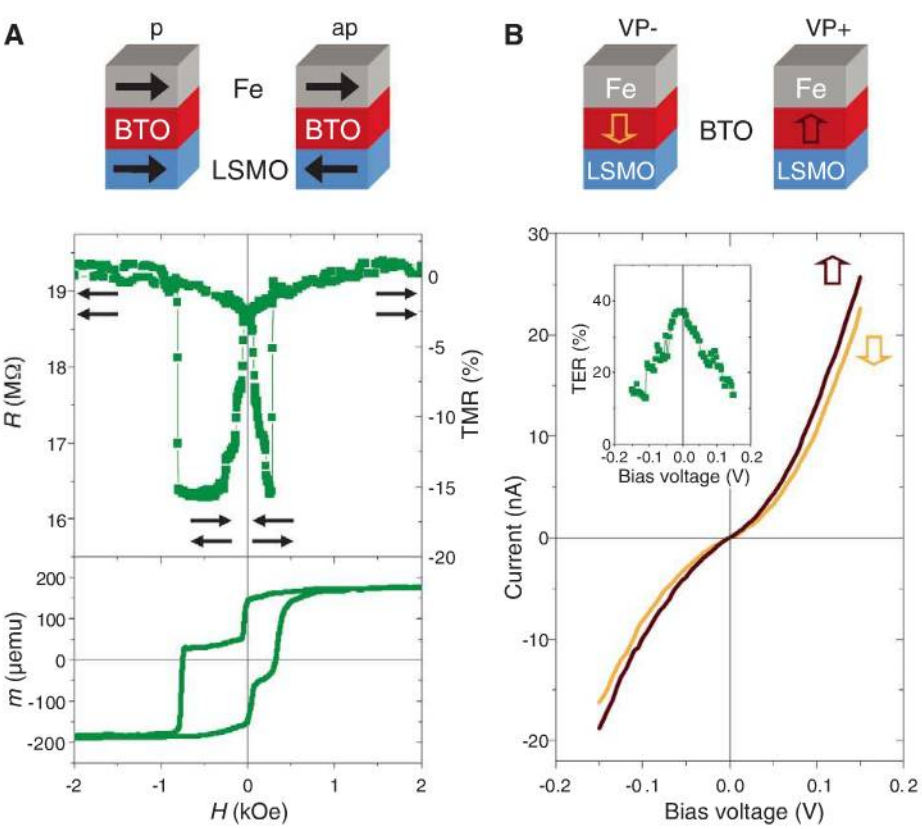

Fig. 2. **(A)** (Top) Device schematic with black arrows to indicate magnetizations. p, parallel; ap, antiparallel. (Middle) $R(H)$ recorded at –2 mV and 4.2 K showing negative *TMR*. (Bottom) $m(H)$ recorded at 30 K with a SQUID magnetometer. emu, electromagnetic units. **(B)** (Top) Device schematic with arrows to indicate ferroelectric polarization. (Bottom) $I(V_{DC})$ curves recorded at 4.2 K after poling the ferroelectric down (orange curve) or up (brown curve). The bias dependence of the *TER* is shown in the inset.

of the barrier potential profile that is created by the incomplete screening of polarization charges by different Thomas-Fermi screening lengths at Fe/BTO and LSMO/BTO interfaces. Piezoelectric-related *TER* effects (*35*, *38*) can be neglected as the piezoelectric coefficient estimated from PFM experiments is too small in our clamped films (*29*). *TER* measurements performed on a BTO(1 nm)/LSMO(30 nm) bilayer with the use of a CTAFM boron-doped diamond tip as the top electrode showed values of ~200% (*29*). Given the strong sensitivity of the *TER* on barrier parameters and barrier-electrode interfaces, these two values are not expected to match precisely. We anticipate that the *TER* variation between Fe/BTO/LSMO junctions and CTAFM-based measurements is primarily the result of different electrostatic boundary conditions.

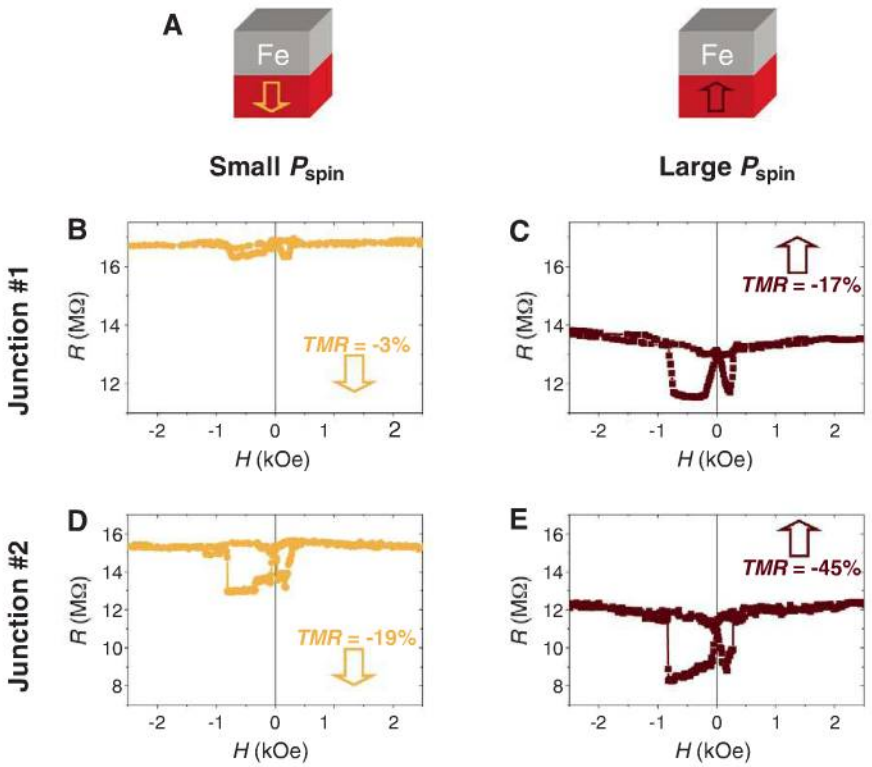

Fig. 3. (**A**) Sketch of the electrical control of spin polarization at the Fe/BTO interface. (**B** and **C**) *R*(*H*) curves for junction #1 (V_{DC} = −50 mV, *T* = 4.2 K) after poling the ferroelectric barrier down or up, respectively. (**D** and **E**) *R*(*H*) curves for junction #2 (V_{DC} = −50 mV, *T* = 4.2 K) after poling the ferroelectric barrier down or up, respectively.

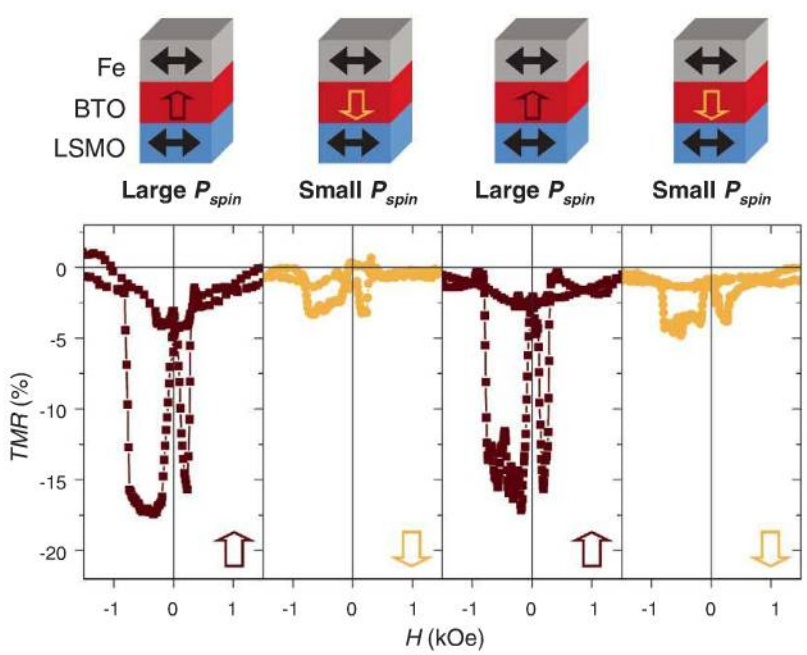

Fig. 4. *TMR*(*H*) curves recorded for junction #1 (V_{DC} = −50 mV, *T* = 4.2 K) after poling the ferroelectric up (*VP*+), down (*VP*–), up (*VP*+), and down (*VP*–).

Switching the ferroelectric polarization of a tunnel barrier with voltage pulses is also expected to affect the spin-dependent DOS of electrodes at a ferromagnet/ferroelectric interface. Interfacial modifications of the spin-dependent DOS of the half-metallic LSMO by the ferroelectric BTO are not likely, as no states are present for the minority spins up to ~350 meV above E_F (*40*, *41*). For 3d ferromagnets such as Fe, large modifications of the spin-dependent DOS are expected, as charge transfer between spin-polarized empty and filled states is possible. For the Fe/BTO interface, large changes have been predicted through ab initio calculations of 3d electronic states of bcc Fe at the interface with BTO by several groups (*18*–*20*).

To experimentally probe possible changes in the spin polarization of the Fe/BTO interface, we measured *R*(*H*) at a fixed bias voltage of –50 mV after aligning the ferroelectric polarization of BTO toward Fe or LSMO. *R*(*H*) cycles were collected for each direction of the ferroelectric polarization for two typical tunnel junctions of the same sample (Fig. 3, B and C, for junction #1; Fig. 3, D and E, for junction #2). In both junctions at the saturating magnetic field, high- and low-resistance states are observed when the ferroelectric polarization points toward LSMO or Fe, respectively, with a variation of ~ 25%. This result confirms the *TER* observations in Fig. 2B.

More interestingly, here, the *TMR* is dramatically modified by the reversal of BTO polarization. For junction #1, the *TMR* amplitude changes from –17 to –3% when the ferroelectric polarization is aligned toward Fe or LSMO, respectively (Fig. 3, B and C). Similarly for junction #2, the *TMR* changes from –45 to –19%. Similar results were obtained on Fe/BTO (1.2 nm)/LSMO junctions (*28*). Within the Jullière model (*23*), these changes in *TMR* correspond to a large (or small) spin polarization at the Fe/BTO interface when the ferroelectric polarization of BTO points toward (or away from) the Fe electrode. These experimental data support our interpretation regarding the electrical manipulation of the spin polarization of the Fe/BTO interface by switching the ferroelectric polarization of the tunnel barrier.

To quantify the sensitivity of the *TMR* with the ferroelectric polarization, we define a term, the tunnel electromagnetoresistance, as $TEMR = (TMR_{VP+} - TMR_{VP-})/TMR_{VP-}$. Large values for the *TEMR* are found for junctions #1 (450%) and #2 (140%), respectively. This electrical

control of the *TMR* with the ferroelectric polarization is repeatable, as shown in Fig. 4 for junction #1 where *TMR* curves are recorded after poling the ferroelectric up, down, up, and down, sequentially (*28*).

For tunnel junctions with a ferroelectric barrier and dissimilar ferromagnetic electrodes, we have reported the influence of the electrically controlled ferroelectric barrier polarization on the tunnel-current spin polarization. This electrical influence over magnetic degrees of freedom represents a new and interfacial magnetoelectric effect that is large because spin-dependent tunneling is very sensitive to interfacial details. Ferroelectrics can provide a local, reversible, nonvolatile, and potentially low-power means of electrically addressing spintronics devices.

References and Notes

1. C. Chappert, A. Fert, F. N. Van Dau, *Nat. Mater.* **6**, 813 (2007).
2. I. Žutić, J. Fabian, S. Das Sarma, *Rev. Mod. Phys.* **76**, 323 (2004).
3. J. C. Slonczewski, *J. Magn. Magn. Mater.* **159**, L1 (1996).
4. J. Nitta, T. Akazaki, H. Takayanagi, T. Enoki, *Phys. Rev. Lett.* **78**, 1335 (1997).
5. H. Ohno *et al.*, *Nature* **408**, 944 (2000).
6. D. Chiba *et al.*, *Nature* **455**, 515 (2008).
7. M. Weisheit *et al.*, *Science* **315**, 349 (2007).
8. T. Maruyama *et al.*, *Nat. Nanotechnol.* **4**, 158 (2008).
9. S. W. E. Riester *et al.*, *Appl. Phys. Lett.* **94**, 063504 (2009).
10. I. Stolichnov *et al.*, *Nat. Mater.* **7**, 464 (2008).
11. C. Bihler *et al.*, *Phys. Rev. B* **78**, 045203 (2008).
12. M. Overby, A. Chernyshov, L. P. Rokhinson, X. Liu, J. K. Furdyna, *Appl. Phys. Lett.* **92**, 192501 (2008).
13. C. Thiele, K. Dörr, O. Bilani, J. Rödel, L. Schultz, *Phys. Rev. B* **75**, 054408 (2007).
14. W. Eerenstein, M. Wiora, J. L. Prieto, J. F. Scott, N. D. Mathur, *Nat. Mater.* **6**, 348 (2007).
15. T. Kanki, H. Tanaka, T. Kawai, *Appl. Phys. Lett.* **89**, 242506 (2006).
16. Y.-H. Chu *et al.*, *Nat. Mater.* **7**, 478 (2008).
17. S. Sahoo *et al.*, *Phys. Rev. B* **76**, 092108 (2007).
18. C.-G. Duan, S. S. Jaswal, E. Y. Tsymbal, *Phys. Rev. Lett.* **97**, 047201 (2006).
19. M. Fechner *et al.*, *Phys. Rev. B* **78**, 212406 (2008).
20. J. Lee, N. Sai, T. Cai, Q. Niu, A. A. Demkov, preprint available at http://arxiv.org/abs/0912.3492v1.
21. K. Yamauchi, B. Sanyal, S. Picozzi, *Appl. Phys. Lett.* **91**, 062506 (2007).
22. M. K. Niranjan, J. P. Velev, C.-G. Duan, S. S. Jaswal, E. Y. Tsymbal, *Phys. Rev. B* **78**, 104405 (2008).
23. M. Jullière, *Phys. Lett. A* **54**, 225 (1975).
24. J. F. Scott, *Science* **315**, 954 (2007).
25. M. Bowen *et al.*, *Appl. Phys. Lett.* **82**, 233 (2003).
26. J. P. Velev *et al.*, *Nano Lett.* **9**, 427 (2009).
27. F. Yang *et al.*, *J. Appl. Phys.* **102**, 044504 (2007).
28. Materials and methods are available as supporting material on *Science* Online.
29. V. Garcia *et al.*, *Nature* **460**, 81 (2009).
30. K. J. Choi *et al.*, *Science* **306**, 1005 (2004).
31. K. Bouzehouane *et al.*, *Nano Lett.* **3**, 1599 (2003).
32. T. J. Regan *et al.*, *Phys. Rev. B* **64**, 214422 (2001).
33. N. Hollmann *et al.*, *Phys. Rev. B* **80**, 085111 (2009).
34. M. Abbate *et al.*, *Phys. Rev. B* **44**, 5419 (1991).
35. E. Y. Tsymbal, H. Kohlstedt, *Science* **313**, 181 (2006).
36. M. Ye. Zhuravlev, R. F. Sabirianov, S. S. Jaswal, E. Y. Tsymbal, *Phys. Rev. Lett.* **94**, 246802 (2005).
37. M. Ye. Zhuravlev, R. F. Sabirianov, S. S. Jaswal, E. Y. Tsymbal, *Phys. Rev. Lett.* **102**, 169901 (2009).
38. H. Kohlstedt, N. A. Pertsev, J. Rodriguez Contreras, R. Waser, *Phys. Rev. B* **72**, 125341 (2005).
39. M. Gajek *et al.*, *Nat. Mater.* **6**, 296 (2007).
40. M. Bowen *et al.*, *Phys. Rev. Lett.* **95**, 137203 (2005).
41. J. D. Burton, E. Y. Tsymbal, *Phys. Rev. B* **80**, 174406 (2009).

42. We thank R. Guillemet, C. Israel, M. E. Vickers, R. Mattana, J.-M. George, and P. Seneor for technical assistance, and C. Colliex for fruitful discussions on the microscopy measurements. This study was partially supported by the France-U.K. Partenariat Hubert Curien Alliance program, the French Réseau Thématique de Recherche Avancée Triangle de la Physique, the European Union (EU) Specific Targeted Research Project (STReP) Manipulating the Coupling in Multiferroic Films, EU STReP Controlling Mesoscopic Phase Separation, U.K. Engineering and Physical Sciences Research Council grant EP/E026206/I, French C-Nano Île de France, French Agence Nationale de la Recherche (ANR) Oxitronics, French ANR Alicante, the European Enabling Science and Technology through European Elelctron Microscopy program, and the French Microscopie Electronique et Sonde Atomique network. X.M. acknowledges support from Comissionat per a Universitats i Recerca (Generalitat de Catalunya).

Supporting Online Material

www.sciencemag.org/cgi/content/full/science.1184028/DC1
Materials and Methods
Figs. S1 to S5
References

30 October 2009; accepted 4 January 2010
Published online 14 January 2010;
10.1126/science.1184028
Include this information when citing this paper.

Integrated Catalytic Conversion of γ-Valerolactone to Liquid Alkenes for Transportation Fuels

Jesse Q. Bond, David Martin Alonso, Dong Wang, Ryan M. West, James A. Dumesic*

Efficient synthesis of renewable fuels remains a challenging and important line of research. We report a strategy by which aqueous solutions of γ-valerolactone (GVL), produced from biomass-derived carbohydrates, can be converted to liquid alkenes in the molecular weight range appropriate for transportation fuels by an integrated catalytic system that does not require an external source of hydrogen. The GVL feed undergoes decarboxylation at elevated pressures (e.g., 36 bar) over a silica/alumina catalyst to produce a gas stream composed of equimolar amounts of butene and carbon dioxide. This stream is fed directly to an oligomerization reactor containing an acid catalyst (e.g., H ZSM-5, Amberlyst-70), which couples butene monomers to form condensable alkenes with molecular weights that can be targeted for gasoline and/or jet fuel applications. The effluent gaseous stream of CO_2 at elevated pressure can potentially be captured and then treated or sequestered to mitigate greenhouse gas emissions from the process.

Diminishing fossil fuel resources and increasing amounts of CO_2 in the atmosphere require the development and implementation of strategies for the production of renewable transportation fuels (*1*–*4*). Although first-generation biofuels, such as corn ethanol and biodiesel, have the capacity to mitigate worldwide dependence on petroleum, new processes using lignocellulosic biomass must be developed to produce sustainable biofuels to meet worldwide demand (*5*). In this respect, γ-valerolactone (GVL) has been identified as a renewable platform molecule (*6*) with potential impact as a feedstock in the production of both energy (*6*, *7*) and fine chemicals (*8*). GVL is produced by hydrogenation of levulinic acid, which can be produced, potentially at low cost, from agricultural waste (*3*) by processes already demonstrated on a commercial scale (*9*). Recently, researchers have minimized the demand for an external source of hydrogen in this process by using the formic acid formed in equimolar amounts with levulinic acid through decomposition of cellulose (*7*) and C_6 sugars (*10*).

GVL retains 97% of the energy content of glucose and performs comparably to ethanol when used as a blending agent (10% v/v) in conventional gasoline (*6*). It has also been applied as a renewable cosolvent in splash blendable diesel fuel (*11*). GVL suffers, however, from several limitations for widespread use in the transportation sector, such as high water solubility, blending limits for use in conventional combustion engines, and lower energy density compared to petroleum-derived fuels. Although these limitations can be at least partially alleviated by reduction of GVL with an external source of hydrogen to produce methyltetrahydrofuran (*12*), which can be blended up to 70% in gasoline (*3*), the limitations would be completely eliminated by converting GVL to liquid alkenes (or alkanes) with molecular weights targeted for direct use as gasoline, jet, and/or diesel fuels.

Regarding the economic feasibility and environmental impact of biofuels, two commonly cited considerations are the demand for external hydrogen in producing a surrogate fuel and CO_2 emissions arising from its combustion (*13*). By processing GVL with a combined decarboxylation and oligomerization strategy, it is possible to

Department of Chemical and Biological Engineering, University of Wisconsin-Madison, Madison, WI 53706, USA.

*To whom correspondence should be addressed. E-mail: dumesic@engr.wisc.edu

mitigate both concerns simultaneously. As shown in the stoichiometric relations below (Eq. 1), the conversion of GVL to alkenes and CO_2 does not require an external source of hydrogen:

$$C_5O_2H_8 \longrightarrow C_4H_8 + CO_2$$
$$C_4H_8 \longrightarrow \sum_{n=2}^{5} \frac{1}{n}[C_{4n}H_{8n}] \quad (1)$$

(The hydrogenation of an alkene to an alkane requires one equivalent of H_2; however, the amount of H_2 required for the overall conversion of GVL to an alkane decreases as the molecular weight of the alkane increases.) Although the combustion of biomass-derived alkenes is equivalent to the combustion of GVL in terms of energy, an additional advantage in isolating the alkenes is that the first equivalent of CO_2 in Eq. 1 can be liberated under conditions more conducive to capture than in an automotive or jet engine. The same argument can be used to describe the conversion of glucose to ethanol, as indicated in the stoichiometric relation below (Eq. 2):

$$C_6O_6H_{12} \longrightarrow 2C_2OH_6 + 2CO_2 \quad (2)$$

However, an important difference between these two approaches for the production of biofuels is that the conversion of GVL to alkenes can produce a CO_2 stream at elevated pressure (e.g., 36 bar, as demonstrated in this report), appropriate for sequestration (*14*, *15*), conversion to methanol (*16*, *17*) upon reaction with a renewable source of hydrogen (*18*, *19*), or copolymerization with epoxides to yield polycarbonates (*20*, *21*). By contrast, the production of CO_2 during fermentation of glucose to ethanol is carried out at atmospheric pressure in the presence of air (*22*).

Figure 1 shows our integrated approach to convert GVL in aqueous solution to liquid alkenes with molecular weights appropriate for transportation fuels. The sequence entails catalytic decarboxylation of GVL to butene and CO_2, combined with the oligomerization of butene at elevated pressures, with a single catalytic system involving two tubular flow reactors connected in series with an interreactor separator (*23*). The first step is the ring opening of GVL to produce an isomeric mixture of unsaturated pentenoic acids, which can then undergo decarboxylation to produce butene isomers and a stoichiometric quantity of CO_2. We demonstrate here that both of these transformations can be carried out over a solid acid catalyst, SiO_2/Al_2O_3, in the presence of water in a single, fixed bed reactor. Moreover, these reactions can be carried out at pressures ranging from ambient to 36 bar. After a separation step in which water is condensed to the liquid state, the butene/CO_2 gas stream is upgraded in a second reactor to higher molecular weight alkenes through acid-catalyzed oligomerization (*24*, *25*). This oligomerization process is favored at elevated pressures and can be tuned to yield alkenes with a targeted range of molecular weights and varied degrees of branching in the product stream (*26*, *27*). In a second separation step, the alkenes are condensed to form a liquid product stream, while CO_2 remains as a high-pressure gas. This approach does not require an external source of hydrogen as is necessary, for example, in the catalytic upgrading of bio-oils produced by pyrolysis of biomass (*28*).

Table 1 summarizes effects of pressure, temperature, and feed composition for the conversion of aqueous solutions of GVL to butene and CO_2 over a SiO_2/Al_2O_3 catalyst (*23*). For a given temperature (entries 1 to 3), the conversion of GVL is approximately constant at pressures ranging from 1 to 36 bar; however, the yield of butenes decreases at higher pressures. Increased pressure has minimal effect on the ring opening (conversion) of GVL; however, the rate of decarboxylation of the reactive intermediate, pentenoic acid (Fig. 1), is hindered at elevated pressures. As system pressure increases, we observe a loss of selectivity to butene and a corresponding increase in selectivity to pentenoic acid. We propose that GVL decarboxylation proceeds through acid-catalyzed protonation to cleave the cyclic ester linkage, followed by proton transfer leading to C-C bond scission and deprotonation to yield butene and an equivalent of CO_2 [see fig. S4 and related text (*23*)]. The selectivity to butene can be improved by operating the reactor at higher temperatures, and good yields of butene (60%) were observed at 673 K and 36 bar (entry 4); however, higher temperature leads to coke formation, likely by polymerization of pentenoic acid, which causes catalyst deactivation with time on stream. Increasing the concentration of GVL in the feed has a positive effect on butene yield (entries 5 and 6), although coke formation eventually becomes problematic, leading to catalyst deactivation at GVL concentrations higher than 80 weight % (wt %) [figs. S1 and S2 and related text (*23*)]. Deactivation of SiO_2/Al_2O_3 is reversible, and catalytic activity can be restored by calcination at 723 K. An appropriate compromise between obtaining a high rate of GVL conversion and maintaining stable catalyst operation is achieved with an aqueous feed solution containing 60 wt % GVL at 648 K and at a pressure of 36 bar (entry 5). Under these conditions, catalytic activity remains constant for more than 100 hours of time on stream [fig. S2 (*23*)]. We observe 85% conversion of the GVL feed to form butene and stoichiometric CO_2 (67% yield), pentenoic acid isomers (15% yield), small oxygenates such as butanol and propionaldehyde (2% yield), and aromatization or oligomerization products including octene and ethylbenzene (1% yield). The butene yield is limited by the unconverted pentenoic acid intermediate, and yields >90% are achieved with a 60 wt % feed at lower space velocities (entry 7) with 100% of GVL conversion. Under these conditions, pentenoic acid is not observed, and 93% yield to butene is achieved. The fraction of butene converted to C_{8+} alkenes and aromatics increases and accounts for the remainder of products observed (7% yield). The percentage of butene present as 1-butene (33%) compared to and cis/trans 2-butene (67%) is higher than at thermodynamic equilibrium, suggesting that 1-butene is the primary product.

The effluent from the GVL decarboxylation reactor is a mixture of butene, CO_2, and water at elevated temperature and pressure. This mixture must subsequently be passed to the butene oligomerization reactor, operating at lower temperature to favor alkene coupling and minimize cracking

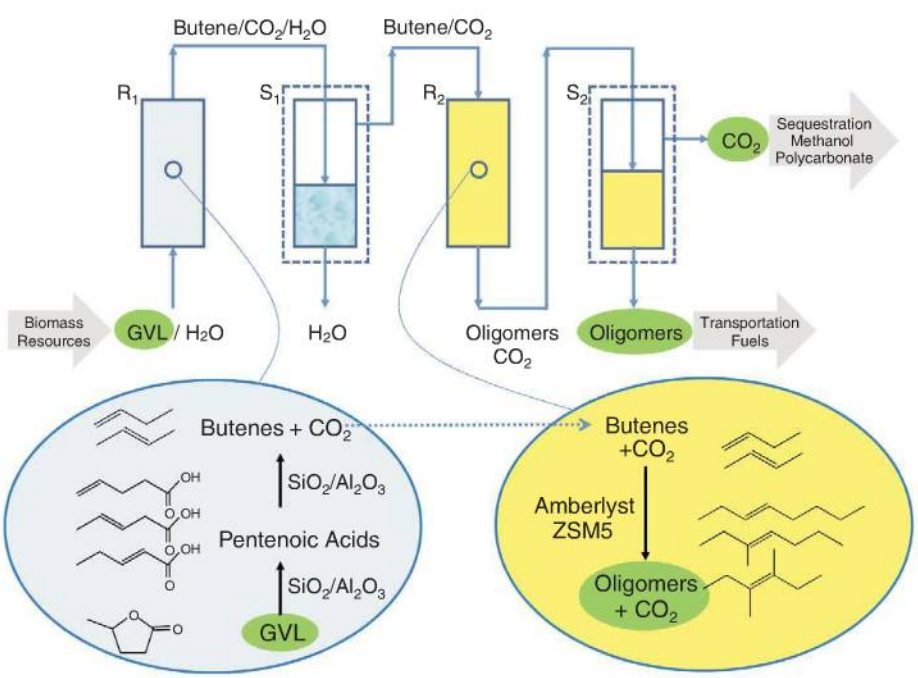

Fig. 1. Reaction pathways for conversion of GVL to butenes and CO_2, and the integrated conversion of GVL to both a liquid stream of alkenes for use in transportation fuels and a gaseous stream rich in CO_2 that is appropriate for further processing options.

reactions. Although the oligomerization of alkenes is practiced widely in the petrochemical industry (*24*, *25*, *29*), we found no reports of processing butene/CO_2 mixtures in the presence of water at elevated pressures, thus necessitating studies to identify catalysts and reaction conditions for our integrated catalytic process. Table 2 summarizes experimental results for butene oligomerization with HZSM-5 and Amberlyst-70 as catalysts (*23*). The conversion of butene over HZSM-5 reaches ~50% at ambient pressure and moderate temperature (523 K, entry 1). Higher conversions are achieved by increasing the reaction temperature to 573 K (entry 2); however, a larger fraction of the products observed are low molecular weight alkenes, produced via cracking, and the selectivity for desired products (C_{8+} alkenes for jet fuel applications) decreases from 80 to 55%. Increasing the pressure to 17 bar leads to an increase in the conversion of butene, accompanied by a decrease in selectivity for C_{8+} alkenes (entry 3). Higher selectivities (>88%) can be achieved at elevated pressure (17 bar) by decreasing the temperature to 498 K (entry 4). A further decrease in temperature to 473 K leads to minimal improvement in selectivity but causes a decrease in butene conversion (entry 5). An increase in pressure to 36 bar at 498 K allows for high overall yields of C_{8+} alkenes (77%) at high butene conversion (87%) (entry 6).

The addition of an equimolar co-feed of CO_2 to the butene oligomerization reactor leads to a decrease in butene conversion (entry 7), although the selectivity to C_{8+} alkenes remains unchanged. This decrease in butene conversion is caused by the corresponding decrease in butene partial pressure in the reactor, and the initial activity is restored upon removal of CO_2 from the feed (entry 8). The conversion of butene can be increased to 90% in the presence of an equimolar amount of CO_2, without modifying the selectivity to C_{8+} alkenes, by decreasing the weight hourly space velocity (WHSV) to 0.09 $hour^{-1}$ (entry 9). Low amounts of water in the feed decrease the conversion of butene from 90 to 82% (entry 10). As the concentration of water in the oligomerization feed increases, inhibition becomes more pronounced, and only 47% of the butene is converted when equimolar quantities of butene, CO_2, and water are fed to the reactor. When the water co-feed is stopped after 100 hours time on stream [supporting online material (SOM) Text (*23*)], 96% of the initial activity is recovered, indicating reversible inhibition and long-term stability. In all experiments reported using HZSM-5 at 498 K, the selectivity to C_{8+} alkenes is higher than 85%, indicating minimal extent of cracking.

Complete butene conversion can be achieved over Amberlyst-70 with high selectivity to C_{8+} oligomers at elevated space velocities (0.63 $hour^{-1}$, entry 14). The conversion of butene decreases upon introducing an equimolar co-feed of CO_2 (entry 15), as found for HZSM-5. The inhibiting effect of water is minimal at low feed concentrations (entry 16). As the fraction of water in the feed increases, inhibition becomes more pronounced, and complete loss of activity is observed at high amounts of water (entries 17 and 18). When the co-feed of water is stopped after 100 hours time on stream [SOM Text (*23*)], Amberlyst-70 regains 100% of its initial activity.

Results from Tables 1 and 2 suggest that GVL decarboxylation can be coupled with butene oligomerization in a single system at elevated pressures, thereby reducing the overall capital expenditure that would be required to separate, purify, and pressurize the butene obtained from GVL. Another advantage of the integrated system is that the vapor pressure of the CO_2 co-product formed by GVL decarboxylation is sufficiently high to achieve and sustain elevated system pressures appropriate for oligomerization,

Table 1. GVL conversion and butene yield at different reaction conditions over a SiO_2/Al_2O_3 catalyst operating at a weight hourly space velocity (WHSV) equal to 0.9 $hour^{-1}$.

Entry	*T* (K)	*P* (bar)	Feed GVL concentration (wt %)	GVL conversion (%)	Butene yield (%)
1	648	1	30	97	75
2	648	18	30	94	65
3	648	36	30	70	35
4	673	36	30	95	60
5	648	36	60	85	67
6	648	36	80	99	96
7*	648	36	60	99	93

*WHSV = 0.18 $hour^{-1}$

Table 2. 1-Butene conversion, selectivity, and yield to liquid C_8-C_{16} alkenes (hydrocarbons of appropriate molecular weight for direct use in liquid transportation fuels) and C_{8+} alkenes (distribution includes all the above class in addition to all oligomers larger than C_{16}) over HZSM-5 and Amberlyst-70 catalysts.

Entry	Catalyst	Feed composition	*T* (K)	*P* (bar)	Butene conversion (%)	Liquid selectivity ($C_8 - C_{16}$)/C_{8+} alkenes (%)	Liquid yield ($C_8 - C_{16}$)/C_{8+} alkenes (%)
1*	HZSM-5	Butene	523	1	51	77/80	40/41
2*	HZSM-5	Butene	573	1	87	50/55	43/48
3*	HZSM-5	Butene	523	17	90	59/73	53/66
4*	HZSM-5	Butene	498	17	64	78/88	50/56
5*	HZSM-5	Butene	473	17	38	89/91	34/35
6*	HZSM-5	Butene	498	36	87	82/88	71/77
7*	HZSM-5	Butene/CO_2 50/50	498	36	64	77/85	49/54
8*	HZSM-5	Butene	498	36	90	80/89	72/80
9†	HZSM-5	Butene/CO_2 50/50	498	17	90	65/88	58/79
10†	HZSM-5	Butene/CO_2/H_2O 47.5/47.5/5	498	17	82	72/89	59/73
11†	HZSM-5	Butene/CO_2/H_2O 45/45/10	498	17	72	72/86	52/62
12†	HZSM-5	Butene/CO_2/H_2O 33/33/33	498	17	47	79/89	37/42
13†	HZSM-5	Butene/CO_2 50/50	498	17	86	78/93	67/80
14‡	Amberlyst 70	Butene	443	17	99	72/96	71/95
15‡	Amberlyst 70	Butene/CO_2 50/50	443	17	93	69/95	64/88
16‡	Amberlyst 70	Butene/CO_2/H_2O 47.5/47.5/5	443	17	90	74/95	66/86
17‡	Amberlyst 70	Butene/CO_2/H_2O 45/45/10	443	17	50	85/92	43/46
18‡	Amberlyst 70	Butene/CO_2/H_2O 33/33/33	443	17	0	—	—
19‡	Amberlyst 70	Butene/CO_2 50/50	443	17	93	58/93	54/87

*WHSV = 0.11 $hour^{-1}$. †WHSV =0.09 $hour^{-1}$. ‡WHSV = 0.63 $hour^{-1}$.

Table 3. Performance of integrated catalytic system consisting of two flow reactors in series with an interreactor separator. Second reactor operated at 36 bar.

Entry	Reactor 1 (GVL to butene)				Reactor 2 (butene to alkenes)				GVL to liquid (C_8-C_{16})/ C_{8+}(%)
	T (K)	GVL conversion (%)	Butene yield (%)	Butene out of first separator (%)	Catalyst	*T* (K)	Butene conversion (%)	Liquid selectivity to (C_8-C_{16})/ C_{8+} (%)	
1*	648	63	37	75	HZSM-5 (14 g)	498	95	63/90	17/24
2†	648	98	91	90	HZSM-5 (14 g)	498	44	76/86	28/31
3†	648	99	92	88	Amberlyst (3 g)	443	92	74/94	50/62
4‡	648	99	90	89	Amberlyst (4 g)	443	94	64/93	48/66
5§	648	99	94	93	Amberlyst (4 g)	443	81	79/94	53/63
6‖	648	99	98	95	Amberlyst (12 g)	443	90	75/95	60/77

*Reactor 1: 2.7 g SiO_2-Al_2O_3.WHSV = 0.68 $hour^{-1}$. First separator at 373 K. †Reactor 1: 10 g SiO_2-Al_2O_3.WHSV = 0.18 $hour^{-1}$. First separator at 383 K. ‡Reactor 1: 10 g SiO_2-Al_2O_3. WHSV = 0.18 $hour^{-1}$. First separator at 388 K. §Reactor 1: 10 g SiO_2-Al_2O_3.WHSV = 0.22 $hour^{-1}$. First separator at 398 K. ‖Reactor 1: 8 g SiO_2-Al_2O_3.WHSV = 0.22 $hour^{-1}$. First separator at 398 K.

which eliminates the need for external compression strategies in continuous operation. Because water has a strong negative effect on oligomerization, the reaction system depicted in Fig. 1 was designed to carry out the desired conversion of GVL to liquid alkenes by including a separation unit between the GVL decarboxylation reactor and the butene oligomerization reactor to minimize the amount of water carried downstream. This system allows a high-pressure stream of gaseous butene to be delivered from the first separator to the inlet of the oligomerization reactor, while >98% of the water in the effluent from the first reactor is removed as a liquid. The total pressure of the system is set at 36 bar, a value that is appropriate for GVL conversion (Table 1) as well as for butene oligomerization (Table 2), and the temperature of the interreactor separator is set at a value (e.g., 373 to 398 K) that is sufficiently low to liquefy most of the water for removal but sufficiently high to maintain butene in the gaseous state for transfer to the oligomerization reactor. The products from the second reactor are collected in a second phase separator operating at ambient temperature, producing a liquid effluent stream of C_{8+} alkenes and unreacted butene, and a gaseous effluent stream of CO_2 with trace quantities of organic compounds.

Table 3 shows results for the conversions of GVL and butene in the integrated catalytic system depicted in Fig. 1 (*23*). [The product distributions for the liquid alkene effluent streams of these experiments are presented in table S2 (*23*).] The conversion of GVL and yield of butene in the first reactor, as well as butene conversion and selectivity to liquid C_{8+} alkenes in the second reactor, are similar in the integrated system (entry 1) to those values obtained for the isolated processes operating at similar conditions (Tables 1 and 2), illustrating the reproducibility of the experiments. This experiment was carried out for 85 hours [fig. S3 (*23*)] while the interreactor separator was operated at 373 K and a pressure of 36 bar; under these conditions, no aqueous phase was observed in the effluent from the oligomerization reactor, and the overall yield from GVL to C_{8+} alkenes was 24%. This overall yield was limited by the decarboxylation of GVL and loss of butene in the first separation step.

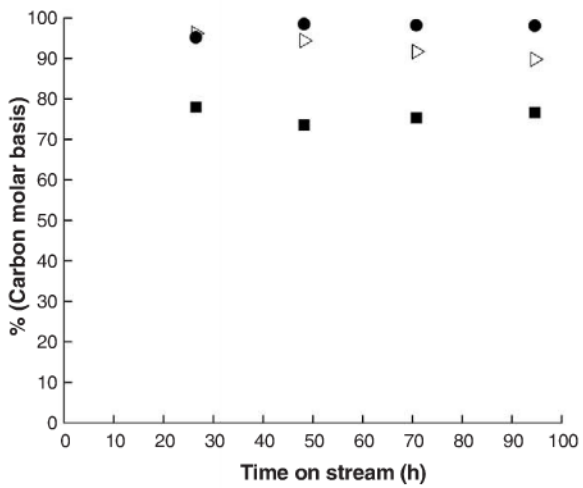

Fig. 2. Yield of butene from GVL in reactor 1 (●), butene conversion in reactor 2 (▷), and overall yield of liquid C_{8+} alkenes from GVL in the integrated process (■) versus time on stream. First reactor operated at 36 bar, 648 K and WHSV = 0.22 $hour^{-1}$. First separator operated at 36 bar and 398 K. Second reactor operated at 36 bar and 443 K with 12 g of Amberlyst-70. Second separator operated at 36 bar and 298 K.

To increase the total yield to liquid alkenes from GVL, we carried out experiments at lower space velocity of GVL (entry 2) and higher separator temperature (383 K). Under these conditions, GVL is almost quantitatively converted to butene with minimal formation of side products such as C_{8+} alkenes and aromatics. Operating the separator at higher temperature increases the extent of both butene and water vaporization and subsequent delivery to the oligomerization reactor. The increased WHSV of butene in the second reactor, combined with the inhibiting effect of water, causes a decrease in butene oligomerization, although the total yield of C_{8+} oligomers is improved to 31%.

Amberlyst-70 was identified to be a more active oligomerization catalyst than HZSM-5, and it can be used at lower temperatures to decrease the extent of cracking reactions and to improve the oligomerization selectivity to C_{8+} alkenes (Table 2). When Amberlyst-70 is used in the second reactor, the conversion of butene increases to 92%, with 94% selectivity to C_{8+} alkenes. Under these conditions, the total yield of C_{8+} alkenes from GVL increases to 62% (entry 3). The total yield to C_{8+} alkenes can be increased by decreasing the WHSV in the second reactor to increase the butene conversion (entry 4). To maximize the amount of butene delivered to the second reactor, we increased the WHSV in the first reactor from 0.18 to 0.22 $hour^{-1}$, which decreases decarboxylation by-products, such as higher alkenes and aromatics, and increases the butene yield to 94%. Additionally, by operating the initial separator at 398 K, 93% of the butene formed is delivered to the oligomerization reactor (entry 5). The higher separator temperature increases the amount of water in the second reactor, which inhibits butene oligomerization (81% conversion) and results in an overall yield of C_{8+} alkenes equal to 63%. A final yield over 75% can be achieved by increasing the amount of catalyst in the second reactor to compensate for water inhibition and reducing the amount of catalyst in the first reactor to maintain the same WHSV (entry 6). Under these conditions, the integrated catalytic system operates for more than 90 hours of time on stream (Fig. 2) with high conversions of GVL and butene in the first and second reactors, respectively, and with a high overall yield to C_{8+} alkenes (>75%). Increasing

the amount of catalyst in the oligomerization reactor modifies the selectivity, decreasing the C_8-C_{16} fraction and increasing the percentage of larger alkenes [see table S2 and related text (*23*)].

The integrated system reported here for conversion of GVL to liquid alkenes in the transportation fuel range consists of two flow reactors, two phase separators, and a simple pumping system for delivery of an aqueous solution of GVL, thereby minimizing secondary processing steps and equipment (e.g., purification of feeds, compression and pumping of gases). In addition, this approach does not require the use of precious metal catalysts, further decreasing capital costs. The catalytic system described in this report provides an efficient and inexpensive processing strategy for GVL. The cost of producing either butene or jet fuel with the approaches described here would be governed by the market value of GVL, and further research should be carried out toward optimizing production of GVL from renewable biomass resources, thereby minimizing the cost of the GVL feed to our process, and toward utilization of the high-pressure CO_2 coproduct stream formed in our process. Additionally, the yield of high molecular weight alkenes from GVL would benefit from the development of water-tolerant oligomerization catalysts.

References and Notes

1. E. L. Kunkes *et al.*, *Science* **322**, 417 (2008).
2. A. J. Ragauskas *et al.*, *Science* **311**, 484 (2006).
3. G. W. Huber, S. Iborra, A. Corma, *Chem. Rev.* **106**, 4044 (2006).
4. D. A. Simonetti, J. Rass-Hansen, E. L. Kunkes, R. R. Soares, J. A. Dumesic, *Green Chem.* **9**, 1073 (2007).
5. G. W. Huber, B. E. Dale, *Sci. Am.* **301**, 52 (2009).
6. I. T.Horváth, H. Mehdi, V. Fábos, L. Boda, L. T. Mika, *Green Chem.* **10**, 238 (2008).
7. H. Mehdi *et al.*, *Top. Catal.* **48**, 49 (2008).
8. L. E. Manzer, *Appl. Catal. Gen.* **272**, 249 (2004).
9. S. W. Fitzpatrick, "Final Technical Report: Commercialization of the Biofine Technology for Levulinic Acid Production from Paper Sludge," *Tech. Report No. DOE/CE/41178* (BioMetics, Inc, Waltham, MA, 2002); www.osti.gov/bridge.
10. H. Heeres *et al.*, *Green Chem.* **11**, 1247 (2009).
11. I. Ahmed, U.S. Patent 6,190,427 (2001).
12. D. C. Elliott, J. G. Frye, U.S. Patent 5,883,266 (1999)
13. G. W. Huber, "Breaking the Chemical and Engineering Barriers to Lignocellulosic Biofuels: Next Generation Hydrocarbon Biorefineries" (Univ. of Massachusetts Amherst, 2007); www.ecs.umass.edu/biofuels/Images/Roadmap2-08.pdf.
14. R. S. Haszeldine, *Science* **325**, 1647 (2009).
15. K. S. Lackner, *Science* **300**, 1677 (2003).
16. H. Sakurai, M. Haruta, *Catal. Today* **29**, 361 (1996).
17. J. Toyir, P. R. de la Piscina, J. L. G. Fierro, N. Homs, *Appl. Catal. Environ.* **34**, 255 (2001).
18. S. Koppatz *et al.*, *Fuel Process. Technol.* **90**, 914 (2009).
19. R. D. Cortright, R. R. Davda, J. A. Dumesic, *Nature* **418**, 964 (2002).
20. G. W. Coates, D. R. Moore, *Angew. Chem. Int. Ed.* **43**, 6618 (2004).
21. D. J. Darensbourg, *Chem. Rev.* **107**, 2388 (2007).
22. M. Wick, J. M. Lebeault, *Appl. Microbiol. Biotechnol.* **56**, 687 (2001).
23. Materials and methods are available as supporting material on *Science* Online.
24. S. Matar, L. F. Hatch, *Chemistry of Petrochemical Processes* (Gulf Professional Publishing, Houston, TX, ed. 2, 2000), pp. 248–250.
25. J. Čejka, H. van Bekkum, A. Corma, F. Schüth, in *Introduction to Zeolite Science and Practice* (Elsevier, Amsterdam, rev. ed. 3, 2007), pp. 895–899.
26. A. Mantilla *et al.*, *Catal. Today* **107-108**, 707 (2005).
27. R. J. Quann, L. A. Green, S. A. Tabak, F. J. Krambeck, *Ind. Eng. Chem. Res.* **27**, 565 (1988).
28. G. Centi, R. Van Santen, in *Catalysis for Renewables: From Feedstock to Energy Production* (Wiley-VCH, Weinheim, Germany, 2007), p. 137.
29. J. Skupinska, *Chem. Rev.* **91**, 613 (1991).

30. This work was supported through funding from the Defense Advanced Research Projects Agency (DARPA) (Surf-cat: Catalysts for Production of JP-8 range molecules from Lignocellulosic Biomass). The views, opinions, and/or findings contained here are those of the authors and should not be interpreted as representing the official views or policies, either expressed or implied, of DARPA or the Department of Defense. In addition, this work was supported in part by the U.S. Department of Energy (DOE), Office of Basic Energy Sciences, and by the DOE Great Lakes Bioenergy Research Center (www.greatlakesbioenergy.org), which is supported by the U.S. DOE, Office of Science, Office of Biological and Environmental Research, through Cooperative Agreement between The Board of Regents of the University of Wisconsin System and the U.S. DOE. A patent application has been filed in association with the Wisconsin Alumni Research Foundation based on the technology reported here. We thank R. Oakes, T. Reigle, and C. Skadahl for their assistance in our investigation of the production of butene from GVL.

Supporting Online Material

www.sciencemag.org/cgi/content/full/327/5969/1110/DC1
Materials and Methods
Figs. S1 to S4
Tables S1 and S2

6 November 2009; accepted 7 January 2010
10.1126/science.1184362

Reconstructing Past Seawater Mg/Ca and Sr/Ca from Mid-Ocean Ridge Flank Calcium Carbonate Veins

Rosalind M. Coggon,[1] Damon A. H. Teagle,[2]* Christopher E. Smith-Duque,[2] Jeffrey C. Alt,[3] Matthew J. Cooper[2]

Proxies for past seawater chemistry, such as Mg/Ca and Sr/Ca ratios, provide a record of the dynamic exchanges of elements between the solid Earth, the atmosphere, and the hydrosphere and the evolving influence of life. We estimated past oceanic Mg/Ca and Sr/Ca ratios from suites of 1.6- to 170-million-year-old calcium carbonate veins that had precipitated from seawater-derived fluids in ocean ridge flank basalts. Our data indicate that before the Neogene, oceanic Mg/Ca and Sr/Ca ratios were lower than in the modern ocean. Decreased ocean spreading since the Cretaceous and the resulting slow reduction in ocean crustal hydrothermal exchange throughout the early Tertiary may explain the recent rise in these ratios.

Cation ratios in seawater reflect the balance between their supply to and removal from the oceans, and these ratios can control important geochemical processes. For example, the influence of the seawater Mg/Ca ratio on calcium carbonate ($CaCO_3$) precipitation [high Mg/Ca ratios favor the formation of aragonite, whereas low Mg/Ca ratios favor calcite (*1*)] has important effects on marine biota and the distribution of carbonate sediments. Seawater chemistry has varied with global climate throughout Earth's history, making past seawater cation ratios such as Mg/Ca and Sr/Ca attractive proxies for determining paleo-ocean conditions (*2*–*4*). Previous estimates of seawater cation ratios have been developed from mass-balance modeling (*5*, *6*) and analyses of marine cements (*7*), fossils (*8*–*10*), and fluid inclusions trapped in halite (*11*–*13*). Unfortunately, marine sedimentary carbonates are susceptible to diagenesis (*14*), and reactions during halite formation may perturb elemental ratios from those of contemporaneous seawater, requiring careful sample selection and analysis (*11*).

Here we propose a new method for reconstructing past variations in seawater Mg/Ca and Sr/Ca ratios from the composition of $CaCO_3$ veins (CCVs) formed in oceanic crust, as recovered by ocean drilling (*15*). CCVs are formed as seawater flows through the upper ocean crust on mid-ocean ridge flanks and reacts with basalt (*16*). Calcite and aragonite precipitate from these fluids to form veins within the basement lavas (*17*). The cation composition of the carbonates therefore records the chemistry of the basement fluid, provided that the temperature at which the veins formed can be determined and the temperature dependence of element partitioning between fluid and mineral is known (*15*, *18*).

If CCVs form on ridge flanks with thin sediment cover at near-bottom water temperatures (<6°C), the reaction between seawater and basalt is minimal and the carbonate data define the seawater Mg/Ca and Sr/Ca ratios at the age determined by their $^{87}Sr/^{86}Sr$ ratios and the well-established seawater Sr isotope record (*19*). However, if CCVs form at moderate tem-

[1]Department of Earth Science and Engineering, Imperial College London, South Kensington Campus, Exhibition Road, London SW7 2AZ, UK. [2]School of Ocean and Earth Science, National Oceanography Centre, University of Southampton, Southampton SO14 3ZH, UK. [3]Department of Geological Sciences, University of Michigan, Ann Arbor, MI 48109-1005, USA.

*To whom correspondence should be addressed. E-mail: damon.teagle@soton.ac.uk

peratures (<60°C) on ridge flanks, where early, rapid sedimentation thermally blankets the basement (*20*), carbonates precipitate after substantial seawater-basalt exchange. The composition of the seawater is derived from the trends of evolving fluid chemistry versus temperature that are calculated for the suite of CCVs from a particular site by extrapolating back to the temperature of contemporaneous seawater (*15*). This was previously demonstrated for a suite of young CCVs from the 1.6- to 3.6-million-year-old Juan de Fuca Ridge (JdFR) basement, where a faithful record of the chemical evolution of near-basement pore waters during active ridge-flank circulation was preserved (Fig. 1) (*18*). In these samples, both the pore fluids and CCVs record fluid Sr/Ca, Mg/Ca, and $^{87}Sr/^{86}Sr$ ratios that show a progressive decrease from modern seawater values and indicate increased fluid-rock interaction with increasing temperature. These linear trends with temperature project back to the modern seawater values for each parameter.

We reconstructed past seawater Mg/Ca and Sr/Ca ratios from CCVs formed in 1.6- to 170-million-year-old upper ocean crust in the Atlantic and Pacific Oceans (table S1). CCVs from older crust, where the carbonate-precipitating hydrothermal systems are now extinct, mostly display similar behavior to that observed on the JdFR. For example, basement CCVs at site 843 precipitated at temperatures from 13° to 31°C from ~109-million-year-old fluids whose cation ratios and Sr isotope compositions varied with temperature (Fig. 1 and table S3). The preservation of chemical trends in ancient ocean crust gives confidence that basement CCVs are resistant to post-precipitation alteration. Consequently, the Sr/Ca, Mg/Ca, and $^{87}Sr/^{86}Sr$ ratios (and hence age) of the contemporaneous seawater from which the basement fluids developed are determined by the back extrapolation of the geochemical temperature trends recorded by the CCVs to the temperature of the contemporaneous bottom water (*15*) (Fig. 1).

From the reconstruction of seawater chemistry (Fig. 2), it is apparent that the Sr/Ca and Mg/Ca ratios were lower from the Middle Jurassic to the Oligocene than they are at present. We estimate that the molar Mg/Ca ratio of seawater remained around 1.5 to 2.5 between 170 and 24 million years ago (Ma) and then rose rapidly to ~5. Our independent record of past seawater Mg/Ca ratios from CCVs is generally in good agreement with seawater Mg/Ca records derived from evaporite inclusions (*11*–*13*) and echinoderm ossicles (*8*) (Fig. 2). We also observe that basalt-hosted CCVs that were precipitated during the Cretaceous and Paleogene are predominantly calcitic, whereas aragonite veins are more common in younger basalts with coexisting calcite veins that were generally precipitated at higher temperatures (>35°C) from fluids with lower Mg/Ca ratios produced by fluid rock exchange. This is in accordance with the greater abundance of aragonitic nonskeletal and biogenic marine carbonate since the early Cenozoic (*21*, *22*), which is attributed to an increase in the seawater Mg/Ca ratio (*22*). Similarly, the molar Sr/Ca ratio of seawater was relatively constant ($\sim 2.8 \times 10^{-3} \pm 1 \times 10^{-3}$) at approximately 30% of the modern value between 170 and 24 Ma before increasing to $\sim 8 \times 10^{-3}$ in the modern oceans. The correlations between estimated fluid Sr/Ca and temperature, and the similar estimates for ~80-million-year-old seawater Sr/Ca from sites in different oceans (for example, sites 1179 and 417/418) that had contrasting sedimentation histories, provide further support for this approach.

Our data suggest that the low Sr/Ca ratio of deep sea carbonates precipitated during the Cretaceous [~30% of modern carbonates (*23*)] is an original sedimentary signature (Fig. 2), resolving a long-standing debate. However, our seawater Sr/Ca determination is much lower than estimates based on benthic foraminifera and macrofossil calcite (*4*, *24*, *25*). We attribute this discrepancy to the great uncertainties in biogenic carbonate-Sr partitioning. Elemental partition coefficients are highly variable between different biominerals because of poorly understood physiological effects (*2*, *9*, *26*), and it is often necessary to assume that partition coefficients determined from modern biogenic carbonate are appropriate for past biomineralization and for species for which there are no modern equivalents. For example, Cretaceous and Jurassic seawater Sr/Ca ratios have been estimated from analyses of bivalves and belemnites using the average partition coefficient for modern brachiopods and bivalves (*10*). However, these coefficients vary by at least a factor of 4 (*24*, *27*) and are dependent on both temperature and calcification rate (*28*).

To evaluate the processes that are responsible for an increase in both the seawater Mg/Ca and Sr/Ca ratios since the Oligocene (Fig. 2), we consider the effects of changes in the magnitude and composition of the major ocean sources and sinks of these elements, namely river discharge, sediment burial, and hydrothermal exchange (Fig. 3). Past variation in the composition of global river discharge is difficult to quantify (*29*), but the discharge-weighted average composition of global rivers has most likely varied within the collective range of modern rivers (Fig. 3). The majority of modern rivers have

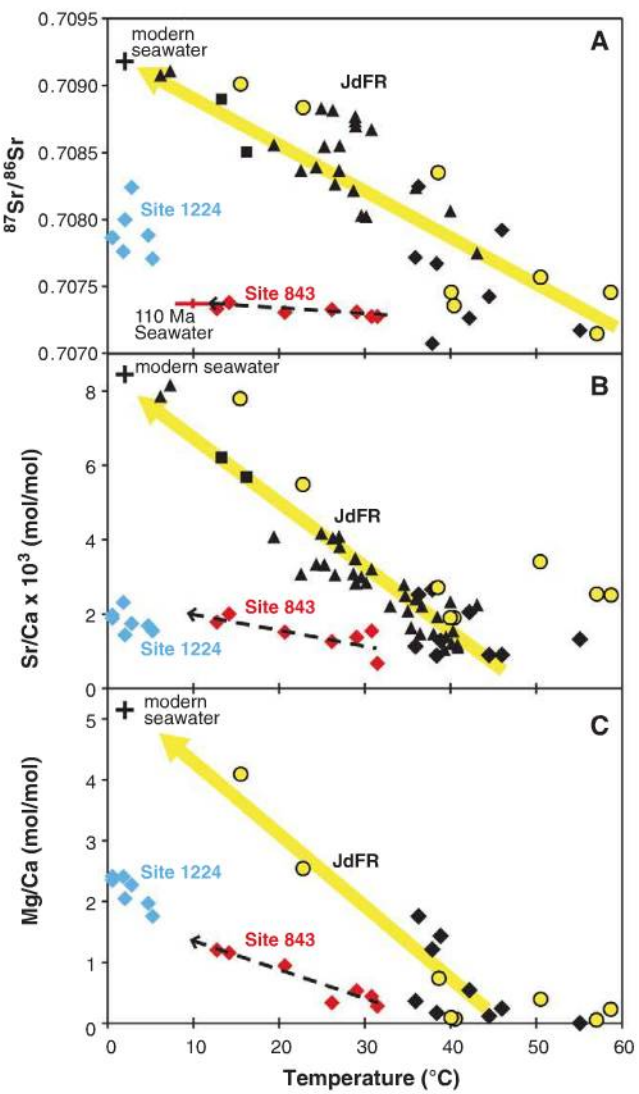

Fig. 1. Plots of fluid $^{87}Sr/^{86}Sr$ (**A**), Sr/Ca (**B**), and Mg/Ca (**C**) ratios against temperature for three sites showing contrasting styles of fluid evolution. Basement fluid compositions recorded by calcite (black diamonds), high-Mg calcite (black squares), and aragonite (black triangles) veins from the JdFR (*18*) record the same geochemical fluid evolution as near-basement pore fluids do [yellow circles (*16*)]. These trends extrapolate back to the composition of modern seawater (black cross), as indicated by the yellow arrows. CCVs from the warm 110-million-year-old site 843 crust (calcite; red diamonds) record fluid evolution trends that project back to ~10°C, 110-million-year-old seawater [red cross (*19*)] and have lower Sr/Ca and Mg/Ca ratios than modern seawater does. CCVs from the cool 46-million-year-old site 1224 crust [blue diamonds (*33*)] all precipitated at near-bottom seawater temperatures (<6°C) and are assumed to have undergone insignificant reaction with the basement.

Mg/Ca ratios that are lower than the Mg/Ca ratio of seawater since 170 Ma, whereas they display a much wider range of Sr/Ca ratios (Fig. 3). This suggests that a decrease in global river discharge in the Neogene would have increased the Mg/Ca ratio of seawater but not the Sr/Ca ratio. Decreased river discharge could therefore account for some of our proposed change in seawater composition.

The impact of sedimentation on seawater Sr/Ca and Mg/Ca ratios depends on mineralogy (Fig. 3A); conditions favoring the precipitation of calcite and aragonite have varied throughout the Phanerozoic (*21*). The most recent shift in the early Cenozoic, to conditions favoring aragonite precipitation, cannot account for our proposed increase in seawater Mg/Ca and Sr/Ca ratios (Fig. 3B). Post-burial alteration of carbonate may also affect the composition of seawater. Mg-Ca exchange during dolomite [$Ca,Mg(CO_3)_2$] formation would decrease seawater Mg/Ca, but its influence on seawater Sr/Ca depends on the carbonate mineral being altered and the time elapsed between deposition and dolomitization.

High-temperature black smoker–type reactions completely remove Mg from seawater during hydrothermal circulation and decrease the fluid Sr/Ca ratio (*30*), indicating that axial hydrothermal fluids should always have lower Sr/Ca and Mg/Ca ratios than contemporaneous seawater does. The major decrease (>30%) in ocean crust production rates (*31*) from the Cretaceous to the Tertiary and consequent lower black smoker fluid volumes would have increased seawater Sr/Ca and Mg/Ca ratios, albeit earlier than was observed in our record. Decreased low-temperature ridge flank hydrothermal alteration has a similar effect on seawater cation ratios. However, because of the vast area of the ridge flanks and the persistence of hydrothermal circulation for ~65 million years off axis, there

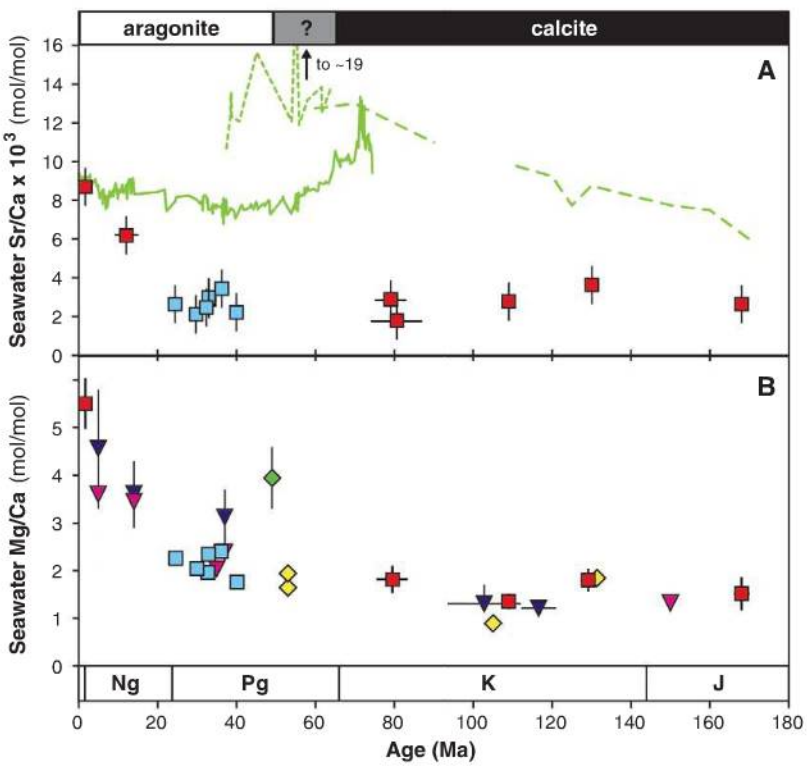

Fig. 2. Comparisons of past seawater cation ratios determined from CCVs from warm sites (red squares) and cool site 1224 (blue squares) with previous estimates of (**A**) seawater Sr/Ca estimates from benthic foraminifera [solid green line (*4*)], bivalves and belemnites [dashed green line (*10*)], and the minimum Sr/Ca estimated from marine turritellid snails [dotted green line (*25*)]; and (**B**) seawater Mg/Ca estimates from halite-trapped fluid inclusions [pink triangles (*11*) and dark blue triangles (*12*), Cretaceous estimates as updated by (*13*)], benthic foraminifera [green diamond (*9*)], and echinoderm ossicles [yellow diamonds (*8*)]. The upper bar indicates intervals when marine conditions favored the precipitation of calcite and aragonite (*21*), and the lower bar shows the geological periods. J, Jurassic; K, Cretaceous; Pg, Paleogene; and Ng, Neogene.

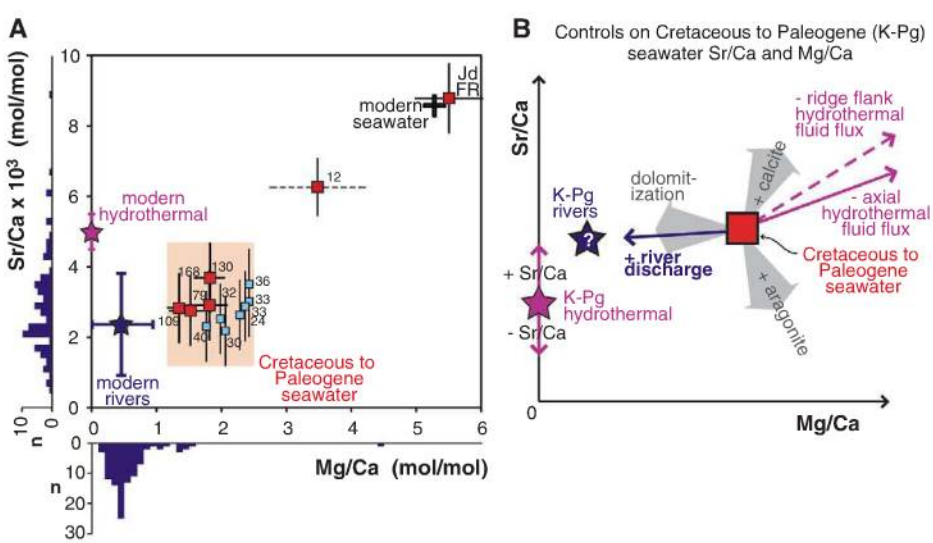

Fig. 3. (**A**) Variation in seawater Sr/Ca and Mg/Ca ratios with time recorded by CCVs [labels indicate age (Ma)] from warm ridge flanks (large red squares) and cool ridge flank site 1224 (smaller light blue squares) relative to modern seawater (black cross). Shown for comparison are the present-day ocean inputs from hydrothermal circulation [purple star; average black smoker fluid (*30*)] and rivers [dark blue star; discharge-weighted average river composition (*34*–*36*), ±1 SD]. The variability of modern river compositions is shown by the histograms along the figure's axes (*n* indicates number of rivers). The Mg/Ca ratio of 12-million-year-old seawater (dashed line) is estimated from evaporite fluid inclusion studies (*11*, *12*). The composition of seawater during the Cretaceous and Paleogene is highlighted (pink box). (**B**) Sketch illustrating the effects on the Sr/Ca and Mg/Ca ratios of Cretaceous-Paleogene (K-Pg) seawater of decreased axial or ridge flank hydrothermal fluid fluxes (purple arrows), or increased global river discharge (blue arrow), calcite or aragonite sedimentation, and dolomitization of sediments (gray arrows). We assume that K-Pg global river discharge (blue star) was compositionally similar to modern discharge. The effect of increasing (+) or decreasing (–) the Sr/Ca ratio of seawater on hydrothermal fluids (purple star) is illustrated.

will be a substantial delay in the impact of lower crustal production rates on decreased low-temperature fluid fluxes, because the age spectrum of the ridge flanks changes only slowly. Presently, only ~55% of the ocean floor is less than 65 million years old and contributes to ridge flank hydrothermal circulation, compared with ~85% in the Late Cretaceous (*32*). Decreasing fluid-rock exchange on the ridge flanks throughout the Tertiary, superimposed on decreases in global mid-ocean ridge axial hydrothermal activity since the Cretaceous, could therefore explain the observed increase in seawater Mg/Ca and Sr/Ca ratios since the Oligocene.

References and Notes

1. J. W. Morse, Q. W. Wang, M. Y. Tsio, *Geology* **25**, 85 (1997).
2. A. L. Cohen, K. E. Owens, G. D. Layne, N. Shimizu, *Science* **296**, 331 (2002).
3. C. H. Lear, H. Elderfield, P. A. Wilson, *Science* **287**, 269 (2000).
4. C. H. Lear, H. Elderfield, P. A. Wilson, *Earth Planet. Sci. Lett.* **208**, 69 (2003).
5. R. A. Berner, A. C. Lasaga, R. M. Garrels, *Am. J. Sci.* **283**, 641 (1983).
6. F. T. Mackenzie, R. M. Garrels, *Am. J. Sci.* **264**, 507 (1966).
7. S. J. Carpenter *et al.*, *Geochim. Cosmochim. Acta* **55**, 1991 (1991).
8. J. A. D. Dickson, *Science* **298**, 1222 (2002).
9. C. H. Lear, Y. Rosenthal, N. Slowey, *Geochim. Cosmochim. Acta* **66**, 3375 (2002).
10. T. Steuber, J. Veizer, *Geology* **30**, 1123 (2002).
11. J. Horita, H. Zimmerman, H. D. Holland, *Geochim. Cosmochim. Acta* **66**, 3733 (2002).
12. T. K. Lowenstein, M. N. Timofeeff, S. T. Brennan, L. A. Hardie, R. V. Demicco, *Science* **294**, 1086 (2001).
13. M. N. Timofeeff, T. K. Lowenstein, M. A. Martins da Silva, N. B. Harris, *Geochim. Cosmochim. Acta* **70**, 1977 (2006).
14. F. M. Richter, D. J. DePaolo, *Earth Planet. Sci. Lett.* **83**, 27 (1987).
15. Materials and methods are available as supporting material on *Science* Online.
16. H. Elderfield, C. G. Wheat, M. J. Mottl, C. Monnin, B. Spiro, *Earth Planet. Sci. Lett.* **172**, 151 (1999).
17. J. C. Alt, D. A. H. Teagle, *Geochim. Cosmochim. Acta* **63**, 1527 (1999).
18. R. M. Coggon, D. A. H. Teagle, M. J. Cooper, D. A. Vanko, *Earth Planet. Sci. Lett.* **219**, 111 (2004).
19. J. M. McArthur, R. J. Howarth, T. R. Bailey, *J. Geol.* **109**, 155 (2001).
20. A. T. Fisher *et al.*, *Nature* **421**, 618 (2003).
21. P. A. Sandberg, *Nature* **305**, 19 (1983).
22. S. M. Stanley, L. A. Hardie, *Palaeogeogr. Palaeoclimatol. Palaeoecol.* **144**, 3 (1998).
23. F. M. Richter, Y. Liang, *Earth Planet. Sci. Lett.* **117**, 553 (1993).
24. T. Steuber, *Int. J. Earth Sci.* **88**, 551 (1999).
25. A. K. Tripati, W. D. Allmon, D. E. Sampson, *Earth Planet. Sci. Lett.* **282**, 122 (2009).
26. D. W. Lea, T. A. Mashiotta, H. J. Spero, *Geochim. Cosmochim. Acta* **63**, 2369 (1999).
27. U. Brand, A. Logan, N. Hiller, J. Richardson, *Chem. Geol.* **198**, 305 (2003).
28. P. S. Freitas, L. J. Clarke, H. Kennedy, C. A. Richardson, F. Abrantes, *Geochim. Cosmochim. Acta* **70**, 5119 (2006).
29. M. T. Gibbs, L. R. Kump, *Paleoceanography* **9**, 529 (1994).
30. K. L. Von Damm, *Geophys. Monogr.* **91**, 222 (1995).
31. R. D. Müller, M. Sdrolias, C. Gaina, B. Steinberger, C. Heine, *Science* **319**, 1357 (2008).
32. M. Seton, C. Gaina, R. D. Müller, C. Heine, *Geology* **37**, 687 (2009).
33. H. J. Paul, K. M. Gillis, R. M. Coggon, D. A. H. Teagle, *Geochem. Geophys. Geosyst.* **7**, Q02003 (2006).
34. J. Gaillardet, B. Dupré, P. Louvat, C. J. Allègre, *Chem. Geol.* **159**, 3 (1999).
35. M. Meybeck, A. Ragu, *River Discharges to the Oceans. An Assessment of Suspended Solids, Major Ions, and Nutrients, Environment Information and Assessment Report* (United Nations Environment Programme, Nairobi, Kenya, 1996).
36. D. Vance, D. A. H. Teagle, G. L. Foster, *Nature* **458**, 493 (2009).

37. This research was supported by National Environment Research Council research grants NER/T/S/2003/00048 and NE/E001971/1 to D.A.H.T. and NE/C513242/1 to R.M.C. and D.A.H.T. This research used samples provided by the Ocean Drilling Program (ODP) and the Integrated Ocean Drilling Program (IODP). ODP was sponsored by NSF and participating countries under the management of Joint Oceanographic Institutions. IODP is supported by NSF; Japan's Ministry of Education, Culture, Sports, Science and Technology; the European Consortium for Ocean Drilling Research; and the People's Republic of China, Ministry of Science and Technology. We thank M. Palmer, P. Wilson, D. Vance, R. James, and three anonymous reviewers for insightful comments that greatly improved this manuscript.

Supporting Online Material

www.sciencemag.org/cgi/content/full/science.1182252/DC1
Materials and Methods
Figs. S1 and S2
Tables S1 to S4
References

21 September 2009; accepted 19 January 2010
Published online 4 February 2010;
10.1126/science.1182252
Include this information when citing this paper.

Climate-Modulated Channel Incision and Rupture History of the San Andreas Fault in the Carrizo Plain

Lisa Grant Ludwig,[1]* Sinan O. Akçiz,[1] Gabriela R. Noriega,[1] Olaf Zielke,[2] J Ramón Arrowsmith[2]

The spatial and temporal distribution of fault slip is a critical parameter in earthquake source models. Previous geomorphic and geologic studies of channel offset along the Carrizo section of the south central San Andreas Fault assumed that channels form more frequently than earthquakes occur and suggested that repeated large-slip earthquakes similar to the 1857 Fort Tejon earthquake illustrate typical fault behavior. We found that offset channels in the Carrizo Plain incised less frequently than they were offset by earthquakes. Channels have been offset by successive earthquakes with variable slip since ~1400. This nonuniform slip history reveals a more complex rupture history than previously assumed for the structurally simplest section of the San Andreas Fault.

Knowledge of the age and associated slip distribution for surface-rupturing earthquakes is essential for understanding fault rupture and the recurrence of large, potentially destructive earthquakes (*1*). Paleoseismological data about previous large earthquakes are needed to characterize rupture patterns and assess the associated seismic hazard (*2*). Dates of past earthquakes are obtained from excavations across active faults, where the disruption of the ground surface at the time of the event is encased in datable sediments. Channels offset along faults are used as markers to determine displacements in successive earthquakes and to infer earthquake recurrence on the basis of two assumptions: (i) Strain release rate along that section of the fault is constant during the period of interest, and (ii) the channels form more frequently than they are offset by earthquakes.

The south central San Andreas Fault (SAF) last ruptured in the great 1857 earthquake (all dates are calendar years C.E.) and displaced channels that crossed the fault (*3*, *4*). In the Carrizo Plain, measurements of slip rate over different time intervals agree with geodetically measured loading rates of ~35 mm/year (*2*, *3*, *5*). Several studies have analyzed offset channels to infer slip distribution from the great 1857 earthquake and prior ruptures (*3*, *4*, *6*–*8*) in the semi-arid Carrizo Plain. Near Wallace Creek (Fig. 1), channels offset by approximately 33 m, 21.8 m, and 9.5 m (*3*, *4*) were interpreted to be caused by three successive earthquakes with surface slip of 11.2 m, 12.3 m, and 9.5 m, respectively (*3*). However, determining the incision age of offset ephemeral stream channels is difficult if only the channel fill sediments are dated, because transported organic material may have inherited age (*7*, *9*–*12*).

We sought to determine the age, and consequently the slip history, of channels that are offset by commonly measured offset values of ~8 to 10 m and ~16 m in the Carrizo Plain and along the 1857 rupture of the southern SAF (*4*, *7*, *8*). To test the hypothesis that incision occurred more frequently than offset, we used traditional stratigraphic analysis, with high-resolution radiocarbon dating and new records of extreme climate events (*9*, *13*, *14*), to determine the relative sequence of earthquake rupture and channel incision. We focused on a section of the SAF between Wallace

[1]Program in Public Health and California Institute for Hazards Research, University of California, Irvine, CA 92697, USA. [2]School of Earth and Space Exploration, Arizona State University, Tempe, AZ 85287, USA.

*To whom correspondence should be addressed. E-mail: lgrant@uci.edu

Creek and the Bidart Fan (BF) paleoseismic site (Figs. 1 and 2) in the northern Carrizo Plain (*7*, *10*–*12*), where excavations provide unique exposures of faulted sediment adjacent to offset channels (*11*, *15*).

In the BF, drainage from the Temblor Range deposits alluvial sediments and forms channels nearly perpendicular to the SAF (Fig. 1). Drainage areas of these channels vary over several orders of magnitude along strike of the fault. BF shows evidence of recent deposition and incision of two offset channels (Fig. 1). Deposition of sediment on the BF surface and erosion of channels into it was driven by varying climatic conditions over the past 700 years (*9*). Many non-offset channels that now cross the SAF in the Carrizo Plain might have incised during the unusually wet decades from 1861 to 1891, possibly during 1861–1862, when floodwaters cut arroyos in southern California (*16*). Stratigraphic correlation and radiocarbon dating of sediments across the fan show that alluvium deposition was strongly controlled by incision of deep channels into the BF (*17*). The location of the depositional lobe has shifted through time (*11*), and those sections of the fan with deep channels experienced limited sedimentation. These incision events caused depositional hiatuses on the fan surface near the northwest and southeast channels (Fig. 1). Alluvial sediments that were deposited before incision of the adjacent (>2 m) deep channels were exposed in trenches 2, 3, and 4 (Fig. 1) and radiocarbon-dated to constrain the approximate dates of incision. Near the northwest channel, layers exposed in trenches 3 and 4 that are ~10 cm, ~50 cm, and ~60 cm below the surface were dated approximately 1340 to 1400 (*15*, *17*), indicating that most deposition ceased around 1400 or later. Likewise, near the southeast channel, radiocarbon dates of detrital samples from the channel fill and alluvial deposits 20 to 30 cm below the fan surface indicate that incision occurred approximately 1616 to 1771 (*17*).

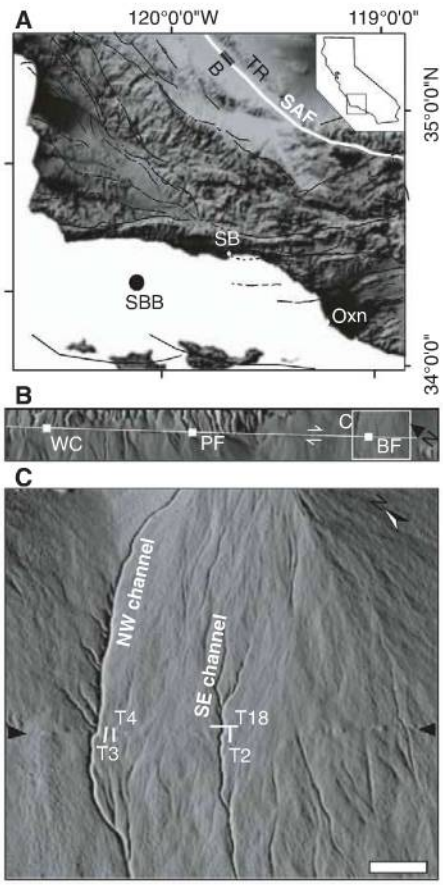

Fig. 1. (**A**) The San Andreas fault (SAF; white) and Quaternary faults (black) in southwestern California (SB, Santa Barbara; Oxn, the coastal region near Oxnard; SBB, the offshore Santa Barbara Basin). TR, Temblor Range; SAF region shown in (B) is indicated. (**B**) Hillshade map generated from LIDAR-based digital elevation map, showing the geomorphic expression of strike-slip faulting in the Carrizo Plain in the study area from Wallace Creek (WC) and Phelan Fan (PF) to Bidart Fan (BF). (**C**) A portion of the Bidart Fan zoomed in on the hillshade plot (grid size 0.5 m) showing southwest-flowing alluvial drainage system bisected by the northwest-trending SAF (between black triangles), which offsets two incised channels (NW and SE). Samples for radiocarbon dating were collected from three trenches (T2, T3, and T4) and the southeast channel (T18) for determining age of channel incision and surface abandonment (*17*). Scale bar, 200 m.

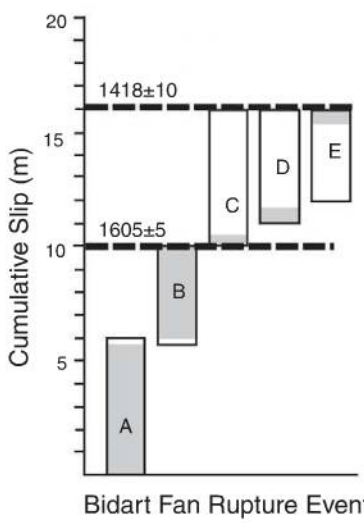

Fig. 2. Summary of cumulative slip, incision model, and slip per earthquake at BF. Five earthquakes and two incision events occurred since ~1400. Slip per earthquake is shown as shaded vertical bar, with maximum slip in open bars. The northwest channel is offset 15.9 m by five earthquakes (Table 1). The 1857 earthquake A generated 5.8 to 6.0 m of slip at BF. Total slip of the 1857 and penultimate earthquake B, 10.2 m, is constrained by offset of the southeast channel, incised around 1605 ± 5 (black dashed line). Three prior earthquakes (boxes labeled 3, 4, and 5) collectively offset the northwest channel as much as 5.6 m. Slip was at least 50 cm each (shaded bars).

Paleoclimate data provide an environmental context for interpreting alluvial deposits and identifying fluvial events that could have caused channel incision. High-resolution paleoclimate proxy data (*9*, *13*, *14*, *18*) between 1300 and 1857 show that two prehistoric extreme flooding events eroded sediment from the coastal region near the Carrizo Plain and deposited sediment in anoxic basins offshore (*13*, *14*). Cores from the offshore Santa Barbara Basin (SBB, Fig. 1) contain two unusually thick layers of terrigenous sediment deposited by floods from the Coast Ranges during the years 1605 ± 5 and 1418 ± 10. The extreme floods in ~1605 and ~1418 have been linked to extreme ENSO (El Niño–Southern Oscillation) events and global reorganizations of atmospheric circulation that left recognizable evidence from California to South America (*14*). In coastal central California, ENSO events are associated with unusually high precipitation and streamflow within ~100 km of the coast (*18*), which includes the Carrizo Plain. Extreme floods in the Santa Clara and Ventura watersheds (draining to the SBB) most likely also occurred in the Carrizo and could have left recognizable sedimentary or geomorphic evidence. Radiocarbon ages of near-surface sediments at BF are consistent with incision of the northwest channel in the ~1418 extreme coastal flooding event, and with incision of the southeast BF channel in the ~1605 extreme flooding event or shortly thereafter (*17*).

These incision ages are also consistent with the offset and apparent ages of the BF channels. Assuming a constant slip rate (*2*, *3*, *5*, *19*), the southeast BF channel should have accumulated 8.8 m of slip between 1605 and 1857. Likewise, the northwest BF channel should have accumulated 15.4 m of slip between 1418 and 1857. Recent LIDAR (light detection and ranging)–based measurements show that the northwest channel is offset by ~15.9 m and the southeast channel is offset by ~10.2 m (*8*). Ground-based measurements of the southeast channel offset are 7 to 10 m (*17*). Excavations of buried offset channels near Wallace Creek yielded similar offset measurements for two channels—7.8 to 8.0 m and 15.1 to 15.8 m (*12*)—which suggests that they could have incised during these regional flooding events.

If the southeast BF channel incised around 1605, it must have been displaced by at least two earthquakes (*15*) instead of a single event, as initially assumed (*4*, *10*, *11*). LIDAR analysis results suggest that average slip during the 1857 earthquake in the Carrizo Plain was 5.3 ± 1.4 m (*8*), although it may have been as high as 6.9 m at the nearby Phelan Fan site (*10*). To account for possible slip variability, we interpolate BF slip as the average of the two nearest offset channels, which measured 6 ± 1 m (~750 m northwest of BF) and 5.8 ± 0.5 m (*8*) (2 km southeast of BF). Subtracting this amount, 5.9 ± 0.6 m, from the total offset of the southeast channel (10.2 ± 1.2 m), we obtain 4.3 ± 1.3 m of slip at BF from the penultimate earthquake. Similarly, correlating

Table 1. Bidart Fan earthquake sequence, channel incision, and offset events.

Earthquake date*	Inferred incision date	Channel	Total offset (m)	Number of offsets
(A) 1857			5.9	
(B) 1631–1823				
	1605 ± 5	SE	10.2†	2§
(C) 1547–1617§				
(D) ~1450–1547‡				
(E) ~1450–1547‡				
	1418 ± 10	NW	15.9†	5
(F) 1360–1425#				
(G) 1280–1340				

*Dates from (*15*) except as noted. Earthquake F is rupture event BDT4-d at trench T4. Earthquake G is rupture BDT4-e at T4. Earthquakes BDT3-f and BDT3-g at T3 (*15*) are older than earthquakes F and G in this table. †Measurements from (*8*). ‡Approximate age (*21*). §Inferred incision age of southeast channel overlaps with dates of second and third earthquakes reported by Akçiz *et al.* (*15*). They presented evidence that event BDT2-b is the third oldest earthquake, event C, and predates incision. New radiocarbon dates of BDT2-b (*17*) eliminate age overlap of earthquakes B and C. #The sixth earthquake, F, caused surface rupture between deposition of two near-surface sedimentary units (*17*) and therefore is inferred to predate incision of the adjacent northwest channel.

same-age sediments in trenches ~ 200 m away suggests that the northwest channel has been displaced by five surface ruptures (Table 1). Ages of sediments and their stratigraphic position in trench 4 support an interpretation of incision between the fifth and sixth earthquakes, during a time interval that includes the ~1418 extreme flood (*17*) (Table 1). Thus, the northwest channel has been offset in three additional earthquakes by as much as 5.6 m more than the offset of the southeast channel (Fig. 2). Slip in individual earthquakes at the BF is not directly measurable, but we can assume at least 50 cm of slip on the basis of expression in trench exposures (*15*). With minimum slip of 1 m in two earthquakes, maximum slip would be 4.6 m in the other earthquake.

Comparison of channel incision dates with the rate of occurrence of surface ruptures suggests that channel incision events are less frequent than earthquakes in the Carrizo Plain, which implies that some channels have been offset by more earthquakes than previously thought (*9*). Our observations do not support previous interpretations of ~9 m of slip in the 1857 earthquake (*3*, *4*) or any of the earthquakes that ruptured since 1400. However, slip in the 1857 earthquake was apparently greater than in any of the four prior ruptures. This variable slip history is not consistent with repeated characteristic slip (*20*) at BF in the Carrizo, one of two areas where characteristic slip was defined (*6*). Since the 1857 earthquake, >5 m of strain has accumulated in the Carrizo, an amount greater than or similar to slip released in the last five ruptures.

References and Notes

1. Ch. H. Scholz, *The Mechanics of Earthquakes and Faulting* (Cambridge Univ. Press, Cambridge, ed. 2, 2002).
2. Working Group on California Earthquake Probabilities, *The Uniform California Earthquake Rupture Forecast, v2, USGS Open File Report 2007* (2008).
3. K. E. Sieh, R. H. Jahns, *Geol. Soc. Am. Bull.* **95**, 883 (1984).
4. K. E. Sieh, *Bull. Seismol. Soc. Am.* **68**, 1421 (1978).
5. G. Schmalzle, T. Dixon, R. Malservisi, R. Govers, *J. Geophys. Res.* **111**, B05403 (2006).
6. D. P. Schwartz, K. J. Coppersmith, *J. Geophys. Res.* **89**, 568 (1984).
7. J. Liu, Y. Klinger, K. Sieh, C. Rubin, *Geology* **32**, 649 (2004).
8. O. Zielke, J R. Arrowsmith, L. Grant Ludwig, S. O. Akçiz, *Science* **327**, 1119 (2010); published online 21 January 2010 (10.1126/science.1182781).
9. G. R. Noriega, thesis, University of California, Irvine (2009).
10. L. B. Grant, K. E. Sieh, *Bull. Seismol. Soc. Am.* **83**, 619 (1993).
11. L. B. Grant, K. E. Sieh, *J. Geophys. Res.* **99**, 6819 (1994).
12. J. Liu-Zeng, Y. Klinger, K. Sieh, C. Rubin, G. Seitz, *J. Geophys. Res.* **111**, B02306 (2006).
13. A. Schimmelmann, M. Zhao, C. C. Harvey, C. B. Lange, *Quat. Res.* **49**, 51 (1998).
14. A. Schimmelmann, C. B. Lange, B. J. Meggers, *Holocene* **13**, 763 (2003).
15. S. O. Akçiz, L. Grant Ludwig, J. R. Arrowsmith, *J. Geophys. Res.* **114**, B01313 (2009).
16. W. N. Engstrom, *Quat. Res.* **46**, 141 (1996).
17. See supporting material on *Science* Online.
18. D. R. Cayan, K. T. Redmond, L. G. Riddle, *J. Clim.* **12**, 2881 (1999).
19. G. R. Noriega, J. R. Arrowsmith, L. B. Grant, J. J. Young, *Bull. Seismol. Soc. Am.* **96**, 33 (2006).
20. L. B. Grant, *Science* **272**, 826 (1996).
21. S. O. Akçiz *et al.*, *Eos* **87** (fall meet. suppl.), T21E-01 (2006).

22. Supported by NSF grants EAR 0409500 and 0711518, USGS grant 07HQGR0092, and the Southern California Earthquake Center (SCEC). SCEC is funded by NSF Cooperative Agreement EAR-0529922 and USGS Cooperative Agreement 07HQAG0008. The SCEC contribution number for this paper is 1305. Thanks to anonymous reviewers, student field assistants, L. Bidart for access to field sites, and J. Southon, M. Kirby, D. Cayan, K. Whipple, A. Heimsath, and E. Vivoni for discussions.

Supporting Online Material

www.sciencemag.org/cgi/content/full/science.1182837/DC1
Materials and Methods
Figs. S1 and S2
References

5 October 2009; accepted 9 January 2010
Published online 21 January 2010;
10.1126/science.1182837
Include this information when citing this paper.

Slip in the 1857 and Earlier Large Earthquakes Along the Carrizo Plain, San Andreas Fault

Olaf Zielke,[1]* J Ramón Arrowsmith,[1] Lisa Grant Ludwig,[2] Sinan O. Akçiz[2]

The moment magnitude (M_w) 7.9 Fort Tejon earthquake of 1857, with a ~350-kilometer-long surface rupture, was the most recent major earthquake along the south-central San Andreas Fault, California. Based on previous measurements of its surface slip distribution, rupture along the ~60-kilometer-long Carrizo segment was thought to control the recurrence of 1857-like earthquakes. New high-resolution topographic data show that the average slip along the Carrizo segment during the 1857 event was 5.3 ± 1.4 meters, eliminating the core assumption for a linkage between Carrizo segment rupture and recurrence of major earthquakes along the south-central San Andreas Fault. Earthquake slip along the Carrizo segment may recur in earthquake clusters with cumulative slip of ~5 meters.

Recent earthquake ruptures along the North Anatolian fault in Turkey [moment magnitude (M_w) 7.4 Izmit earthquake, 1999] (*1*), the Kunlun Fault in China (M_w 7.8 Kokoxili earthquake, 2001) (*2*), the Denali fault in Alaska (M_w 7.9 Denali earthquake, 2002) (*3*), and the Longmenshan fault in China (M_w 7.9 Wenchuan earthquake, 2008) (*4*) present dramatic manifestations of large-earthquake phenomena, exemplifying the destructive potential of tectonically active faults. A primary step toward assessing the time and magnitude of future large earthquakes is the identification of earthquake recurrence intervals and along-fault slip-release patterns.

Previous work along the San Andreas Fault (SAF) (*5*, *6*) reported that the largest slip associated with the surface rupture of the M_w 7.9 Fort Tejon earthquake of 1857—the most recent earthquake along the south-central SAF—occurred with ~9 m along the Carrizo segment (Fig. 1). Further investigation along the 1857 rupture trace (*7*) suggested that individual fault segments experienced essentially the same amount of slip in preceding earthquakes as they did in 1857 (e.g., the largest slip associated with preceding earthquakes occurred with ~9 m along the Carrizo segment). These and similar observations for the Wasatch fault in Utah led to the formulation of the uniform-slip and the characteristic earthquake model (*7*, *8*), which dominate current

seismic hazard assessment and earthquake forecast. Both earthquake recurrence models propose that slip per earthquake at a point along a fault is essentially the same (i.e., characteristic) and can be inferred to have occurred by similar-magnitude major earthquakes. Assuming a constant slip rate along the fault and a direct relation between repeat time and amount of slip released in an earthquake, it was proposed that the relatively strong (i.e., high slip per event) Carrizo segment defines the reported 240- to 450-year recurrence time of major earthquakes along the south-central SAF (*7*, *9*). This widely accepted model is now used to estimate long-term earthquake probabilities along the SAF (*10*). However, the relation between Carrizo segment rupture and the recurrence of major 1857-like earthquakes, as well as the formulation of the aforementioned earthquake recurrence models, relied on aerial photography and field investigations to reconstruct surface slip of the 1857 earthquake and preceding large earthquakes.

A recently collected light detection and ranging (LIDAR) topographic data set (*11*) covers the 1857 rupture trace and provides previously unavailable, high-resolution data. LIDAR-based digital elevation models permit identification and measurement of subtle tectono-geomorphic features (*12*) (Fig. 2A), therefore justifying the reevaluation of surface slip along the Carrizo segment associated with the 1857 and preceding earthquakes. Here, we present measurements of the lateral surface displacement of well-defined offset stream channels along the Carrizo segment, assuming that channel incision events generally occur more frequently (decadal time scale) than large earthquakes (centennial time scale) (*5*–*7*, *9*, *13*, *14*). Consequently, the smallest observable offsets correspond to the most recent earthquake along the Carrizo segment (1857 earthquake), and successive larger offset groups record the cumulative slip of prior events. Channels along the Carrizo segment that show no displacement as they cross the fault trace therefore formed after the 1857 earthquake (*5*, *6*). After fault line and offset stream channels were identified and traced, we determined the position (distance to fault trace) of upstream and downstream topographic, cross-sectional profiles and back-slipped them with respect to one another to determine the channel offset (*13*) (Fig. 2). Ninety-eight new measurements were combined with 51 remeasured offsets (*5*) (table S2) along the 60-km-long Carrizo segment (Fig. 1B).

Offset probabilities between 0 and 25 m are spatially well distributed along the fault segment southeast of Wallace Creek (Fig. 3A). The number of offset observations decreases as the respective offset increases, largely due to the steady degradation of inactive channels by geomorphic processes. The cumulative offset probability distribution (COPD)—stacked offset measurements weighted by assigned quality rating (*13*)—forms distinct peaks at 5.3, 9.8, 14.9, 20.1, and 24.5 m (Fig. 3B). These peaks, particularly those at 5.3, 9.8, and 14.9 m, are narrow and well separated, indicating that channel offsets along the Carrizo segment fall into small, well-defined ranges. Variation within each offset group appears to be local and random (Fig. 3A). Similar high-frequency and apparently random offset variation has been

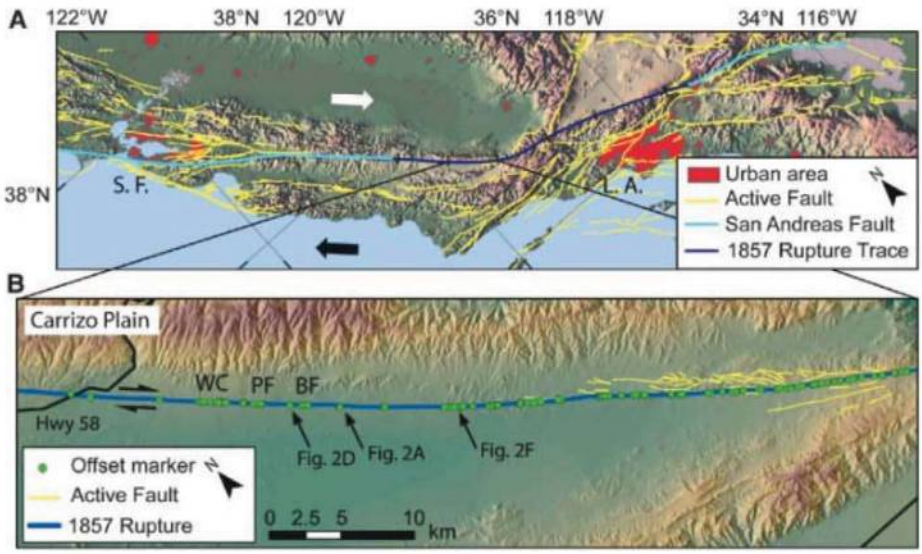

Fig. 1. (**A**) Overview of Quaternary active faults (*27*), including the surface rupture of the great 1857 Fort Tejon earthquake along the SAF, and their geographic relation to urban areas (S.F., San Francisco; L.A., Los Angeles). The southern SAF is divided into five major segments (*10*). Relative motion of North American and Pacific plate is indicated by block arrows. (**B**) Carrizo Plain segment and the 1857 surface rupture trace. The locations where offset geomorphic markers were measured, as well as selected paleoseismic sites (WC, Wallace Creek; PF, Phelan Fan; BF, Bidart Fan), are indicated.

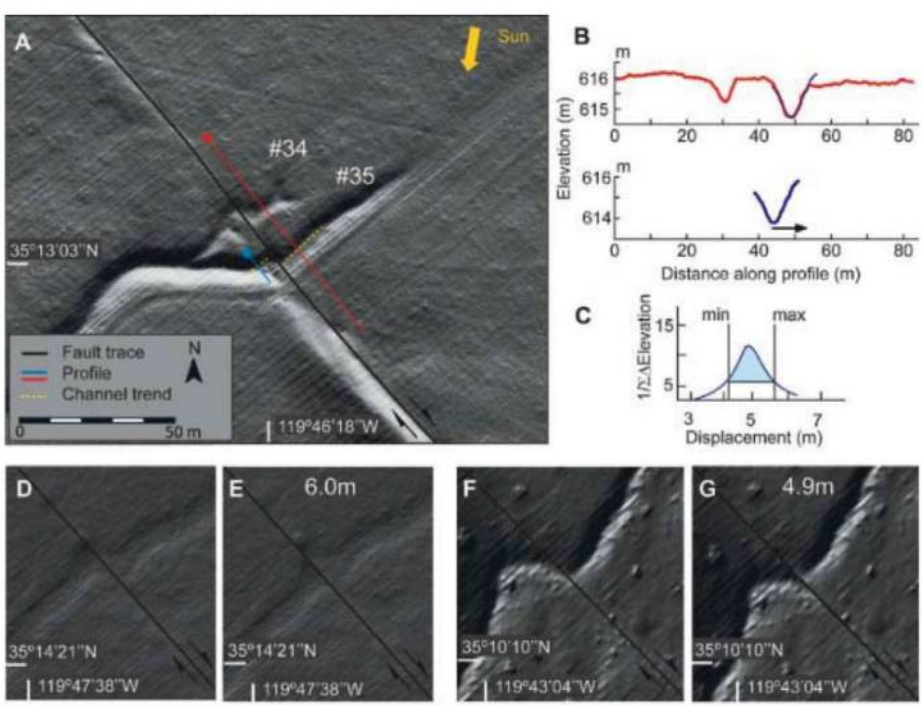

Fig. 2. (**A**) Hillshade map of channels #34 and #35 (*5*) generated from LIDAR-based digital elevation models. (**B**) Topographic profiles along red and blue lines are projected onto the fault plane based on channel obliquity [yellow dashed line in (A)]. Also shown is the blue profile, back-slipped by optimal offset estimate. (**C**) 1/Σ(Δelevation) is a measure of goodness of fit, calculated for each back-slip increment. (**D** to **G**) Current and back-slipped hillshade plot of two channels in the Carrizo Plain area that intersect the SAF and were offset during the 1857 earthquake (Fig. 1B).

[1]School of Earth and Space Exploration, Arizona State University, Tempe, AZ 85287, USA. [2]Program in Public Health, University of California Irvine, Irvine, CA 92697, USA.

*To whom correspondence should be addressed. E-mail: olaf.zielke@asu.edu

observed for essentially all large historical ruptures—for example, the 1999 Izmit (*1*) and 2002 Denali earthquakes (*3*).

The smallest observable offsets are attributed to the 1857 earthquake (Fig. 3). Surface slip distribution and respective COPD peaks reveal that average right-lateral surface displacement of the 1857 rupture along the Carrizo segment was 5.3 ± 1.4 m—distinctly lower than the previously reported 9.0 ± 2.0 m (*5*–*7*, *9*). We suggest that the latter offsets correspond to the COPD peak at 9.8 m, recording the cumulative slip of two or more earthquakes (*15*). Prior association of these offsets with the 1857 earthquake is primarily due to the relative geomorphic expression of both channel offset groups. Offset channels contributing to the COPD peak at 9.8 m form a stronger geomorphic signal (relatively deeply incised, wide channels) than the presumably younger but locally only weakly developed channels that were offset by 5.3 ± 1.4 m; spatiotemporal variations in storm severity are likely the controlling factor (*16*–*18*). As a result, earlier studies using aerial photography and field observations to measure the 1857 surface slip distribution may have missed those often weakly developed 5.3 ± 1.4 m offsets or interpreted them as outliers not representative of the 1857 surface slip (*5*–*7*). Paleoseismic studies at Phelan Fan and Wallace Creek (Fig. 1B) determined minimum channel offsets of 6.7 and 7.9 m, respectively (*9*, *14*), associating them with the 1857 earthquake. Their observations were of uniquely matching and singly incised offset channel margins and fill units. Whereas the former offset lies marginally in the observed range for the 1857 event, the latter offset does not. The discrepancy between the Wallace Creek record [reporting a cumulative slip of 7.9, 15.8, 20.7, 22.0, and 30.0 m (*9*)] and our COPD peaks (Fig. 3B) may be related to along-fault slip variations or spatiotemporal variations in relative frequency of channel incision and earthquake occurrence. A recent study on modern earthquakes (*19*) showed that the ratio between average and maximum surface slip is ~0.4. Considering a ~5-m average slip during the 1857 event in the Carrizo Plain, the observed 7.9 m at Wallace Creek may reflect the maximum slip of this event. However, it was noted (*9*) that channel offsets may record the cumulative slip of multiple events when earthquake recurrence was more frequent than channel formation. We suggest that the 7.9-m offset channel formed before the penultimate earthquake and therefore records the slip of more than one earthquake (*15*).

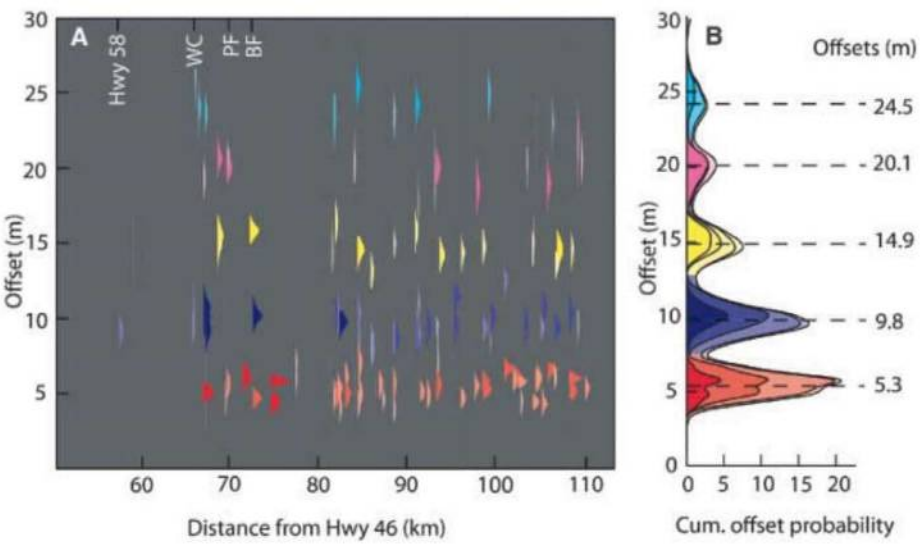

Fig. 3. (**A**) Offset probability for individual measurements along the Carrizo segment. The goodness-of-fit measurements were truncated by visually determining minimum and maximum offsets for each offset (*13*). Color is assigned based on the respective optimal offset measurement (red: 5 ± 2.5 m; blue: 10 ± 2.5 m; yellow: 15 ± 2.5 m; magenta: 20 ± 2.5 m; and cyan: 25 ± 2.5 m), indicating to which COPD peak it contributes most. Color intensity is based on the quality rating assigned to the measurement. (**B**) COPD color intensity is based on the quality rating of the offset estimates used in the stacking. The COPD forms narrow, well-separated peaks.

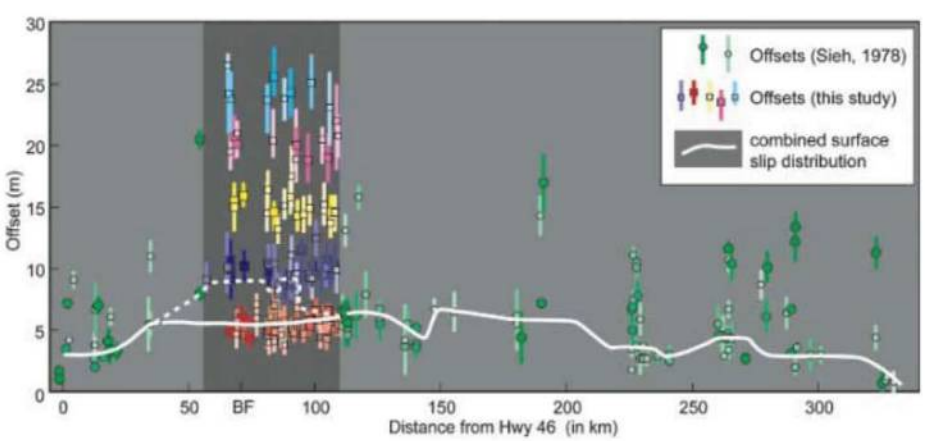

Fig. 4. Combined surface slip distribution associated with the 1857 earthquake (solid white line). Measurements show quality rating increasing with increasing color intensity. Our measurements along the Carrizo Plain suggest an average slip of 5.3 ± 1.4 m during this event. The previously reported 9.0 ± 2.0 m offsets (dashed white line) represent the cumulative slip of at least two earthquakes.

Estimates of seismic moment (M_0) and M_w for the 1857 earthquake change by only a fraction if the new offsets for the Carrizo segment are used; the respective values change from $M_0 \sim 8.71 \times 10^{20}$ Nm to $M_0 \sim 8.12 \times 10^{20}$ Nm and from M_w 7.93 to M_w 7.90 (table S3). The new combined surface slip distribution for the 1857 earthquake (Fig. 4) suggests that the Carrizo segment may not be considered an individual fault segment because its respective offset is not distinctly different from that of the neighboring segments (Fig. 1A). Neither distinctively large slip along the Carrizo segment (relative to other sections of the 1857 rupture) nor high slip gradients at its proposed boundaries (*5*, *7*) were observed. These observations challenge the long-held view that the Carrizo segment is an unusually strong fault segment, responsible for the recurrence of major 1857-like earthquakes along the south-central SAF (*7*–*10*). The 1857 multisegment rupture may not be the typical (i.e., characteristic) earthquake for the south-central SAF. The Carrizo Plain and other fault sections involved in the great 1857 earthquake may therefore rupture individually and in smaller but still hazardous events; major, 1857-like rupture may occur only infrequently.

Previous work along the SAF system described bimodality in the magnitude-frequency distribution (*20*–*22*); small- to moderate-magnitude earthquakes follow the Gutenberg-Richter inverse power-law relation, whereas large-size earthquakes occur more frequently. According to earthquake simulations (*23*), bimodality may be explained by systematic variations of coseismic stress drop with depth and a resulting abrupt increase in down-dip rupture width at the transition from moderate- to large-magnitude earthquakes. Total strain release along faults is presumably dominated by large-earthquake slip (*7*, *8*, *20*–*23*). If

bimodal behavior is a property of SAF earthquake recurrence, the observed COPD peaks at 5.3, 9.8, 14.9, 20.1, and 24.5 m (Fig. 3B) represent the cumulative slip of the five most recent clusters of earthquakes, each consisting of a single large earthquake and an undefined number of small- to moderate-size earthquakes (*15*). Recent work at the Bidart Fan site (*18*) on the Carrizo Plain (Fig. 1B) provides support for clusters of earthquakes that add up to 5-m slip. An alternative interpretation is that slip varies from event to event unsystematically and that the observed COPD peaks (Fig. 3B) are caused by infrequent but highly episodic channel incision events, recording the earthquake slip that was accumulated along the fault in between incision events. Then channel incision—not earthquake slip—has a characteristic recurrence pattern (*16*). Assuming that total strain release along the Carrizo segment is dominated by large-earthquake slip (*7*, *8*, *21*–*23*) and considering the Holocene slip rate of 35 mm/year along the SAF in the Carrizo Plain (*7*), we estimate a 140 ± 46 year interval for large-earthquake recurrence (*24*). This recurrence time is consistent with findings of past paleoseismic studies in the Carrizo Plain (*25*, *26*), which may have recognized primarily large earthquakes with compelling rupture evidence. Surface-rupturing earthquakes along the Carrizo segment therefore occur more frequently and with lower (but still high) slip than previously reported (*5*–*7*, *9*, *14*, *26*).

References and Notes

1. T. Rockwell *et al.*, *Bull. Seismol. Soc. Am.* **92**, 79 (2002).
2. A. Lin *et al.*, *Science* **296**, 2015 (2002).
3. P. J. Haeussler *et al.*, *Bull. Seismol. Soc. Am.* **94** (6B), S23 (2004).
4. X. W. Xu *et al.*, *Geology* **37**, 515 (2009).
5. K. E. Sieh, *Bull. Seismol. Soc. Am.* **68**, 1421 (1978).
6. R. E. Wallace, in *Proceedings of Conference on Geologic Problems of the San Andreas Fault System*, W. R. Dickinson, A. Grantz, Eds. (Stanford Univ. Publications in the Geological Sciences, 1968), vol. 11, p. 6.
7. K. E. Sieh, R. H. Jahns, *Geol. Soc. Am. Bull.* **95**, 883 (1984).
8. D. P. Schwartz, K. J. Coppersmith, *J. Geophys. Res.* **89**, (B7), 5681 (1984).
9. J. Liu-Zeng, Y. Klinger, K. Sieh, C. Rubin, G. Seitz, *J. Geophys. Res.* **111** (B2), B02306 (2006).
10. 2007 Working Group of California Earthquake Probabilities, *The Uniform California Earthquake Rupture Forecast, Version 2 (UCERF 2)* (USGS Open File Report 2007-1437, 2008; http://pubs.usgs.gov/of/2007/1437/).
11. LiDAR data freely available at www.opentopography.org/.
12. J. R. Arrowsmith, O. Zielke, *Geomorphology* **113**, 70 (2009).
13. Materials and Methods are available as supporting material on *Science* Online.
14. L. B. Grant, K. E. Sieh, *Bull. Seismol. Soc. Am.* **83**, 619 (1993).
15. The number of earthquakes contributing to individual COPD peaks (Fig. 3B) is a priori not known. Cumulative offset from two or more events might be misinterpreted as single-event offset because short interevent time and temporal variations in storm severity (*16*–*18*) may suppress channel incision between successive events, so that no or only weak evidence for the latter event might be created.
16. A. Schimmelmann, C. B. Lange, B. J. Meggers, *Holocene* **13**, 763 (2003).
17. M. A. Cane, S. E. Zebiak, *Science* **228**, 1085 (1985).
18. L. Grant Ludwig, S. O. Akçiz, G. R. Noriega, O. Zielke, J R. Arrowsmith, *Science* **327**, 1117 (2010); published online 21 January 2010 (10.1126/science.1182837).
19. S. G. Wesnousky, *Bull. Seismol. Soc. Am.* **98**, 1609 (2008).
20. L. Knopoff, *Proc. Natl. Acad. Sci. U.S.A.* **97**, 11880 (2000).
21. S. G. Wesnousky, *Bull. Seismol. Soc. Am.* **84**, 1940 (1994).
22. J. Ben-Zion, *Rev. Geophys.* **46**, RG4006 (2008).
23. O. Zielke, J. R. Arrowsmith, *Geophys. Res. Lett.* **35**, L24301 (2008).
24. The 140 ± 46 year interval presents a maximum for the recurrence of major earthquakes along the Carrizo segment because it neglects the potential slip contribution of moderate-size earthquakes.
25. S. O. Akçiz, L. Grant Ludwig, J. R. Arrowsmith, *J. Geophys. Res.* **114**, B01313 (2009).
26. L. Grant, K. E. Sieh, *J. Geophys. Res.* **99**, 6819 (1994).
27. U.S. Geological Survey and California Geological Survey, *Quaternary Fault and Fold Database of the United States* (http://earthquake.usgs.gov/regional/qfaults/).

28. This research was supported by the NSF Tectonics Program and the Southern California Earthquake Center (SCEC). SCEC is funded by NSF Cooperative Agreement EAR-0529922 and U.S. Geological Survey Cooperative Agreement 07HQAG0008. The SCEC contribution number for this paper is 1310. We thank T. Jordan, D. Schwartz, and anonymous reviewers for constructive comments.

Supporting Online Material

www.sciencemag.org/cgi/content/full/science.1182781/DC1
Materials and Methods
Figs. S1 to S4
Tables S1 to S3
References

2 October 2009; accepted 5 January 2010
Published online 21 January 2010;
10.1126/science.1182781
Include this information when citing this paper.

Plant Peptides Govern Terminal Differentiation of Bacteria in Symbiosis

Willem Van de Velde,[1] Grigor Zehirov,[2] Agnes Szatmari,[1,3] Monika Debreczeny,[4] Hironobu Ishihara,[2] Zoltan Kevei,[4] Attila Farkas,[4] Kata Mikulass,[4] Andrea Nagy,[4] Hilda Tiricz,[4] Beatrice Satiat-Jeunemaître,[1] Benoit Alunni,[1] Mickael Bourge,[1] Ken-ichi Kucho,[2] Mikiko Abe,[2] Attila Kereszt,[4] Gergely Maroti,[4] Toshiki Uchiumi,[2] Eva Kondorosi,[1,4]* Peter Mergaert[1]

Legume plants host nitrogen-fixing endosymbiotic *Rhizobium* bacteria in root nodules. In *Medicago truncatula*, the bacteria undergo an irreversible (terminal) differentiation mediated by hitherto unidentified plant factors. We demonstrated that these factors are nodule-specific cysteine-rich (NCR) peptides that are targeted to the bacteria and enter the bacterial membrane and cytosol. Obstruction of NCR transport in the *dnf1-1* signal peptidase mutant correlated with the absence of terminal bacterial differentiation. On the contrary, ectopic expression of NCRs in legumes devoid of NCRs or challenge of cultured rhizobia with peptides provoked symptoms of terminal differentiation. Because NCRs resemble antimicrobial peptides, our findings reveal a previously unknown innovation of the host plant, which adopts effectors of the innate immune system for symbiosis to manipulate the cell fate of endosymbiotic bacteria.

Symbiotic nitrogen fixation by legumes is a major contributor to the combined nitrogen pool in the biosphere. It takes place in specialized root organs called nodules (*1*). The symbiotic nodule cells are large polyploid cells (*2*) housing thousands of bacteroids. Bacteroids are differentiated *Rhizobium* bacteria with specialized metabolic activity, capable of reducing atmospheric nitrogen and supplying the plant with ammonium as a nitrogen source (*3*). In addition to this metabolic adaptation, the endosymbionts of *Medicago truncatula* and related legumes undergo striking morphological changes such as cell elongation coupled to genome amplification, membrane modifications, and the loss of reproductive capacity (*4*–*6*). The polyploid state of bacteroids and the induction of bacteroid-like cells by genetic interference with the rhizobial cell cycle (*7*–*10*) suggest that terminal bacteroid differentiation is a cell cycle–related process.

This terminal bacteroid differentiation is specific for legumes belonging to the inverted repeat–lacking clade (IRLC) such as *Medicago*, *Pisum*, or *Trifolium*, whereas bacteroids in the non-IRLC legumes, such as *Lotus japonicus*, show no sign of terminal differentiation as they maintain their normal bacterial size, genome content, and reproductive capacity (*6*). The same *Rhizobium* strains that form symbiosis with both IRLC and non-IRLC legumes have different bacteroid differentiation fates in the two legume types. Therefore, it was concluded that terminal bacteroid differentiation is determined by unknown host factors that are produced by the IRLC legumes and do not exist in the non-IRLC legumes (*6*). The nodule-specific cysteine-rich (NCR) peptides were likely candidates for these factors (*11*, *12*). *NCR* genes were found only in

[1]Institut des Sciences du Végétal, Centre National de la Recherche Scientifique, 91198 Gif-sur-Yvette Cedex, France. [2]Graduate School of Science and Engineering, Kagoshima University, 890 0065 Kagoshima, Japan. [3]Plant Protection Institute of the Hungarian Academy of Sciences, 1022 Budapest, Hungary. [4]Institute for Plant Genomics, Human Biotechnology and Bioenergy, Bay Zoltan Foundation for Applied Research, 6726 Szeged, Hungary.

*To whom correspondence should be addressed. E-mail: eva.kondorosi@isv.cnrs-gif.fr

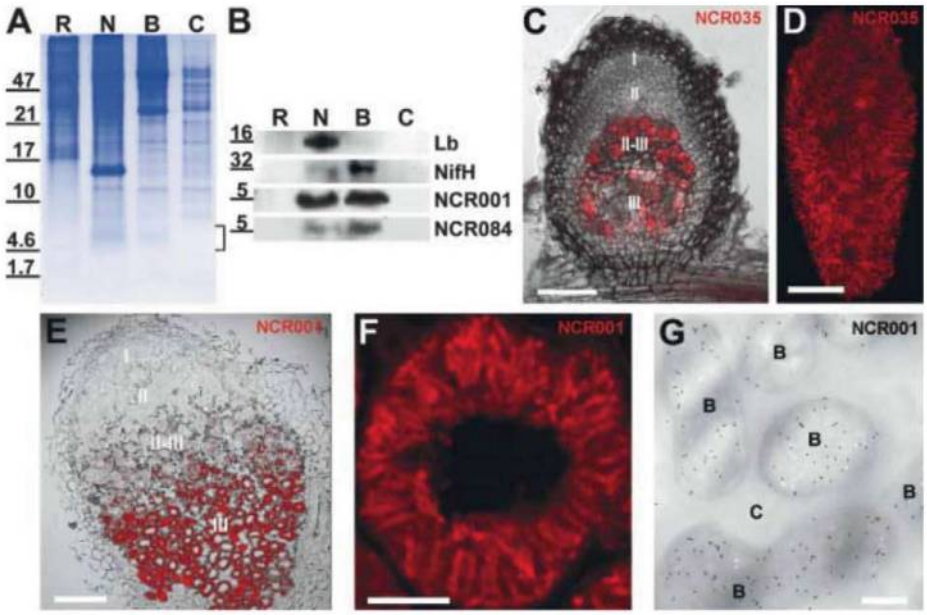

Fig. 1. NCR peptides colocalize with bacteroids in *M. truncatula* nodules. (**A**) SDS-PAGE analysis and Coomassie blue staining of total protein extracts of roots (R), nodules (N), bacteroids (B), and cultured *S. meliloti* cells (C) reveal the specific presence of low-molecular-weight peptides (bracket) in nodules and bacteroids. (**B**) Western blot analysis of identical extracts with antibodies against plant leghemoglobin (Lb), bacterial dinitrogenase reductase (NifH), NCR001, and NCR084 confirms the presence of NCR peptides in nodules and their copurification with bacteroids. (**C** and **D**) In a nodule (C) and a symbiotic cell (D) expressing *NCR035-mCHERRY*, NCR035-mCHERRY (red signal) localizes to bacteroids in symbiotic cells of the interzone (II-III) and fixation zone (III). I, meristem; II, infection zone. (**E** and **F**) Immunofluorescence localization of NCR001 with Alexa 633 (red signal) in a nodule (E) and a symbiotic cell (F) demonstrates that NCR001 colocalizes with bacteroids in symbiotic cells of the fixation zone. (**G**) Immunogold localization (black dots) of NCR001 in a nitrogen-fixing symbiotic cell, confirming the presence of NCR001 in the bacteroids. B, bacteroid; C, cytoplasm of the symbiotic cell. Scale bars, 100 μm in (C) and (E); 10 μm in (D) and (F); 1 μm in (G).

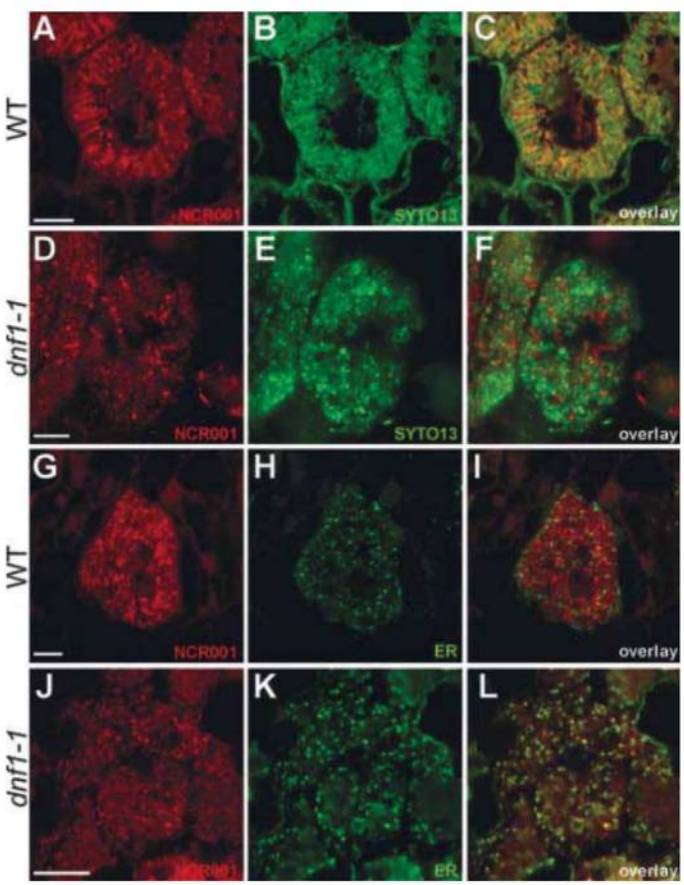

Fig. 2. NCR001 peptides localize to the ER in the secretory pathway mutant *dnf1-1*. (**A** to **F**) Immunofluorescence localization of NCR001 [(A) and (D)], SYTO13 (a nucleic acid marker) staining of bacteroids [(B) and (E)], and an overlay [(C) and (F)] in a WT [(A) to (C)] and *dnf1-1* [(D) to (F)] symbiotic cell shows that NCR001 no longer colocalizes with bacteroids in the *dnf1-1* mutant background. (**G** to **L**) Immunofluorescence localization of NCR001 [(G) and (J)], the KDEL epitope (ER marker) [(H) and (K)], and an overlay [(I) and (L)] in a WT [(G) to (I)] and *dnf1-1* [(J) to (L)] symbiotic cell revealing colocalization of NCR001 with the ER in *dnf1-1*. Scale bars, 10 μm.

the IRLC legumes (*11*, *12*). In the tested cases, the expression of *NCR* genes was restricted to the *Rhizobium*-infected plant cells, where different subsets of *NCR* genes were activated during distinct developmental stages of the symbiotic cells (*11*). The *NCR* gene family encodes more than 300, highly divergent peptides in *M. truncatula*, which are most similar to defensin-type antimicrobial peptides (AMPs) (*11*–*13*). Increased membrane permeability and definitive inhibition of cell division can be mediated by AMPs (*14*); therefore, we postulated that NCRs may have AMP-like activities and could be the critical plant factors that mediate terminal bacteroid differentiation.

We tested whether *NCRs* are translated and targeted to the bacteroids (*15*). SDS–polyacrylamide gel electrophoresis (SDS-PAGE) analysis of total protein extracts revealed the presence of peptides with molecular weight in the range of 3 to 5 kD in *M. truncatula* nodules and purified bacteroids, which were absent in roots or free-living *Sinorhizobium meliloti*, the endosymbiont of *M. truncatula* (Fig. 1A). This size range corresponded to the predicted molecular weight of the mature NCR peptides, and mass spectrometry confirmed their presence in the bacteroid extracts. Out of the eight sequenced peptides, seven corresponded to five different NCR peptides, whereas one peptide derived from a small protein of *S. meliloti* (table S1). Likewise, the NCR084 and NCR001 peptides were detected only in the nodule and bacteroid extracts by Western blot analysis (Fig. 1B). Different approaches were undertaken for in situ localization of NCR peptides inside the symbiotic cells. Transgenic *M. truncatula* nodules expressing NCR035 as a translational fusion with the mCHERRY red fluorescent protein under the control of its own promoter demonstrated that the NCR035 peptides were present only in the infected nodule cells, where they colocalized with the bacteroids (Fig. 1, C and D). Immunofluorescence localization of NCR001 with affinity purified antibodies also labeled the bacteroids in the symbiotic cells (Fig. 1, E and F), in accordance with the predicted role of NCRs in bacteroid differentiation. Immunogold transmission electron microscopy (TEM) demonstrated the localization of NCR001 in the bacteroid membrane but predominantly in the bacteroid cytosol (Fig. 1G

and fig. S1), indicating that NCRs may have intracellular rhizobial targets, and their mode of action is not restricted to an interaction with the bacterial membrane.

Because of the high complexity of the *NCR* gene family and the probable redundancy of NCRs, reverse genetics approaches were unlikely to be effective to elucidate NCR functions. Bacteroids in symbiotic nodule cells are not in direct contact with the host cell cytoplasm, because they are surrounded by a plant-derived membrane forming an organelle-like structure, the symbiosome. This suggested that protein trafficking to symbiosomes probably depends on the secretory pathway (*16*). NCRs have a characteristic signal peptide which, as we showed in onion cells, targets them into the secretory pathway (*11*). Therefore, it was expected that interference with NCR trafficking may have a general effect and block the function of all NCR peptides. The *M. truncatula dnf1-1* mutant is deficient in a nodule-specific component of the signal peptidase complex (SPC) of the secretory pathway (*17*). The SPC resides in the endoplasmic reticulum (ER) and removes the signal peptide of secretory proteins during their translocation into the ER lumen, which is an essential step for their proper targeting (*18*). The *dnf1-1* mutant forms nonfunctional nodules (*17*), with comparable structure to wild-type (WT) nodules in which symbiotic cells are infected (fig. S2, A and B), but the bacteroids remain undifferentiated (fig. S2, C to F). This raised the possibility that the lack of bacteroid differentiation in this mutant is caused by improper targeting of NCRs. *NCR001* and other *NCR*s were expressed at similar levels in *dnf1-1* and WT nodules (fig. S2G). In the *dnf1-1* nodules, low-molecular-weight peptides were present in the nodule extracts but absent in the bacteroid extracts (fig. S2H). Immunoblotting revealed the absence of mature NCR001 peptide in both the *dnf1-1* nodules and bacteroids, as well as the presence of a higher-molecular-weight form of NCR001 only in the *dnf1-1* nodules, probably corresponding to the full-length unprocessed NCR001 because the SPC is nonfunctional (fig. S2I). Immunofluorescence localization confirmed that NCR001 was not targeted to the bacteroids in the *dnf1-1* mutant (Fig. 2, A to F). Instead, it colocalized with the ER (Fig. 2, G to L). Thus, prevention of proper targeting of NCR peptides to the bacteroids correlated with the absence of bacterial differentiation in this plant mutant.

To further support the role of NCRs in terminal bacteroid differentiation, we tested whether expression of *NCR* genes could induce features of the IRLC-specific bacteroid differentiation in *L. japonicus* nodules, where this bacteroid differentiation does not occur and the *NCR* genes are absent (*11*, *12*). Different transgenic *Lotus* lines were created with nodule-specific expression of one of eight NCRs (*15*), selected on the basis of their expression pattern (*11*) or the β-glucuronidase (*GUS*) reporter gene as a control. Expression of each gene was controlled by the *M. truncatula leghemoglobin 1* promoter (*pMtLb1*) that was active in *L. japonicus* symbiotic cells (fig. S3, A and B). Moreover, targeting of the NCRs to the symbiosomes was also confirmed in transgenic *L. japonicus* nodules expressing an NCR035-mCHERRY translational fusion under the control of *pMtLb1* (fig. S3, C to E). TEM and scanning electron microscopy (SEM) of *pMtLb1::GUS* control transgenic nodules showed that symbiosomes generally harbored multiple small bacteroids (Fig. 3, A, C, and E), which is indicative of bacteroid division within the symbiosomes, similarly to WT *L. japonicus* nodules (*19*). Out of the eight NCR peptides, NCR035 produced the most pronounced effects on the bacteroids in *L. japonicus* nodules: The majority of the symbiosomes contained a single bacteroid, and many bacteroids were remarkably elongated (Fig. 3, B, D, and E) as in *M. truncatula* nodules, indicating that these bacteroids, in the presence of NCR035, had lost their capacity to multiply within symbiosomes. Moreover, an increased fraction (25% versus 18% in the control) of isolated bacteroids became permeable by the DNA-staining dye propidium iodide (PI), indicating that NCR035 affected the membrane structure of bacteroids. Thus, expression of *NCR* genes in *L. japonicus* nodules was sufficient to induce bacteroid morphologies reminiscent of terminally differentiated *M. truncatula* bacteroids.

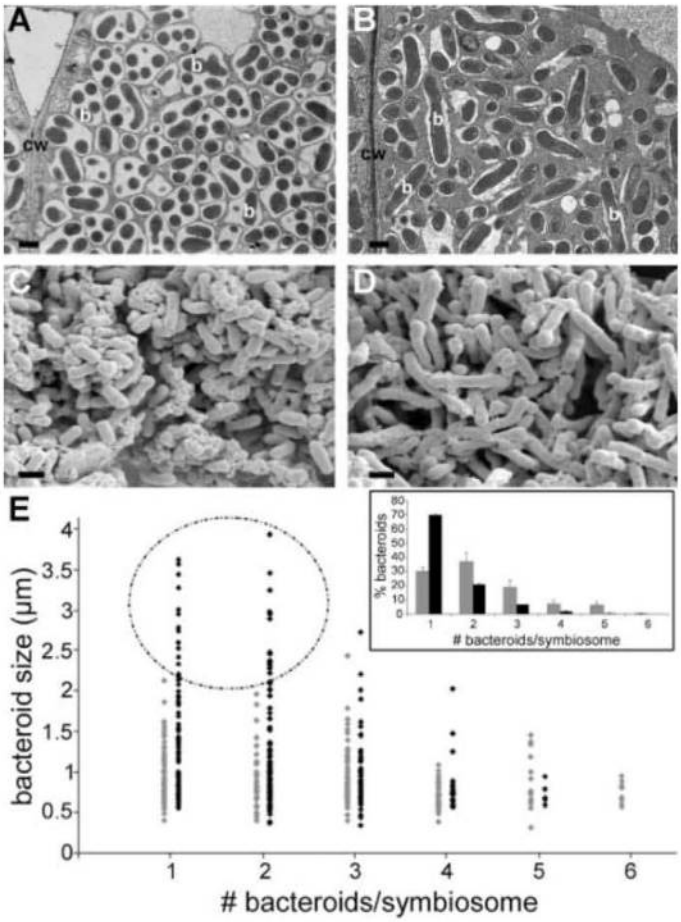

Fig. 3. Expression of *NCR* genes in *L. japonicus* leads to features of terminal bacteroid differentiation. (**A** and **B**) TEM of a symbiotic nodule cell expressing *GUS* (A) and *NCR035* (B) demonstrates an increase in bacteroid size in the case of *NCR035* expression. b, bacteroid; cw, cell wall. (**C** and **D**) SEM of bacteroids in a symbiotic cell expressing *GUS* (C) and *NCR035* (D) visualizes the morphological differences of bacteroids upon *NCR035* expression. (**E**) Plotting of bacteroid size as a function of bacteroid number per symbiosome shows the presence of bacteroid populations with enlarged size in *NCR035* transgenic lines (encircled); $n = 132$ bacteroids from two independent transgenic lines. The inset shows the proportion of bacteroids as a function of the number of bacteroids per symbiosome. In the control nodules, most symbiosomes contain more than one bacteroid, whereas in the NCR035-expressing lines, there is most frequently one bacteroid per symbiosome. Gray is the quantification for control lines and black for NCR035-expressing lines. Scale bars, 1 μm.

The observation that NCRs are important for terminal bacteroid differentiation in planta led us to postulate that synthetic NCR peptides may be active in vitro and provoke certain features of terminal bacteroid differentiation when added to *S. meliloti* cultures. When log-phase bacteria were treated with the peptides, membrane permeabilization was detected by the uptake of the PI dye in a peptide- and concentration-dependent manner (Fig. 4A). NCR035, NCR055, and NCR247 induced bacterial cell death, indicated by the decrease of colony-forming units in plating assays (Fig. 4B) and by the loss of respiratory activity quantified by a decrease in 5-cyano-2,3-di-4-tolyl tetrazolium chloride fluorescence (fig. S4A). These findings show that some NCR peptides possess antimicrobial activity and can therefore be classified as AMPs. Defensins can interact with negatively charged membrane components, and their activity is inhibited by divalent cations (*14*). Likewise, the activity of NCR peptides was inhibited by Ca^{2+} (fig. S4B), indicating that NCRs can

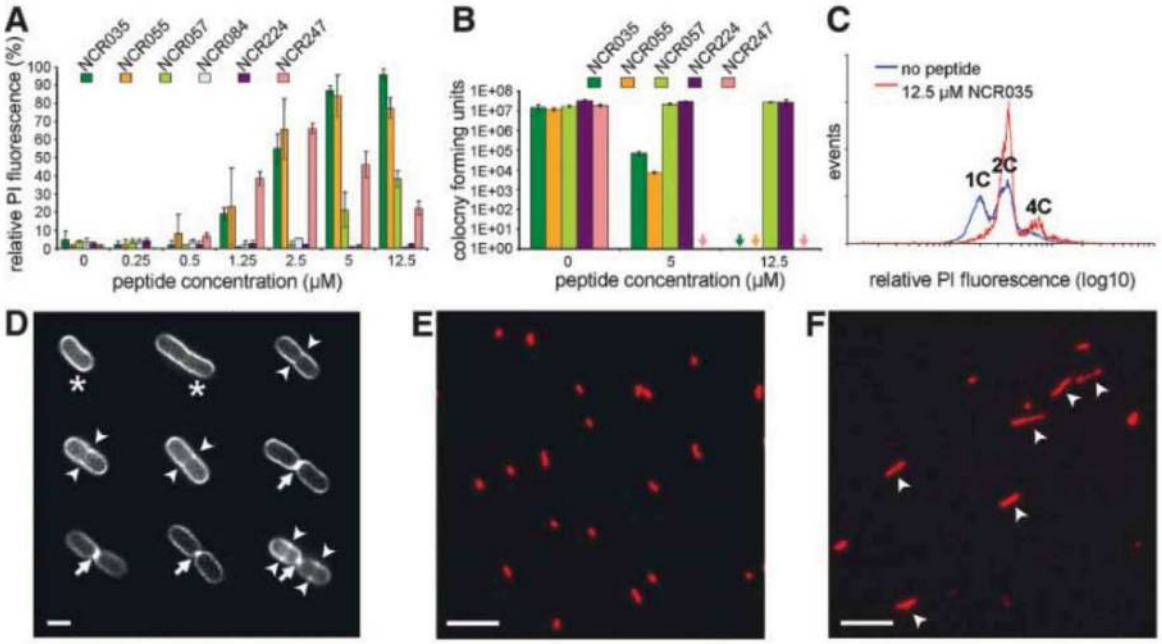

Fig. 4. NCR peptides provoke features of terminal bacteroid differentiation in vitro. (**A**) PI uptake of *S. meliloti* cells after treatment with different NCRs, showing that NCRs provoke membrane permeabilization of *S. meliloti* cells. Data are means ± SD ($n = 4$ measurements). (**B**) Cell kill assay of *S. meliloti* cells after treatment with NCRs disposing different cell killing capacities. Data are means ± SD ($n = 3$). (**C**) Increased DNA content of *S. meliloti* cells after NCR035 treatment in comparison to the control. (**D**) FITC-NCR035 localization in *S. meliloti* cells, initially at the cell envelope (asterisks), and later, intracellularly at the bacterial division site (arrowheads and arrows). (**E** and **F**) Control (E) and NCR-treated (F) *S. meliloti* cells showing an increase in size upon treatment with NCR peptides (arrowheads). Cells were stained with PI. Scale bars, 1 μm in (D); 10 μm in (E) and (F).

also interact with negatively charged membrane components such as phospholipids or lipopolysaccharide. A distinctive feature of terminally differentiated bacteroids is their high DNA content, achieved by repeated replication cycles (*6*). To examine whether NCR peptides affect the bacterial cell cycle, the DNA content was measured by flow cytometry of *S. meliloti* cells treated with NCR035. Cell populations both in the haploid (1C) and diploid (2C) phase were present in the untreated control sample, whereas in the NCR035-treated sample, haploid cells were not detected; the majority of cells were diploid and a new population appeared with a 4C DNA content (Fig. 4C), indicating that the peptide inhibited cytokinesis while DNA synthesis was ongoing. Investigating further, we followed the uptake and localization of a bioactive fluorescein isothiocyanate (FITC)–labeled NCR035 peptide (fig. S4B) in bacterial cells. Two main patterns could be discerned: labeling of the cell envelope (Fig. 4D, asterisk) and intracellular marking of the bacterial cell division plane (Fig. 4D, arrow and arrowhead), which is in agreement with a role of NCR035 in cytokinesis inhibition. The inhibition of cytokinesis by NCR peptides resulted in enlarged *S. meliloti* cells, reminiscent of *S. meliloti* bacteroids (Fig. 4, E and F). Taken together, the in vitro responses of *S. meliloti* to NCR peptides partially mimicked characteristics of terminally differentiated bacteroids, notably provoking membrane modifications, inhibition of bacterial cytokinesis, and DNA amplification coupled with cell enlargement. However, the effect of NCR peptides on free-living bacteria was more dramatic than on bacteroids in *M. truncatula* nodules. NCR peptides rapidly abolished respiration and killed the free-living bacteria, in contrast to the nodule, where the bacteroid metabolic activity was maintained for symbiotic nitrogen fixation (*6*). These observations could be explained by a possibly lower concentration of peptides in the plant than the concentrations used in the in vitro assays. Moreover, the concerted action of many different NCRs produced within the same symbiotic cell or the particular physiological conditions prevalent in nodules (such as low free oxygen concentration or oxidative stress) might also be essential to modulate the bacterial responses in such a way that bacteroids remain alive, although with complete loss of their proliferative ability.

Cysteine-rich peptides are extremely abundant in plants (*13*, *20*, *21*). Some of these peptides have signaling roles (*22*, *23*), but many of them are thought to have antimicrobial activity (*20*, *21*). Our results demonstrate that in *Medicago* and probably in other IRLC legumes, the nodule-specific NCR peptides act as symbiotic plant effectors to direct the bacteroids into a terminally differentiated state and that these peptides have in vitro antimicrobial activity. Therefore, one can speculate that IRLC legumes recruited cysteine-rich AMPs in the context of symbiosis to evolve the nodule-specific NCR family and to dominate the endosymbionts. Although the fitness benefits to the host plant from such a bacteroid differentiation pathway remain to be clarified, the high number and diversity of peptides lead us to propose that NCR peptides interfere with many aspects of the bacteroid metabolism to allow the efficiency of the nitrogen fixation process to be optimized. For example, the peptides could be part of a mechanism to avoid the cheating of rhizobia that could use host resources to accumulate carbon storage compounds instead of fixing nitrogen. Such "freeloading" by bacteroids is often observed in the non-IRLC legumes but not in the IRLC (*24*). In addition, suppressing bacterial reproduction in conjunction with genome amplification and weakening of bacterial membranes by NCR peptides might be of benefit during nodule senescence, when the fragilized bacteroids can be efficiently digested by the plant cells (*5*, *25*) and their nutrients reused by the host. Alternatively, the enlarged and polyploid bacteroids might have a more efficient metabolism, like polyploid eukaryotic cells (*2*), resulting in higher nitrogen fixation (*24*).

References and Notes

1. K. M. Jones, H. Kobayashi, B. W. Davies, M. E. Taga, G. C. Walker, *Nat. Rev. Microbiol.* **5**, 619 (2007).
2. E. Kondorosi, F. Roudier, E. Gendreau, *Curr. Opin. Plant Biol.* **3**, 488 (2000).
3. J. Prell, P. Poole, *Trends Microbiol.* **14**, 161 (2006).
4. M. W. Beijerinck, *Bot. Ztg.* **46**, 725 (1888).
5. J. Vasse, F. de Billy, S. Camut, G. Truchet, *J. Bacteriol.* **172**, 4295 (1990).
6. P. Mergaert *et al.*, *Proc. Natl. Acad. Sci. U.S.A.* **103**, 5230 (2006).
7. J. N. Latch, W. Margolin, *J. Bacteriol.* **179**, 2373 (1997).
8. R. Wright, C. Stephens, L. Shapiro, *J. Bacteriol.* **179**, 5869 (1997).
9. C. D. Sibley, S. R. MacLellan, T. Finan, *Microbiology* **152**, 443 (2006).
10. J. Cheng, C. D. Sibley, R. Zaheer, T. M. Finan, *Microbiology* **153**, 375 (2007).
11. P. Mergaert *et al.*, *Plant Physiol.* **132**, 161 (2003).
12. B. Alunni *et al.*, *Mol. Plant Microbe Interact.* **20**, 1138 (2007).
13. M. A. Graham, K. A. T. Silverstein, S. B. Cannon, K. A. VandenBosch, *Plant Physiol.* **135**, 1179 (2004).

14. K. A. Brogden, *Nat. Rev. Microbiol.* **3**, 238 (2005).
15. Information on materials and methods is available as supporting material on *Science* Online.
16. D. P. Verma, Z. Hong, *Trends Microbiol.* **4**, 364 (1996).
17. D. Wang *et al.*, *Science* **327**, 1126 (2010).
18. M. Paetzel, A. Karla, N. C. Strynadka, R. E. Dalbey, *Chem. Rev.* **102**, 4549 (2002).
19. K. Szczyglowski *et al.*, *Mol. Plant Microbe Interact.* **11**, 684 (1998).
20. K. A. T. Silverstein, M. A. Graham, T. D. Paape, K. A. VandenBosch, *Plant Physiol.* **138**, 600 (2005).
21. K. A. T. Silverstein *et al.*, *Plant J.* **51**, 262 (2007).
22. C. R. Schopfer, M. E. Nasrallah, J. B. Nasrallah, *Science* **286**, 1697 (1999).
23. S. Okuda *et al.*, *Nature* **458**, 357 (2009).
24. R. Oono, R. F. Denison, E. T. Kiers, *New Phytol.* **183**, 967 (2009).
25. W. Van de Velde *et al.*, *Plant Physiol.* **141**, 711 (2006).
26. We thank S. Long, T. Bisseling, G. Ferguson, and R. Whitford for helpful comments on the manuscript; S. Brown, M. Yamaura, P. Laporte, P. Durand, É. Klement, E. Magyaródi, and the IMAGIF platform for technical support; and S. Long, D. Wang, D. Barker, P. Ludden, and N. Suganuma for providing materials. This work was supported by the Agence National de la Recherche project ANR-05-BLAN-0129 (W.V.d.V., A.S., E.K. and P.M.), the Japanese Society for the Promotion of Science (G.Z. and T.U.), the Hungarian National Office for Research and Technology Teller program OMFB-00441/2007 (M.D., A.F., K.M., A.N., H.T., A.K., G.M. and E.K.), and a Ph.D. fellowship from the French Ministry of Research (B.A.). E. Kondorosi *et al.* European patent no. 09305547.3-2107 related to the antimicrobial activity of NCR peptides is pending.

Supporting Online Material

www.sciencemag.org/cgi/content/full/327/5969/1122/DC1
Materials and Methods
Figs. S1 to S4
Table S1
References

30 October 2009; accepted 21 January 2010
10.1126/science.1184057

A Nodule-Specific Protein Secretory Pathway Required for Nitrogen-Fixing Symbiosis

Dong Wang,[1] Joel Griffitts,[1]* Colby Starker,[1]† Elena Fedorova,[2,3] Erik Limpens,[2] Sergey Ivanov,[2,3] Ton Bisseling,[2] Sharon Long[1]‡

The nitrogen-fixing symbiosis between *Sinorhizobium meliloti* and its leguminous host plant *Medicago truncatula* occurs in a specialized root organ called the nodule. Bacteria that are released into plant cells are surrounded by a unique plant membrane compartment termed a symbiosome. We found that in the symbiosis-defective *dnf1* mutant of *M. truncatula*, bacteroid and symbiosome development are blocked. We identified the *DNF1* gene as encoding a subunit of a signal peptidase complex that is highly expressed in nodules. By analyzing data from whole-genome expression analysis, we propose that correct symbiosome development in *M. truncatula* requires the orderly secretion of protein constituents through coordinated up-regulation of a nodule-specific pathway exemplified by DNF1.

To study the mechanisms governing bacterial infection and nodule organogenesis, we previously isolated a number of *Medicago truncatula* fast neutron bombardment mutants that were defective in nitrogen fixation (*dnf* mutants) (*1*). Among these, *dnf1* is blocked at an intermediate stage of nodule development, as indicated by abolished induction of a set of host and bacterial genes and by microscopic analyses of thin longitudinal sections of nodules (Fig. 1, A and B) (*2*). After release from infection threads into the host cytoplasm, rhizobial bacteria in wild-type (WT) nodule cells divide and quickly differentiate into very large, elongated bacteroids that are dedicated to nitrogen fixation (Fig. 1, A and E, and fig. S1). Bacteria in *dnf1* nodules are released from infection threads, are surrounded by symbiosome membrane, and divide, as do bacteria in WT plants. However, the bacteroids in *dnf1* mutant hosts remain small and resemble freshly released rhizobia (Fig. 1B and fig. S1) or stage 1 bacteroids (*3*) (Fig. 1, C and D) that are present in about 10 cell layers of plant tissue. This is in contrast to WT nodules, which contain the stage 1 bacteroids only in the first one or two cell layers of the infection zone, beyond which they rapidly enlarge (fig. S1) to become about 5 to 10 times longer than freshly released rhizobia. Light and electron microscopic analyses show that bacteroids in *dnf1* nodules are arrested at a very early stage of development. Further, numerous (pre-)autophagic bodies/autophagosomes (*4*) were observed in *dnf1* nodule cells (Fig. 1C), whereas they are rare in WT cells. Whether the accumulation of autophagosomes is a primary or more indirect consequence of the *dnf1* mutation remains to be determined. This accumulation of autophagosomes may reflect delayed vesicle maturation in the *dnf1* mutant, or may relate to overall impaired vacuole development seen in young nodule cells of *dnf1* (Fig. 1B) (*4*).

Recently, we showed that the symbiosome membrane has a "mosaic" identity (*5*). The plasma membrane SNARE SYP132 is present directly after the release of the bacteria from the

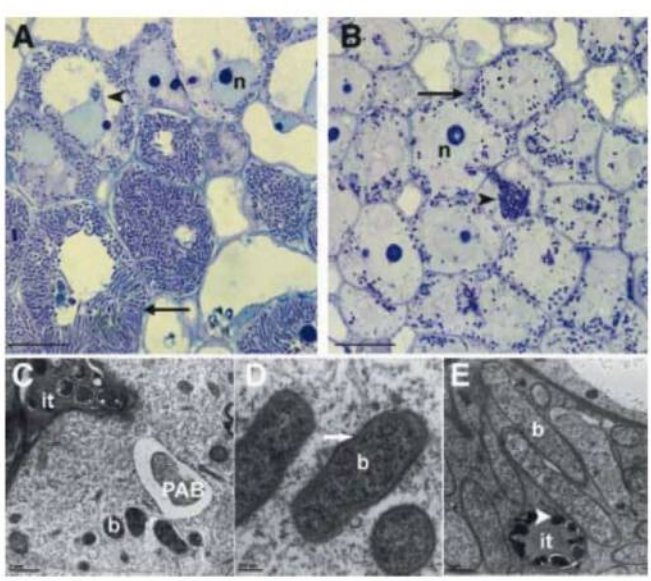

Fig. 1. Cytological characterization of *dnf1* root nodules. (**A** and **B**) High-magnification light microscopic image of longitudinal sections of a WT (A) and *dnf1* (B) nodule 12 dpi, showing that, in all layers of the central tissue, the bacteroids in *dnf1* are arrested at stage 1 (*20*). In WT, after release from the infection thread (it, arrowhead), the bacteria soon differentiate into elongated bacteroids (arrow). In *dnf1*, although many bacteroids are visible in the central part of the nodule, they have a size similar to that of the bacteria that are present in the infection threads. n, nucleus. (**C**) Transmission electron microscope (TEM) image of a freshly infected *dnf1* nodule cell showing the infection thread (it), several bacteroids surrounded by a symbiosome membrane (b), and a pre-autophagic body (PAB) containing cytoplasm. (**D**) TEM image of an infected *dnf1* nodule cell containing symbiosomes that remain arrested at stage 1. Arrows indicate symbiosome membrane. (**E**) Mature bacteroids in a WT nodule. These bacteroids are markedly bigger than the bacteria that are present in the it (arrowhead). Scale bars in (A) and (B), 10 μm; (C), 1 μm; (D), 200 nm; (E), 1 μm.

[1]Department of Biology, Stanford University, Stanford, CA 94305, USA. [2]Laboratory of Molecular Biology, Graduate School of Experimental Plant Sciences, Wageningen University, Droevendaalsesteeg 1, 6708 PB Wageningen, Netherlands. [3]K.A. Timiryazev Institute of Plant Physiology, Russian Academy of Sciences, Botanicheskaya 35, Moscow 127392, Russia.

*Present address: Department of Microbiology and Molecular Biology, Brigham Young University, Provo, UT 84602, USA.
†Present address: Department of Plant Biology, University of Minnesota, St. Paul, MN 55108, USA.
‡To whom correspondence should be addressed. E-mail: SRL@stanford.edu

infection threads (*5*, *6*) and is maintained on the symbiosome membrane through later stages of development. The late endosome marker Rab7 appears only when the symbiosomes stop dividing, whereas the vacuolar SNAREs occur on the symbiosome membrane only at the onset of senescence. To test whether the arrest of symbiosome development in *dnf1* correlates with an altered symbiosome membrane identity, *dnf1* roots were transformed with constructs, each encoding a fusion of green fluorescent protein (GFP) to one of these membrane identity markers (*5*). Our data showed that *dnf1* symbiosomes obtain Rab7 (fig. S2A) as well as the vacuolar SNARE VTI11 before senescence (fig. S2B). Because the occurrence of membrane identity markers on *dnf1* symbiosome membranes is very similar to that of WT symbiosomes, a changed membrane identity cannot explain the block in symbiosome development.

To identify candidate genes for *DNF1*, we compared the transcriptomes of WT versus *dnf1* plants. Such an analysis has previously been used to isolate the *M. truncatula DMI3* calcium- and calmodulin-dependent (CCaM) kinase gene (*7*), because fast neutron-bombardment mutagenesis frequently causes deletions in the genome, and the consequent abolition of transcript can be detected by array hybridization. In plants that are homozygous for the *dnf1-1* mutant allele, a set of sequences showed drastically reduced expression, including the sequence of TC121074. Further investigation identified a large deletion of at least 20 kb that removed the entire gene for TC121074. A second allele, *dnf1-2*, displayed an independent disruption of the TC121074 locus as a result of chromosome rearrangement. The deletion of TC121074 in *dnf1-1* cosegregated with the mutant phenotype (32 F2 individuals), implying a causal relationship.

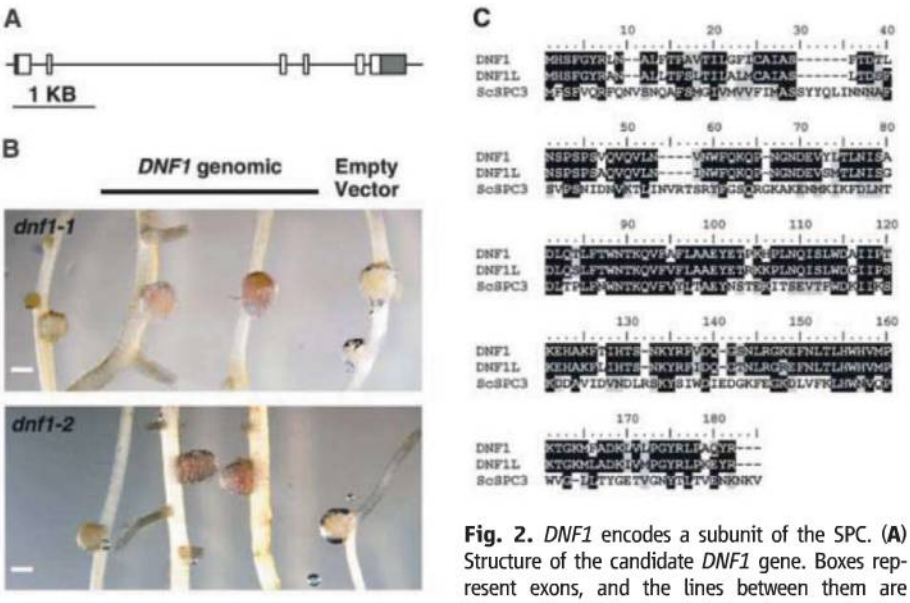

Fig. 2. *DNF1* encodes a subunit of the SPC. (**A**) Structure of the candidate *DNF1* gene. Boxes represent exons, and the lines between them are introns. 5′ and 3′ untranslated regions are shaded. (**B**) Complementation of mutant nodule phenotype by introducing the genomic fragment of the predicted *DNF1* gene. Pink color indicates the presence of leghemoglobin. Scale bars, 1 mm. (**C**) Alignment of protein sequences between DNF1, DNF1L of *M. truncatula*, and the *Sa. cerevisiae* homolog ScSPC3.

By using the *dnf1-1* and *dnf1-2* mutants, we transformed roots with a genomic copy of the predicted coding region (Fig. 2A) for TC121074 under its inferred native promoter (3 kb upstream of the translational start site). At 14 days post inoculation (dpi) with *Sinorhizobium meliloti* Rm1021, transgenic roots produced pink nodules that were indistinguishable from those of WT (Fig. 2B). We concluded that *DNF1* corresponds to TC121074.

The DNF1 protein is annotated as the 22-kD subunit (SPC22) of the signal peptidase complex (SPC). Being an early component of the protein secretory pathway in the endoplasmic reticulum (ER), the SPC cleaves signal peptides off nascent polypeptides that are destined for intracellular compartments and the extracellular matrix (*8*). Although it is not the catalytic domain, SPC22 is nonetheless essential for viability in species where it has been tested (*9*, *10*). In the available genome and expressed sequence tag (EST) databases, we found another SPC22 gene (*DNF1L*), whose protein had a sequence that is almost identical to that of DNF1. Both proteins display substantial sequence similarity to the *Saccharomyces cerevisiae* SPC3 (*8*–*11*) (Fig. 2C). We hypothesize that housekeeping activities important for viability can be performed by DNF1L alone, while DNF1 has evolved to specialize in symbiosis.

To test this hypothesis, we queried the *M. truncatula* Gene Expression Atlas (*12*) for the expression profiles of *DNF1* and *DNF1L*. Their profiles are essentially uncorrelated ($R^2 = 0.024$). *DNF1L* is expressed evenly in all organs at a low level, with modestly higher levels being expressed in pods and nodules (fig. S3). In contrast, *DNF1* expression is highly elevated in the nodule compared with other source tissues (Fig. 3A). The nodule expression of *DNF1* reaches the highest level at 4 dpi, which is the earliest available time point in the dataset (Fig. 3B). This early induction of *DNF1* expression is consistent with the mutant phenotype. Previous transcriptional profiling studies have also noted the up-regulation of *DNF1* during nodule formation (*13*, *14*).

We further investigated the tissue specificity of *DNF1* expression in the nodule. The *DNF1*

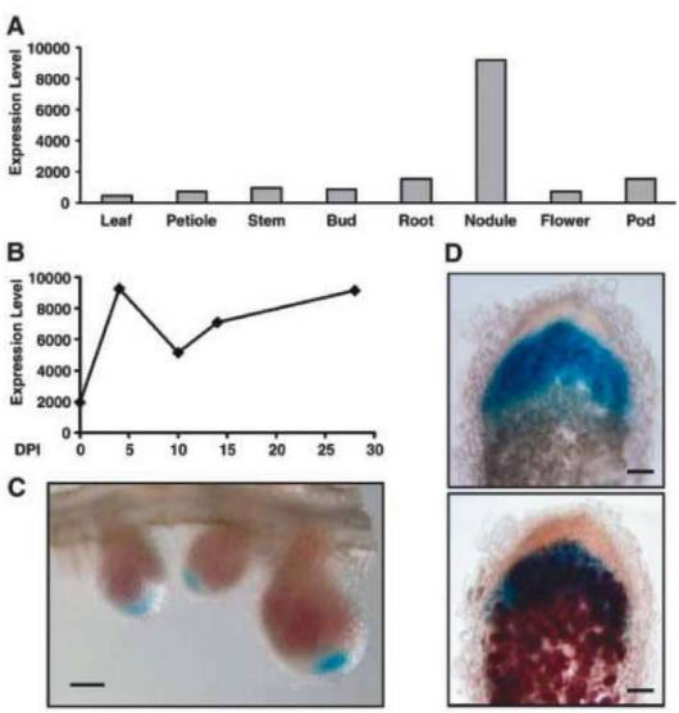

Fig. 3. *DNF1* expression pattern. (**A**) Expression level of *DNF1* in various tissues. (**B**) Temporal profile of *DNF1* expression in nodule. (**C**) Spatial pattern of *DNF1* expression revealed by a promoter::GUS construct in 14-day-old nodules. Nodule samples were stained briefly to preserve the color of leghemoglobin. (**D**) *DNF1* promoter activity in nodules inoculated with Rm1021 carrying *hemA::lacZ*. A *DNF1* promoter::GUS transgenic nodule was stained for GUS activity, photographed (top), briefly fixed, sectioned manually, and then stained with Salmon-gal (bottom). Values in (A) and (B) are levels of Affymetrix probe signal based on microarray data from the *M. truncatula* Gene Expression Atlas. DPI: days post inoculation. Scale bars in (C), 1 mm; (D), 100 μm.

promoter was fused to β-glucuronidase (GUS) and transformed into roots. In roots before inoculation, the promoter is active in the vasculature. GUS activity becomes visible inside very young nodules (fig. S4). By 14 dpi, the nodule has differentiated into distinct zones. GUS activity appears the highest in the growing tip of the nodule (Fig. 3C). By visualizing bacteria in transgenic nodules, we found that the *DNF1* gene is expressed in the infection zone, where bacteria invade the host cell and symbiosomes subsequently differentiate (Fig. 3D). Its expression decreases but is still detectable in differentiated cells of the fixation zone (fig. S5). This expression pattern is consistent with a function of DNF1 in the differentiation of symbiosomes.

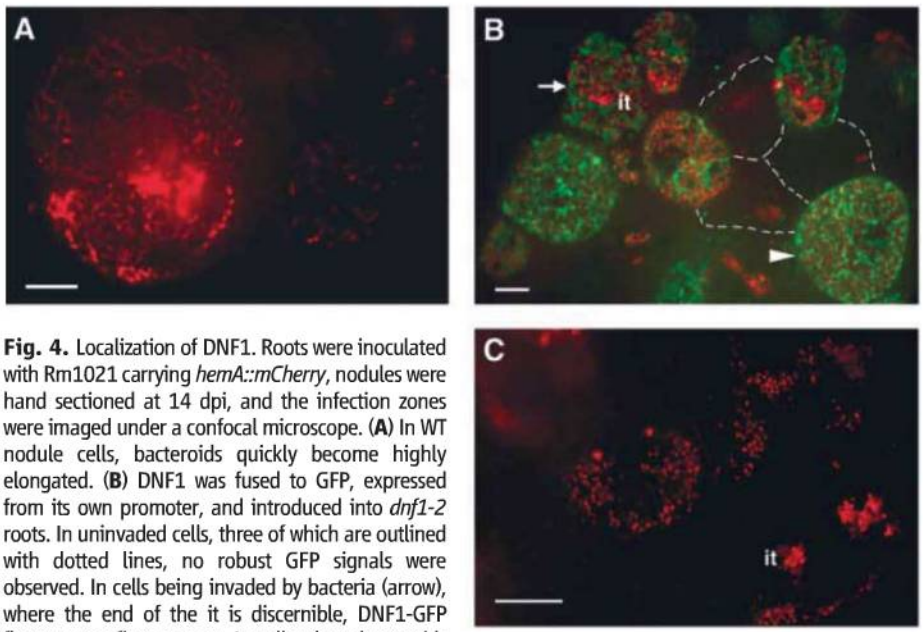

Fig. 4. Localization of DNF1. Roots were inoculated with Rm1021 carrying *hemA::mCherry*, nodules were hand sectioned at 14 dpi, and the infection zones were imaged under a confocal microscope. (**A**) In WT nodule cells, bacteroids quickly become highly elongated. (**B**) DNF1 was fused to GFP, expressed from its own promoter, and introduced into *dnf1-2* roots. In uninvaded cells, three of which are outlined with dotted lines, no robust GFP signals were observed. In cells being invaded by bacteria (arrow), where the end of the it is discernible, DNF1-GFP fluorescence first appears. In cells where bacteroids are fully mature (arrowhead), DNF1-containing structures are numerous and appear elongated and closely associated with symbiosomes. (**C**) In *dnf1-2* mutant nodule cells, bacteroids remain small and undifferentiated after release from the it. Green, DNF1-GFP; red, Rm1021 *hemA::mCherry*. Scale bars, 10 μm.

The ER is a dynamic, multifunctional structure with roles in protein targeting and secretion (*15*, *16*). We made a translational DNF1-GFP fusion under its own promoter, transformed the construct into *dnf1-2* mutant roots, and then inoculated them with mCherry-labeled *S. meliloti*. Transgenic nodules recovered the pink color of leghemoglobin, which is an indication of normal nitrogen-fixing activity. The bacteria were able to differentiate into elongated bacteroids similar to WT, proving that the GFP moiety does not interfere with DNF1 function (Fig. 4). DNF1-GFP exhibits a robust signal in cells containing bacteria, and shows ER-like distributions (Fig. 4B). In an accompanying study, Van de Velde *et al*. demonstrate that *M. truncatula* produces nodule-specific cysteine rich proteins (NCRs) governing bacteroid differentiation, which require DNF1 to be processed from the preprotein (*11*). Failure to process the propeptides in *dnf1* results in the accumulation of these propeptides in the ER.

In plants, the SPC complex is composed of four subunits. In the *M. truncatula* Gene Expression Atlas, the three genes with the highest expression correlation to *DNF1* encode SPC25, SPC12, and SPC18 (the catalytic subunit) (*17*). The correlation at the transcript level suggests that their protein products probably form the SPC complex in nodule cells. Therefore, we named them *DAS12* (for *DNF1*-associated *SPC12*), *DAS18*, and *DAS25* (Fig. 5A). Following the *DAS* genes on the correlation list is a gene that encodes a signal peptide peptidase (*18*), which degrades the signal peptides after cleavage (Fig. 5A). Further strengthening the notion of a common regulatory mechanism of the protein secretory pathway during symbiosome biogenesis, the expression of genes coding for the small GTPase Rab11b and an isoform of SYP132 is also highly correlated to that of *DNF1* (Fig. 5A). In *Nicotiana tabacum*, Rab11b regulates vesicle trafficking for protein secretion in the pollen tube (*19*). The comparatively lower correlation for *Rab11b* may reflect additional mechanisms to regulate Rab protein activity beyond transcriptional control.

We produced promoter::GUS fusions for two genes, *DAS12* and *DAS25*, to both verify the transcriptome data and probe their spatial expression. Reporter fusion data indicate that both genes are expressed in the infection zone of the nodule in a pattern that is indistinguishable from that of *DNF1* (Fig. 5, B to D). Overall, the high correlation among the expression profiles of multiple functionally related genes strongly supports the

A

Gene name	Affymetrix microarray ID	Correlation with *DNF1*
DAS25	Mtr.37516.1.S1_at	0.97
DAS12	Mtr.7213.1.S1_at	0.96
DAS18	Mtr.21175.1.S1_at	0.95
Signal peptide peptidase	Mtr.12523.1.S1_s_at	0.95
	Mtr.43325.1.S1_s_at	0.92
SYP132	Mtr.31873.1.S1_at	0.93
RAB11B	Mtr.19206.1.S1_at	0.90

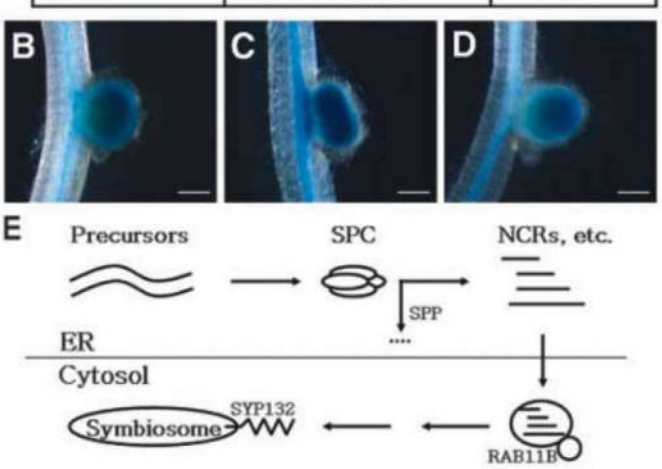

Fig. 5. Coordinated up-regulation of a nodule-specific protein secretory pathway. (**A**) Correlation in gene expression between *DNF1* and additional components of the protein secretory pathway. Correlation values are provided by the *M. truncatula* Gene Expression Atlas (*12*) based on microarray data on vegetative and reproductive tissues, seed development, nodulation, mycorrhization, and chemical treatments. The signal peptide peptidase gene is represented by two probe sets. (**B** to **D**) Promoter::GUS activity in the nodule of *DNF1* and its associated SPC genes *DAS12* and *DAS25*. Transgenic roots were inoculated with Rm1021, and nodules were photographed at 14 dpi. (B) *pDNF1::GUS*; (C) *pDAS12::GUS*; and (D) *pDAS25::GUS*. Background GUS activity in the vasculature confirmed the presence of the transgene. In (C), a nodule with double primodia is being formed. (**E**) A model for a nodule-specific pathway dedicated to secrete protein constitutes toward the developing symbiosome. SPC denotes the DNF1-containing SPC, SPP refers to the signal peptide peptidase listed in (A), and NCRs are mature peptides from precursor proteins processed by SPC and SPP. Scale bar, 1 mm.

hypothesis that upon rhizobial infection, the plant machinery for processing secretory proteins is mobilized coordinately (Fig. 5E).

In *dnf1* mutants, bacterial release into the host cell is apparently normal, but the subsequent differentiation of the bacteria is blocked. Such a phenotype suggests that among the substrates of the DNF1 complex are important host determinants of symbiosome development, such as the processed NCR peptides described by Van de Velde *et al.* (*11*). The NCR proteins are found only in legumes such as *Medicago* spp. that subject their microbial partners to terminal differentiation; however, it is possible that the DNF1 apparatus is present even in legume species that lack NCR type proteins, such as *Lotus* or bean (*18*). If so, it will be interesting to test whether disrupting function of a DNF1 homolog affects symbiosome function in these legumes. Such a result would imply that there are other substrates for the DNF1 SPC, a possibility that can be empirically tested. Potential substrates include the A1b/leginsulin family proteins ENOD8, ENOD16, and nodulin-25, all of which are proteins with a signal peptide, are up-regulated during nodulation, and in some cases are shown to localize to the symbiosome (*13*, *20*, *21*). Some of these proteins are conserved in *Lotus japonicus* and soybean, suggesting that they may be processed by a common mechanism in a variety of legume species. Alternatively, the *DNF1* and co-expressed signal peptidase genes may have co-evolved with the *NCR* genes within the clade of legumes that show terminal bacteroid differentiation as a specialized means to control bacterial proliferation and function within the host cells.

References and Notes

1. C. G. Starker, A. L. Parra-Colmenares, L. Smith, R. M. Mitra, S. R. Long, *Plant Physiol.* **140**, 671 (2006).
2. R. M. Mitra, S. R. Long, *Plant Physiol.* **134**, 595 (2004).
3. J. Vasse, F. de Billy, S. Camut, G. Truchet, *J. Bacteriol.* **172**, 4295 (1990).
4. A. R. Thompson, R. D. Vierstra, *Curr. Opin. Plant Biol.* **8**, 165 (2005).
5. E. Limpens *et al.*, *Plant Cell* **21**, 2811 (2009).
6. C. M. Catalano, K. J. Czymmek, J. G. Gann, D. J. Sherrier, *Planta* **225**, 541 (2007).
7. R. M. Mitra *et al.*, *Proc. Natl. Acad. Sci. U.S.A.* **101**, 4701 (2004).
8. M. Paetzel, A. Karla, N. C. Strynadka, R. E. Dalbey, *Chem. Rev.* **102**, 4549 (2002).
9. H. Fang, C. Mullins, N. Green, *J. Biol. Chem.* **272**, 13152 (1997).
10. H. A. Meyer, E. Hartmann, *J. Biol. Chem.* **272**, 13159 (1997).
11. W. Van de Velde *et al.*, *Science* **327**, [THIS ISSUE] (2010).
12. V. A. Benedito *et al.*, *Plant J.* **55**, 504 (2008).
13. F. El Yahyaoui *et al.*, *Plant Physiol.* **136**, 3159 (2004).
14. K. Manthey *et al.*, *Mol. Plant Microbe Interact.* **17**, 1063 (2004).
15. N. Raikhel, M. J. Chrispeels, in *Biochemistry and Molecular Biology of Plants*, B. B. Buchanan, W. Gruissem, R. L. Jones, Eds. (American Society of Plant Biologists, Rockville, MD, 2000) pp. 160–201.
16. Y. Du, S. Ferro-Novick, P. Novick, *J. Cell Sci.* **117**, 2871 (2004).
17. R. E. Dalbey, M. O. Lively, S. Bron, J. M. van Dijl, *Protein Sci.* **6**, 1129 (1997).
18. P. Mergaert *et al.*, *Plant Physiol.* **132**, 161 (2003).
19. B. H. de Graaf *et al.*, *Plant Cell* **17**, 2564 (2005).
20. C. M. Catalano, W. S. Lane, D. J. Sherrier, *Electrophoresis* **25**, 519 (2004).
21. L. Coque *et al.*, *Mol. Plant Microbe Interact.* **21**, 404 (2008).

22. We thank D. Ehrhardt for assistance with confocal microscope and E. Kondorosi, P. Mergaert, and W. Van de Velde for critical reviews of the manuscript and for sharing unpublished results. This work was supported by the Helen Hay Whitney Foundation (to J.G.), a National Institutes of Health training grant (to C.S.), The Netherlands Organisation for Scientific Research (NWO, to E.L., S.I., E.F., and T.B.), the Hoover Circle fund, and prior support from the Howard Hughes Medical Institute and the U.S. Department of Energy grant no. DE–FG03–90ER20010 (to S.R.L.).

Supporting Online Material

www.sciencemag.org/cgi/content/full/327/5969/1126/DC1
Materials and Methods
Figs. S1 to S5
References

2 November 2009; accepted 21 January 2010
10.1126/science.1184096

Individuals and the Variation Needed for High Species Diversity in Forest Trees

James S. Clark

In the past, explanations for high species diversity have been sought at the species level. Theory shows that coexistence requires substantial differences between species, but species-level data rarely provide evidence for such differences. Using data from forests in the southeastern United States, I show here that variation evident at the individual level provides for coexistence of large numbers of competitors. Variation among individuals within populations allows species to differ in their distributions of responses to the environment, despite the fact that the populations to which they belong do not differ, on average. Results are consistent with theory predicting that coexistence depends on competition being stronger within than between species, shown here by analysis of individual-level responses to environmental fluctuation.

The paradox of low diversity predicted by theory and the high diversity in nature has been recognized for a half-century (*1*). Forest trees compete intensely for a small number of resources, including light, water, and several nutrients (*2*, *3*). Models of competition for few resources predict low diversity and precise parameter trade-offs that limit the strength of competition among those species that do coexist. It has become increasingly apparent that mean demographic rates or responses to resources in the few dimensions that can be measured are not significantly different among many species (*4*–*7*). The weak trends in data are inconsistent with the precise parameter relations and trade-offs needed to explain coexistence in models; yet there is abundant evidence for long-term coexistence of competitors in nature and rapid return to previous densities after disturbance (*8*). In summary, there are apparently few dimensions along which species can partition the resources for which they compete intensively. Evidence is lacking for the species differences required for coexistence, but there is pervasive evidence for long-term persistence of competitors at high diversity.

Nicholas School of the Environment, Department of Biology and Department of Statistical Science, Duke University, Durham, NC 27708, USA. E-mail: jimclark@duke.edu

Recent demonstration that variation within tree species exceeds the differences in species-level averages (*4*–*6*) motivated the present analysis of how variation in many dimensions might provide the explanation for high biodiversity, made possible by extensive data and alternative methods for analysis. Six to 18 years of annual, individual-level demographic estimates on 11 forests in three regions in the southeastern U.S. include 33 tree species, >22,000 trees, and >226,000 tree years (*9*, *10*). The data have sufficient detail to resolve responses to environmental fluctuations at high frequency (annual or less) and sufficient duration to permit inference at the individual level. This combination of annual resolution and long duration is not available from previous studies, which are either short- (a few years or less) or long-term, but with 5- to 10-year resolution. A hierarchical Bayesian analysis quantifies the structure of variation among individuals within populations and over time. From observations on tree diameter, canopy status, reproductive status, survival, remote sensing of canopy stature, and seed rain, we inferred annual demographic estimates of growth, fecundity, and survival risk for every individual in 11 forest stands (*9*, *10*). The structure in these estimates of demographic rates can be used to evaluate how species compare at the level of individual responses to environmental variation.

The analysis of individual variation expands on two relations demonstrated from theory and simulation. First, analytical models have long shown that coexistence is promoted when intraspecific competition is stronger than interspecific

competition (*11*–*13*). Simulation studies confirm low diversity of competitors and the prediction that coexistence depends on resource partitioning (*13*–*16*). Such criteria for coexistence can be met by trade-offs among species, such as negative correlations in consumption of different resources, colonization versus competitive ability, and low-light survival versus high-light growth (*2*). The problem is that most studies do not find such trade-offs. Although trends in data are sometimes consistent with the assumption of trade-offs for a few species within some communities, we still require an explanation for the persistence of large numbers of competing species that do not possess such trade-offs. None of the trade-offs traditionally postulated for trees is evident in the extensive, long-term data sets analyzed here (*4*, *9*).

Second, coexistence is promoted when species differ in how they respond to fluctuations (*17*). Negative correlation between species in response to environmental fluctuation can promote coexistence (*5*, *18*, *19*). For example, a trade-off between growth potential and low-resource tolerance may allow desert annual species to partition variation, with different species benefiting in different years (*20*). However, many competitors do not show such temporal partitioning. *Acer rubrum* and *Nyssa sylvatica*, examples from this analysis, illustrate a general pattern. These species have coexisted in shaded understories throughout the eastern U.S. at least since the early Holocene, but their growth responses are positively correlated across years (Fig. 1A). The responses broadly overlap, with no indication that one experiences high growth when the other does not; at the species level, there is no evidence of partitioning environmental fluctuations in the form of negative correlation. The positive correlation is not surprising for species limited, on average, by the same few resources. This is one example of a large number of species that show no tendency to trade off (*9*). Thus, the high diversity of southeastern U.S. forests analyzed in this study is not consistent with the prediction that species are negatively correlated in their responses, at least when applied at the species level.

Despite small differences in species means, there is substantial variation within species, and the structure of variation shows that species partition environmental variation in higher dimensions. This can be the case if competition between individuals of the same species is stronger than with individuals of other species, even if there is no apparent trade-off in species mean traits in a few dimensions and also if there is positive correlation in species means over time. To illustrate this concept, I now shift focus from species to individuals. Consider individual variation in a demographic rate, such as growth or fecundity. Individuals responding to environmental variation in similar ways show positive correlation and vice versa (Fig. 1B). Clearly, the negative correlation between individuals shown in the lower-left panel of Fig. 1B is evidence that individuals are responding differently. In the lower-right panel of the same figure, they are responding similarly. However, to promote coexistence, the question is not whether correlations are negative, but rather if correlations are lower when comparing different species. The latter indicates that intraspecific competition will be stronger than interspecific competition. For n_A and n_B individuals of two species (denoted by A and B, respectively), there will be $n_A n_B$ interspecific and $\frac{1}{2}[n_A(n_A - 1) + n_B(n_B - 1)]$ intraspecific comparisons. For the example in Fig. 1B, histograms of comparisons between individuals of the same species in the same neighborhoods tend toward positive correlation, reflecting similar resource requirements and physiological constraints as the environment varies over time and among sites. If individual-level variation promotes coexistence, correlations involving individuals of different species (*Acer:Nyssa*) are lower than those between individuals of the same species (*Acer:Acer* and *Nyssa:Nyssa*). In more general terms, the strength of competition experienced by an individual i from a neighbor of its own species A exceeds that from a neighbor of species B if $R_{iA} > R_{iB}$, where R_{iA} and R_{iB} are the correlations between individual i and others of species A and i and others of species B, respectively (*10*). The more similarity existing between individual i and its own species A (large R_{iA}), the more likely it is to coexist with species B, because it experiences stronger competition when its own species A is abundant. Competition can be stronger within than between species, even where correlations between species mean responses are positive (Fig. 1A). This basic relation can be extended to spatial neighborhoods of multiple individuals $\mathbf{S}_{iA}\mathbf{S}_{AA}^{-1}\mathbf{S}_A > \mathbf{S}_{iB}\mathbf{S}_{BB}^{-1}\mathbf{S}_B$, where $\mathbf{S}_{iA}$ and $\mathbf{S}_{iB}$ are the vectors of covariances between growth of individual i and those of n_A and n_B competitors of the two species, $\mathbf{S}_{AA}$ and $\mathbf{S}_{BB}$ are the growth covariance matrices for A and B, and $\mathbf{S}_A$ and $\mathbf{S}_B$ are the vectors of growth standard deviations for neighbors of A and B (*10*).

To determine if the relations between individuals of different species contribute to coexistence, I evaluated correlation and covariance structure for all individuals of all 33 co-occurring species in the 11 forest stands. These species are light-limited in shaded understories and occur on plots that experience annual moisture deficits:

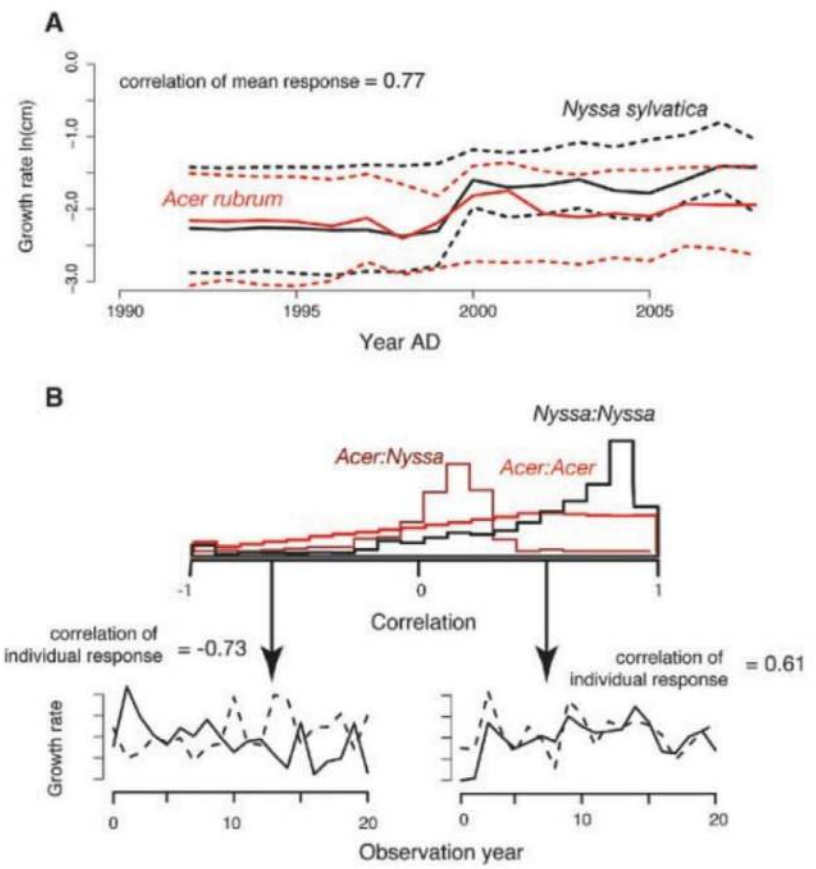

Fig. 1. (**A**) At the species level, growth responses over time overlap broadly [included are median (solid lines) and 95% variation (dashed lines) among individuals], as shown for the example of *A. rubrum* and *N. sylvatica*. The correlation between mean species response is high (0.77). (**B**) Frequency distribution of correlations for intra- (*Nyssa:Nyssa*, *Acer:Acer*) and interspecific (*Acer:Nyssa*) comparisons of growth rate for individuals that occur in the same neighborhoods, defined as 20 m in radius. Although the correlation between species means is high (A), the mean correlations for interspecific comparisons is lower than is the mean for intraspecific comparisons. The lower panels in (B) show examples of low (left) and high (right) correlation between the growth of two individuals.

They compete both above- and belowground. Individual-level estimates of year-to-year growth and fecundity are available for each tree. The correlation and covariance was determined for every pair of individuals occurring in local neighborhoods of radii 20 m for growth and 60 m for fecundity. These distances represent approximate interaction neighborhoods for growth, which determine resource capture through their effect on tree size, and dispersal, which determines capture of recruitment sites. The qualitative results reported here also hold for much larger neighborhoods.

The analysis confirms that individual responses contribute the species differences that are lacking in species-level comparisons. The vertical axis in Fig. 2 shows the fraction of species-level comparisons in which mean correlations (solid lines) and mean growth or fecundity deviations (dashed lines) were greater when comparing individuals of the same versus different species. Correlations between individuals of different species were lower than those for the same species, for both growth (Fig. 2A) and fecundity (Fig. 2B). As the environment fluctuates, individuals respond in different ways, depending on fine-scale variation in resources such as moisture, nutrients, and light and their genotypic differences. Because individuals are responding in many dimensions, but with more similarity to individuals of the same species than to individuals of different species, intraspecific comparisons have higher correlation than interspecific comparisons. More similar responses translate to stronger competition: Growth influences long-term competitive ability by changing size (and, thus, resource capture), and fecundity determines capture of new recruitment sites.

Although trade-offs evident at the species level do not explain coexistence, species partition the environment without showing species-level correlations. Responses can differ between species, even if species mean responses in a few observable dimensions do not differ (Fig. 1A). If individuals of each species exploit variation in many dimensions in different ways, then species-level analysis misses the factors responsible for coexistence. The individual level dominates species interactions, because the few environmental axes that are measured account for only a small fraction of the variation between species (*4*). For example, two species may be limited by moisture, but they differ in their capacity to exploit high moisture versus tolerate extended drought (*21*). Species-level comparisons can show both species increasing in wet years (positive correlation), whereas each is actually competing more with individuals of its own species, depending on moisture variation in space and time. On average, both species benefit in wet years, but it is not the same individuals that are benefiting and not to the same degree on sites with differing moisture

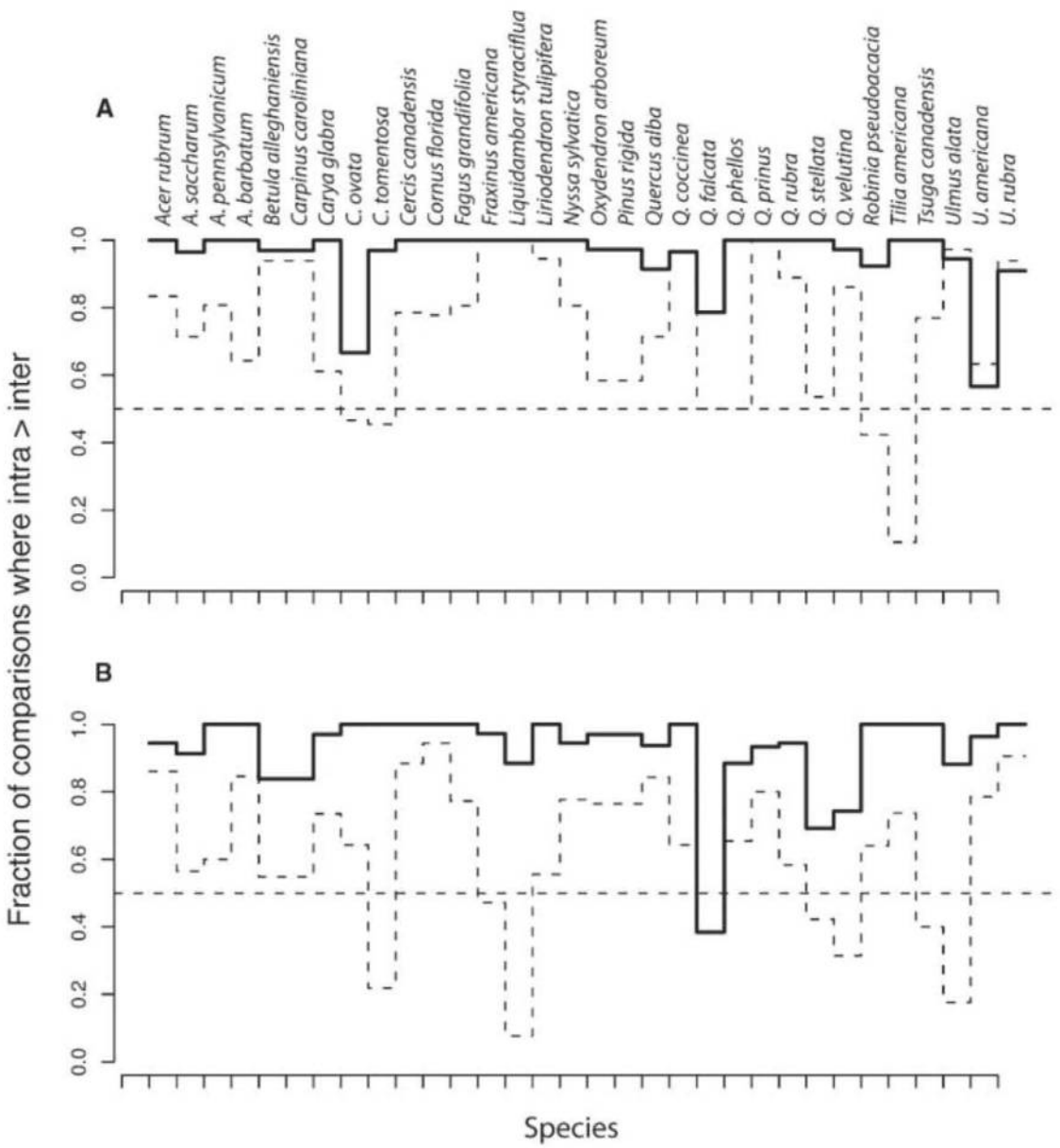

Fig. 2. Fractions of comparisons consistent with promoting coexistence at the individual level, including correlations ($R_{iA} > R_{iB}$) (solid lines) and conditional responses ($\mathbf{S}_{iA}\mathbf{S}_{AA}^{-1}\mathbf{S}_{A} > \mathbf{S}_{iB}\mathbf{S}_{BB}^{-1}\mathbf{S}_{B}$) (dashed lines). For both growth rate (**A**) and fecundity (**B**), the majority of values greater than 0.5 indicates that individuals respond more like individuals of their own species, thus focusing intraspecific competition in space and time. Interspecific correlations are weaker, thus providing opportunity for partitioning the environment.

status. Variation within populations, be it genetic or not, can differ between species in many dimensions that are not documented in species-level data. Species-level analyses fail to capture variation that contributes to diversity if variation among individuals in many dimensions is species-specific. This analysis shows that the massive variation within populations documented in previous studies (*4*–*6*) is structured in such a way that it contributes to coexistence.

The explanation that diversity depends on individual variation is consistent with the lack of evidence that individuals recognize the species identities of their competitors. Most competition theory is based on interaction coefficients specific to each species pair, often termed the "community matrix." This concept has prompted substantial study to quantify interaction strength between species pairs. Neutral theory (*22*, *23*) and the belief that all species are functionally equivalent was partly motivated by the implausibility that plant competition operates differently for each species pair. The individual-level maintenance of biodiversity shown here involves only differences in the ranges of response to the environment and the tendency to respond like conspecifics, and not species-by-species recognition. Those differences translate into differences in individual growth, which determines resource capture, and fecundity, which determines capture of new sites. In contrast to neutral theory, which posits no difference, high diversity is possible because species differ in so many ways. The mechanism demonstrated here is also more general than a rare-species advantage, which invokes host-specific natural enemies (one to control each species when it becomes abundant) and disappearance of the effect when the host becomes rare (*24*, *25*), or N natural enemies to explain coexistence of N hosts. The tendency to respond like other individuals of the same species can promote coexistence independent of local frequency or density and does not require a large number of host-specific enemies.

The biodiversity paradox of many coexisting competitors in which the number of limiting resources seems low can be resolved at the individual level. Just as variation among individuals is required to maintain species by natural selection, providing a means for adaptive evolution in response to many factors in many dimensions, variation at the individual scale is also needed to explain why large numbers of intensely competing species coexist. Individual-level variation need not be genetic (although genotypic variation can be large), but species do need to differ in how individuals respond in many dimensions. In the absence of precise information on the many dimensions in which species differ, individual-level data provide evidence for species differences.

References and Notes

1. G. E. Hutchinson, *Am. Nat.* **95**, 137 (1961).
2. M. Rees, R. Condit, M. Crawley, S. Pacala, D. Tilman, *Science* **293**, 650 (2001).
3. J. Silvertown, *Trends Ecol. Evol.* **19**, 605 (2004).
4. J. S. Clark, S. LaDeau, I. Ibanez, *Ecol. Monogr.* **74**, 415 (2004).
5. J. S. Clark *et al.*, *Ecol. Lett.* **10**, 647 (2007).
6. J. E. Mohan, J. S. Clark, W. H. Schlesinger, *Ecol. Appl.* **17**, 1198 (2007).
7. R. Condit *et al.*, *Science* **313**, 98 (2006); published online 8 June 2006 (10.1126/science.1124712).
8. J. S. Clark, J. S. McLachlan, *Nature* **423**, 635 (2003).
9. J. S. Clark *et al.*, in *Handbook of Bayesian Analysis*, T. O'Hagan, M. West, Eds. (Oxford Univ. Press, New York, 2010), pp. 431–481.
10. Materials and methods are available as supporting material on *Science* Online.
11. R. H. MacArthur, R. Levins, *Proc. Natl. Acad. Sci. U.S.A.* **51**, 1207 (1964).
12. S. A. Levin, *Am. Nat.* **104**, 413 (1970).
13. D. Tilman, *Plant Strategies and the Dynamics and Structure of Plant Communities* (Princeton Univ. Press, Princeton, NJ, 1988).
14. D. Tilman, *Proc. Natl. Acad. Sci. U.S.A.* **101**, 10854 (2004).
15. D. Gravel, C. D. Canham, M. Beaudet, C. Messier, *Ecol. Lett.* **9**, 399 (2006).
16. T. Zillio, R. Condit, *Oikos* **116**, 931 (2007).
17. R. Levins, *Am. Nat.* **114**, 765 (1979).
18. P. Chesson, *Annu. Rev. Ecol. Syst.* **31**, 343 (2000).
19. P. B. Adler, J. HilleRisLambers, P. C. Kyriakidis, Q. Guan, J. M. Levine, *Proc. Natl. Acad. Sci. U.S.A.* **103**, 12793 (2006).
20. A. L. Angert, T. E. Huxman, P. Chesson, D. L. Venable, *Proc. Natl. Acad. Sci. U.S.A.* **106**, 11641 (2009).
21. N. McDowell *et al.*, *New Phytol.* **178**, 719 (2008).
22. S. P. Hubbell, *The Unified Neutral Theory of Biodiversity and Biogeography* (Princeton Univ. Press, Princeton, NJ, 2001).
23. S. P. Hubbell, *Ecology* **87**, 1387 (2006).
24. D. H. Janzen, *Am. Nat.* **104**, 501 (1970).
25. J. H. Connell, in *Dynamics of Numbers in Populations*, P. J. Boer, G. R. Graadwell, Eds. (Centre for Agricultural Publishing and Documentation, Wageningen, Netherlands, 1971), pp. 298–312.

Supporting Online Material

www.sciencemag.org/cgi/content/full/327/5969/1129/DC1
Materials and Methods
Figs. S1 to S3
Tables S1 to S3
References

19 October 2009; accepted 18 January 2010
10.1126/science.1183506

Generating a Prion with Bacterially Expressed Recombinant Prion Protein

Fei Wang,[1]* Xinhe Wang,[1]* Chong-Gang Yuan,[2] Jiyan Ma[1,2]†

The prion hypothesis posits that a misfolded form of prion protein (PrP) is responsible for the infectivity of prion disease. Using recombinant murine PrP purified from *Escherichia coli*, we created a recombinant prion with the attributes of the pathogenic PrP isoform: aggregated, protease-resistant, and self-perpetuating. After intracerebral injection of the recombinant prion, wild-type mice developed neurological signs in ~130 days and reached the terminal stage of disease in ~150 days. Characterization of diseased mice revealed classic neuropathology of prion disease, the presence of protease-resistant PrP, and the capability of serially transmitting the disease; these findings confirmed that the mice succumbed to prion disease. Thus, as postulated by the prion hypothesis, the infectivity in mammalian prion disease results from an altered conformation of PrP.

Transmissible spongiform encephalopathies (TSEs or prion disease) are infectious neurodegenerative disorders. The prion hypothesis (*1*) proposes that the infectious agent is an aberrant conformational isoform of the normal PrP (PrP^C), a glycosylphosphatidylinositol (GPI)–anchored glycoprotein. By virtue of its self-perpetuating characteristic, the aberrant isoform (PrP^{Sc}) converts host PrP^C into the PrP^{Sc} conformation and leads to neurodegeneration (*2*–*4*). Despite strong supporting evidence (*5*–*11*), a crucial prediction derived from the prion hypothesis—that an infectious prion can be generated with bacterially expressed recombinant PrP (recPrP)—remains unfulfilled (*2*, *12*), leaving lingering doubts about the prion hypothesis (*13*).

Recombinant PrP has been folded into various forms similar to PrP^{Sc}, but none of them fully recapitulates the characteristics of the infectious agent (*2*, *12*). The amyloid fiber of a recPrP fragment (recPrP89-230) causes prion disease in transgenic mice overexpressing PrP89-231 (*10*), but a prolonged incubation time in mice overexpressing PrP has led to uncertainty about whether the infectivity is indeed derived from recPrP89-230 amyloid fibers (*2*, *12*). The difficulty in creating a recombinant prion is likely due to the lack of proper facilitating factors (*14*). Polyanions, particularly RNA, have been found to facilitate PrP conversion and promote de novo prion formation (*9*, *15*–*17*). We investigated lipid as a potential facilitating factor because GPI-anchored PrP^C is in the vicinity of lipid membranes and the interfacial lipid bilayer region strongly influences protein structure (*18*). Encouraged by the findings that lipid interaction converts recPrP to a PrP^{Sc}-like form (*19*), we applied protein misfolding cyclic amplification (PMCA) (*8*) to study recPrP

[1]Department of Molecular and Cellular Biochemistry, Ohio State University, Columbus, OH 43210, USA. [2]School of Life Science, East China Normal University, Shanghai 200062, China.

*These authors contributed equally to this work.
†To whom correspondence should be addressed. E-mail: ma.131@osu.edu

conversion in the presence of both lipid and RNA.

Using a serial PMCA protocol (*20*), we tested 16 different conditions in which recPrP was mixed with various combinations of lipids and/or total RNA isolated from normal mouse liver. In the presence of the synthetic anionic phospholipid POPG (1-palmitoyl-2-oleoylphosphatidylglycerol) and RNA, a 15-kD proteinase K (PK)–resistant band was detected after 17 rounds of PMCA (Fig. 1A). Once formed, the PK-resistant recPrP (rPrP-res) was able to serially propagate (Fig. 1A and fig. S1). The same procedure was repeated several times, and the overall efficiency of de novo rPrP-res formation was found to be ~20% (fig. S2).

Serial PK-digestion of rPrP-res revealed that the PK-resistant band was detectable after digestion with high concentrations of PK (200 μg/ml; PK:recPrP molar ratio > 50:1) (Fig. 1B). After centrifugation, the rPrP-res was detected only in the pellet fraction (Fig. 1C); moreover, the 15-kD PK-resistant band was not recognized by the 8B4 antibody, which detects an N-terminal epitope of PrP (*21*) (Fig. 1C). These findings show that, similar to PrP^{Sc}, rPrP-res is aggregated, is PK-resistant, and contains a C-terminal PK-resistant core.

Next, we performed PMCA and cell culture analyses to determine whether rPrP-res could seed glycosylated and GPI-anchored endogenous PrP^{C}. With normal mouse brain homogenate as substrate, PMCA was carried out with or without rPrP-res seed. The PK-resistant endogenous PrP, as demonstrated by higher molecular weights of glycosylated PrP, was detected in samples seeded with rPrP-res (Fig. 1D). In reactions without rPrP-res seed, no PK-resistant PrP was detected, allowing us to rule out de novo PrP-res formation or insufficient PK digestion. The cell infection assay was performed on SN56 cells, a murine neuronal cell line susceptible to prion infection (*22*). Endogenous PrP^{C} in SN56 cells was glycosylated and sensitive to PK digestion (Fig. 1E). After rPrP-res infection, the PK-resistant endogenous PrP was detected in cells after 2 passages and remained detectable after 17 passages (Fig. 1E). A similar experiment revealed that the rPrP-res–converted normal mouse brain homogenate (Fig. 1D) could infect SN56 cells as well (fig. S3). Thus, rPrP-res is able to propagate its PK-resistant conformation to endogenous PrP^{C}.

To determine whether rPrP-res was capable of causing bona fide prion disease, we infected 8-week-old female CD-1 mice by intracerebral injection. The rPrP-res (inoculum 4) was prepared by propagating rPrP-res through 24 rounds of PMCA. All PMCA products were pooled together and centrifuged through a sucrose cushion. The pellet was washed, resuspended, and used for inoculation. Three control inocula were used for animal study (Table 1). Inoculum 1, consisting of all the components used for rPrP-res propagation except for recPrP and rPrP-res seed, was subjected to the same treatments as inoculum 4. Inoculum 2, consisting of all the components of rPrP-res propagation except for rPrP-res seed, was incubated at 37°C for 24 days without sonication and subjected to the same pelleting and washing treatments. Omitting the sonication step prevented the de novo rPrP-res formation in this control sample, as confirmed by the PK digestion analysis described below (Fig. 2A). Inoculum 3 was prepared by directly mixing recPrP, POPG, and RNA in the inocu-

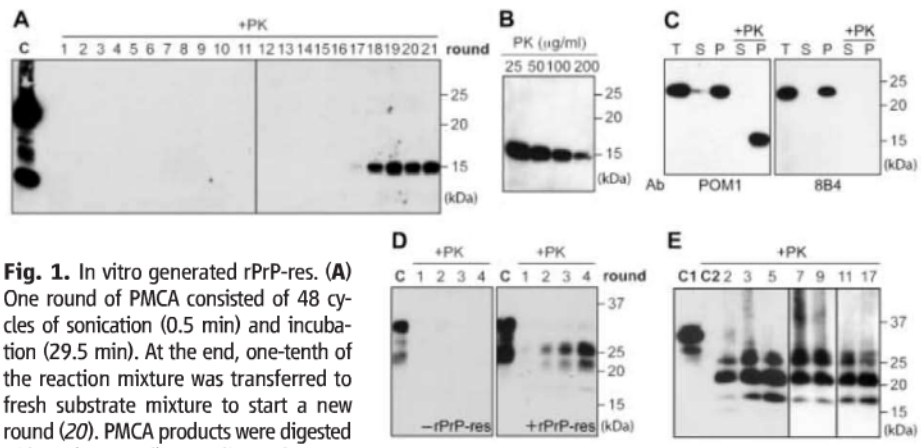

Fig. 1. In vitro generated rPrP-res. (**A**) One round of PMCA consisted of 48 cycles of sonication (0.5 min) and incubation (29.5 min). At the end, one-tenth of the reaction mixture was transferred to fresh substrate mixture to start a new round (*20*). PMCA products were digested with PK (25 μg/ml); C, undigested recPrP. (**B**) Serial PK digestion of PMCA products. (**C**) PMCA product was separated into supernatant (S) and pellet (P) by a 1-hour 100,000*g* centrifugation at 4°C. T, total input; +PK, digested with PK (25 μg/ml). (**D**) With normal mouse brain homogenate (NMBH) as substrate, PMCA was performed with or without rPrP-res seed. Product was digested with PK (100 μg/ml); C, undigested NMBH. (**E**) After rPrP-res infection, SN56 cells were lysed, digested with PK (25 μg/ml), and centrifuged. The PK-resistant PrP in the pellet was detected by immunoblot analysis. Numbers indicate cell passages. C1, undigested SN56 cell lysate; C2, pellet of PK-digested, uninfected SN56 cell lysates. In all panels, PrP was detected by immunoblot analysis with POM1 antibody to PrP except for the right panel of (C), where 8B4 antibody was used. PK digestion was carried out at 37°C for 30 min [(A), (B), and (C)] or 1 hour [(D) and (E)].

Table 1. Intracerebral inoculation of rPrP-res.

Inoculum	Component	Processing	Preparation for injection	Diseased/ inoculated	Survival time (dpi)*
1	Buffer + POPG + RNA (the amount of each component equaled that in the rPrP-res propagation reaction)	Serial PMCA	Pelleting through a sucrose cushion and washing twice with PBS	0/15	>360
2	Buffer + POPG + RNA + recPrP (the amount of each component equaled that in the rPrP-res propagation reaction)	Incubated at 37°C without sonication	Pelleting through a sucrose cushion and washing twice with PBS	1†/14	>360 (286†)
3	POPG + RNA + recPrP (the amount of each component equaled that in the final pool of inoculum 4)	No processing	No preparation	0/5	>360
4 (rPrP-res)	Buffer + POPG + RNA + recPrP + rPrP-res seed	Serial PMCA	Pelleting through a sucrose cushion and washing twice with PBS	15/15	150 ± 2.2 (mean ± SEM)

*One mouse from each group was euthanized at 275 dpi to serve as controls. †One mouse died from an unrelated disease at 286 dpi. It had no neurological signs or weight loss.

lum diluent. The amount of each component was equal to the total amount in the final pool of inoculum 4, ensuring that the result was not influenced by insufficient dosage of recPrP or any other component. The inoculation and animal care were carried out in an animal vivarium that had never been exposed to animals with prion disease.

After the injection, the remaining inocula were analyzed (Fig. 2A). Inoculum 1 did not contain PrP, and, accordingly, no PrP was detected. Of three inocula that contained recPrP, inoculum 4 had the lowest amount of recPrP (Fig. 2A). However, the 15-kD PK-resistant band was detected only in inoculum 4; hence, it was the only inoculum containing rPrP-res.

Around 130 days post-inoculation (dpi), all 15 rPrP-res–inoculated mice developed clinical signs of prion disease. The earliest sign was clasping, an indication of neurological dysfunction (Fig. 2B). Soon after that, mice developed tail plasticity and akinesia—that is, they remained stationary in response to external stimuli (Fig. 2B and movie S1). The disease progressed rapidly; mice developed kyphosis, head twitching, and mild ataxia, and eventually they became cachexic and lethargic (Fig. 2B and movie S2). The rPrP-res–inoculated mice reached the terminal stage at 136 to 161 dpi, with an average survival time of 150 ± 2.2 days (mean ± SEM) (Table 1 and fig. S4). None of the mice injected with control inocula developed prion disease after more than 360 days. Thus, intracerebral rPrP-res injection caused neurodegenerative disorders in wild-type mice, and infectivity was specifically associated with the rPrP-res conformation.

To ensure that every rPrP-res–inoculated mouse received both pathological and biochemical analyses, we bisected each mouse brain sagittally and subjected brain halves to histological or biochemical analysis. Severe spongiosis was detected in multiple brain regions (figs. S5 and S6). Dense small vacuoles were observed in the frontal cortex and caudate nucleus (Fig. 3B and fig. S6), whereas larger vacuoles were detected in the pons, midbrain (areas around raphe nuclei and periaqueductal gray), and cerebellar white matter (areas around cerebellar dentate and fastigial nuclei). Moderate spongiosis was present in the occipital cortex, thalamus, medulla, and hippocampus, whereas little spongiosis was detected in the superior or inferior colliculus, hypothalamus, or olfactory bulb (figs. S6 and S7). Prominent astrogliosis and microgliosis were detected in rPrP-res–inoculated mouse brains (Fig. 3D and fig. S8). PrP immunohistochemistry revealed abnormal PrP deposition in a pattern similar to the diffuse synaptic accumulation (Fig. 3F). The densest PrP deposition was in the thalamus (fig. S8), a finding supported by paraffin-embedded tissue blot (PET blot) analysis (fig. S9). Collectively, rPrP-res–inoculated mouse brains exhibited the classic neuropathological features of prion disease: spongiosis, astrogliosis, microgliosis, and abnormal PrP deposition.

To determine whether PrP^{Sc} was specifically present in rPrP-res–inoculated mice, we euthanized one mouse from each control group at 275 dpi. PrP^{Sc} was detected in the rPrP-res–inoculated mouse brain but not in any other control brains (Fig. 3G). Histological analysis confirmed that there was no spongiosis in the control mice. The glycosylation and the electrophoretic pattern of PrP^{Sc} were similar among all 15 mice (fig. S10), in agreement with the similar neuropathology and relatively synchronized disease onset observed among these mice.

To determine whether the rPrP-res–induced disease could be serially transmitted, we prepared 1% brain homogenates from six diseased mice and inoculated each sample intracerebrally into four or five wild-type CD-1 mice. Around 130 dpi, all mice ($n = 29$) developed disease, and the behavior phenotypes were essentially the same as those of the rPrP-res–inoculated mice (movie S3). These mice reached the terminal stage of disease at 151 to 180 dpi; the average survival

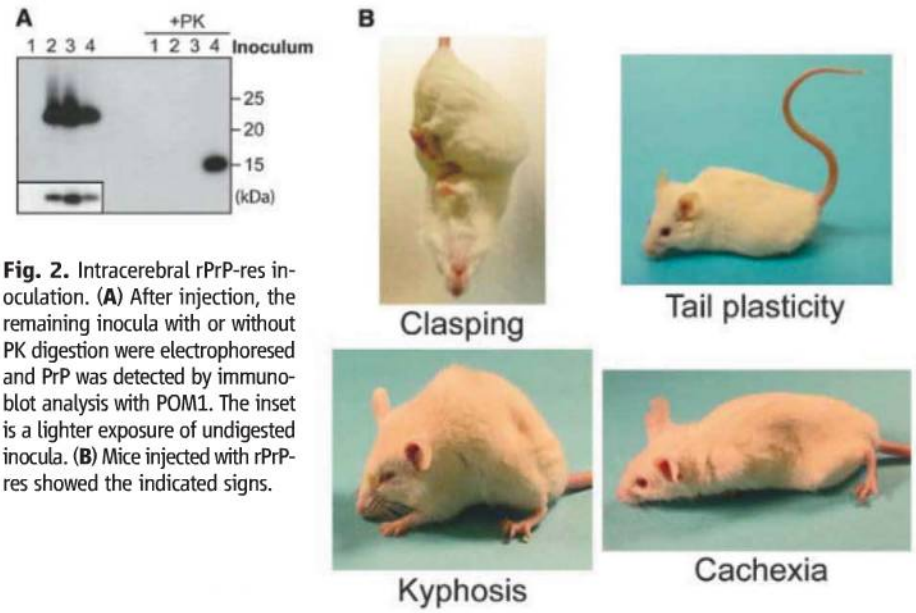

Fig. 2. Intracerebral rPrP-res inoculation. (**A**) After injection, the remaining inocula with or without PK digestion were electrophoresed and PrP was detected by immunoblot analysis with POM1. The inset is a lighter exposure of undigested inocula. (**B**) Mice injected with rPrP-res showed the indicated signs.

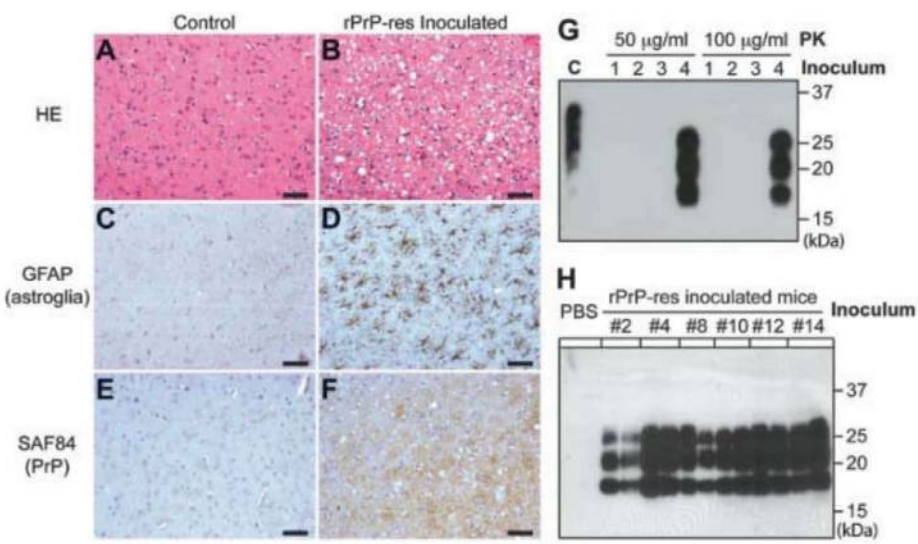

Fig. 3. Characterization of rPrP-res–caused prion disease. (**A** to **F**) Histological analyses of age- and sex-matched control mice [(A), (C), and (E)] and rPrP-res injected mice [(B), (D), and (F)]. Brain sections were stained by hematoxylin and eosin [(A) and (B)], an antibody to GFAP (glial fibrillary acidic protein) [(C) and (D)], and SAF84 antibody to PrP [(E) and (F)]. Immunohistochemical stains were counterstained with hematoxylin. Scale bars, 50 μm. (**G**) Brain homogenates of an rPrP-res–inoculated mouse or mice inoculated with control inocula 1 to 3 were digested at 37°C for 1 hour with the indicated concentrations of PK. PrP was detected by immunoblot analysis with M20 antibody to PrP. (**H**) Brain homogenates of mice that received second-round transmission or control mice inoculated with inoculum diluent [phosphate-buffered saline (PBS)] were digested by PK (50 μg/ml) at 37°C for 1 hour. PrP was detected by immunoblot analysis with POM1 antibody to PrP. Number indicates the mouse from which the inocula were prepared.

time was 166 ± 1.5 days (fig. S11). The marginal increase in the survival time of second-round transmission could be due to the reported variation among inoculation experiments (*23*) or to the influence of other components in the brain homogenate used in second-round transmission. Nonetheless, PrP^{Sc} was detected in all groups of mice inoculated with diseased mouse brain homogenates, but not in control mice (Fig. 3H). The spongiosis pattern remained similar to that of rPrP-res–inoculated mice (fig. S12). Thus, similar to natural prion disease, the rPrP-res–caused disease can be serially transmitted.

Inadvertent contamination is always a concern for PMCA. The only naturally occurring prion used in our lab was the RML strain, which was used only three times in our failed attempts to convert recPrP. During the past 2 years while we were working with rPrP-res, absolutely no naturally occurring prion was used. Our latest de novo rPrP-res formation (fig. S2) was achieved in a new sonicator, and the substrate was prepared in a lab that has never been exposed to prion. Furthermore, both the behavioral and pathological phenotypes of rPrP-res–inoculated mice were clearly different from those reported for RML-infected mice (*24*). Thus, it is highly unlikely that rPrP-res formation was due to an inadvertent contamination. Note also that before the inoculum was prepared, the rPrP-res had been propagated for more than 35 rounds of PMCA. Thus, even if the initial rPrP-res formation were due to contamination, the $>10^{35}$ dilution had ensured that recPrP was the only PrP in the inoculum (Fig. 2A). We therefore conclude that the disease-causing agent was rPrP-res.

The three main components in our system were recPrP, POPG, and RNA. The purity of recPrP was verified by silver staining, and recPrP was the only protein detected (fig. S13). The mouse liver RNA was chosen because PrP is not normally expressed in liver and because ectopic PrP expression in the liver of PrP-null mice does not support prion propagation (*25*). Because synthetic polyanions that do not encode protein can replace RNA in cell-free prion formation and propagation (*9*, *16*, *17*), the likely role of RNA in generating infectious prions is to facilitate PrP conversion rather than to encode an infectious protein. Indeed, we were able to propagate rPrP-res with the use of synthetic polyadenylated RNA (fig. S14), which shows that rPrP-res can be generated with virtually completely defined components. The requirement of lipid is in accordance with previous reports of higher prion infectivity in lipid membrane–associated PrP^{Sc} (*22*, *26*). Notably, the purified GPI-anchored PrP^{C}, which was used to produce infectious prion de novo (*9*), contained stoichiometric amounts of copurified lipids, supporting a general role of lipid in PrP conversion. Of note, the POPG and RNA used here may simply mimic one or more unknown in vivo facilitating factors. Further studies are required to identify these factors.

Our results provide direct evidence in support of the prion hypothesis. We found that rPrP-res is in a conformational state similar to the pathogenic PrP^{Sc} isoform, that rPrP-res possesses the self-perpetuating characteristic of a prion, and that rPrP-res causes bona fide prion disease in wild-type mice. The fact that only rPrP-res–inoculated mice developed prion disease establishes that prion disease is caused by the altered conformational form of PrP.

References and Notes

1. S. B. Prusiner, *Science* **216**, 136 (1982).
2. B. Caughey, G. S. Baron, B. Chesebro, M. Jeffrey, *Annu. Rev. Biochem.* **78**, 177 (2009).
3. A. Aguzzi, F. Baumann, J. Bremer, *Annu. Rev. Neurosci.* **31**, 439 (2008).
4. J. Collinge, A. R. Clarke, *Science* **318**, 930 (2007).
5. H. Büeler *et al.*, *Cell* **73**, 1339 (1993).
6. D. A. Kocisko *et al.*, *Nature* **370**, 471 (1994).
7. R. A. Bessen *et al.*, *Nature* **375**, 698 (1995).
8. J. Castilla, P. Saá, C. Hetz, C. Soto, *Cell* **121**, 195 (2005).
9. N. R. Deleault, B. T. Harris, J. R. Rees, S. Supattapone, *Proc. Natl. Acad. Sci. U.S.A.* **104**, 9741 (2007).
10. G. Legname *et al.*, *Science* **305**, 673 (2004).
11. G. C. Telling *et al.*, *Science* **274**, 2079 (1996).
12. C. Weissmann, *Cell* **122**, 165 (2005).
13. L. Manuelidis, *J. Cell. Biochem.* **100**, 897 (2007).
14. B. Caughey, G. S. Baron, *Nature* **443**, 803 (2006).
15. N. R. Deleault, R. W. Lucassen, S. Supattapone, *Nature* **425**, 717 (2003).
16. N. R. Deleault *et al.*, *J. Biol. Chem.* **280**, 26873 (2005).
17. J. C. Geoghegan *et al.*, *J. Biol. Chem.* **282**, 36341 (2007).
18. S. H. White, A. S. Ladokhin, S. Jayasinghe, K. Hristova, *J. Biol. Chem.* **276**, 32395 (2001).
19. F. Wang *et al.*, *Biochemistry* **46**, 7045 (2007).
20. See supporting material on *Science* Online.
21. T. Pan *et al.*, *J. Virol.* **79**, 12355 (2005).
22. G. S. Baron, A. C. Magalhães, M. A. Prado, B. Caughey, *J. Virol.* **80**, 2106 (2006).
23. G. Tamgüney *et al.*, *J. Gen. Virol.* **89**, 1777 (2008).
24. J. Castilla *et al.*, *EMBO J.* **27**, 2557 (2008).
25. A. J. Raeber *et al.*, *Proc. Natl. Acad. Sci. U.S.A.* **96**, 3987 (1999).
26. R. Gabizon, M. P. McKinley, S. B. Prusiner, *Proc. Natl. Acad. Sci. U.S.A.* **84**, 4017 (1987).

27. We thank. A. Aguzzi, M.-S. Sy, and B. Wainer for reagents and A. Steele for comments on the manuscript. Supported by the Ellison Medical Foundation, NIH grant R01NS060729, and Ministry of Education of China project 985.

Supporting Online Material

www.sciencemag.org/cgi/content/full/science.1183748/DC1
Materials and Methods
Figs. S1 to S14
Movies S1 to S3
References

23 October 2009; accepted 18 January 2009
Published online 28 January 2009;
10.1126/science.1183748
Include this information when citing this paper.

Inhibition of NF-κB Signaling by A20 Through Disruption of Ubiquitin Enzyme Complexes

Noula Shembade,[1]* Averil Ma,[2] Edward W. Harhaj[1]*

A20 negatively regulates inflammation by inhibiting the nuclear factor κB (NF-κB) transcription factor in the tumor necrosis factor receptor (TNFR) and Toll-like receptor (TLR) pathways. A20 contains deubiquitinase and E3 ligase domains and thus has been proposed to function as a ubiquitin-editing enzyme downstream of TNFR1 by inactivating ubiquitinated RIP1. However, it remains unclear how A20 terminates NF-κB signaling downstream of TLRs. We have shown that A20 inhibited the E3 ligase activities of TRAF6, TRAF2, and cIAP1 by antagonizing interactions with the E2 ubiquitin conjugating enzymes Ubc13 and UbcH5c. A20, together with the regulatory molecule TAX1BP1, interacted with Ubc13 and UbcH5c and triggered their ubiquitination and proteasome-dependent degradation. These findings suggest a mechanism of A20 action in the inhibition of inflammatory signaling pathways.

The zinc finger protein A20 (also known as TNFAIP3) has an essential role in limiting the strength and duration of NF-κB signaling (*1*). A20-deficient mice die prematurely from multiorgan inflammation and cachexia, and A20-deficient cells exhibit a defect in the termination of tumor necrosis factor–α (TNF-α) and lipopolysaccharide (LPS)–induced NF-κB signaling (*2*, *3*). A20 requires several regulatory proteins, including Tax1 binding protein 1 (TAX1BP1), and the E3 ubiquitin ligases Itch and ring finger protein 11 (RNF11), to restrict NF-κB activation (*4*–*6*). A20 functions as a ubiquitin-editing enzyme with both deubiquitinating (DUB) and ubiquitin E3 ligase activity toward the adaptor protein and death-domain containing protein kinase, receptor-interacting protein 1 (RIP1) in the TNFR pathway (*7*). A20 first cleaves lysine 63 (K63)–linked polyubiquitin chains on RIP1 and then conjugates lysine 48 (K48)–linked polyubiquitin chains that target RIP1 for degradation by the proteasome (*7*). A20 also inhibits the polyubiquitination and activation of the E3 ubiquitin ligase TNF receptor–associated factor 6 (TRAF6) in the Toll-like receptor 4 and interleukin-1 receptor (TLR4/IL-1R) pathways

[1]Department of Microbiology and Immunology, Sylvester Comprehensive Cancer Center, The University of Miami, Miller School of Medicine, Miami, FL 33136, USA. [2]Department of Medicine, University of California at San Francisco, San Francisco, CA 94143, USA.

*To whom correspondence should be addressed. E-mail: nshembade@med.miami.edu (N.S.); eharhaj@med.miami.edu (E.W.H.)

(*3*); however, it is unclear whether A20 functions by a similar mechanism to inhibit TRAF6.

To investigate the mechanism of TRAF6 regulation by A20, we examined TRAF6 protein-protein interactions by coimmunoprecipitation in cells stimulated with IL-1. Wild-type mouse embryonic fibroblasts (MEFs) or MEFs that lack expression of A20 (*A20*$^{-/-}$) or TAX1BP1 (*Tax1bp1*$^{-/-}$) were treated with IL-1 for various times, and the interactions between TRAF6, A20, and TAX1BP1 were monitored by immunoprecipitations and protein immunoblotting (Fig. 1 and fig. S1). A20 and TAX1BP1 were recruited to TRAF6 with distinct kinetics. Whereas TAX1BP1 interacted with TRAF6 after 15 min of IL-1 treatment, A20 recruitment to TRAF6 was delayed until 45 min of stimulation (Fig. 1A). No binding was observed when immunoprecipitations were performed with a control rabbit immunoglobulin antibody (Fig. 1B). TAX1BP1 recruitment to TRAF6 was impaired in A20-deficient MEFs (Fig. 1A). Interaction of A20 with TRAF6 was also dependent on TAX1BP1 (fig. S1A). The A20 and TAX1BP1 regulatory proteins Itch and RNF11 were also recruited to TRAF6 at early time points, together with TAX1BP1, although the interactions with TRAF6 were transient (Fig. 1A). TRAF6 polyubiquitination and activation is dependent on the E2 enzyme Ubc13 (*8*, *9*). TRAF6 interaction with Ubc13 was stimulus-dependent and was lost after 45 min of IL-1 stimulation, coinciding with the recruitment of A20 to TRAF6. The TRAF6-Ubc13 interaction was more persistent in *A20*$^{-/-}$ and *Tax1bp1*$^{-/-}$ MEFs treated with IL-1 (Fig. 1A and fig. S1A). Because Ubc13 may regulate NF-κB in stimulus- and cell type–specific ways (*10*), we also examined interactions of TRAF6 with the E2 enzyme UbcH5c (also known as Ube2D3), which functions with TRAF6 to synthesize unanchored polyubiquitin chains that activate IκB kinase (IKK) (*11*). TRAF6 and UbcH5c interacted transiently after IL-1 stimulation in control MEFs (Fig. 1A). However, binding of TRAF6 to UbcH5c was prolonged in A20-deficient MEFs (Fig. 1A). The persistent interactions between TRAF6 and the E2 enzymes Ubc13 and UbcH5c coincided with enhanced

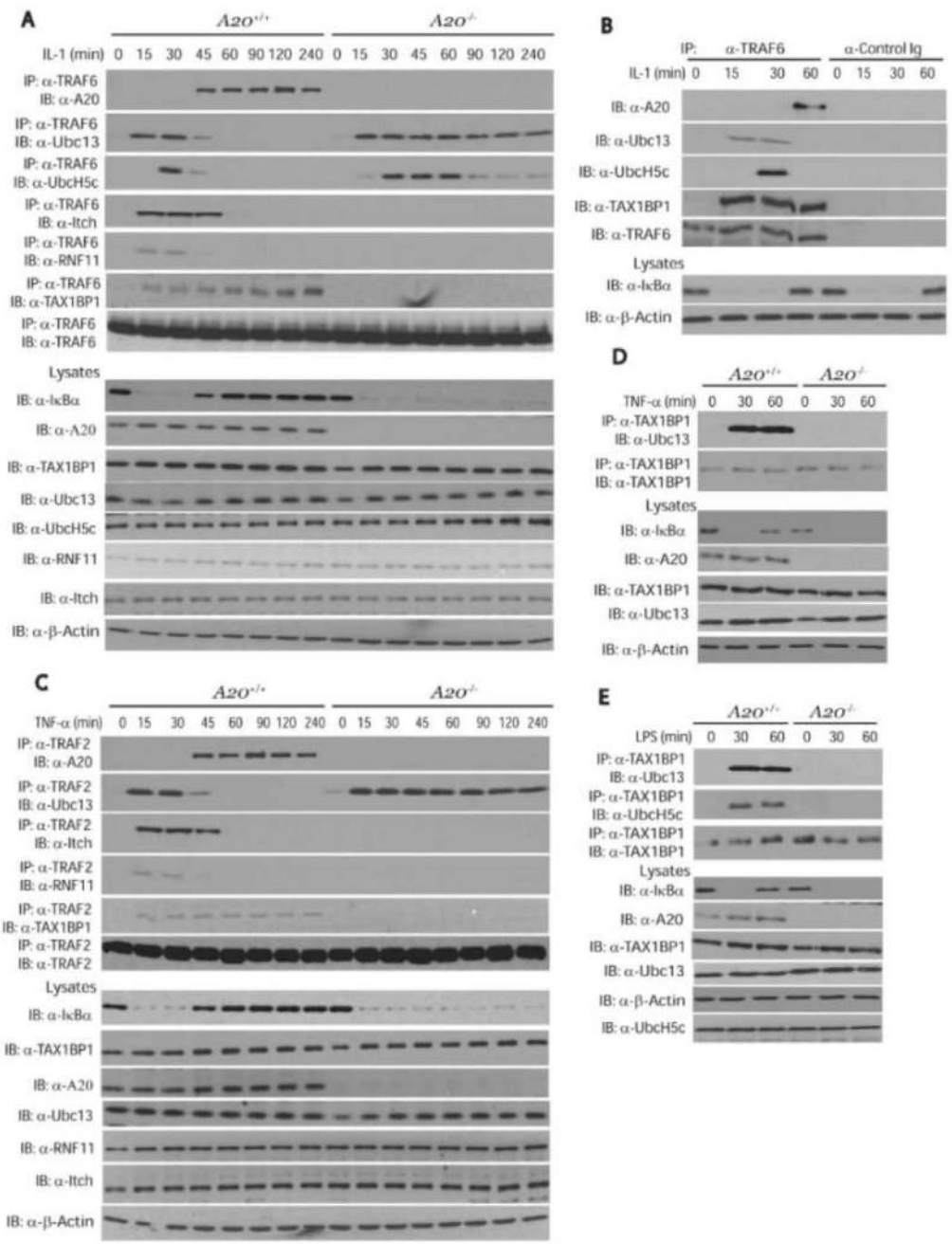

Fig. 1. Disruption of interactions between E2 and E3 enzymes in the TNFR and TLR4/IL-1R pathways by A20 and TAX1BP1. (**A**) Kinetics of TRAF6, Ubc13, UbcH5c, Itch, RNF11, A20, and TAX1BP1 interactions in control and A20-deficient MEFs. *A20*$^{+/+}$ and *A20*$^{-/-}$ MEFs were stimulated with IL-1 for the indicated times. Proteins from lysates were immunoprecipitated with TRAF6 antibody and detected by immunoblotting with antibodies to A20, Ubc13, UbcH5c, Itch, RNF11, TAX1BP1, or TRAF6. Lysates were subjected to immunoblotting with antibodies to IκBα, A20, TAX1BP1, Ubc13, UbcH5c, RNF11, Itch, and β-actin. (**B**) Specificity of TRAF6, Ubc13, A20, UbcH5c, and TAX1BP1 interactions. *A20*$^{+/+}$ MEFs were stimulated with IL-1 for the indicated times. Proteins from lysates were immunoprecipitated with TRAF6 or control rabbit antibody [Cont. IgG (immunoglobulin G)] and detected by immunoblotting with antibodies to A20, Ubc13, UbcH5c, TAX1BP1, or TRAF6. Lysates were subjected to immunoblotting with antibodies to IκBα and β-actin. (**C**) Kinetics of TRAF2, Ubc13, Itch, RNF11, A20, and TAX1BP1 interactions in control and A20-deficient MEFs. *A20*$^{+/+}$ and *A20*$^{-/-}$ MEFs were stimulated with TNF-α, and proteins from lysates were immunoprecipitated with TRAF2 antibody followed by immunoblotting with antibodies to A20, Ubc13, Itch, RNF11, TAX1BP1, and TRAF2. Lysates were subjected to immunoblotting with antibodies to IκBα, TAX1BP1, A20, Ubc13, RNF11, Itch, and β-actin. (**D** and **E**) Interaction of TAX1BP1 with Ubc13. *A20*$^{+/+}$ and *A20*$^{-/-}$ MEFs were stimulated with TNF-α (D) or LPS (E) for 30 and 60 min, and proteins from lysates were immunoprecipitated with antibody to TAX1BP1, followed by immunoblotting with antibodies to Ubc13, UbcH5c, or TAX1BP1. Lysates were subjected to immunoblotting with antibodies to IκBα, A20, TAX1BP1, Ubc13, and β-actin. The results shown are representative of three independent experiments. IP, immunoprecipitation; IB, immunoblot.

degradation of IκBα and activation of NF-κB in *A20*$^{-/-}$ and *Tax1bp1*$^{-/-}$ MEFs (Fig. 1A) (*3*, *4*).

Ubc13 also functions as an E2 enzyme for other E3 ligases, including TRAF2 and cIAP1 in the TNFR pathway (*12*, *13*). Therefore, we investigated whether A20 targeted TRAF2-Ubc13 and cIAP1-Ubc13 complexes for inactivation in the TNFR1 pathway. TRAF2 interacted transiently with Ubc13 in a TNF-α–dependent manner, and the interaction was disrupted upon recruitment of A20 to TRAF2 (Fig. 1C). However, in *A20*$^{-/-}$ and *Tax1bp1*$^{-/-}$ MEFs, the TRAF2-Ubc13 interaction was persistent after stimulation with TNF-α (Fig. 1C and fig. S1B). Similar results were obtained with cIAP1 and Ubc13 (fig. S1C). We also confirmed that A20 interacted with Ubc13 in a stimulus-dependent manner in both primary bone marrow–derived macrophages (BMDMs) and dendritic cells (BMDCs) (fig. S1, D and E). A20 and TAX1BP1 were dependent on each other to interact with Ubc13 in cells treated with TNF-α or LPS (Fig. 1, D and E, and fig. S1, F and G). Collectively, these results indicate that A20 and TAX1BP1 function together to disrupt interactions among the E3 ligases TRAF6, TRAF2, and c-IAP1 and the E2 enzymes Ubc13 and UbcH5c.

TRAF6 is activated in cells treated with LPS or IL-1 and is auto-ubiquitinated in a Ubc13-dependent manner (*8*, *14*, *15*). As expected, TRAF6 ubiquitination was transient in control

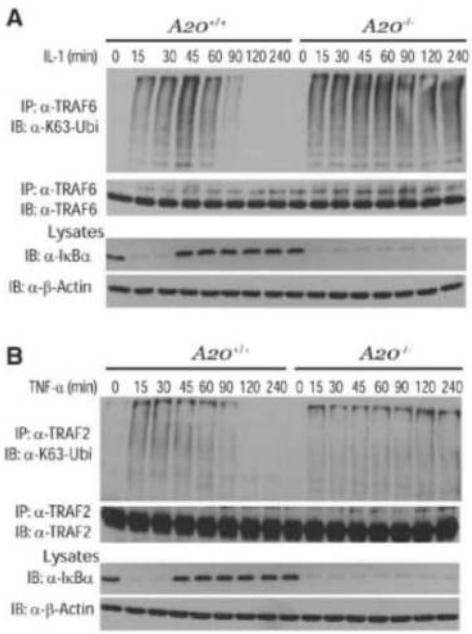

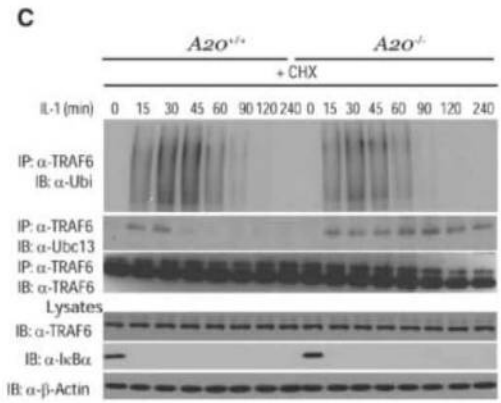

Fig. 2. Negative regulation of TRAF2 and TRAF6 polyubiquitination by A20. (**A**) Kinetics of TRAF6 ubiquitination. *A20*$^{+/+}$ and *A20*$^{-/-}$ MEFs were stimulated with IL-1 for the indicated times. Proteins from lysates were immunoprecipitated with antibody to TRAF6, eluted with 1% SDS, diluted in lysis buffer, reimmunoprecipitated with TRAF6 antibody followed by immunoblotting with K63-specific antibody to Ubi or antibody to TRAF6. Lysates were subjected to immunoblotting with antibodies to IκBα or β-actin. (**B**) Kinetics of TRAF2 ubiquitination. *A20*$^{+/+}$ and *A20*$^{-/-}$ MEFs were stimulated with TNF-α for the indicated times. Proteins from lysates were immunoprecipitated with antibody to TRAF2, eluted with 1% SDS, diluted in lysis buffer, and reimmunoprecipitated with TRAF2 antibody, followed by immunoblotting with antibodies to Ubi or TRAF2. Lysates were subjected to immunoblotting with antibodies to IκBα and β-actin. (**C**) Stability of ubiquitinated TRAF6. *A20*$^{+/+}$ and *A20*$^{-/-}$ MEFs were pretreated with cycloheximide, followed by IL-1 stimulation for the indicated times. Proteins from lysates were immunoprecipitated with antibody to TRAF6 as described (A), followed by immunoblotting with antibodies to Ubi, Ubc13, or TRAF6. Lysates were subjected to immunoblotting with antibodies to TRAF6, IκBα, and β-actin. The results shown are representative of three independent experiments.

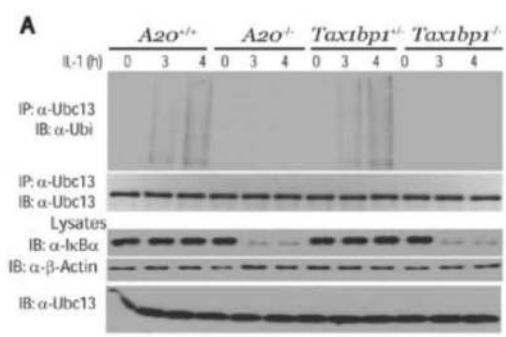

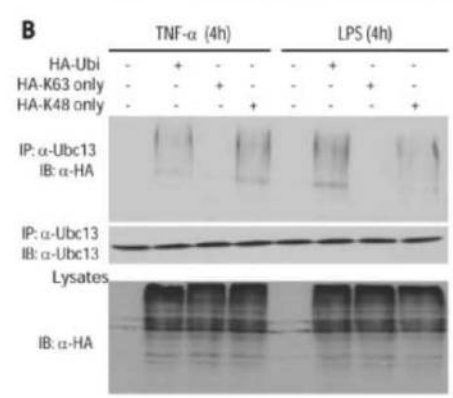

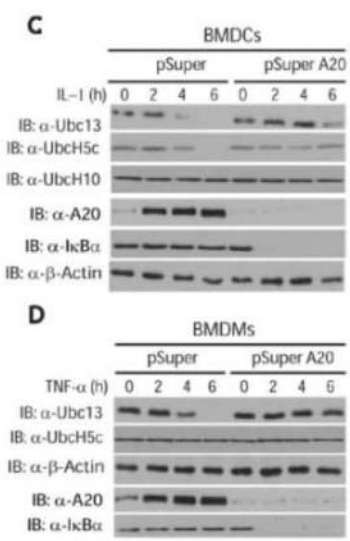

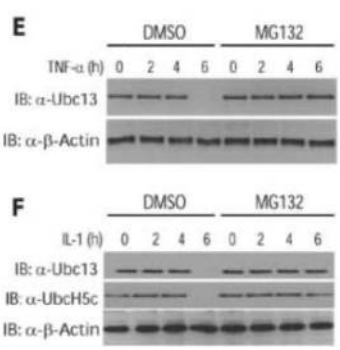

Fig. 3. The ubiquitination and degradation of Ubc13 is promoted by A20 and TAX1BP1. (**A**) Polyubiquitination of Ubc13 in cells stimulated with IL-1. Control, *A20*$^{-/-}$, or *Tax1bp1*$^{-/-}$ MEFs were treated with IL-1 for the indicated times. Proteins from lysates were immunoprecipitated with antibody to Ubc13, eluted with 1% SDS, diluted in lysis buffer, and reimmunoprecipitated with Ubc13 antibody, followed by immunoblotting with antibodies to Ubi or Ubc13. Lysates were subjected to immunoblotting with antibodies to IκBα, Ubc13, and β-actin. (**B**) K48-linked polyubiquitination of Ubc13. Control MEFs were transiently transfected with plasmids encoding HA-Ubi, HA-Ubi-K63 only, or HA-Ubi-K48 only. After 36 hours, cells were stimulated for 4 hours with either TNF-α or LPS. Ubiquitination assays were performed as described in (A). Lysates were subjected to immunoblotting with antibody to HA. (**C** and **D**) Requirement of A20 for the degradation of Ubc13 and UbcH5c. BMDCs (C) or BMDMs (D) were transiently transfected with pSuper or pSuper A20 siRNA plasmids. After 36 hours, cells were stimulated with either IL-1 or TNF-α for the indicated times. Lysates were subjected to immunoblotting with antibodies to Ubc13, UbcH5c, UbcH10, A20, IκBα, or β-actin. (**E** and **F**) Proteasome-dependent degradation of Ubc13. Control MEFs were treated with TNF-α (E) or IL-1 (F) for the indicated times in the presence of MG132 or vehicle [dimethyl sulfoxide (DMSO)]. Lysates were subjected to immunoblotting with antibodies to Ubc13, UbcH5c, and β-actin. The results shown are representative of three independent experiments.

MEFs, in sharp contrast to the persistent TRAF6 ubiquitination observed in *A20*$^{-/-}$ and *Tax1bp1*$^{-/-}$ MEFs upon IL-1 stimulation (Fig. 2A and fig. S2A). Interleukin-1 receptor-associated kinase 1 (IRAK1) functions upstream of TRAF6 in the IL-1R pathway and is regulated by K63-linked polyubiquitination (*16*). However, A20 or TAX1BP1 deficiency had no effect on the ubiquitination or degradation of IRAK1 (fig. S2B). TRAF2 and RIP1 ubiquitination were also prolonged in *A20*$^{-/-}$ and *Tax1bp1*$^{-/-}$ MEFs upon stimulation with TNF-α (Fig. 2B and fig. S2D). Finally, the stability of ubiquitinated TRAF6 was similar in control and *A20*$^{-/-}$ or *Tax1bp1*$^{-/-}$ MEFs treated with IL-1 and the protein synthesis inhibitor cycloheximide (CHX) (Fig. 2C and fig. S2F).

Because A20 promotes K48-linked ubiquitination and proteasomal degradation of RIP1 in the TNFR pathway (*7*), but does not promote degradation of TRAF6 in cells stimulated with IL-1 (Fig. 2C), we next investigated whether A20 targeted Ubc13 for degradation. Treatment of cells with IL-1 or TNF-α triggered the ubiquitination of endogenous Ubc13 in control MEFs but not in *A20*$^{-/-}$ or *Tax1bp1*$^{-/-}$ MEFs (Fig. 3A and fig. S3). To determine the type of Ubc13 polyubiquitin chains, we transfected MEFs with a hemagglutinin (HA)–tagged wild-type ubiquitin or ubiquitin mutants with substitution of arginine for all lysine residues except the lysine at position 48 (K48-only mutant) or the lysine at position 63 (K63-only mutant). Ubc13 polyubiquitination was observed in cells treated with either TNF-α or LPS and expressing either wild-type HA-Ubi or HA-Ubi K48-only (Fig. 3B), which suggests that Ubc13 ubiquitination was predominantly K48-linked, leading to proteasome-mediated degradation. Indeed, Ubc13 degradation was observed in primary BMDCs or BMDMs after treatment with IL-1 (Fig.

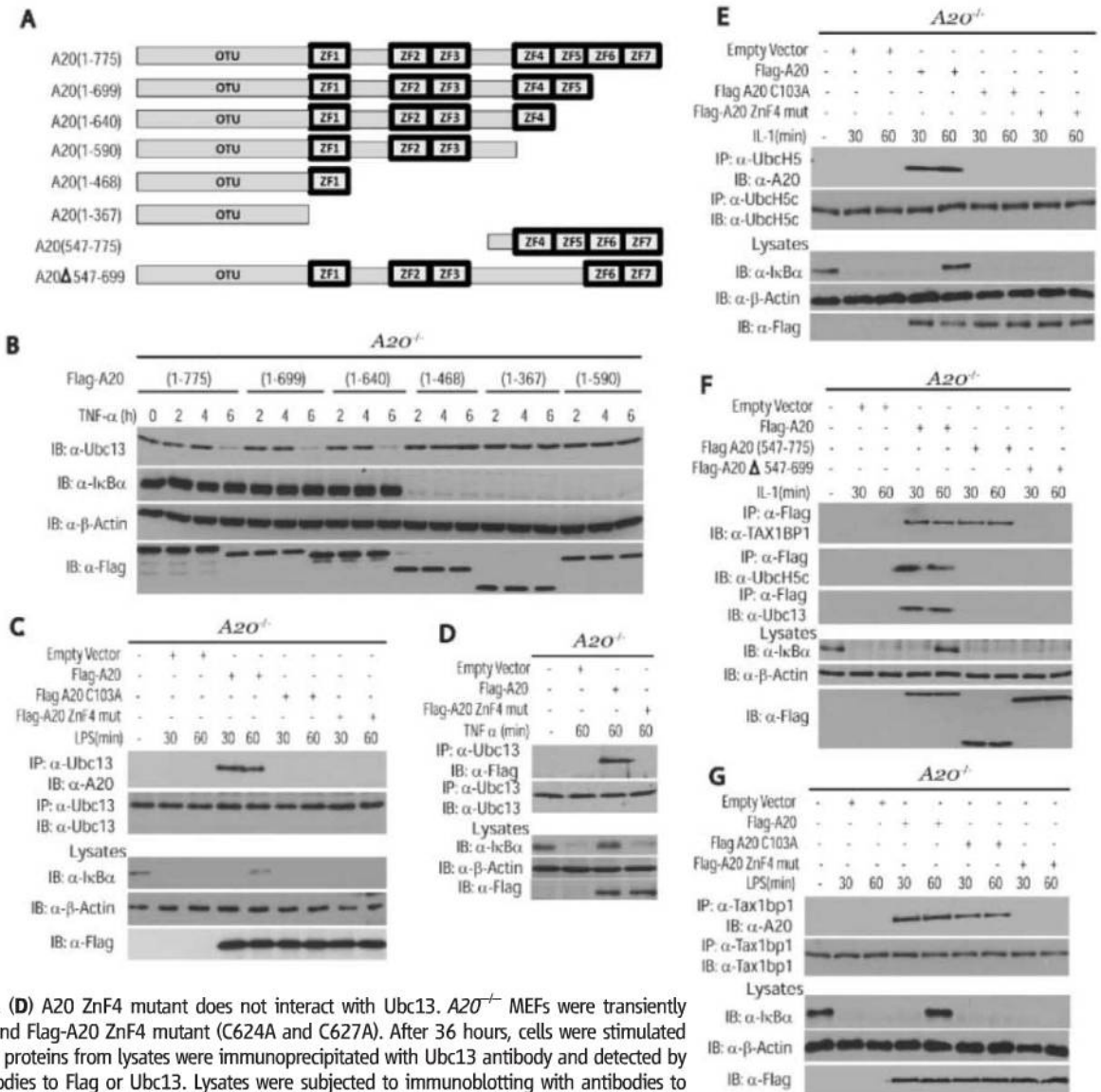

Fig. 4. Requirement of A20 zinc finger 4 for TAX1BP1 binding and degradation of Ubc13 and UbcH5c. (**A**) Schematic of A20 deletion mutants. (**B**) Requirement of A20 ZnF4 for the degradation of Ubc13. *A20*$^{-/-}$ MEFs were transiently transfected with the indicated mutants. After 36 hours, cells were treated with TNF-α for the indicated times. Lysates were subjected to immunoblotting with antibodies to Ubc13, IκBα, β-actin, or Flag. (**C**) A20 DUB and ZnF4 mutants do not interact with Ubc13. *A20*$^{-/-}$ MEFs were transiently transfected with Flag-A20, Flag-A20 (C103A), and Flag-A20 ZnF4 mutant (C624A and C627A). After 36 hours, cells were stimulated with LPS for the indicated times, and proteins from lysates were immunoprecipitated with Ubc13 antibody and detected by immunoblotting with antibodies to A20 or Ubc13. Lysates were subjected to immunoblotting with antibodies to Flag, IκBα, and β-actin. (**D**) A20 ZnF4 mutant does not interact with Ubc13. *A20*$^{-/-}$ MEFs were transiently transfected with Flag-A20 and Flag-A20 ZnF4 mutant (C624A and C627A). After 36 hours, cells were stimulated with TNF-α for 60 min, and proteins from lysates were immunoprecipitated with Ubc13 antibody and detected by immunoblotting with antibodies to Flag or Ubc13. Lysates were subjected to immunoblotting with antibodies to Flag, IκBα, and β-actin. (**E**) A20 DUB and ZnF4 mutants do not interact with UbcH5c. *A20*$^{-/-}$ MEFs were transiently transfected with plasmids as described in (C). After 36 hours, cells were stimulated with IL-1 for the indicated times, and proteins from lysates were immunoprecipitated with UbcH5c antibody and detected by immunoblotting with antibodies to A20 or UbcH5c. Lysates were subjected to immunoblotting with antibodies to Flag, IκBα, and β-actin. (**F**) Differential requirement for the A20 OTU domain and C-terminal zinc fingers in binding to TAX1BP1, Ubc13, and UbcH5c. *A20*$^{-/-}$ MEFs were transiently transfected with empty vector, Flag-A20, Flag-A20 (547-775) or Flag-A20Δ547-699. After 36 hours, cells were treated with IL-1 for either 30 or 60 min. Proteins from lysates were immunoprecipitated with antibody to Flag, followed by immunoblotting with antibodies to TAX1BP1, UbcH5c, or Ubc13. Lysates were subjected to immunoblotting with antibodies to IκBα, Flag, and β-actin. (**G**) A20 ZnF4 mutant does not interact with TAX1BP1. *A20*$^{-/-}$ MEFs were transiently transfected with plasmids as described in (C). After 36 hours, cells were stimulated with LPS for the indicated times, and proteins from lysates were immunoprecipitated with TAX1BP1 antibody and detected by immunoblotting with antibodies to A20 and TAX1BP1. Lysates were subjected to immunoblotting with antibodies to Flag, IκBα, and β-actin. The results shown are representative of three independent experiments.

3C) or TNF-α (Fig. 3D). Stimulus-dependent degradation of UbcH5c also occurred, but only in response to IL-1 and not to TNF-α (Fig. 3, C and D, and fig. S4, A and C). Knockdown of A20 with small interfering RNA (siRNA) prevented the degradation of both Ubc13 and UbcH5c (Fig. 3, C and D). However, the E3 ubiquitin ligases RNF11 and Itch were both dispensable for Ubc13 degradation, despite the requirement of Itch for the attenuation of TRAF6 ubiquitination (fig. S5). Ubc13 was also degraded in response to IL-1 and TNF-α in MEFs in an A20- and TAX1BP1-dependent manner (fig. S4). Finally, TNF-α and IL-1–induced Ubc13 and UbcH5c degradation was blocked by the proteasome inhibitor MG-132 (Fig. 3, E and F).

A20 inhibits RIP1 activation in the TNFR pathway through its deubiquitinase and E3 ligase activities; however, whether these activities are required for the down-regulation of Ubc13 and UbcH5c is unknown. A20 contains an N-terminal ovarian tumor (OTU) DUB domain and seven C-terminal zinc finger domains (Fig. 4A). A20-deficient MEFs were reconstituted with various Flag-tagged A20 deletion mutants to determine the domain(s) important for the degradation of Ubc13 and UbcH5c. Deletion of zinc fingers 5 through 7 had no effect on the degradation of Ubc13 or UbcH5c (Fig. 4B and fig. S6). However, deletion of zinc finger 4 (ZnF4) abrogated A20-mediated degradation of Ubc13 and UbcH5c (Fig. 4B and fig. S6), correlating with published reports on the importance of ZnF4 in A20-mediated inhibition of NF-κB (*17*). The degradation of Ubc13 and UbcH5c by A20 appeared to be specific because UbcH10 (also known as Ube2c) was not degraded in cells treated with IL-1 (fig. S6). Reconstitution studies in *A20*$^{-/-}$ MEFs revealed that wild-type A20, but not A20 C103A, disrupted the binding of TRAF6 and Ubc13 (fig. S7A). Overexpression of the deubiquitinating enzyme cylindromatosis (CYLD) exerted no effect on TRAF6 and Ubc13 binding, which suggests that CYLD uses a distinct mechanism to inhibit TRAF6 ubiquitination (fig. S7A). Similarly, A20, but not A20 C103A or CYLD, efficiently inhibited TRAF2-Ubc13 binding in TNF-α–stimulated *A20*$^{-/-}$ MEFs (fig. S7B). Although wild-type A20 interacted with endogenous Ubc13 and UbcH5c in cells stimulated with LPS or IL-1, both A20 C103A and A20 ZnF4 mutants were defective for binding to Ubc13 and UbcH5c (Fig. 4, C to E) and thus were unable to inhibit TRAF6 ubiquitination or promote Ubc13 degradation (fig. S8, A to C). A20 C103 and ZnF4 were also required for TAX1BP1 to interact with Ubc13 (fig. S8D). Furthermore, A20 deletion mutants lacking either the OTU domain or zinc fingers 4 and 5 were not associated with Ubc13 or UbcH5c (Fig. 4F). However, for TAX1BP1 binding, the OTU domain was dispensable and only ZnF4 was critical (Fig. 4, F and G) (*17*). Collectively, these results indicate that A20 ZnF4 is important for binding to TAX1BP1, whereas the OTU domain and ZnF4 are important for binding to Ubc13 and UbcH5c.

The human T cell leukemia virus type I (HTLV-I) Tax oncoprotein promotes a persistent NF-κB response, in part, by interacting with TAX1BP1 and disrupting the interactions between A20, TAX1BP1, and Itch (*5*). Because Tax interacts with Ubc13 (*18*), we hypothesized that Tax would prevent A20 from binding to Ubc13, thereby protecting Ubc13 from degradation. Indeed, Tax impaired the TNF-α–dependent interaction of A20 with Ubc13 (fig. S9A), as well as TNF-α–mediated degradation of Ubc13 (fig. S9B). Tax also prevented A20 from binding to TRAF6 in response to IL-1 stimulation (fig. S9C). The Tax point mutant Tax M22, but not Tax M47, is defective for NF-κB activation (*19*). Tax M22, but not Tax M47, failed to bind to Ubc13 (fig. S9D). Thus, Tax preserves E2:E3 enzyme complexes essential for NF-κB activation and prevents Ubc13 degradation, which is essential for Tax polyubiquitination (*18*).

The importance of A20 in limiting inflammation is underscored by the numerous human autoimmune diseases associated with polymorphisms in the A20 genomic region (*20*–*22*). A20 also functions as a tumor suppressor gene for B cell lymphomas (*23*, *24*). Our findings indicate that A20 disrupts key E2 and E3 ubiquitin enzyme complexes in both TNFR and TLR pathways. A20 binding to E2 or E3 enzymes may sterically interfere with their interactions, or alternatively A20 may directly modify E2 or E3 enzymes that antagonize their interactions.

References and Notes

1. B. Coornaert, I. Carpentier, R. Beyaert, *J. Biol. Chem.* **284**, 8217 (2009).
2. E. G. Lee *et al.*, *Science* **289**, 2350 (2000).
3. D. L. Boone *et al.*, *Nat. Immunol.* **5**, 1052 (2004).
4. N. Shembade, N. S. Harhaj, D. J. Liebl, E. W. Harhaj, *EMBO J.* **26**, 3910 (2007).
5. N. Shembade *et al.*, *Nat. Immunol.* **9**, 254 (2008).
6. N. Shembade, K. Parvatiyar, N. S. Harhaj, E. W. Harhaj, *EMBO J.* **28**, 513 (2009).
7. I. E. Wertz *et al.*, *Nature* **430**, 694 (2004).
8. B. Lamothe *et al.*, *J. Biol. Chem.* **282**, 4102 (2007).
9. T. Fukushima *et al.*, *Proc. Natl. Acad. Sci. U.S.A.* **104**, 6371 (2007).
10. M. Yamamoto *et al.*, *Nat. Immunol.* **7**, 962 (2006).
11. Z. P. Xia *et al.*, *Nature* **461**, 114 (2009).
12. C. S. Shi, J. H. Kehrl, *J. Biol. Chem.* **278**, 15429 (2003).
13. M. J. Bertrand *et al.*, *Mol. Cell* **30**, 689 (2008).
14. J. Wooff, L. Pastushok, M. Hanna, Y. Fu, W. Xiao, *FEBS Lett.* **566**, 229 (2004).
15. L. Deng *et al.*, *Cell* **103**, 351 (2000).
16. D. B. Conze, C. J. Wu, J. A. Thomas, A. Landstrom, J. D. Ashwell, *Mol. Cell. Biol.* **28**, 3538 (2008).
17. M. Klinkenberg, S. Van Huffel, K. Heyninck, R. Beyaert, *FEBS Lett.* **498**, 93 (2001).
18. N. Shembade, N. S. Harhaj, M. Yamamoto, S. Akira, E. W. Harhaj, *J. Virol.* **81**, 13735 (2007).
19. M. R. Smith, W. C. Greene, *Genes Dev.* **4**, 1875 (1990).
20. R. Dieguez-Gonzalez *et al.*, *Arthritis Res. Ther.* **11**, R42 (2009).
21. S. L. Musone *et al.*, *Nat. Genet.* **40**, 1062 (2008).
22. E. Y. Fung *et al.*, *Genes Immun.* **10**, 188 (2009).
23. M. Compagno *et al.*, *Nature* **459**, 717 (2009).
24. M. Kato *et al.*, *Nature* **459**, 712 (2009).

25. We thank S. C. Sun, L. Matesic, D. Abbott, C. Vincenz, P. Storz, R. Beyaert, and the Belgian Coordinated Collections of Microorganisms/Laboratory of Molecular Biology of Ghent University (BCCM™/LMBP) for reagents and H. Ishikawa for assistance in the preparation of BMDMs and BMDCs. The project described was supported by NIH grants RO1GM083143 and RO1CA135362 awarded to E.W.H. The content is solely the responsibility of the authors and does not necessarily represent the official views of the National Cancer Institute/National Institute of General Medical Sciences or the National Institutes of Health.

Supporting Online Material

www.sciencemag.org/cgi/content/full/327/5969/1135/DC1
Materials and Methods
Figs. S1 to S9
References

23 September 2009; accepted 14 January 2010
10.1126/science.1182364

Photorhabdus luminescens Toxins ADP-Ribosylate Actin and RhoA to Force Actin Clustering

Alexander E. Lang,[1,2]* Gudula Schmidt,[1]* Andreas Schlosser,[3] Timothy D. Hey,[4] Ignacio M. Larrinua,[4] Joel J. Sheets,[4] Hans G. Mannherz,[5,6] Klaus Aktories[1]†

The bacterium *Photorhabdus luminescens* is mutualistically associated with entomopathogenetic nematodes. These nematodes invade insect larvae and release the bacteria from their intestine, which kills the insects through the action of toxin complexes. We elucidated the mode of action of two of these insecticidal toxins from *P. luminescens*. We identified the biologically active components TccC3 and TccC5 as adenosine diphosphate (ADP)–ribosyltransferases, which modify unusual amino acids. TccC3 ADP-ribosylated threonine-148 of actin, resulting in actin polymerization. TccC5 ADP-ribosylated Rho guanosine triphosphatase proteins at glutamine-61 and glutamine-63, inducing their activation. The concerted action of both toxins inhibited phagocytosis of target insect cells and induced extensive intracellular polymerization and clustering of actin. Several human pathogenic bacteria produce related toxins.

Photorhabdus luminescens colonizes the intestine of infective entomophathogenetic nematodes from the genera *Heterorhabditis* in a symbiotic manner (*1*). The nematodes invade larvae of susceptible insects and release bacteria (*2*). The bacteria reach the insect hemocoel, inhibit insect immunity, proliferate rapidly, and kill the insect larvae usually within 2 days. After proliferation and recolonization by *P. luminescens*, the nematodes invade and kill new insect hosts. Thus, nematodes, harboring the bacteria, can be used as biological insecticides.

P. luminescens produces an array of toxins that are likely involved in pathogenicity against insect hosts and the symbiotic relationship with nematodes (*2*). One major toxin family of *P. luminescens* is the group of the Tc toxin complexes with masses of ~1 million daltons. Each complex is characterized by at least three basic types of functional components: TcA, TcB, and TcC (fig. S1) (*3*, *4*). TcA-like components appear to form tetramers and may be responsible for binding and/or translocation of the toxin complex (*5*). TcB-like components may function as a chaperone and/or a linker between TcA and TcC components (*6*). However, so far the mode of action of Tc toxins has not been understood.

Initially, we studied the effects of the toxins on the phagocytic activity of hemocytes from *Galleria mellonella* because *P. luminescens* infection alters their phagocytic activity. Treatment of hemocytes with the *Photorhabdus* toxin complex 3 (PTC3), which consists of TcdA1 and TcdB2/TccC3 (fig. S1), inhibited phagocytosis (Fig. 1A) (*7*). A similar effect was induced by the *Photorhabdus* toxin complex PTC5, which consists of TcdA1 and TcdB2/TccC5. PTC3 plus PTC5 in combination completely blocked phagocytosis (Fig. 1A). The biological activity depended on the complete toxin complex: TcdA1 or the TcdB2/TccC3 fusion protein alone was ineffective, and TcdB2/TccC5 did not influence phagocytosis in the absence of TcdA1 (Fig. 1A).

Because microfilaments are involved in phagocytic activity, we studied the effects of the toxins on the actin cytoskeleton. PTC3 caused extensive clustering of F-actin in *G. mellonella* hemocytes (Fig. 1B). Again, this effect was not observed when TcdA1 was missing or only the fusion protein TcdB2/TccC3 was applied (fig. S2A). A similar effect was observed with human HeLa cells (Fig. 1B), although it was less strong. To study the effects of TccC3 independently of TcdA1 and TcdB2, we introduced the toxin into target cells by means of the protective antigen (PA), which is the anthrax toxin binding and translocation component. Thus, a His-tag was added to TccC3, which allowed transport via PA into target cells without TcdA1 or TcdB2. His-tagged TccC3 caused the same formation of actin aggregates as observed with PTC3 (fig. S2B). Thus, the biological activity of PTC3 is located in the TccC3 component of the toxin.

PTC5 caused strong stress fiber formation but no actin clustering in *Galleria mellonella* hemocytes and in HeLa cells (Fig. 1B). Application of both PTC3 and PTC5 caused even stronger effects. The actin cytoskeleton was completely aggregated, forming star-like clusters all over the target cell. In HeLa cells, the cortical actin was redistributed, and actin clusters were also observed below the plasma membrane (Fig. 1B). Thus, both toxins induce major changes of the actin cytoskeleton, which most likely cause the inhibition of hemocyte phagocytosis.

TccC3 and TccC5 exhibit sequence similarities with adenosine diphosphate (ADP)–ribosyltransferases (*8*)—especially the "R, S, E" motif, which is typical for almost all ADP-ribosyltransferases and was also found in TccC3 and TccC5 (fig. S3). Using [^{32}P]NAD$^+$, we tested the ADP-ribosylation of proteins in lysates of cells by TccC3. An ~45 kDa protein was selectively labeled by TccC3 in lysates of insect Sf9 and human HeLa cells (fig. S4A). Because the labeled protein comigrated with actin, we directly tested the ADP-ribosylation of purified actin with TccC3 in the presence of [^{32}P]NAD$^+$ (Fig. 2A). This resulted in strong labeling of actin. ADP-ribosylation of actin was also catalyzed by the 32 kDa C-terminal fragment of TccC3, which shows sequence similarity with ADP-ribosyltransferases, indicating a harboring of the enzyme activity (Fig. 2A). Actin is also ADP-ribosylated by the family of binary ADP-ribosylating toxins, including C2 toxin from *C. botulinum* and iota toxin from *C. perfringens* (*9*). However, these toxins, which modify actin at arginine-177 (*10*), cause depolymerization and not polymerization or clustering of actin (*11*). Accordingly, TccC3 did not modify arginine-177. When actin was ADP-ribosylated by C2 toxin, addition of TccC3 and [^{32}P]NAD$^+$ further increased labeling, indicating modification at a different site (fig. S4B). C2 toxin–ADP-ribosylated actin (arginine-177) can be cleaved by neutral hydroxylamine. In contrast, actin ADP-ribosylated by TccC3 was not affected by hydroxylamine (fig. S4C).

Mass analytical data suggested modification of actin at threonine-148 or threonine-149 by TccC3 (fig. S5A). Mutation of both threonine-148 and threonine-149 to alanine of in vitro synthesized (β/γ)-actin confirmed that only threonine-148 was ADP-ribosylated by TccC3 (Fig. 2B).

Threonine-148 is located in the interaction site of actin with the actin monomer-binding protein thymosin-β4, which is involved in the sequestering of monomeric actin and prevents actin polymerization (fig. S6) (*12*). Cross-linking experiments demonstrated that ADP-ribosylation inhibited the interaction of thymosin-β4 with α-actin (Fig. 2C and fig. S7A). To quantify the effect of ADP-ribosylation, the rates of association and dissociation of thymosin-β4 to α-actin covalently modified at Cys374 by N-iodoacetyl-N′-(5-sulfo-1-naphthyl)ethylenediamine (AEDANS) before and after TccC3–ADP-ribosylation were determined by means of fast reaction kinetics (*13*). The rate constant of association of thymosin-β4 decreased from 0.97×10^6 to 0.37×10^6 M^{-1} s^{-1}, and its rate constant of dissociation increased from 3.11 to 8.5 s^{-1} for control and TccC3–ADP-ribosylated actin, respectively (fig. S7B), resulting in an eight-fold higher dissociation constant of the TccC3–ADP-ribosylated actin:thymosin-β4 complex (from 3.2 to 23 μM, under the conditions used).

Next, we studied the effects of thymosin-β4 on actin polymerization after ADP-ribosylation of actin by TccC3. Actin polymerization induced by

[1]Institut für Experimentelle und Klinische Pharmakologie und Toxikologie, Albert-Ludwigs-Universität Freiburg, 79104 Freiburg, Germany. [2]Fakultät für Biologie, Albert-Ludwigs-Universität Freiburg, 79104 Freiburg, Germany. [3]Zentrum für Biosystemanalyse, Core Facility Proteomics, Albert-Ludwigs-Universität Freiburg, 79104 Freiburg, Germany. [4]Discovery Research, Dow AgroSciences, Indianapolis, IN 46268, USA. [5]Physikalische Biochemie, Max-Planck-Institut für molekulare Physiologie, 44227 Dortmund, Germany. [6]Abteilung für Anatomie und Embryologie, Ruhr-Universität Bochum, 44801 Bochum, Germany.

*These authors contributed equally to this work.
†To whom correspondence should be addressed. E-mail: klaus.aktories@pharmakol.uni-freiburg.de

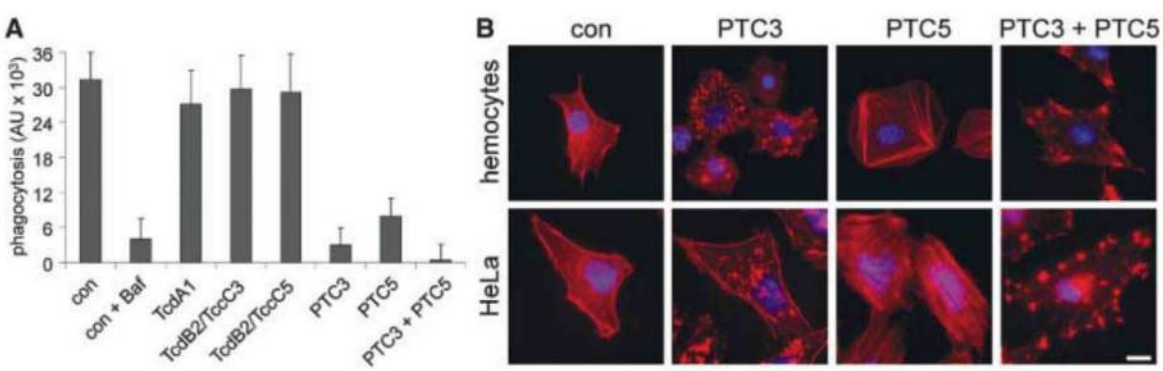

Fig. 1. Influence of *Photorhabdus* Tc proteins on phagocytosis and on the actin cytoskeleton of *G. mellonella* hemocytes and human HeLa cells. (**A**) *G. mellonella* hemocytes were treated with TcdA1, TcdB2/TccC3 or TcdB2/TccC5, PTC3 (TcdA1 + TcdB2/TccC3), or PTC5 (TcdA1 + TcdB2/TccC5) for 30 min. Phagocytosis was measured by increase in fluorescence of hemocytes. Background fluorescence was determined in the presence of bafilomycin A1 (Baf). Data are mean ± SD; $n = 3$ replicates. (**B**) *G. mellonella* hemocytes and HeLa cells were treated with the indicated toxin complexes for 2 hours (hemocytes) or 4 hours (HeLa cells). Then, the cells were fixed and stained with tetramethyl rhodamine isothiocyanate–conjugated phalloidin and 4′,6′-diamidino-2-phenylindole (scale bar, 10 μm).

addition of Mg^{2+} ions was completely prevented in the presence of equimolar thymosin-β4 (Fig. 2D). Polymerization of TccC3–ADP-ribosylated actin was faster than under control conditions. In contrast, addition of thymosin-β4 led to only a slight reduction of the initial velocity of actin polymerization but did not block polymerization of modified actin. Similar results were obtained in studies of the critical concentration of polymerization of actin (Cc) in the presence of thymosin-β4 (fig. S7C). Thus, ADP-ribosylation of actin at threonine-148 reduces the affinity of thymosin-β4 binding to actin and therefore largely eliminates actin sequestration, which may explain the observed increased intracellular content of F-actin. Cross-linking experiments of actin with profilin, which can also sequester actin (*14*), revealed that ADP-ribosylation had no or only a minor effect on the actin-profilin interaction (fig. S7D).

As shown above, PTC5 caused stress fiber formation. We studied the activity of TccC5 by means of in vitro ADP-ribosylation with [^{32}P]NAD$^+$ using insect Sf9 and human HeLa cell lysates. TccC5 catalyzed radioactive labeling of ~20 kDa proteins (Fig. 3A). Because activation of RhoA is known to induce stress fiber formation, we tested recombinant Rho guanosine triphosphatases (GTPases) as substrates of TccC5. TccC5 ADP-ribosylated RhoA and Cdc42 (Fig. 3B). The Rho isoforms RhoA, RhoB, and RhoC are well-known targets of ADP-ribosyltransferase C3 from *C. botulinum* (*15*). This modification occurs at asparagine-41 of RhoA and inhibits the biological activity of RhoA, suggesting a different target site for TccC5. To identify the site of TccC5-catalyzed ADP-ribosylation of Rho, we treated recombinant RhoA with TccC5 in the presence of NAD$^+$ and subjected peptides to mass spectrometric analysis. TccC5 ADP-ribosylated RhoA at glutamine-63 (fig. S5B). The modification site was confirmed by using the mutant proteins Q63E-RhoA or Q63L-RhoA (Q61E-Cdc42 and Q61L-Cdc42), which were not substrates of TccC5, whereas the mutants were still modified by C3 exoenzyme (Fig. 3B). Glutamine-63 of RhoA is deamidated by *Escherichia coli* cytotoxic necrotizing factor 1 (CNF1) (*16*). Accordingly, pretreatment of HeLa cells with CNF1 inhibited subsequent ADP-ribosylation by TccC5 without affecting C3-induced ADP-ribosylation at asparagine-41 (fig. S8A).

Glutamine-63 (glutamine-61 of Rac and Cdc42) plays a pivotal role in the turn-off reaction of Rho GTPases. This amino acid (or an equivalent glutamine residue) is highly conserved in G proteins and is essential for hydrolysis of GTP by the

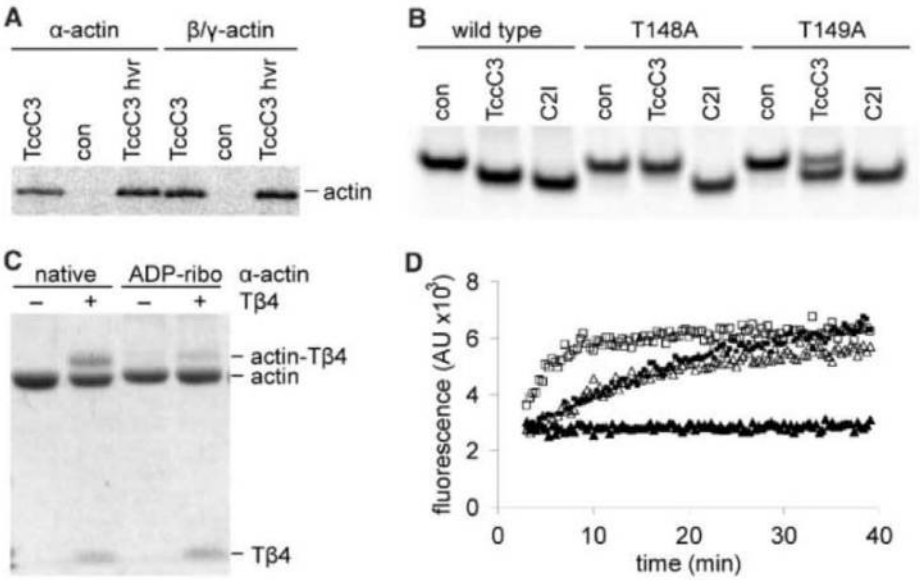

Fig. 2. ADP-ribosylation of actin by TccC3. Toxin effects on thymosin-β4 binding of actin and actin polymerization. (**A**) Purified α-actin and β/γ-actin were incubated for 45 min with [^{32}P]NAD$^+$ and TccC3 or the C-terminal (hvr) ~32 kDa fragment of TccC3. Radio-labeled proteins were detected by means of sodium dodecyl sulfate–polyacrylamide gel electrophoresis (SDS-PAGE) and phosphorimaging. (**B**) In vitro translated and [^{35}S]methionine-radiolabeled β-actin and the actin mutants T148A and T149A were ADP-ribosylated with NAD$^+$ by TccC3 or C2I. Proteins were analyzed by means of native gel electrophoresis and phosphorimaging. (**C**) Native α-actin and TccC3–ADP-ribosylated actin were cross-linked without and with thymosin-β4 (Tβ4) by 1-ethyl-3[3-(dimethylamino)-propyl]carbodiimide (EDC) and, thereafter, analyzed by means of SDS-PAGE (*24*). (**D**) Native α-actin supplemented with pyrene-actin (Δ, ▲) or TccC3–ADP-ribosylated α-actin supplemented with TccC3–ADP-ribosylated pyrene-actin (□, ■) was polymerized by the addition of $MgCl_2$ in the absence (Δ, □) or presence (▲, ■) of thymosin-β4. Polymerization was followed by the increase in pyrene-fluorescence.

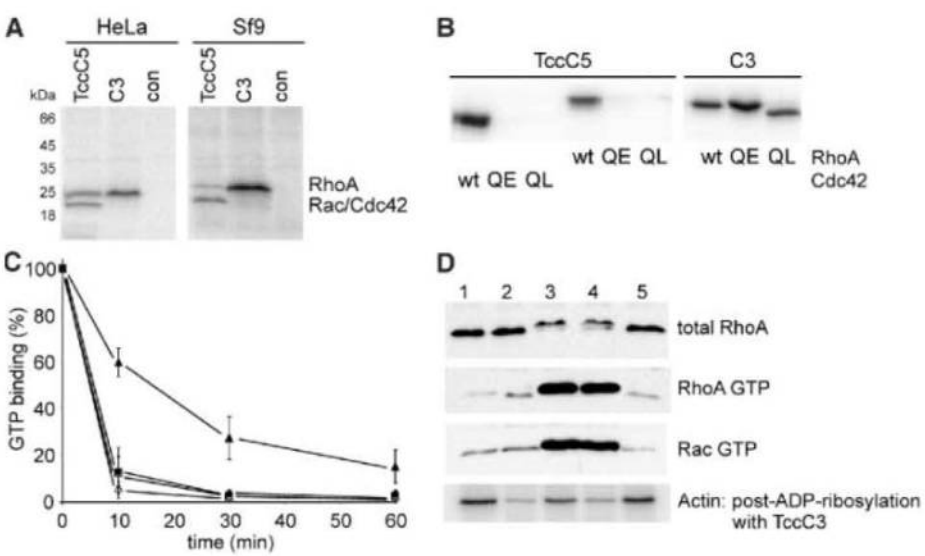

Fig. 3. ADP-ribosylation by TccC5. (**A**) Lysates of serum-starved HeLa or Sf9 cells or (**B**) recombinant GTPases (Cdc42 and RhoA) and indicated mutants (RhoAQ63E, RhoAQ63L, Cdc42Q61E, and Cdc42Q61L) were [^{32}P]ADP-ribosylated by TccC5, *C. botulinum* exoenzyme C3 (C3), or buffer (control). Labeled proteins were analyzed by means of SDS-PAGE and phosphorimaging. (**C**) Influence of TccC5-induced ADP-ribosylation of Cdc42 on GTP hydrolysis. Recombinant Cdc42 was incubated with TccC5 (▲, Δ) or the inactive N-terminal part of TccC5 (■, □) with (▲, ■) or without (Δ, □) NAD$^+$ for 1 hour. Then, the GTPase was loaded with [γ-^{32}P]GTP. Remaining nonhydrolyzed GTP bound to Cdc42 was measured with a filter binding assay. Data are percentage of initial loading (mean ± SD, $n = 3$ independent experiments). (**D**) Toxin effects on Rho GTPases and actin. Intact HeLa cells were treated without (lane 1) or with PTC3 (lane 2), PTC5 (lane 3), PTC3 and PTC5 (lane 4), or TcdA1 alone (lane 5) for 3 hours. Thereafter, RhoA was detected in cell lysates by means of immunoblotting (top, total RhoA). Activation of RhoA and Rac was analyzed through pull-down with rhotekin- and PAK-coupled beads, respectively. Bound GTPases were detected by means of immunoblotting. (Bottom) Each lysate was post–ADP-ribosylated with TccC3 with [^{32}P]NAD$^+$. Radio-labeled actin was analyzed by means of SDS-PAGE and autoradiography.

GTPases (*17*). Accordingly, ADP-ribosylation of Rho GTPases by TccC5 inhibited the GTP hydrolysis catalyzed by the GTPases (Fig. 3C and fig. S8C). Thus, TccC5 may cause persistent activation of Rho GTPases by ADP-ribosylation. To confirm that the toxins caused selective modification of target proteins in intact cells, we treated HeLa cells with PTC3 or PTC5 and also with the combination of PTC3 and PTC5. As an additional control, cells were treated with TcdA1 only. Thereafter, activated RhoA and Rac proteins were identified in lysates of these cells by rhotekin and PAK pull-down assays. Furthermore, actin was ADP-ribosylated in the cell lysates by TccC3 and [^{32}P]NAD^{+}. Treatment of cells with PTC3 caused ADP-ribosylation of actin, which was detected by the reduction of radioactive labeling of actin by TccC3 but no activation of Rac or RhoA (Fig. 3D). PTC5 caused activation of RhoA and Rac but did not modify actin. In the presence of PTC3 and PTC5, both activation of RhoA and Rac and ADP-ribosylation of actin was determined. As expected, TcdA1 alone did not activate Rho GTPases or modify actin. Thus, PTC5 activates Rho GTPases in intact cells. Activation of RhoA is probably the reason for massive formation of stress fibers. RhoA activation by PTC5 also occurs in Sf9 insect cells (fig. S8B).

Here, we have elucidated the causal mechanisms of the alterations of the actin cytoskeleton induced by the Tc toxins and suggest a model for the mode of action of the toxins [supporting online material (SOM) text and fig. S10]. Both TccC3 and TccC5, which enter the target cell cytosol via TcdA1, ADP-ribosylate actin and Rho-GTPases, respectively. The toxins thus cause actin clustering by means of a concerted action. TccC3 releases actin from its thymosin-β4 complex, probably supplying monomeric actin to the filament-promoting activities of profilin and actin nucleators such as the formins (*18*, *19*), and TccC5 activates signal pathways, which support stress fiber formation. In addition, because Rho GTPases are also involved in a large array of other biological functions (*20*, *21*), their alteration by Tc toxins may be of major importance for the host-pathogen interaction of *P. luminescens*. Tc toxins are a common principle in insect pathogenicity of a broad spectrum of bacteria and have been identified in human pathogenic *Yersinia pseudotuberculosis* and *Yersinia pestis* (*22*, *23*). Thus, the molecular mechanism of the prototypical Tc complexes aids the understanding of other types of Tc toxins in insecticidal bacteria and potentially human pathogens.

References and Notes

1. S. A. Joyce, R. J. Watson, D. J. Clarke, *Curr. Opin. Microbiol.* **9**, 127 (2006).
2. R. H. ffrench-Constant *et al.*, *FEMS Microbiol. Rev.* **26**, 433 (2003).
3. N. R. Waterfield, D. J. Bowen, J. D. Fetherston, R. D. Perry, R. H. ffrench-Constant, *Trends Microbiol.* **9**, 185 (2001).
4. D. Bowen *et al.*, *Science* **280**, 2129 (1998).
5. S. C. Lee *et al.*, *J. Mol. Biol.* **366**, 1558 (2007).
6. N. Waterfield, M. Hares, G. Yang, A. Dowling, R. ffrench-Constant, *Cell. Microbiol.* **7**, 373 (2005).
7. Materials and methods are available as supporting material on *Science* Online.
8. R. J. Fieldhouse, A. R. Merrill, *Trends Biochem. Sci.* **33**, 546 (2008).
9. H. Barth, K. Aktories, M. R. Popoff, B. G. Stiles, *Microbiol. Mol. Biol. Rev.* **68**, 373 (2004).
10. K. Aktories *et al.*, *Nature* **322**, 390 (1986).
11. K. Aktories, A. Wegner, *J. Cell Biol.* **109**, 1385 (1989).
12. E. Irobi *et al.*, *EMBO J.* **23**, 3599 (2004).
13. E. M. De La Cruz *et al.*, *Biophys. J.* **78**, 2516 (2000).
14. H. Q. Sun, K. Kwiatkowska, H. L. Yin, *Curr. Opin. Cell Biol.* **7**, 102 (1995).
15. M. Vogelsgesang, A. Pautsch, K. Aktories, *Naunyn Schmiedebergs Arch. Pharmacol.* **374**, 347 (2007).
16. G. Schmidt *et al.*, *Nature* **387**, 725 (1997).
17. I. R. Vetter, A. Wittinghofer, *Science* **294**, 1299 (2001).
18. M. Pring, A. Weber, M. R. Bubb, *Biochemistry* **31**, 1827 (1992).
19. S. Romero *et al.*, *Cell* **119**, 419 (2004).
20. A. B. Jaffe, A. Hall, *Annu. Rev. Cell Dev. Biol.* **21**, 247 (2005).
21. K. Burridge, K. Wennerberg, *Cell* **116**, 167 (2004).
22. J. Parkhill *et al.*, *Nature* **413**, 523 (2001).
23. M. C. Hares *et al.*, *Microbiology* **154**, 3503 (2008).
24. H. G. Mannherz *et al.*, *J. Mol. Biol.* **366**, 745 (2007).

25. We thank Agilent Technologies for supporting us with instrumentation, R. S. Goody (Dortmund, Germany) for help in stopped-flow measurements, and M. Geyer (Dortmund, Germany) for providing profilin. The study was financially supported by the Deutsche Forschungsgemeinschaft DFG to K.A. and H.G.M.

Supporting Online Material

www.sciencemag.org/cgi/content/full/327/5969/1139/DC1
Materials and Methods
SOM Text
Figs. S1 to S10
References

11 November 2009; accepted 22 January 2010
10.1126/science.1184557

Noise Can Induce Bimodality in Positive Transcriptional Feedback Loops Without Bistability

Tsz-Leung To and Narendra Maheshri*

Transcriptional positive-feedback loops are widely associated with bistability, characterized by two stable expression states that allow cells to respond to analog signals in a digital manner. Using a synthetic system in budding yeast, we show that positive feedback involving a promoter with multiple transcription factor (TF) binding sites can induce a steady-state bimodal response without cooperative binding of the TF. Deterministic models of this system do not predict bistability. Rather, the bimodal response requires a short-lived TF and stochastic fluctuations in the TF's expression. Multiple binding sites provide these fluctuations. Because many promoters possess multiple binding sites and many TFs are unstable, positive-feedback loops in gene regulatory networks may exhibit bimodal responses, but not necessarily because of deterministic bistability, as is commonly thought.

When a cell must unambiguously commit to a particular gene expression program, often a digital change occurs in a key regulator's expression (*1*). Decision-making circuitry within metabolic (*2*), developmental (*3*), and synthetic gene regulatory networks (*4*–*6*) uses positive feedback to provide bimodal, "all-or-none" expression of a regulator. The bimodal population response has been explained with deterministic models that predict bistable gene expression (*7*). Consider a positive-feedback loop where a transcriptional activator binds its own promoter to regulate expression. The open-loop promoter response (in the absence of feedback) is modeled by a Hill-type equation, where the Hill coefficient describes whether the response is linear (Hill coefficient = 1) or sigmoidal (Hill coefficient > 1) before saturating. The basis for sigmoidal responses can be direct cooperative binding of transcription factors (TFs) to promoters, or indirect cooperativity via nucleosome displacement (*8*). Without cooperativity, bistability is not predicted.

To understand how promoter structure relates to the Hill coefficient, we used the widely used tet-Off system, adapted for budding yeast (*9*). The tet–transcriptional activator (tTA) binds to a tet operator (tetO) sequence in the absence of doxycycline. We constructed yeast strains without (open loop) and with feedback (closed loop), using previously designed promoters with one (1xtetO) and seven (7xtetO) binding sites (*9*). With 1xtetO in positive feedback, the reporter exhibits a graded steady-state response to changes in feedback strength, whereas 7xtetO exhibits a bimodal response (Fig. 1A). One explanation is that 7xtetO has a sigmoidal open-loop response due to cooperative binding of tTA to multiple binding sites, resulting in bistability (*6*, *10*). Yet, if one accounts for the binding of doxycycline to the tTA dimer [Supporting Online Material (SOM) Text], both 1xtetO and 7xtetO exhibit a noncooperative open-loop response, with a Hill coefficient of ~1 (Fig. 1B). To eliminate the possibility of altered doxycycline binding, we titrated tTA levels directly, using a galactose-inducible promoter, and confirmed the

Department of Chemical Engineering, Massachusetts Institute of Technology, Cambridge, MA 02139, USA.

*To whom correspondence should be addressed. E-mail: narendra@mit.edu

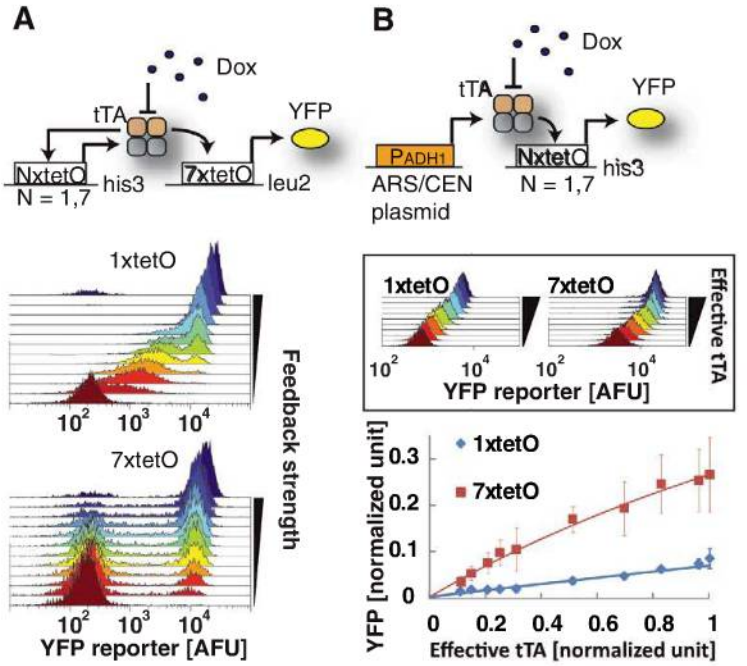

Fig. 1. Bimodal gene expression with noncooperative positive feedback. (**A**) Yeast strains engineered with 1xtetO and 7xtetO in a closed-loop configuration (top) were grown to steady state. Feedback strength was modulated by varying doxycycline concentration from 0 to 2000 ng/ml (bottom) (details in table S3). Resulting steady-state expression distributions were obtained from flow cytometry. (**B**) The open-loop response of both 1xtetO and 7xtetO (top), as determined by titration with doxycycline (0 to 2000 ng/ml), is noncooperative, with a Hill coefficient of ~1 (bottom). Flow cytometric analysis confirms that the response is graded at the single-cell level (middle). The effective tTA level was calculated from doxycycline concentration with Eq. 2 (SOM Text). Error bars indicate the SD of triplicate samples. (**C**) A simulated time series describing expression in positive feedback with infrequent promoter firing and an unstable activator, leading to a bimodal, closed-loop response.

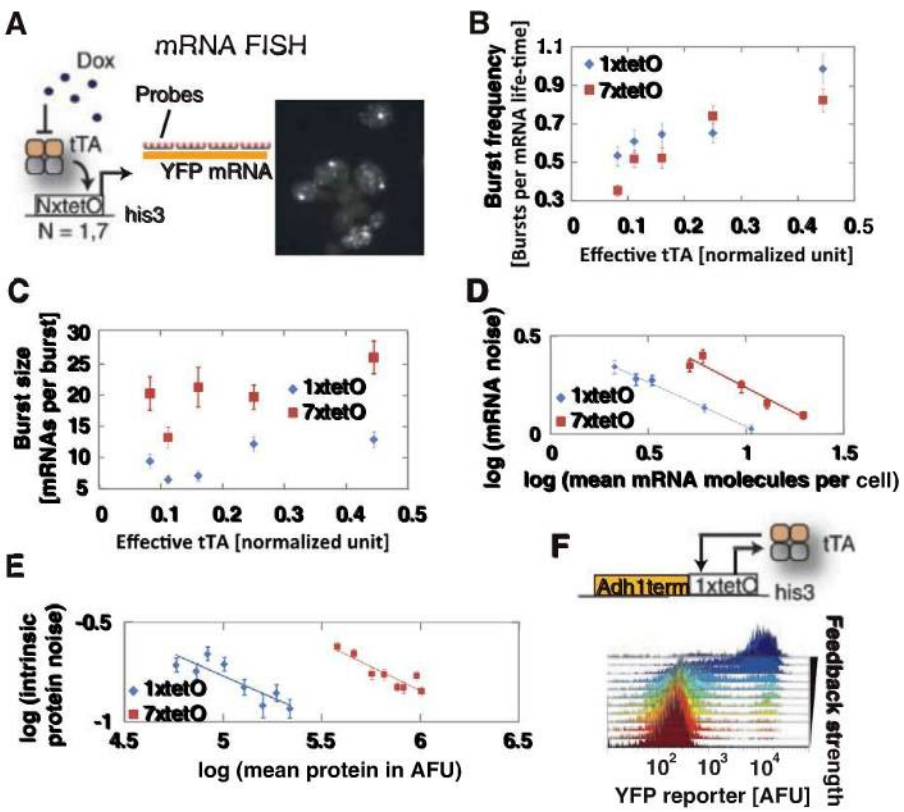

Fig. 2. Multiple TF binding sites increase promoter noise. (**A**) The burst statistics of mRNA of 1xtetO and 7xtetO promoters were determined by mRNA FISH (*14*). The effective tTA level was modulated with doxycycline (250, 500, 750, 1000, and 1250 ng/ml). (**B**) The burst frequency and (**C**) burst size were inferred by fitting the steady-state mRNA distributions to a stochastic model (SOM). Error bars represent 95% confidence intervals (CIs). (**D**) The scaling law (slope ~ −0.5 on the log-log plot) between mRNA noise and mean mRNA expression level suggests that mRNA noise is primarily due to intrinsic sources and burst frequency regulation. (**E**) The intrinsic protein noise was determined by the dual-reporter assay (*16*). The same scaling law applies to the intrinsic protein noise. Error bars in (D) and (E) representing 95% CIs were obtained by bootstrapping. (**F**) The Adh1term-1xtetO promoter was created by inserting an *ADH1* terminator upstream of 1xtetO in the sense direction. The feedback strength was modulated by varying doxycycline from 0 to 1000 ng/ml (details in table S3).

noncooperative response (fig. S1). In addition, the open-loop response of both promoters in a strain that contains a closed-loop promoter is also noncooperative (fig. S2).

Recent single-molecule approaches have revealed that gene expression often occurs in random bursts of transcription and/or translation [reviewed in (*11*)]. Burst statistics can be characterized by the burst size (number of mRNAs or proteins produced per transcriptional activation event) and the burst frequency (number of transcriptional activation events per mRNA or protein lifetime). A theoretical study of the effects of these stochastic bursts by Friedman *et al.* (*12*) predicts that bimodal expression at steady state is possible with positive feedback even when the open-loop response is noncooperative with a Hill coefficient ≤1 [similar results reported in (*13*)]. This requires that the maximum burst frequency is low, the burst size is large enough to turn the promoter on in positive feedback, and the activator regulates burst frequency (exact conditions shown in fig. S6). Infrequent transcriptional bursts of mRNA lead to bursts of a transcriptional activator. Simulations under these conditions (Fig. 1C) show that some bursts lead to large activator levels because of large burst sizes and switch the system to high expression (~3000 min). Because the activator is short-lived, occasionally all activators degrade before the next burst occurs (time ~300 min). This switches the system back to low expression.

We hypothesized that the 7xtetO promoter had a lower maximum burst frequency and larger burst size versus the 1xtetO promoter. Independent support for this hypothesis comes from a study of stochastic gene expression using the tet-Off system in mammalian cells (*14*). As in that study, we combined mRNA fluorescence in situ

hybridization (FISH) measurements (*15*) with a stochastic model of gene expression to determine the burst statistics of mRNA (Fig. 2A). The 7xtetO promoter has a burst size twice as high as that of the 1xtetO promoter (Fig. 2C), whereas the mRNA distributions are consistent with burst frequency regulation (Fig. 2B and fig. S7). Both mRNA and intrinsic protein noise scale with the inverse square root of abundance (Fig. 2, D and E), suggesting that mRNA noise is dominated by intrinsic fluctuations (*16*, *17*) and tTA regulates burst frequency (*18*).

In the open-loop context, the *ADH1* promoter-driven tTA level was not high enough to saturate either promoter. Therefore, we used the closed-loop data, where tTA levels are much higher, to estimate the maximum burst frequency (fig. S2). Consistent with our hypothesis and the mammalian study (*14*), 7xtetO has a maximum burst frequency one-fifth that of 1xtetO. Taken together, multiple tetO binding sites make a promoter more sensitive to tTA, with a lower burst frequency and a higher burst size. We were unable to determine if the increased burst size is due to a longer-duration burst or a more intense burst (fig. S9). A 1xtetO promoter variant containing the yeast *ADH1* terminator upstream of the 1xtetO site has a non-cooperative open-loop response (fig. S11) and also exhibits a bimodal response in positive feedback (Fig. 2F). This promoter has a higher burst size and lower maximum burst frequency compared to 1xtetO (fig. S12 and table S8). Therefore, as expected by the theory, the noise properties of the promoter, and not multiple binding sites per se, are responsible for the bimodal response.

A strong prediction of our model is that stabilization of tTA will increase the maximum burst frequency and eliminate bimodal expression. Global measurements of protein stability in yeast reveal that TFs tend to be less stable than typical proteins (*19*). Although tTA (a fusion between tet repressor and the VP16 activation domain) stability has not been determined, the in vivo half-life of a lexA-VP16 fusion protein in yeast was 6 min (*20*). Moreover, mono-ubiquitination of lexA-VP16 was required to activate the TF, but led to subsequent polyubiquitination via Met30p, targeting it for degradation (*20*). To stabilize tTA, we expressed the active monoubiquitinated version and deleted *MET30* (*21*). As expected, the closed-loop response of the stabilized tTA was more graded (Fig. 3A).

To verify whether a stochastic model could quantitatively describe our results, we measured tTA mRNA and protein half-lives. To determine the mRNA stability, we stopped transcription in a 7xtetO closed-loop strain by adding doxycycline and the transcriptional inhibitor thiolutin. Cells were fixed at specific time points after inhibition, and tTA and YFP (yellow fluorescent protein) mRNA abundance was measured by FISH. Both transcripts have a half-life of ~15 to 20 min (fig. S14). We determined the tTA stability at the population level by stopping tTA production and following tTA levels by Western blotting (Fig. 3B). tTA appears to have an ~70-min half-life, much longer than the 6-min half-life of lexA-VP16 (*20*). With the resulting high maximum burst frequency, neither the Friedman model nor a modified version accounting for all three stages (promoter, mRNA, and protein) of gene expression (SOM Text) even qualitatively describes bimodal expression. Given the short half-life of the lexA-VP16 fusion, we suspected that multiple forms of tTA were present in the cell and only the active form was unstable. Because activation-coupled degradation of tTA occurs only in the nucleus, we hypothesized that cytoplasmic tTA was stable and nuclear transport of tTA was slow. Nuclear transport of the reverse tTA is limiting in yeast, and addition of nuclear localization signals (NLS) alters its subcellular distribution (*22*).

To test the effect of nuclear transport, we fused a mammalian NLS to tTA, confirmed the nuclear localization (fig. S17), and measured the open- and closed-loop responses. As before, the NLS-tTA open-loop response was graded (fig. S15). The closed-loop responses remained bimodal for 7xtetO (Fig. 4A), although more cells were found with intermediate expression levels compared to tTA (Fig. 1A). NLS-tTA stability was reduced to a ~10-min half-life (Fig. 3B), suggesting that the increased stability of tTA was indeed due to a stable cytoplasmic fraction not susceptible to rapid degradation. By incorporating both nuclear transport and the shorter tTA half-life in our model (fig. S16), we could recapitulate the closed-loop responses for

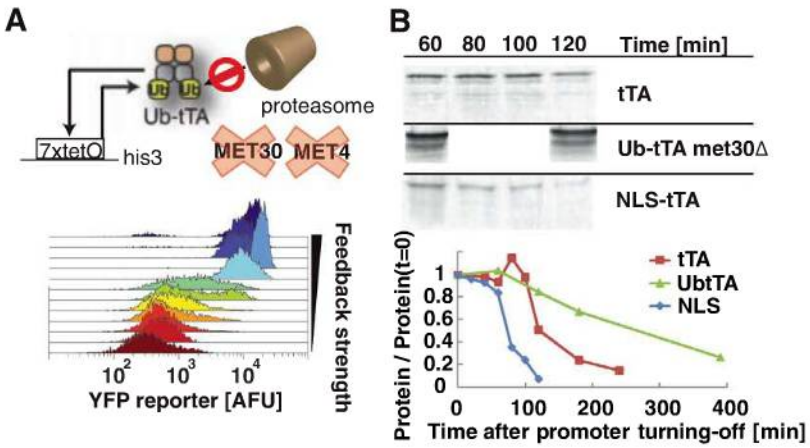

Fig. 3. Stabilizing the TF reduces stochastic fluctuation and eliminates bimodality. (**A**) To create a stabilized TF, a ubiquitin-tTA fusion was expressed in a *met30*Δ *met4*Δ background (upper panel) (*20*). The closed-loop reporter response measured by flow cytometry becomes more graded for 7xtetO (lower panel). Feedback strength was modulated by varying doxycycline, as in Fig. 1A. (**B**) To determine tTA stability, its expression was halted via a galactose-inducible promoter (*27*), and levels were measured by quantitative Western blotting. Lanes contain equivalent amount of total protein as determined by Bradford assay. After accounting for the 60-min lag required for mRNA depletion and tTA folding, tTA was found to have an ~70-min half-life. The stabilized tTA variant has an ~175-min half-life, similar to the doubling time. The SV40 NLS-tagged tTA has an ~15-min half life, suggesting that nuclear transport was rate limiting.

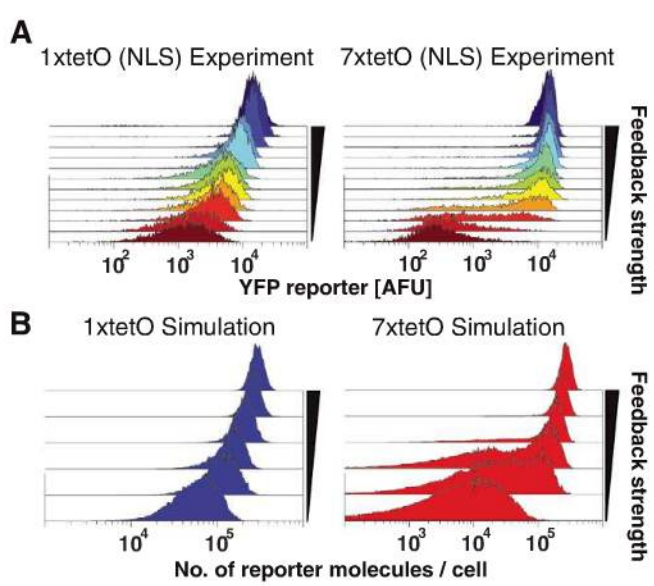

Fig. 4. Stochastic modeling of the closed-loop response reveals the importance of nuclear transport. (**A**) A SV40 NLS was fused to the N terminal of tTA, and the closed-loop reporter response at steady state was measured by flow cytometry. The feedback strength was modulated by varying doxycycline concentration, as in Fig. 1A. The measured expression profiles for NLS-tTA remain bimodal, but less so compared to normal tTA (Fig. 1A). (**B**) Stochastic simulations using the scheme in fig. S16 and parameter values in tables S3 and S7. Results capture differences between the graded versus bimodal expression profiles between 1xtetO and 7xtetO and generally agree with experimental closed-loop NLS-tTA data.

NLS-tTA (Fig. 4B) using measured in vivo parameters for the open-loop promoters (table S7) (*23*).

This work is related to examples where enzymatic cycles (*24*) and positive feedback in spatial organization (*25*) possess bimodal activity that is solely due to stochastic fluctuations. In addition, a stochastic view of noncooperative positive feedback in HIV escape from latency leads to a transient bimodal response (*26*), but we demonstrated a steady-state bimodal response. The hallmarks of noise-induced bimodality in gene expression—positive-feedback loops and unstable proteins—are characteristic of many TFs and promoters and likely widespread in biological systems (table S4). Our findings also suggest that multiple binding sites may be associated with all-or-none responses not by virtue of cooperative binding but because of increased noise. Finally, this work provides new guidelines for the construction of a bistable switch based on positive feedback for applications in synthetic biology and metabolic engineering.

References and Notes

1. U. Alon, *An Introduction to Systems Biology: Design Principles of Biological Circuits* (CRC Press, Boca Raton, FL, 2006).
2. M. Acar, A. Becskei, A. van Oudenaarden, *Nature* **435**, 228 (2005).
3. W. Xiong, J. E. Ferrell Jr., *Nature* **426**, 460 (2003).
4. N. T. Ingolia, A. W. Murray, *Curr. Biol.* **17**, 668 (2007).
5. F. J. Isaacs, J. Hasty, C. R. Cantor, J. J. Collins, *Proc. Natl. Acad. Sci. U.S.A.* **100**, 7714 (2003).
6. C. M. Ajo-Franklin *et al.*, *Genes Dev.* **21**, 2271 (2007).
7. A. D. Keller, *J. Theor. Biol.* **172**, 169 (1995).
8. J. A. Miller, J. Widom, *Mol. Cell. Biol.* **23**, 1623 (2003).
9. E. Garí, L. Piedrafita, M. Aldea, E. Herrero, *Yeast* **13**, 837 (1997).
10. A. Becskei, B. Séraphin, L. Serrano, *EMBO J.* **20**, 2528 (2001).
11. N. Maheshri, E. K. O'Shea, *Annu. Rev. Biophys. Biomol. Struct.* **36**, 413 (2007).
12. N. Friedman, L. Cai, X. S. Xie, *Phys. Rev. Lett.* **97**, 168302 (2006).
13. R. Karmakar, I. Bose, *Phys. Biol.* **4**, 29 (2007).
14. A. Raj, C. S. Peskin, D. Tranchina, D. Y. Vargas, S. Tyagi, *PLoS Biol.* **4**, e309 (2006).
15. A. Raj, P. van den Bogaard, S. A. Rifkin, A. van Oudenaarden, S. Tyagi, *Nat. Methods* **5**, 877 (2008).
16. M. B. Elowitz, A. J. Levine, E. D. Siggia, P. S. Swain, *Science* **297**, 1183 (2002).
17. A. Bar-Even *et al.*, *Nat. Genet.* **38**, 636 (2006).
18. There is sizable extrinsic noise in protein abundance as measured by fluorescence (fig. S10), yet it does not appear to have a major effect (SOM Text).
19. A. Belle, A. Tanay, L. Bitincka, R. Shamir, E. K. O'Shea, *Proc. Natl. Acad. Sci. U.S.A.* **103**, 13004 (2006).
20. S. E. Salghetti, A. A. Caudy, J. G. Chenoweth, W. P. Tansey, *Science* **293**, 1651 (2001).
21. *MET4* must also be deleted, as single deletion of *MET30* is lethal (*20*).
22. A. Becskei, M. G. Boselli, A. van Oudenaarden, *Nat. Cell Biol.* **6**, 451 (2004).
23. The more pronounced bimodal response from nuclear transport–limited tTA (Fig. 1A) compared to NLS-tTA remains unclear, but likely depends on details of tTA transport (see SOM).
24. M. Samoilov, S. Plyasunov, A. P. Arkin, *Proc. Natl. Acad. Sci. U.S.A.* **102**, 2310 (2005).
25. S. J. Altschuler, S. B. Angenent, Y. Wang, L. F. Wu, *Nature* **454**, 886 (2008).
26. L. S. Weinberger, T. Shenk, *PLoS Biol.* **5**, e9 (2007).
27. Materials and methods are available as supporting material in *Science* Online.

28. We thank A. Raj for technical assistance with FISH, and C. J. Zopf, H. Kim, A. Raj, J. Gore, and K. Verstrepen for comments on the manuscript. This work was funded by an NSF Graduate Fellowship (to T.-L. T.), the Human Frontiers Science Program RGY2007 (to N.M.), and Massachusetts Institute of Technology startup funds (to N.M.)

Supporting Online Material

www.sciencemag.org/cgi/content/full/327/5969/1142/DC1
Material and Methods
SOM Text
Figs. S1 to S19
Tables S1 to S9
References

10 July 2009; accepted 8 January 2010
10.1126/science.1178962

Cortical Plasticity Induced by Inhibitory Neuron Transplantation

Derek G. Southwell,[1] Robert C. Froemke,[2] Arturo Alvarez-Buylla,[1]* Michael P. Stryker,[3]* Sunil P. Gandhi[3]*

Critical periods are times of pronounced brain plasticity. During a critical period in the postnatal development of the visual cortex, the occlusion of one eye triggers a rapid reorganization of neuronal responses, a process known as ocular dominance plasticity. We have shown that the transplantation of inhibitory neurons induces ocular dominance plasticity after the critical period. Transplanted inhibitory neurons receive excitatory synapses, make inhibitory synapses onto host cortical neurons, and promote plasticity when they reach a cellular age equivalent to that of endogenous inhibitory neurons during the normal critical period. These findings suggest that ocular dominance plasticity is regulated by the execution of a maturational program intrinsic to inhibitory neurons. By inducing plasticity, inhibitory neuron transplantation may facilitate brain repair.

Once in life, a critical period for ocular dominance plasticity is initiated by the development of intracortical inhibitory synaptic transmission (*1*). Reduction of inhibitory transmission disrupts ocular dominance plasticity (*2*), whereas the early enhancement of inhibitory transmission promotes a precocious period of ocular dominance plasticity (*3*–*6*). After the critical period has passed, however, direct pharmacological augmentation of inhibitory transmission does not induce plasticity (*7*).

Cortical inhibitory neurons are produced in the medial and caudal ganglionic eminences of the embryonic ventral forebrain (*8*–*10*). When transplanted into the brains of older animals, embryonic inhibitory neuron precursors disperse widely (*11*) and develop the characteristics of mature cortical inhibitory neurons (*12*). We have used repeated optical imaging of intrinsic signals (*13*, *14*) to examine whether inhibitory neuron transplantation produces ocular dominance plasticity after the critical period (fig. S1).

In mice, ocular dominance plasticity reaches a peak in the fourth postnatal week, when cortical inhibitory neurons are ~33 to 35 days old (*3*, *10*) (Fig. 1A). At this age, monocular visual deprivation shifts neuronal responses in the binocular visual cortex away from the deprived eye and toward the nondeprived eye. Throughout this study, we have quantified the balance of cortical responses to the two eyes by calculating an ocular dominance index (ODI). An ODI value of –1 indicates responses dominated by the ipsilateral eye, a value of 1 represents responses dominated by the contralateral eye, and a value of 0 represents equal binocular responses. In untreated mice at the peak of the critical period [postnatal day 28 (P28)], the binocular visual cortex responded more to the contralateral eye, with a mean ODI of 0.22 (Fig. 1B, open black circles). After four days of visual deprivation of the contralateral eye, cortical responses were shifted toward the ipsilateral eye, with a mean ODI value of 0.00 (Fig. 1B, filled black circles).

We first examined whether inhibitory neuron transplantation induced ocular dominance plasticity 14 to 18 days after the critical period, at P42 to 46. We transplanted cells from the embryonic day 13.5 to 14.5 (E13.5 to 14.5) medial ganglionic eminence (MGE) into sites flanking the host primary visual cortex at two ages, P0 to 2 and P9 to 11, respectively (Fig. 1A). Host mice that received transplants at P9 to 11 were thus studied 33 to 35 days after transplantation (DAT), whereas hosts that received transplants at P0 to 2 were studied 43 to 46 DAT. Transplantation did not alter the absolute magnitudes of visual responses in the host binocular visual cortex (fig. S2). Before monocular deprivation, host cortex responded more to the contralateral eye (Fig. 1B; P9 to 11 hosts, 33 to 35 DAT ODI mean ± SD = 0.23 ± 0.02, open green squares; P0 to 2 hosts, 43

[1]Department of Neurological Surgery and the Eli and Edythe Broad Center of Regenerative Medicine and Stem Cell Research, University of California, San Francisco, 513 Parnassus Avenue, San Francisco, CA 94143, USA. [2]Department of Otolaryngology, University of California, San Francisco, 513 Parnassus Avenue, San Francisco, CA 94143, USA. [3]Department of Physiology, University of California, San Francisco, 513 Parnassus Avenue, San Francisco, CA 94143, USA.

*To whom correspondence should be addressed. E-mail: abuylla@stemcell.ucsf.edu (A.A.B.); stryker@phy.ucsf.edu (M.P.S.); sunil@phy.ucsf.edu (S.P.G.)

to 46 DAT ODI = 0.24 ± 0.01, open red diamonds). Monocular deprivation shifted visual responses toward the nondeprived eye 33 to 35 DAT into P9 to 11 hosts (Fig. 1B, ODI = 0.05 ± 0.06, solid green squares). By contrast, monocular deprivation produced much weaker effects 43 to 46 DAT into P0 to 2 animals (Fig. 1B, ODI = 0.16 ± 0.04, solid red diamonds, Mann-Whitney test, $U = 1$, $P = 0.005$), consistent with earlier descriptions of the normal decline of ocular dominance plasticity after the critical period (*15*, *16*). These findings demonstrate that transplantation into P9 to 11 animals induces ocular dominance plasticity 33 to 35 DAT, 14 to 18 days after the peak of the critical period.

It remained unclear why transplantation into P0 to 2 hosts did not produce plasticity. We reasoned that the effects of transplantation may have been determined by the age of the host at transplantation (P0 to 2 versus P9 to 11) or by the cellular age of the transplanted population at the time of monocular deprivation (43 to 46 DAT versus 33 to 35 DAT). To distinguish between these possibilities, we transplanted into P0 to 2 and P9 to 11 hosts and then studied plasticity at P33 to 37, shortly after the critical period. Mice transplanted at P0 to 2 were thus studied 33 to 35 DAT, whereas animals transplanted at P9 to 11 were studied 25 to 27 DAT. Monocular deprivation elicited a strong effect 33 to 35 DAT into P0 to 2 hosts (Fig. 1B; ODI = 0.04 ± 0.05, solid green diamonds) but produced a much weaker effect 25 to 27 DAT to P9 to 11 hosts (Fig. 1B; ODI = 0.13 ± 0.07, solid blue squares; $U = 13$, $P = 0.035$). Thus, transplantation into both P0 to 2 and P9 to 11 hosts could produce plasticity, depending on the age of the transplanted cells at the time of monocular deprivation: Transplantation was effective when the cells were 33 to 35 days old but not when the cells were 25 to 27 or 43 to 46 days old.

These results showed that inhibitory neuron transplantation induced plasticity after the critical period, but they did not establish whether transplantation altered the normal plasticity at the peak of the critical period. We therefore studied plasticity 17 DAT into P11 animals (Fig. 1B, solid purple squares). At this age, monocular deprivation produced similar effects in hosts and age-matched, untreated animals (17 DAT ODI = 0.04 ± 0.01; untreated P28 control ODI = 0.00 ± 0.01; $U = 1$, $P = 0.057$). This finding, taken together with the results observed 25 to 27 and 33 to 35 DAT, indicates that transplantation produces a novel period of ocular dominance plasticity, rather than a delay or lengthening of normal critical period plasticity.

To determine whether the effects of transplantation were specific to the introduction of inhibitory precursors from the MGE, we transplanted cells from the lateral ganglionic eminence (LGE), an embryonic ventral forebrain region that produces olfactory bulb inhibitory neurons and striatal medium spiny neurons (*17*) (fig. S3). The transplantation of E13.5 LGE cells into P9 to 11 hosts did not produce a significant effect on ocular dominance plasticity 33 to 35 days later (Fig. 1B; before monocular deprivation, ODI = 0.24 ± 0.02, open green squares with red crosses; after monocular deprivation, ODI = 0.22 ± 0.03, solid green squares with red crosses; $U = 4$, $P = 0.343$). The transplantation of freeze-thawed, dead MGE cells also produced little plasticity (fig. S4; before monocular deprivation, ODI = 0.24 ± 0.01; after monocular deprivation, ODI = 0.19 ± 0.03), further suggesting that the effects of transplantation were specifically caused by live MGE cells (live cell 33 to 35 DAT versus dead cell ODI after monocular deprivation, $U = 0$, $P = 0.006$).

Many of our results were obtained by measuring visual responses in the same host before and after monocular deprivation. For each animal, we calculated an ocular dominance shift, the difference between ODIs measured before and after monocular deprivation (Fig. 1C). The ocular dominance shift observed 33 to 35 DAT into P9

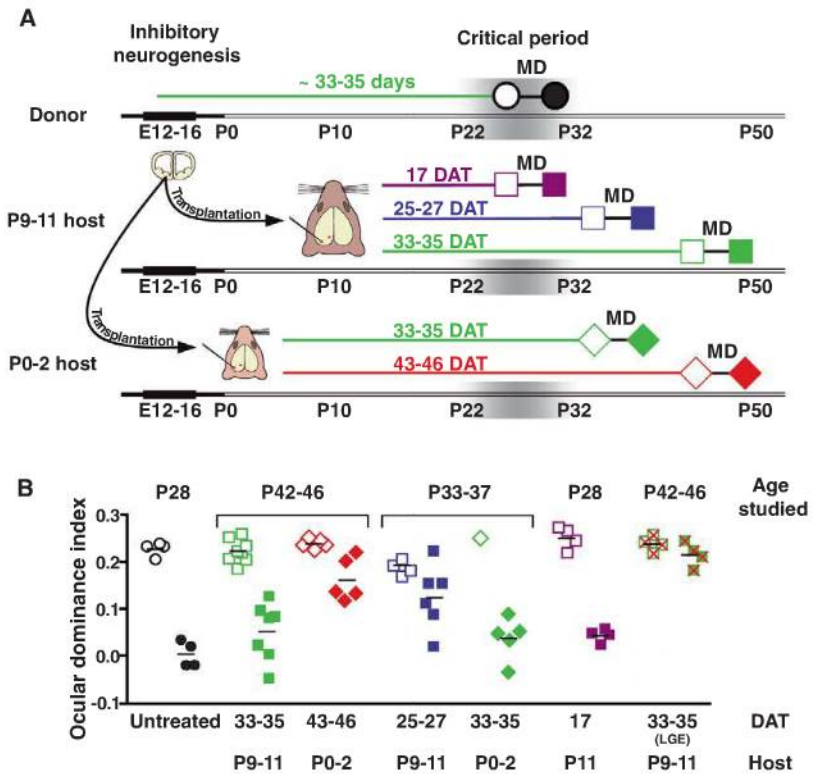

Fig. 1. Ocular dominance plasticity induced by transplantation of inhibitory neuron precursors. (**A**) Experimental design. Cortical inhibitory neurons are produced from E12 to 16. Mouse ocular dominance plasticity peaks at P26 to 28, when inhibitory neurons are 33 to 35 days old. Inhibitory neuron precursors were transplanted from E13.5 to 14.5 donor embryos into host animals of two ages: P0 to 2 (diamonds) and P9 to 11 (squares). Ocular dominance plasticity was assessed 17 (purple), 25 to 27 (blue), 33 to 35 (green), and 43 to 46 (red) DAT by measuring visual responses to the two eyes before (open symbols) and after (solid symbols) 4 days of monocular deprivation (MD). Visual responses were quantified using an ODI. (**B**) Results of plasticity studies. During the critical period (P28) in untreated mice, monocular deprivation shifted responses toward the nondeprived eye (open versus filled black circles). In P42 to 46 host animals, 14 to 18 days after the critical period, monocular deprivation produced a strong shift in responses 33 to 35 DAT (solid green squares). However, 43 to 46 DAT, monocular deprivation produced a weaker shift in responses (solid red diamonds). In P33 to 37 host animals, 5 to 9 days after the critical period, monocular deprivation produced a stronger effect 33 to 35 DAT (solid green diamonds) than at 25 to 27 DAT (solid blue squares). Transplantation did not alter the effects of monocular deprivation during the critical period (solid purple squares), as compared with untreated controls (solid black circles; Mann-Whitney test, $U = 1$, $P = 0.057$). Monocular deprivation produced an insignificant effect at 33 to 35 DAT using cells from the LGE ($U = 4$, $P = 0.343$, solid green squares with red crosses). (**C**) An ocular dominance shift quantified the change in ODI produced by monocular deprivation. Thirty-three to 35 DAT (green) the shift was 2.5 times as high as at 25 to 27 DAT (blue; $P < 0.05$) and 2.2 times as high as at 43 to 46 DAT (red; $P < 0.05$, Kruskal-Wallis test; $H = 8.6$ with Dunn's post test). The shift observed 33 to 35 DAT (green) was 77% of that observed in untreated animals during the critical period (black). Error bars represent SEM.

to 11 hosts (green) was 77% of that observed in untreated animals during the critical period (black). The effects of transplantation 33 to 35 DAT into P9 to 11 hosts were more than double those produced 25 to 27 DAT (blue) and 43 to 46 DAT (red). These findings indicate that transplantation has its strongest effect on plasticity when the transplanted cells reach a cellular age of 33 to 35 days. This age matches the age of endogenous inhibitory neurons at the peak of the normal critical period (*10*, *15*).

In most of our experiments, cells expressing a red fluorescent protein (DsRed) (*18*) were transplanted into hosts containing endogenous inhibitory neurons expressing green fluorescent protein (GAD67-GFP) (*19*). In other experiments, cells expressing GFP (*20*) were transplanted into wild-type hosts. The transplantation of DsRed cells into GAD67-GFP hosts was done to facilitate the identification of the transplanted and host inhibitory cells in electrophysiological recordings. Transplantation of GFP donor cells into wild-type hosts permitted the detailed histological characterization of the transplanted cells. The effects of monocular deprivation in wild-type host animals 33 to 35 DAT were similar to those observed in GAD67-GFP hosts (fig. S5; wild-type ODI = 0.04 ± 0.03; GAD67-GFP ODI = 0.05 ± 0.06).

We next examined whether transplanted MGE cells migrated into the primary visual cortex and developed into inhibitory neurons. After the optical imaging experiments, we labeled the borders of host binocular visual cortex with DiI injections and studied the morphologies, molecular phenotypes, spatial distributions, and densities of transplanted cells within the DiI-labeled binocular visual cortex. Across all experimental groups, transplanted cells had migrated into all layers of

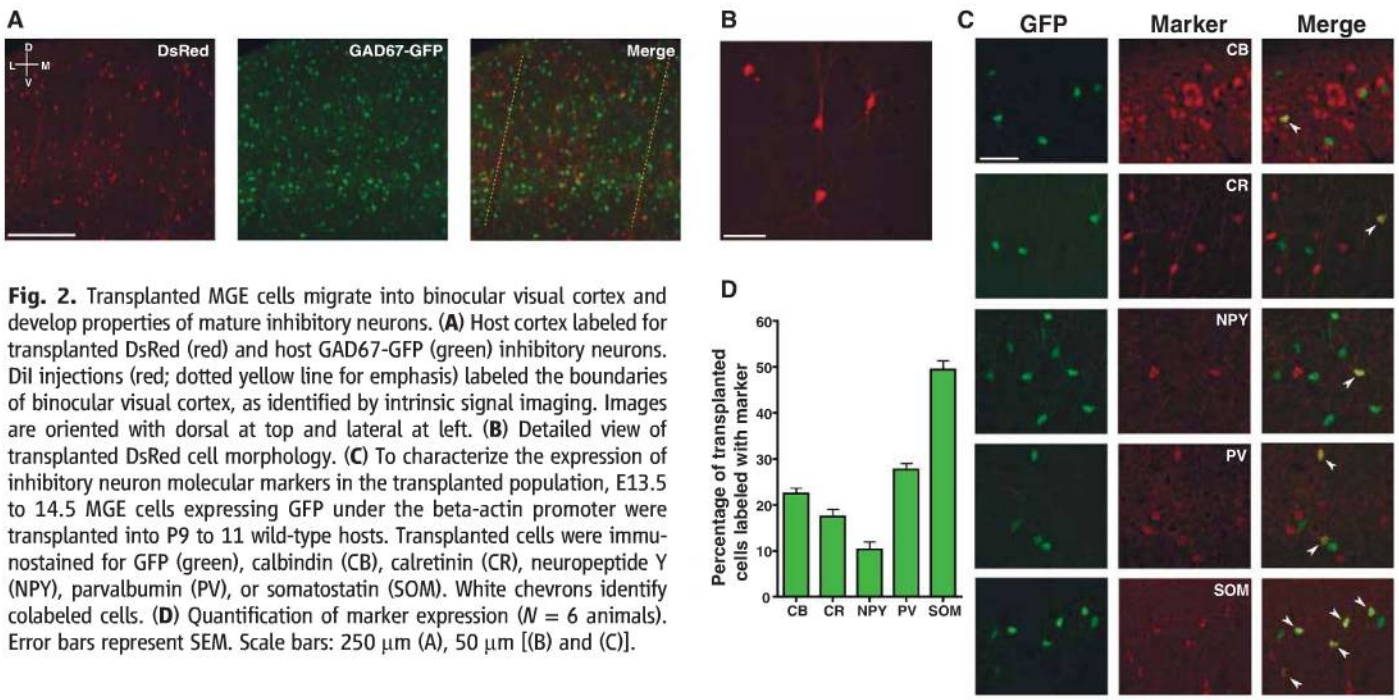

Fig. 2. Transplanted MGE cells migrate into binocular visual cortex and develop properties of mature inhibitory neurons. (**A**) Host cortex labeled for transplanted DsRed (red) and host GAD67-GFP (green) inhibitory neurons. DiI injections (red; dotted yellow line for emphasis) labeled the boundaries of binocular visual cortex, as identified by intrinsic signal imaging. Images are oriented with dorsal at top and lateral at left. (**B**) Detailed view of transplanted DsRed cell morphology. (**C**) To characterize the expression of inhibitory neuron molecular markers in the transplanted population, E13.5 to 14.5 MGE cells expressing GFP under the beta-actin promoter were transplanted into P9 to 11 wild-type hosts. Transplanted cells were immunostained for GFP (green), calbindin (CB), calretinin (CR), neuropeptide Y (NPY), parvalbumin (PV), or somatostatin (SOM). White chevrons identify colabeled cells. (**D**) Quantification of marker expression (N = 6 animals). Error bars represent SEM. Scale bars: 250 μm (A), 50 μm [(B) and (C)].

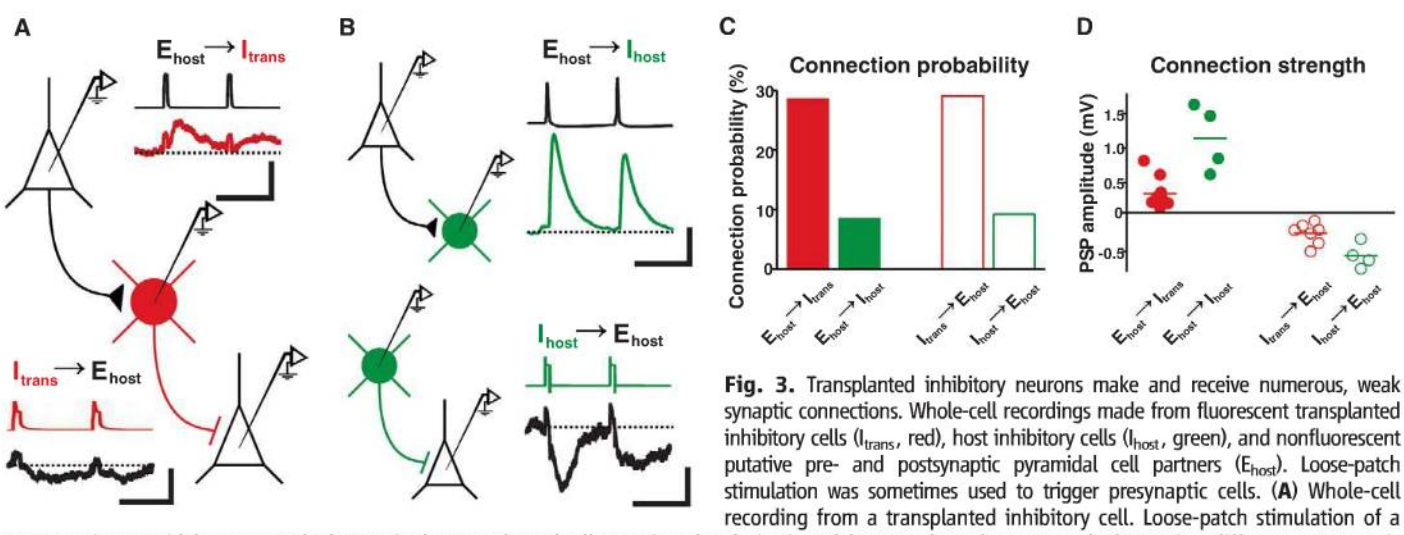

Fig. 3. Transplanted inhibitory neurons make and receive numerous, weak synaptic connections. Whole-cell recordings made from fluorescent transplanted inhibitory cells (I_{trans}, red), host inhibitory cells (I_{host}, green), and nonfluorescent putative pre- and postsynaptic pyramidal cell partners (E_{host}). Loose-patch stimulation was sometimes used to trigger presynaptic cells. (**A**) Whole-cell recording from a transplanted inhibitory cell. Loose-patch stimulation of a presynaptic pyramidal neuron evoked EPSPs in the transplanted cell. Transient depolarization of the transplanted neuron evoked IPSPs in a different postsynaptic pyramidal cell. Scale bars: 25 ms, 90 mV (presynaptic); 25 ms, 0.125 mV (postsynaptic). (**B**) Recordings from pairs of host pyramidal and host inhibitory cells. (Top) Dual whole-cell recording of a presynaptic pyramidal cell and a postsynaptic I_{host}. (Bottom) Loose-patch stimulation of a presynaptic host inhibitory neuron and whole-cell recording of a postsynaptic pyramidal cell. Scale bars: 25 ms, 40 mV (presynaptic); 25 ms, 0.25 mV (postsynaptic). (**C**) Connection probabilities for host-transplanted (red) and host-host (green) cell pairs. Transplanted inhibitory neurons made and received about three times as many connections as host inhibitory neurons ($P < 0.05$; two-tailed Fisher's exact test). (**D**) Connection strengths for all connected host-transplant and host-host cell pairs. Inhibitory and excitatory synapses made and received by transplanted cells were about one-third as strong as synapses of host inhibitory cells ($P < 0.05$).

the host visual cortex (Fig. 2A). Essentially all transplanted cells studied (17 DAT to 43 to 46 DAT) developed morphologies of mature inhibitory neurons (99.8%, Fig. 2B), whereas a very small fraction developed morphologies of glia (0.2%). In P9 to 11 hosts studied 33 to 35 DAT, nearly half of the transplanted neurons (49.5 ± 2.0%) expressed somatostatin, whereas over one-quarter expressed parvalbumin (27.7 ± 1.4%) (Fig. 2, C and D) (*21*, *22*). Smaller fractions of the transplanted neurons expressed calretinin (17.5 ± 1.6%), calbindin (22.5 ± 1.2%), and neuropeptide Y (10.3 ± 1.7%). A wide range of transplanted cell densities were sufficient to induce plasticity 33 to 35 DAT (fig. S6). Variations in the total transplanted cell densities and spatial distributions (fig. S7) could not account for why transplant-induced plasticity was greatest 33 to 35 DAT.

Because of evidence indicating that parvalbumin-expressing inhibitory neurons may regulate critical period ocular dominance plasticity (*1*, *5*, *6*), we examined whether the groups studied at 17, 25 to 27, and 43 to 46 DAT had also received transplanted populations that included parvalbumin-expressing cells (fig. S8). At all ages studied, parvalbumin-expressing cells made up a fraction of the transplanted populations and the fraction of parvalbumin-expressing cells increased with the cellular age of the transplanted population. Thus, the lack of plasticity at 25 to 27 DAT and 43 to 46 DAT cannot be attributed to an absence of parvalbumin-expressing transplanted cells in these groups. Instead, the cellular age of the transplanted population determines the effects on cortical plasticity.

We next examined whether transplanted neurons provided new inhibition to host visual cortex by making whole-cell current-clamp recordings from transplanted and host neurons (*12*, *23*). Transplantation was performed into P0 to 2 or P9 to 11 hosts, and recordings were made from host brain slices at 36 ± 3 DAT (mean ± SD; host ages P43 ± 4), when transplant-induced plasticity was strongest. Transplanted inhibitory neurons (I_{trans}) received excitatory synapses and made inhibitory synapses with host excitatory neurons (E_{host}) (Fig. 3A). We compared the connection probabilities and synaptic strengths of transplanted neurons with those of adjacent host inhibitory neurons in the same slices (I_{host}; P45 ± 6; 38 ± 4 DAT) (Fig. 3B). Compared with host inhibitory neurons, transplanted inhibitory neurons were three times as likely to receive synapses from host excitatory neurons, and were also three times as likely to make inhibitory synapses onto host excitatory neurons (Fig. 3C; connection probability E_{host}-to-I_{trans} = 10/35 or 28.6%; E_{host}-to-I_{host} = 4/47 or 8.5%, $P < 0.04$; I_{trans}-to-E_{host} = 7/24 or 29.2%; I_{host}-to-E_{host} = 4/43 or 9.3%, $P < 0.05$). The synapses received and made by transplanted inhibitory neurons were about one-third as strong as host-to-host synapses [Fig. 3D; synaptic strength, E_{host}-to-I_{trans} EPSPs (excitatory postsynaptic potentials) = 0.34 ± 0.07 mV; E_{host}-to-I_{host} EPSPs = 1.1 ± 0.24 mV, $P < 0.05$; I_{trans}-to-E_{host} IPSPs (inhibitory postsynaptic potentials) = −0.24 ± 0.06 mV; I_{host}-to-E_{host} IPSPs = −0.56 ± 0.09, $P < 0.03$]. These results demonstrate that transplanted inhibitory neurons form weak but numerous synaptic connections with neighboring excitatory neurons, widely modifying inhibitory signaling in host cortex. The presence of numerous connections between transplanted inhibitory neurons and the host brain may explain why lower transplanted cell densities (fig. S6) were sufficient to induce plasticity.

Our results show that inhibitory neuron transplantation induces ocular dominance plasticity after the normal critical period. Thirty-three to thirty-five days after transplantation, monocular deprivation produced a shift in visual responses comparable to that observed during the normal critical period (Fig. 1C). However, at shorter and longer intervals after transplantation (25 to 27 and 43 to 46 DAT, respectively), the effect of monocular deprivation was much smaller (Fig. 1C). Thus, transplant-induced plasticity resembles critical period plasticity in two ways: First, transplant-induced and critical period plasticity both peak when the transplanted and endogenous inhibitory neurons reach cellular ages of 33 to 35 days, respectively. Second, both transplant-induced and critical period plasticity are of short duration. Within the binocular visual cortex, the vast majority of transplanted cells expressed the morphological and molecular characteristics of mature inhibitory neurons. Transplanted inhibitory neurons received excitatory synapses from host neurons and made inhibitory synapses onto host neurons. These synaptic contacts were individually weaker but more numerous than those made by host inhibitory neurons.

At a host age when transplanted inhibitory neurons induce plasticity (P42 to 46), the direct pharmacological enhancement of inhibition does not (*7*). How then, might inhibitory neuron transplantation produce a new period of cortical plasticity? One plausible explanation is that transplanted inhibitory neurons reorganize the cortical circuitry by introducing a new set of weak inhibitory synapses (*6*), rather than simply augmenting the strength of the endogenous, mature inhibitory connections. This pattern of numerous, weak connections is consistent with the form of developing inhibition predicted to enhance Hebbian plasticity mechanisms during the critical period (*24*).

Cortical plasticity can be produced after the critical period by the activation of neuromodulatory systems (*25*, *26*) and the manipulation of molecules that promote structural plasticity (*27*). Each of these manipulations was associated with an accompanying reorganization of inhibitory circuits. Perhaps these experimental manipulations stimulate endogenous inhibitory neurons to form numerous, weak inhibitory synapses similar to those produced by transplanted inhibitory neurons.

It is remarkable that transplanted inhibitory neurons induce plasticity when they reach a cellular age similar to that of endogenous inhibitory neurons during the critical period. This finding suggests (i) that the critical period is regulated by the execution of a developmental program intrinsic to inhibitory neurons and (ii) that embryonic inhibitory neuron precursors retain and execute this program when transplanted into the postnatal cortex. Inhibitory neuron transplantation provides a new experimental preparation for the study of cortical plasticity. Moreover, by promoting cortical plasticity, inhibitory neuron transplantation may facilitate the restoration of normal function to the diseased brain.

References and Notes

1. T. K. Hensch, *Annu. Rev. Neurosci.* **27**, 549 (2004).
2. T. K. Hensch *et al.*, *Science* **282**, 1504 (1998).
3. Z. J. Huang *et al.*, *Cell* **98**, 739 (1999).
4. J. L. Hanover, Z. J. Huang, S. Tonegawa, M. P. Stryker, *J. Neurosci.* **19**, RC40 (1999).
5. M. Fagiolini *et al.*, *Science* **303**, 1681 (2004).
6. S. Sugiyama *et al.*, *Cell* **134**, 508 (2008).
7. M. Fagiolini, T. K. Hensch, *Nature* **404**, 183 (2000).
8. S. A. Anderson, D. D. Eisenstat, L. Shi, J. L. Rubenstein, *Science* **278**, 474 (1997).
9. S. Nery, G. Fishell, J. G. Corbin, *Nat. Neurosci.* **5**, 1279 (2002).
10. C. P. Wonders, S. A. Anderson, *Nat. Rev. Neurosci.* **7**, 687 (2006).
11. H. Wichterle, J. M. Garcia-Verdugo, D. G. Herrera, A. Alvarez-Buylla, *Nat. Neurosci.* **2**, 461 (1999).
12. M. Alvarez-Dolado *et al.*, *J. Neurosci.* **26**, 7380 (2006).
13. J. Cang, V. A. Kalatsky, S. Löwel, M. P. Stryker, *Vis. Neurosci.* **22**, 685 (2005).
14. M. Kaneko, J. L. Hanover, P. M. England, M. P. Stryker, *Nat. Neurosci.* **11**, 497 (2008).
15. J. A. Gordon, M. P. Stryker, *J. Neurosci.* **16**, 3274 (1996).
16. S. Taha, J. L. Hanover, A. J. Silva, M. P. Stryker, *Neuron* **36**, 483 (2002).
17. H. Wichterle, D. H. Turnbull, S. Nery, G. Fishell, A. Alvarez-Buylla, *Development* **128**, 3759 (2001).
18. K. Vintersten *et al.*, *Genesis* **40**, 241 (2004).
19. N. Tamamaki *et al.*, *J. Comp. Neurol.* **467**, 60 (2003).
20. A. K. Hadjantonakis, M. Gertsenstein, M. Ikawa, M. Okabe, A. Nagy, *Mech. Dev.* **76**, 79 (1998).
21. Y. Kawaguchi, Y. Kubota, *Cereb. Cortex* **7**, 476 (1997).
22. Y. Gonchar, Q. Wang, A. Burkhalter, *Front. Neuroanat.* **1**, 1 (2008).
23. A. Maffei, K. Nataraj, S. B. Nelson, G. G. Turrigiano, *Nature* **443**, 81 (2006).
24. S. P. Gandhi, Y. Yanagawa, M. P. Stryker, *Proc. Natl. Acad. Sci. U.S.A.* **105**, 16797 (2008).
25. R. C. Froemke, M. M. Merzenich, C. E. Schreiner, *Nature* **450**, 425 (2007).
26. J. F. Maya Vetencourt *et al.*, *Science* **320**, 385 (2008).
27. T. Pizzorusso *et al.*, *Science* **298**, 1248 (2002).

28. We thank A. Kriegstein, P. Parker, and members of the Kriegstein laboratory for help with the electrophysiological recordings, R. Romero for assistance with histology, and P. McQuillen for sharing histology equipment. This work was funded by grants R01 NS048528 (A.A.-B.) and P50 MH077972 (M.P.S.) from the National Institutes of Health, grant P0001351 from the Dana Foundation (M.P.S.), and a grant from the Adelson Medical Research Foundation (M.P.S.). D.G.S. was supported by a predoctoral training grant from the California Institute for Regenerative Medicine. S.P.G. was supported by postdoctoral fellowship EY016317 from the National Institutes of Health. R.C.F. is a recipient of a NIDCD K99/R00 Career Award.

Supporting Online Material

www.sciencemag.org/cgi/content/full/327/5969/1145/DC1
Materials and Methods
Figs. S1 to S9
References

29 October 2009; accepted 7 January 2010
10.1126/science.1183962

NEW PRODUCTS

LC TECHNOLOGY

The Accela 600 high performance liquid chromatography (HPLC) and Accela 1000 ultra-HPLC systems are designed to enable rapid method development and reduce solvent consumption. Both systems feature Force Feedback Control, which enables the delivery of accurate and precise gradients under all operating conditions and provides the flexibility of quaternary solvent delivery. The systems deliver excellent compositional and flow rate accuracy and precision, resulting in high levels of reproducibility, according to the manufacturer. When coupled with the Thermo Scientific LTQ Velos, these systems create a fast LC-mass spectrometry (MS) system, with increased ion trapping efficiency and lower fragmentation times. The fast scan rates of the LTQ Velos allow more MS^n experiments to be carried out in shorter chromatographic runs.

Thermo Fisher **For information 800-532-4752 | www.thermofisher.com/lc**

FLOW CYTOMETERS

The guava easyCyte 8HT flow cytometry system is a compact, affordable, six-color detection system with 96-well automation that allows scientists to move their research out of the core lab and into their own lab. The system enables researchers to carry out highly multiplexed experiments in which six targets and eight parameters can be simultaneously analyzed in a single sample of cells. In addition to allowing researchers to analyze more targets, the six-color detection range also provides greater freedom to choose fluorescent dyes with well-separated emission spectra, which reduces the chance of overlap in the resulting signals and improves data quality.

Millipore

For information 978-715-1567 | www.millipore.com

COLOR CAMERA

The SC30 is an easy-to-use color camera for high-quality microscopy imaging that offers superior resolution and quality with accurate color reproduction. Suitable for use in both material and life science applications, this camera is designed to capture fast frame rates. Its cost-to-performance ratio makes it a suitable introductory model. With a native resolution of 2048 x 1532 pixels and multiple binning modes, the SC30 camera can achieve high levels of sensitivity and fast frame rates during live cell imaging. Using the 4x binning mode, 49 frames per second can be captured at a resolution of 508 x 384 pixels. Exposure times can be set from 57 microseconds to 1.75 seconds, enabling the user to be in complete control of the image acquisition process.

Olympus

For information +49-40-2-37-73-5426 | www.microscopy.olympus.eu

CYTOMETER FOR LARGE PARTICLES

The Copast Large Particle Flow Cytometers can analyze, sort, and dispense objects that are too large (20 microns to 1,000 microns) or too delicate for traditional flow cytometers. Typical samples that can be analyzed range from small multicellular organisms (*C. elegans, D. melanogaster,* and zebrafish) to delicate large cells and cell clusters (adipocytes, embryoid bodies, pancreatic islets, duct cells, and hepatocytes) to seeds and beads (cells growing in or on beads and bead-based assays). Samples are analyzed one by one in a continuously flowing stream and each object is analyzed and sorted based on size, optical density, and up to three fluorescent parameters. Applications include rapid dispensing into microtiter plates for assay preparation, population enrichment prior to further experiments, isolation of rare events, and quantification of fluorescence levels of each object.

Union Biometrica

For information 508-893-3115 | www.unionbio.com

PROTEIN A COLUMNS

A new range of Protein A columns combines the benefits of BioVyon technology with the economy and convenience of a cartridge-based separation methodology. Designed for laboratories that handle small numbers of discrete samples, the columns offer a simple and rapid method for antibody purification, giving consistent recoveries of purified IgG. The minicolumns have a capacity of about 2.5 mg IgG, and the microcolumns have a capacity of 200 µg IgG. They can be washed and reused several times.

Porvair Sciences

For information +44-1372-824290 | www.porvair-sciences.com

MICROULTRACENTRIFUGES

The Sorvall Micro-ultracentrifuge models offer versatility in rapid, small-volume processing of samples, including viruses, cellular organelles, lipoproteins, nucleic acids, and nanoparticles. Both new models offer an expanded volume range, accommodating tubes from 0.2 ml to 30 ml. These systems offer a cutting-edge drive system, providing maintenance-free performance and rotor imbalance protection for years of reliable and dependable performance. The benchtop Sorvall MTX 150 puts almost any separation within reach with a centrifugal force in excess of 1,048,000 x g. It achieves its maximum rotational speed of 150,000 rpm in just 80 seconds, and features a user-friendly LCD touch-screen interface. The Sorvall MX series offers the same versatility as the Sorvall MTX 150 in a floor model configuration. It is available in two versions, with maximum speeds of 150,000 rpm or 120,000 rpm.

Thermo Fisher

For information 508-742-5254 | www.thermo.com/centrifuge

Electronically submit your new product description or product literature information! Go to **www.sciencemag.org/products/newproducts.dtl** for more information.

Newly offered instrumentation, apparatus, and laboratory materials of interest to researchers in all disciplines in academic, industrial, and governmental organizations are featured in this space. Emphasis is given to purpose, chief characteristics, and availabilty of products and materials. Endorsement by *Science* or AAAS of any products or materials mentioned is not implied. Additional information may be obtained from the manufacturer or supplier.

POSITIONS OPEN

WASHINGTON STATE UNIVERSITY

TENURE-TRACK FACULTY POSITION in Virology/Viral Immunology

The Department of Veterinary Microbiology and Pathology, College of Veterinary Medicine, Washington State University, invites applications for a full-time (12-month), tenure-track research/graduate education position in virology/viral immunology at the level of **ASSISTANT PROFESSOR.** The start date is negotiable and may be as early as August 23, 2010. A Ph.D. or clinical doctorate (D.V.M., M.D.) is required and a minimum of two years of postdoctoral training is highly preferred. The successful candidate will have evidence of conducting and publishing high-quality results from hypothesis-based research in top tier journals, a track record of or strong potential for attracting extramural funding, and a history of or stated intent to contribute to high-quality graduate and professional (D.V.M.) education. The faculty member will be expected to develop and maintain an independent, extramurally funded research program in virology or viral immunology that interfaces with ongoing infectious disease research within the Department, College, and University. Active, well-funded research groups are focused on the immunology, pathogenesis, epidemiology, and genomics of animal pathogens and zoonotic agents (**website: http://www.vetmed.wsu.edu/research_vmp/**). Research training at the undergraduate, graduate, and postdoctoral levels is supported by NIH training programs, and the faculty member is expected to actively participate in these programs at all levels. Review of applications will begin April 19, 2010. Submit letter of application, curriculum vitae, and names and addresses of three references to: **Dr. Robert H. Mealey, c/o Ms. Sue Zumwalt, College of Veterinary Medicine, Washington State University, P.O. Box 647040, Pullman, WA 99164-7040. Or e-mail: szumwalt@vetmed.wsu.edu.** For more information, see **website: http://www.vetmed.wsu.edu/employment/.** *WSU is an Equal Employment Opportunity/Affirmative Action Employer. Protected group members are encouraged to apply.*

DARWIN FELLOW

The Graduate Program in Organismic and Evolutionary Biology at University of Massachusetts Amherst announces a two-year **POSTDOCTORAL FELLOWSHIP/LECTURESHIP.** OEB draws together more than 80 faculty from the Five Colleges (University of Massachusetts Amherst and Smith, Hampshire, Mount Holyoke, and Amherst Colleges), offering unique training and research opportunities in the fields of organismic and evolutionary biology and ecology. Our research/lecture position provides recent Ph.D.s with an opportunity for independent research with an OEB faculty sponsor as well as experience developing and teaching a one-semester undergraduate biology course.

Proven teaching skills are required. Position subject to availability of funds. First-year salary: $35,000; second-year salary: $37,000.

To apply, send curriculum vitae, three letters of reference, and statements of research and teaching interests and arrange for a letter of support from your proposed OEB faculty sponsor. A list of faculty and additional information are available at **website: http://www.bio.umass.edu/oeb**.

OEB Darwin Fellowship
319 Morrill Science Center
611 N. Pleasant Street
University of Massachusetts Amherst
Amherst, MA 01003
Telephone: 413-545-0928
E-mail: darwin@bio.umass.edu

Application review begins April 1, 2010. Start date: August 15, 2010.

The University of Massachusetts Amherst is an Affirmative Action/Equal Opportunity Employer. Women and members of minority groups are encouraged to apply.

POSITIONS OPEN

SAN JOSÉ STATE UNIVERSITY

FACULTY POSITION IN GENETICS

San José State University invites applications for a tenure-track position in genetics to begin August 23, 2010 (**website: http://www.sjsu.edu/facultyaffairs/Unit_3/Tenure_Track/Employment/index.htm**). Preference will be given to applicants that are currently utilizing genomics or proteomics approaches in their research. For full consideration send a letter of application, curriculum vitae, university undergraduate and graduate transcripts, statement of teaching interests/philosophy and research interests, and at least three official letters of reference with contact information to: **Genetics Search Committee, Department of Biological Sciences, San Jose State University, One Washington Square, San Jose, CA 95192-0100. E-mail: shearon.threets@sjsu.edu; telephone: 408-924-4905.** For full consideration apply by March 15, 2010. Please include **Job Opening Identification (JOID) 13749** on all correspondence. *SJSU is an Equal Opportunity/Affirmative Action Employer committed to the core values of inclusion, civility, and respect for each individual.*

ENDOWED SENIOR FACULTY POSITION in the Field of Advanced Materials and Surface Science; Full-time, Tenure-Track Faculty

In a major joint venture, Kent State University, Case Western Reserve University, and Youngstown State University received a multimillion award from the State of Ohio to establish a Research Cluster on Surfaces in Advanced Materials in collaboration with industrial partners: Alpha Micron, Inc., CoAdna Photonics, Inc., Cleveland Botanical Garden, Kent Displays, Inc., Kent Optronics, Inc., and LXD, Inc. The Research Cluster will invest aggressively in senior research talent and related facilities and equipment. As a part of this program, Kent State University has been awarded an endowed senior faculty position for an Ohio Research Scholar in the Liquid Crystal Institute, specializing in the area of soft materials and soft matter interfaces. The Liquid Crystal Institute is a leader in basic and applied liquid crystal science, with a broad range of research activities, partnerships with academic and industrial centers, exemplary facilities, and a vibrant scientific atmosphere. Further information is available on the **website: http://www.lci.kent.edu**. Responsibilities include conducting a vigorous program of innovative and funded research, collaborating with academic and industrial partners, supervising graduate students, and teaching. The Ohio Research Scholar will be considered for tenure in the Chemical Physics Interdisciplinary Program, or departments of Chemistry, Physics, or Biological Sciences, depending on the background. Qualification: Ph.D. in physics, chemistry, materials science, or related field required. Applicants must also have an established record of outstanding scholarly research and the ability to secure extramural funding. Application deadline: open until filled.

For a complete description of the position and to apply online, visit the KSU jobs **website: http://jobs.kent.edu** and complete an academic data form for the **position number 990952.** In addition, please attach a letter of application, curriculum vitae, and contact information for three professional references or mail to: **Oleg D. Lavrentovich, Director, Liquid Crystal Institute, Kent State University, P.O. Box 5190, Kent, OH 44242-0001 U.S.A.** *Kent State University, an Equal Opportunity, Affirmative Action Employer, is committed to attaining excellence through the recruitment and retention of a diverse work force. Women, minorities, veterans, and individuals with disabilities are encouraged to apply.*

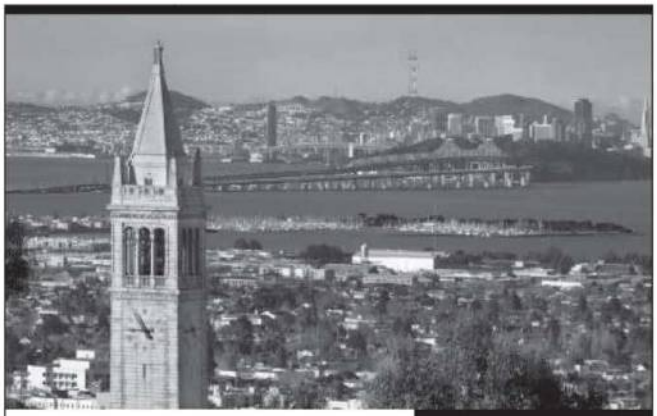

Entry Point!
Students with Disabilities

To meet the challenge of the competitive economy in the new millennium, private industry and government research agencies must expand the pool of technical talent. AAAS started Entry Point!, a program that offers students with disabilities competitive internship opportunities in science, engineering, mathematics, computer science, and some fields of business. And this is just one of the ways that AAAS is committed to advancing science to support a healthy and prosperous world. Join us. Together we can make a difference. aaas.org/plusyou/entrypoint

AAAS + U = Δ

Science Careers is the stage that showcases your talent.

Visit our ENHANCED WEBSITE!

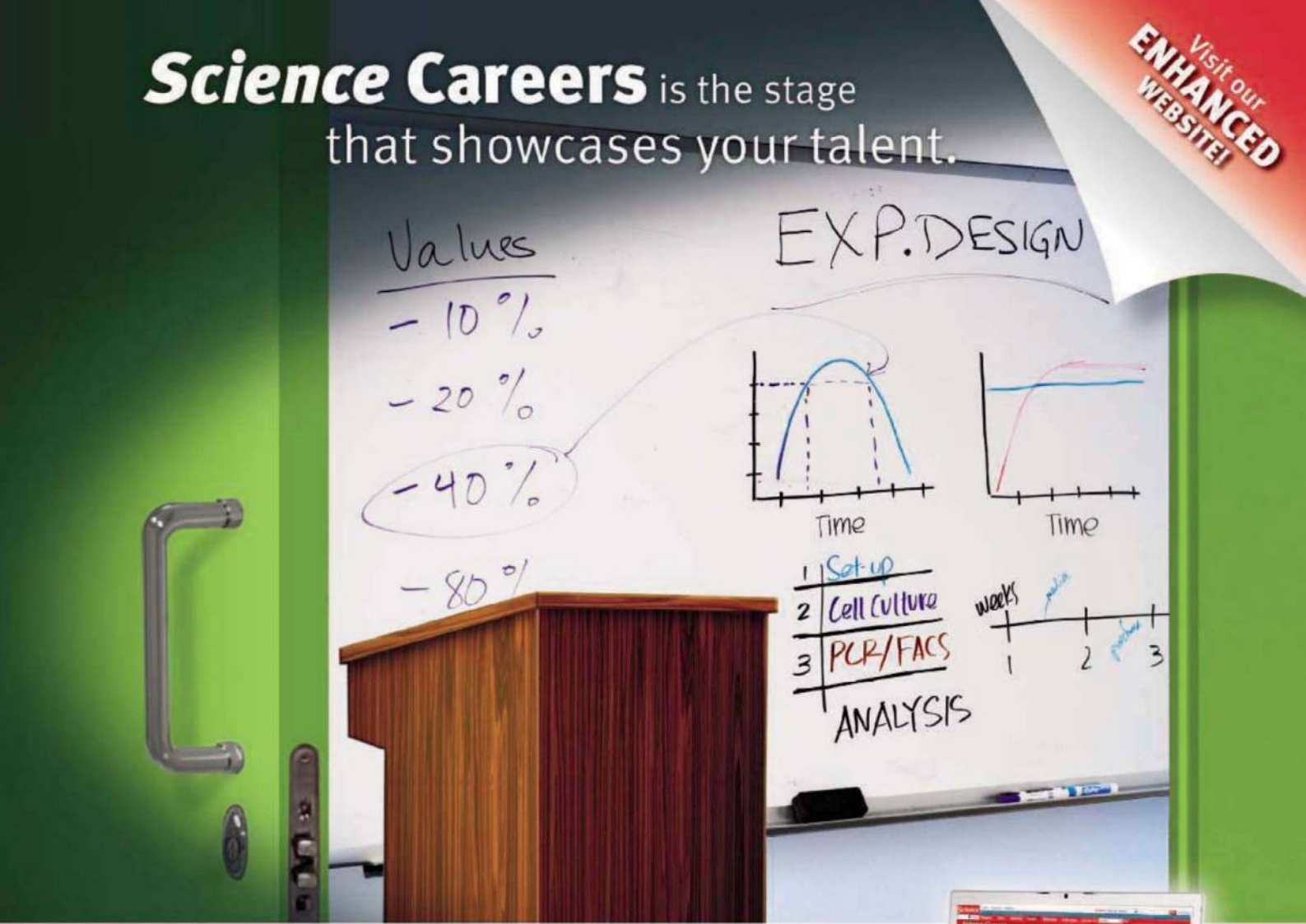

Showcasing your talent is our forte. We're your source for connecting with top employers in industry, academia, and government. We're the experts and platform for accessing the latest and most relevant career information across the globe.

Our newly designed website offers a set of tools that help you discover career opportunities and your personal potential. Whether you're seeking a new job in academia, career advancement in your chosen field, or ways to stay current on industry trends, *Science* Careers is your first stage toward a fulfilling future.

Your Future Awaits.

Improved Website Features:

- » Relevant Job E-mail Alerts
- » Improved Resume Uploading
- » Content Specific Multimedia Section
- » Facebook Profile

Job Search Functionality:

- » Save and Sort Jobs
- » Track Your Activity
- » Search by Geography
- » Enhanced Job Sorting

Science Careers
From the journal *Science* AAAS

ScienceCareers.org

Whitacre Chair in Energy Science and Engineering

The Department of Chemical Engineering at Texas Tech University is actively seeking to fill the newly endowed Whitacre Chair in Sustainable Energy. Candidates for the position will be exceptional individuals whose research areas are aligned with the university goals of creating a strong multi departmental research base in Sustainable Energy at Texas Tech University. The selected individual will be an internationally recognized leader in his or her field as demonstrated by such metrics as the peer reviewed publication and citation records, national recognitions such as major awards or fellowships in technical societies, and a strong track record of competitive research funding. The Department of Chemical Engineering at Texas Tech University has embarked on building a nationally recognized research-intensive department with strengths in Polymers and Materials, Bioengineering and Biotechnology, Computational Chemical Engineering, and Process Systems and Engineering. The successful candidate is expected to expand the research portfolio of the department into Sustainable Energy. The position is an Endowed Chair at the level of Full Professor and incumbents will be expected to participate in research service and teaching at this level. It is anticipated that successful candidates will have very strong records of scholarship supported by extramural funding and that externally sponsored research will be brought to Texas Tech University.

Interested candidates should apply online at **https://jobs.texastech.edu/**. Please use requisition number **80764**. Interested candidates should include a detailed CV, a research statement, and a list of five referees.For further information, please contact the search committee chair, **Dr.Raghu Rengasamy at raghu.rengasamy @ttu.edu**.

Texas Tech is an Equal Opportunity Employer.

Molecular and Cellular Biologist

Molecular and Cellular Oncology

The Department of Molecular and Cellular Oncology at The University of Texas M. D. Anderson Cancer Center is seeking outstanding molecular and cellular oncologists. The department has an opening for a full-time, tenure-track faculty with demonstrated excellence in molecular and cellular approaches to understanding the molecular mechanisms of cancer development. Although not required, the following expertise is encouraged: proteomic/biochemical analysis, and signal pathways to elucidate the molecular mechanisms that cause cancer. Incumbents will be responsible for establishing their own independent research and expected to write grants and papers. Applicants must have a doctoral degree, postdoctoral experience and be eligible to apply for federal grants. Interested applicants should send a letter and curriculum vitae to:

Mien-Chie Hung, Ph.D.
Chair, Department of Molecular and Cellular Oncology, Unit 108
The University of Texas M. D. Anderson Cancer Center
1515 Holcombe Blvd., Houston, Texas 77030
E-mail: nedwards@mdanderson.org

THE UNIVERSITY OF TEXAS
MD ANDERSON
CANCER CENTER
Making Cancer History®

The University of Texas M. D. Anderson Cancer Center is an equal opportunity employer and does not discriminate on the basis of race, color, national origin, gender, sexual orientation, age, religion, disability or veteran status, except where such distinction is required by law. All positions at The University of Texas M. D. Anderson Cancer Center are security sensitive and subject to examination of criminal history record information. Smoke-free and drug-free environment.

Tenure Track Faculty Positions in Neuroscience

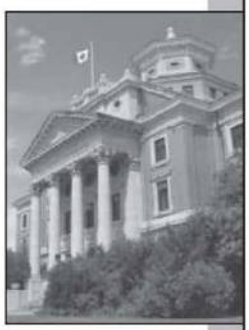

Located in the thriving, multicultural city of Winnipeg, the University of Manitoba offers students and faculty a vibrant learning community, exceptional facilities and the chance to explore ideas, challenge assumptions and turn theory into reality. Our researchers are among the best in the world, finding new ways to protect the environment, improve human health, advance technology and strengthen communities in Canada and beyond. With more than 30,000 students, faculty, and staff, and over 90 degree programs, the University of Manitoba plays a key role in the social, cultural, and economic well-being of our community and our world.

The Faculty of Medicine, University of Manitoba and the Winnipeg Regional Health Authority are developing a new priority initiative, the Neuroscience Research Program. Five (5) tenure-track faculty positions are available at the rank of Assistant or Associate Professor, commensurate with qualifications and experience. **Position # 10631,10632,10633,10634, 10635.**

The candidates must have a PhD and/or MD with strong demonstrated expertise in neuroscience research. The new recruits are expected to teach in, and to develop a rigorous and independently-funded research program in the areas of neurosciences, mental health and addiction. Some examples of research areas of interests are: neuropharmacology, developmental neurobiology, neurobiology of neurological and psychiatric diseases, neuroinflammation, cerebrovascular biology, stroke, neurotrauma, and regenerative neuroscience. The successful candidates will be offered an academic appointment in a basic science department, depending upon each candidate's interests and specialty area. All candidates are also expected to develop strong collaboration in translational research with clinical departments.

The Program will be housed in the new Kleyson Institute of Advanced Medicine which is part of the Health Sciences Centre complex. The successful candidates will be provided with a competitive start-up package and will have access to numerous state-of-the-art facilities and expertise including gene targeting, high throughput screening, RNAi Libraries, Proteomics, cell sorting, animal modeling, imaging and behaviour systems. Learn more about our research at **http://www.umanitoba.ca/faculties/medicine/research/.**

Winnipeg has a strong health research focus. The city has a rich cultural environment, including symphony, opera, dance, theatre, professional sports and ethnic festivals. The region provides many opportunities for outdoor recreation in all seasons. Learn more about Winnipeg at **http://www.city.winnipeg.mb.ca.**

The University of Manitoba encourages applications from qualified women and men, including members of visible minorities, Aboriginal peoples and persons with disabilities. All qualified candidates are encouraged to apply; however, Canadians and permanent residents will be given priority.

Candidates are to forward further enquiries or a letter of application together with curriculum vitae, supportive information, a statement of research interests and the names and contact information of three referees to: **Dr. Kevin Coombs, Associate Dean of Research, E-mail: kcoombs@cc.umanitoba.ca or Dr. Xin-Min Li, Director of the Neuroscience Research Program, E-mail: xinmin_li@umanitoba.ca, Faculty of Medicine, University of Manitoba, Room A108 Chown Bldg, 753 McDermot Ave., Winnipeg, MB R3E 0T6, Tel: (204) 789-3375, Fax: (204) 789-3942**

Selection process begins **March 1, 2010** and will remain open until filled. Anticipated start date is **July 1, 2010** or as soon thereafter as possible.

Application materials, including letters of reference, will be handled in accordance with the *"Freedom of Information and Protection of Privacy Act"* (Manitoba). Please note that curriculum vitaes may be provided to participating members of the search process.

For more information on this opportunity, please visit umanitoba.ca/employment

Winnipeg Regional Health Authority
Office régional de la santé de Winnipeg

One university. Many futures.

UNIVERSITY OF MANITOBA

UNIVERSITÄT BASEL

The Faculty of Medicine of the University of Basel, Switzerland, invites applications for a

Professorship in Anatomy

(with a scientific focus in the fields of Functional Neuroanatomy/Neuro-Imaging or Mechanobiology)

Applicants are expected to have completed their studies in medicine or life sciences, obtained their habilitation or an equivalent qualification and have several years of teaching experience in Anatomy or a related clinical discipline. In addition, candidates must have proven leadership qualities and be willing to promote interdisciplinary cooperation with clinical and pre-clinical research groups.

The successful candidate will be an active researcher in the fields of Functional Neuroanatomy/ Neuro-Imaging or Mechanobiology/Mechanotransduction, have an excellent scientific publication record and demonstrated ability to successfully acquire extramural funding.

Teaching at the University of Basel is in German. Successful non-German speaking candidates will be expected to learn German within 2–3 years.

The University of Basel seeks to increase the proportion of women among the faculty members and therefore specifically encourages female candidates to apply.

For additional information please contact: Prof. Ch. Stippich, Head of the Search Committee, University Hospital, Basel (phone: +41 61 265 49 12, email: cstippich@uhbs.ch).

Application deadline is: 18.4.2010
Details concerning the documents to be included in the application are available at: http://medizin.unibas.ch/dekanat/bewerbungen.html

Please send your letter and your application solely as a pdf file on a CD addressed to:
Medizinisches Dekanat der Universität Basel, Klingelbergstrasse 61, CH-4056 Basel

UNI BASEL

The Pennsylvania State University

PENNSTATE

SCHOOL *of* INTERNATIONAL AFFAIRS

FACULTY SEARCH: PROFESSOR/ASSOCIATE PROFESSOR OF INTERNATIONAL AFFAIRS (Specializing in Science and Technology)

Penn State University's School of International Affairs invites nominations and applications of scholars worldwide for a tenured or tenure track faculty as Professor/Associate Professor of International Affairs specializing in science, technology and policy, with an appreciation of the role and impact of science and technology policy in economic development, communications, society, NGOs and globalization. Applicants should have a relevant Ph.D. and a track record of scholarship and teaching and/or relevant experience in public or private sector entities or international organizations.

Penn State University's School of International Affairs enrolled its first graduate class in fall 2008. The School's mission is to prepare students for careers and leadership positions in both the private and public sectors of an increasingly interdependent world. Our faculty are motivated by and dedicated to the unique opportunity of building a new graduate School of International Affairs with programs and standing appropriate to one of the world's great public research universities.

Please send letter of application, résumé/CV and the names, addresses, telephone numbers and e-mail addresses of three referees or nominations to Faculty Search Committee Chair, Penn State University School of International Affairs, Lewis Katz Building, University Park, PA 16802 at siainfo@psu.edu or Human Resources Coordinator at jls142@psu.edu. For more information visit: www.sia.psu.edu. Review of applications will begin immediately and will continue until position is filled. Penn State is committed to affirmative action, equal opportunity and the diversity of its workforce, and we welcome applications from persons of color, women and other groups traditionally underrepresented in the academic community.

TIGM
TEXAS A&M INSTITUTE FOR GENOMIC MEDICINE

Director and Chief Executive Officer

Texas A&M Institute for Genomic Medicine
Texas A&M Health Science Center

The Texas A&M Health Science Center is seeking a director for the Texas Institute for Genomic Medicine (TIGM). TIGM maintains the world's largest single library of unique genetically modified mouse embryonic stem cell clones, representing over 10,000 inactivated genes. The mission of TIGM is to advance research and education related to human and veterinary diseases through the application of functional genomics, primarily using transgenic and knockout mouse technology. The TIGM core facility provides ES cells and genetically-engineered mice as well as services to investigators, academic partners, and corporate institutions throughout the world on a fee-for-service basis. In addition, TIGM supports basic and applied research and training for scientists from Texas A&M and affiliated institutions.

TIGM is one of four members of the *International Knockout Mouse Consortium* and is a partner within the Texas A&M Institute for Innovative Therapeutics (IIT). TIGM has major research laboratories in Houston and College Station, Texas, and is headquartered in a new state-of-the-art building (40,000 square feet) on the campus of Texas A&M University in College Station. Additional information about TIGM can be found at **http://www.tigm.org/**.

The Director/CEO of the TIGM will provide leadership, strategic direction, and oversight of all TIGM activities and operations. A major responsibility is to develop exciting research and business opportunities with academic and corporate partners.

It is highly desirable that the Director and Chief Executive Officer be qualified for an academic appointment within the Texas A&M Health Science Center or Texas A&M University and that the candidate's research interests be highly aligned with the strategic objectives of TIGM.

The Director/CEO of TIGM should have: (a) fundamental working knowledge of mouse ES cells and technologies associated with their application in modern genomic medicine; (b) proven leadership abilities and strategic vision; and (c) outstanding administrative, managerial, and communication skills. The Director/CEO must have: an advanced degree (PhD, MD, DVM) or commensurate experience from the commercial biotechnology sector; recognition as an outstanding research scientist and/or clinician; and/or leadership experience in a biotechnology corporate environment.

Interested candidates should send a complete CV along with a cover letter including a description of their research and administrative experience, a vision statement, and contact information for three or more references to the following link **https://jobs.tamhsc.edu/applicants/Central?quickFind=51521**.

SCRIPPS FLORIDA
THE SCRIPPS RESEARCH INSTITUTE

Faculty Positions
Department of Neuroscience

Scripps Florida is seeking outstanding applicants for tenure track faculty positions in the Department of Neuroscience at its newly opened, state-of-the-art campus in Jupiter, Florida. TSRI applies integrative molecular genetic, biochemical, biophysical, cellular, anatomical, and behavioral approaches to elucidate the mechanisms underlying brain function. We are particularly interested for this search in highly qualified and interactive investigators working with rodent models for human neurological and psychiatric disorders. Other particular areas of interest include learning and memory, sleep research, synapse formation, and drug discovery efforts for CNS disorders. The state-of-the-art facilities at Scripps Florida house expertise in proteomics, crystallography, pharmacokinetics, medicinal chemistry, rodent behavior, and ultra high-throughput small molecule screening for drug discovery.

Appointments are available at Assistant, Associate, or Full Professor. TSRI offers attractive startup packages and an outstanding intellectual environment for fostering top-tier basic and translational research. Interested candidates should submit their *Curriculum Vitae*, a synopsis of their past, current, and proposed research, and complete contact information for at least three professional references as a single PDF file, to:

Dr. Ronald L. Davis, Chairman, Department of Neuroscience
c/o Hollie Alkema
(hollie@scripps.edu)

The Scripps Research Institute, Scripps Florida
130 Scripps Way
Jupiter, Florida, 33458

Postdoctoral Fellowships
Dartmouth College
Life Sciences

The Department of Biological Sciences at Dartmouth College, with funding from the Howard Hughes Medical Institute, seeks applications for two **HHMI Postdoctoral Fellowships in the Life Sciences**. The HHMI Fellowships are two-year, non-tenure track positions with NIH NRSA scale salaries and Dartmouth health benefits; they are designed to provide training to postdoctoral fellows in the arts of teaching and research. Each fellow will pursue a life science-related research project in the laboratory of a Dartmouth faculty member from an appropriate department in the Arts and Sciences, Medical School, or Engineering School. Collaborative projects that involve more than one laboratory at Dartmouth will also be considered. In addition, during the first year, each fellow will be paired with a senior faculty member with whom they will co-teach an undergraduate course in biology; they will teach a course alone during the second year. Training in teaching will occur through mentoring and workshops designed specifically for the fellows by staff of the Dartmouth Center for the Advancement of Learning. Thus, the fellows will receive substantial training under the guidance of experienced faculty and education mentors. The goal of the HHMI Fellowships is to ensure that the fellows develop strong research and teaching credentials.

Applicants should prepare a cover letter, in which they indicate up to three laboratories with which they would like to be affiliated (contact with these laboratories prior to application submission is strongly encouraged but not required; see **http://www.dartmouth.edu/~biology/HHMIpostdoc.html** for more information), a curriculum vitae, and a statement of career goals and teaching interests. Candidates should also arrange to have three letters of recommendation sent from individuals qualified to comment on the applicant's credentials. Application materials should be sent to **HHMI-Fellows@mac.dartmouth.edu or via U. S. mail (HHMI Fellowship Search Committee, Department of Biological Sciences, 6044 Gilman, Dartmouth College, Hanover, New Hampshire 03755)**. Consideration of applications will begin on 17 May 2010 and continue until the positions are filled. Fellowships will run for two calendar years, beginning on 1 September 2010.

Dartmouth College is an Equal Opportunity/Affirmative Action Employer.

WAYNE STATE UNIVERSITY
CANCER

The Department of Pathology at the Wayne State University School of Medicine in Detroit Michigan is seeking to fill two tenure-track faculty positions at the rank of Assistant/Associate professor in the area of cancer biology. We are interested in identifying qualified scientists with interest in tumor microenvironment, angiogenesis and/or cancer stem cells and expertise in cell biology and mouse models of cancer, but all areas of cancer will be considered. Applicants should have a PhD or equivalent degree. Candidates for Assistant Professor positions should have clear potential for conducting funded independent research. Associate Professor applicants should have a recognized reputation in his/her field of research and extramural funding. A competitive start-up package will be provided.

Send a curriculum vitae and the names and email addresses of three references (all included in a single PDF file) to **Pathology-search-cancer@med.wayne.edu**. Information about the Pathology department is available at **http://Pathology.med.wayne.edu/**.

Wayne State University is an Affirmative Action, Equal Opportunity Employer.

WAYNE STATE UNIVERSITY
METABOLIC

The Department of Pathology at the Wayne State University School of Medicine in Detroit Michigan is seeking to fill two tenure-track faculty positions at the rank of Assistant/Associate professor in the areas of metabolic and/or cardiovascular disease. Although we will consider applicants with research in any area related to metabolic or cardiovascular diseases, we are particularly interested in identifying individuals with interests in cellular energy metabolism, mitochondrial biology, stem cells and/or metabolomics. Applicants should have a PhD or equivalent degree. Assistant Professor applicants should have clear potential for conducting funded independent research. Associate Professor applicants should have a recognized reputation in his/her field of research and extramural funding. A competitive start-up package will be provided.

Send a curriculum vitae and the names and email addresses of three references (all included in a single PDF file) to **Pathology-search-metabolic@med.wayne.edu**. Information about the Pathology department is available at **http://Pathology.med.wayne.edu/**.

Wayne State University is an Affirmative Action, Equal Opportunity Employer.

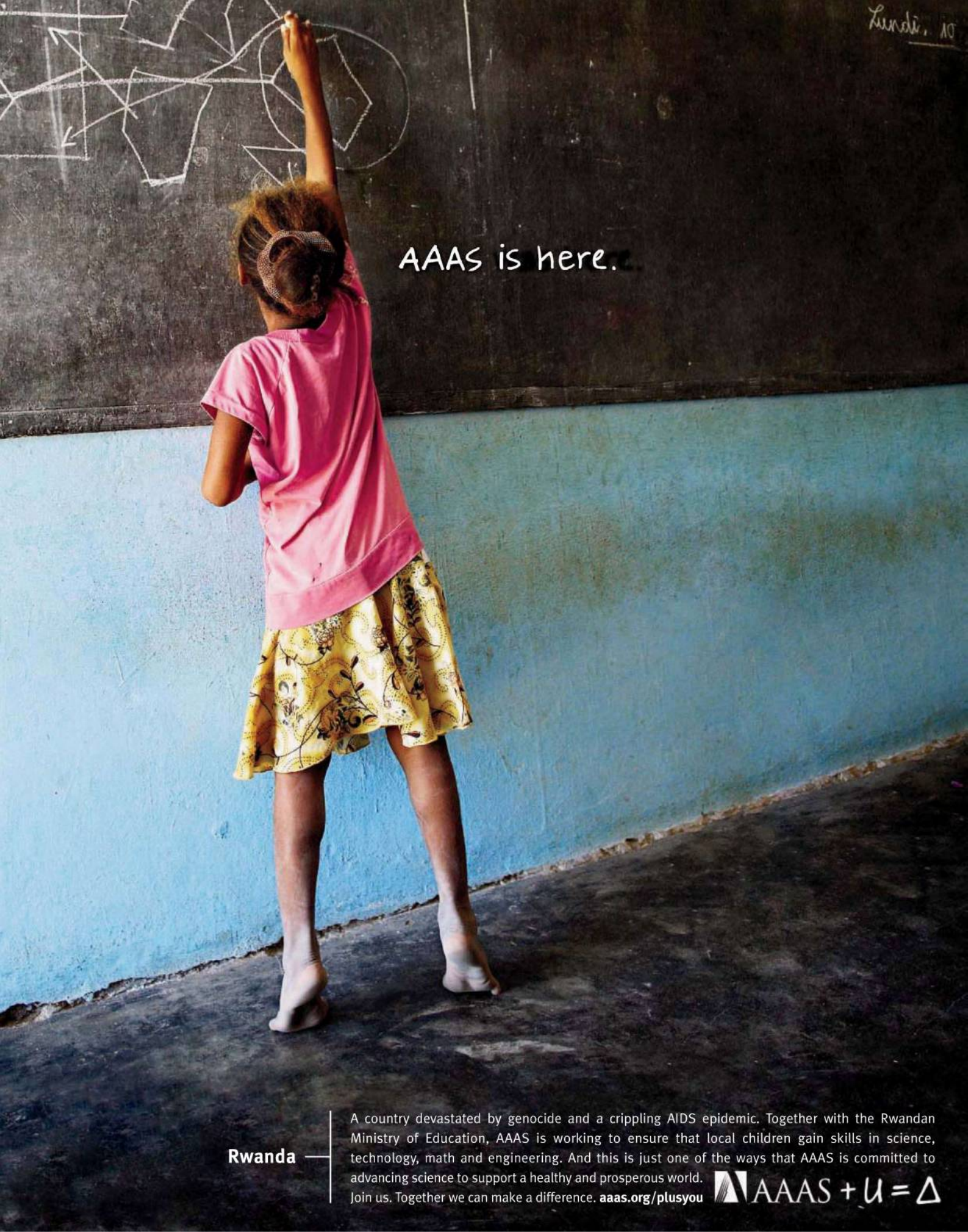

Rwanda

A country devastated by genocide and a crippling AIDS epidemic. Together with the Rwandan Ministry of Education, AAAS is working to ensure that local children gain skills in science, technology, math and engineering. And this is just one of the ways that AAAS is committed to advancing science to support a healthy and prosperous world.
Join us. Together we can make a difference. **aaas.org/plusyou**

AAAS + U = Δ

KUWAIT INSTITUTE FOR SCIENTIFIC RESEARCH

KISR has a vacancy in the following field:

MOLECULAR DIAGNOSTICS

Major duties: Carrying out multidisciplinary research on molecular diagnostic and molecular pathogenesis of livestock and crops diseases. Conducting molecular studies on bacterial and viral pathogens as well as on insect toxins and to develop diagnostic kits.

Qualifications: Applicants should have a Ph.D. in Virology, Microbiology or any other related area with proven experience in molecular diagnostic R&D with broad experience in cell culture, genomics, gene silencing and proteomics techniques. Strong leadership, ability to attract research funding, project management and staff training are highly desirable.

KISR offers attractive tax free salaries commensurate with qualifications and experience that include: gratuity, free furnished accommodation, school tuition fees for children, six weeks annual paid vacation, air tickets and life insurance.

Interested applicants are requested to send their Curriculum Vitae with supporting information not later than one month from the date of this publication, to:

Personnel Manager
Kuwait Institute for Scientific Research
P.O. Box 24885
13109 Safat, Kuwait.
Or e-mail: employment@safat.kisr.edu.kw
For further information, please visit our web site:
www.kisr.edu.kw

FRED **HUTCHINSON**
CANCER RESEARCH **CENTER**

A LIFE OF SCIENCE

Faculty Recruitment, MD or MD-PhD
Physician-Scientist or PhD Translational Scientist

The Fred Hutchinson Cancer Research Center (FHCRC) is recruiting a faculty member at the ASSISTANT, ASSOCIATE or FULL MEMBER level with active laboratory research related to breast cancer. Physician-Scientists with strong laboratory research and clinical expertise in a breast cancer-related discipline or PhD scientists with active translational research interests in breast cancer are strongly encouraged to apply. The successful candidate will join the large Women's Cancer Research Program within the Fred Hutchinson/University of Washington Cancer Consortium; a dynamic cross-disciplinary research team dedicated to improving prevention, detection, diagnosis, prognosis and treatment of breast cancer. The primary appointment will be in the Clinical Research Division of the FHCRC. If appropriate, a joint appointment may be offered in other divisions at the Center (Human Biology, Basic Sciences or Public Health Sciences) and/or to the full-time faculty in an appropriate department at the University of Washington.

Interested individuals should forward their curriculum vitae, including a research plan and the names of five references, to:

Suzanne Lentz
Administrator, Women's Cancer Research: Breast Section
Fred Hutchinson Cancer Research Center
srlentz@fhcrc.org

Fred Hutchinson Cancer Research Center is an Affirmative Action, Equal Opportunity Employer. We are dedicated to building a culturally diverse faculty and strongly encourage applications from women, minorities, individuals with disabilities, and covered veterans.

Cold Spring Harbor Asia
Conferences & Summer School
Suzhou, China

Cold Spring Harbor Asia programs will be held at the new Suzhou Dushu Lake Center in Suzhou, China, sixty miles west of Shanghai and in easy reach of international and domestic airports. Symposia, conferences and summer schools follow the Cold Spring Harbor tradition in showcasing merit-based scientific advances in an informal but intense atmosphere. Nearby Suzhou is an ancient city known as the Venice of China, famous for its canals and gardens and home to scholars for over two millenia.

2010 Summer School

COMPUTATIONAL & COGNITIVE NEUROBIOLOGY
July 11 - 24, 2010
Application deadline: April 15, 2010
Upinder Bhalla (India), Zachary Mainen (Portugal)
Xiao-Jing Wang (USA), Si Wu (China)
Speakers include:
Larry Abbott, Carlos Brody, Robert Desimone, Yang Dan, Kenji Doya, Michael Hausser, Eve Marder, Barry Richmond, Mike Shadlen, Keiji Tanaka, Daniel Wolpert

2010 Conferences

James Watson Cancer Symposium April 6 - 11
Francis Crick Neuroscience Symposium April 12 - 17
Membrane Proteins: Structure & Function May 10 - 14
Epigenetics, Chromatin & Transcription May 17 - 21
Human Genetics & Genomics September 6 - 10
Molecular Switches and Genome Function in Stem Cells & Development September 20 - 24
Computational Biology September 27 - October 1
Emerging Infectious Diseases October 18 - 22
From Plant Biology to Crop Biotechnology October 25 - 29
RNA Biology November 1 - 5
Frontiers of Immunology in Health and Diseases November 8 - 10

To encourage significant international participation, all scientific programs will be conducted in English. Stipends may be available to partially offset registration/tuition, room and board costs for qualified applicants.

Supported by Suzhou Ventures Group, Life Technologies

Cold Spring Harbor Asia Conferences
Suzhou Dushu Lake Conference Center
299 Qiyue Rd, SIP/Suzhou, Jiangsu Province, China
T +86 512 6272 9029 F+86 512 6272 9028
meetings@csh-asia.org

POSITIONS OPEN

VISITING ASSISTANT PROFESSOR POSITIONS IN GENETICS, IN VERTEBRATE PHYSIOLOGY, AND IN VERTEBRATE ANATOMY
The Joint Science Department of Claremont McKenna, Pitzer, and Scripps Colleges

The Joint Science Department of Claremont McKenna, Pitzer, and Scripps Colleges, three of the five undergraduate Claremont Colleges in southern California, seeks to hire three visiting assistant professors for the 2010-2011 academic year, beginning August 2010. Anticipated teaching responsibilities: Position 1: vertebrate physiology, a course for nonscience majors, and a laboratory section of introductory biology (molecular, cell, genetics, metabolism, physiology, and development). Position 2: vertebrate anatomy, a course for nonscience majors, and laboratory sections of introductory biology (ecology, evolution, biodiversity). Position 3: genetics, introductory biology lecture and laboratory (molecular, cell, genetics, metabolism, physiology, and development), and a course for nonscience majors.

Participation in research, particularly directing undergraduate research projects, may be possible. A Ph.D. in biology or related subject is required, and prior teaching experience is preferred.

Please submit curriculum vitae and a statement of interest, and arrange to have three letters of reference sent to: **Temporary Biology Position # (1, 2, or 3), W.M. Keck Science Center, 925 N. Mills Avenue, Claremont, CA 91711-5916. Telephone: 909-621-8298.** Inquiries for Positions 1 and 2 to **Dr. Marion Preest, e-mail: mpreest@jsd.claremont.edu**; for Position 3 to **Dr. Emily Wiley, e-mail: ewiley@jsd.claremont.edu**. Review of applications begins immediately. The positions will remain open until filled.

In a continuing effort to enrich their academic environment and provide equal educational employment opportunities, The Claremont Colleges actively encourage applications from women and members of historically underrepresented groups in higher education. The Claremont Colleges are an Equal Opportunity Employer.

XEUS

MICROBIOLOGIST

XEUS in Boston, Massachusetts, seeks a Microbiologist. Position requires an exceptional understanding of microbial fermentation, along with a solid working knowledge of common microorganisms utilized in the biofuels area, including yeasts and bacteria. Applicant should also have a solid understanding of metabolic engineering techniques. Applicant will identify potential bacterial and yeast strains, and then will optimize fermentation conditions for the strains identified. Applicant will team with bioprocessing engineers in the scaling and commercialization of our cellulosic biofuels technology. The candidate preferably has a Ph.D. in microbiology or the equivalent. The ideal candidate should have a minimum of five years of relevant industrial experience. The candidate should have experience with bioreactors and various purification and recovery methods, such as centrifugation, cell disruption, cryopreservation, seed flask development, distillation, chromatography, and lyophilization. Experience with standard laboratory instrumentation, such as Nova, Cedex, microscopes, gas analyzers, spectrophotometers, YSI analyzers, and high performance liquid chromatography, is also required. Send curriculum vitae to **e-mail: microbiologist@xeus.info**.

POSITIONS OPEN

ASSISTANT PROFESSOR
Physical Geography (Watershed or Aquatic Science) Department of Watershed Sciences Utah State University

The Department of Watershed Sciences (**website: http://www.cnr.usu.edu/wats**) at Utah State University seeks applications for a nine-month, tenure-track position. We are interested in applicants whose primary expertise is in an area of watershed or aquatic science and who can contribute to the curricula in both Watershed Sciences and Physical Geography. The division of activities will be approximately 50 percent research, 40 percent teaching, and 10 percent service. See **website: https://jobs.usu.edu (requisition ID 052010)** for a complete position description and application instructions.

ASSISTANT PROFESSOR HISTOLOGY/ANATOMY

Applications for appointment at the Assistant Professor level in the tenure track at the University of Florida, Department of Physiological Sciences, are invited from individuals engaged in environmental health research. Applicants should hold a Ph.D. and/or D.V.M. degree and have significant postdoctoral training. The successful candidate will be expected to establish an independent, externally funded research program and to teach in University of Florida, College of Veterinary Medicine professional veterinary medicine curriculum. The successful candidate will be required to teach histology and/or anatomy. This full-time position offers outstanding scholarly and scientific resources in a collegial environment with existing neuroscience and toxicology programs. The University of Florida has state-of-the-art core facilities, including transgenic mouse and targeted mutagenesis, confocal and multiphoton microscopy, imaging and morphometry, cell sorting, and microarray cores. Applicants with outstanding accomplishments in integrative environmental health research, especially transgenic models related to environmental health, are encouraged to apply. The successful candidate will have the opportunity to add to existing departmental strengths in toxicology and cardiovascular, respiratory, urogenital and comparative neurobiology. Beyond the individual's area of expertise, the successful candidate will have the ability to bridge basic and clinical science. This recruitment is part of a growing commitment at the College of Veterinary Medicine to increase the understanding and treatment of diseases related to environmental health in all species. Salary is commensurate with experience. The start date is expected to be July 1, 2010.

Applications will be considered as they are received, but in order to ensure full consideration, applicants should send curriculum vitae, a three-page statement of research accomplishments, teaching statement and future goals, and three letters of recommendation by April 15, 2010, to **Thomas Wronski, Ph.D., Search Committee Chair.** Please direct electronic submissions to **e-mail: wronskit@vetmed.ufl.edu**.

The University of Florida is an Affirmative Action, Equal Opportunity Employer. Hiring is contingent upon eligibility to work in the U.S.A. Women and minorities are especially encouraged to apply.

POSITIONS OPEN

Yale

CHANNEL ELECTROPHYSIOLOGIST RESEARCH ASSOCIATE

Superb opportunity to work at Yale University Medical School as a member of multidisciplinary team including physiologists, pharmacologists, molecular and cell biologists, and pain physiologists. Research Associate position available for a Ph.D. or M.D. electrophysiologist, with prior experience and publications in patch clamp analysis of ion channels in heterologous expression systems and in mammalian neurons. Experience with the physiology and pharmacology of voltage-gated channels, and current-clamp as well as voltage-clamp analysis is highly desirable. Electronically send curriculum vitae and three letters of reference to **Stephen Waxman, M.D., Ph.D., e-mail: stephen.waxman@yale.edu**, and/or via surface mail to: **Neuroscience and Regeneration Research Center of Yale University, VA Connecticut, 950 Campbell Avenue, Building 34, West Haven, CT 06516.** *Equal Opportunity, Affirmative Action Employer.*

POSTDOCTORAL RESEARCH SCIENTIST/ ASSOCIATE RESEARCH SCIENTIST/ ASSISTANT PROFESSOR
Columbia University College of Dental Medicine Stem Cell Biology/Biomaterials/ Tissue Engineering/Regenerative Medicine

Several full-time Faculty and several Postdoctoral positions are available at the Columbia University Medical Center campus. This research involves collaboration opportunities among the College of Dental Medicine (CDM), the College of Physicians and Surgeons, and the Department of Biomedical Engineering at the School of Engineering and Applied Sciences. The primary appointment is at CDM. Research experience in biomaterials, controlled release, polymer chemistry, cell and molecular biology, stem cell biology, tissue engineering, and animal surgery techniques required. The central focus is to engineer human tissue and/or organ analogs under the sponsorship of NIH grants. Good verbal and written communication skills required. Ph.D. required. Experience in working with a team preferable. Academic rank and compensation commensurate with experience. Positions available immediately. For more information about these positions and to apply, please visit the following **website: https://academicjobs.columbia.edu/applicants/Central?quickFind=52820**.

Columbia University is an Equal Opportunity/Affirmative Action Employer.

Two to three **POSTDOCTORAL FELLOW** or **RESEARCH ASSISTANT PROFESSOR** positions are open in the lung cancer genetics group at the Siteman Cancer Center of Washington University School of Medicine. Experience with large-scale genomewide datasets, next generation sequencing experience, genomewide association studies (GWAS) knowledge, and expression arrays and full understanding of genetics of complex disease are required. The starting salaries will be $36,000 to $45,000 for Fellows and $75,000 to $85,000 for Research Assistant Professors. Please send a resume and three references to **Dr. Ming You, e-mail: youm@wustl.edu**.

MARKETPLACE

AAAS, publisher of *Science*,
thanks the sponsors and supporters of the

2010 Annual Meeting

Bridging Science and Society

18—22 February ▸ San Diego

Presenting Sponsor

SUBARU

OSA The Optical Society

Canada

HELMHOLTZ ASSOCIATION

EUROPEAN RESEARCH
SUCCESS THROUGH COOPERATION
www.ec.europa.eu/research

Johnson & Johnson
PHARMACEUTICAL RESEARCH & DEVELOPMENT, L.L.C.

UCSD

SOYCONNECTION.COM

THE ROYAL SOCIETY

PATHWAY GENOMICS

THE KAVLI FOUNDATION

In addition generous funding for AAAS Awards is provided by the ***Kavli Foundation*** and ***Affymetrix.***

AAAS
ADVANCING SCIENCE, SERVING SOCIETY

Can you see how they'll be different 30 years from now?

applied biosystems
part of life technologies

SOLiD™ 4
SYSTEM SEQUENCING

Introducing the new, more accurate, higher throughput SOLiD™ 4 System.

Next-generation sequencing just leaped to the next level in accuracy. The SOLiD™ 4 System leverages advanced informatics and optimized reagents to enable scientist to obtain the highest accuracy of any NGS system. With throughputs of 100 GB per run and workflow automation, the SOLiD™ 4 System accelerates your large-scale genomic analysis to an unprecedented pace. Plus, new paired-end library options enable detection of novel splice variation and fusion transcripts with less input DNA. Using the SOLiD™ 4 System, your laboratory will have the ability to detect more variation and spend less time and money doing it. Take a look at the new SOLiD™ 4 System. See what's never been seen before.

For more information, visit us at **www.appliedbiosystems.com/solid4**

life technologies™